The Synthesis and Characterization of Lanthanide Complexes with Phenalenide and Aromatic-Fused Cyclopentadienyls as Ligands

By

Jianlong Sun

BSc, Shandong University, China, 2001

A Dissertation Submitted in Partial Fulfillment of the
Requirements for the Degree of

DOCTOR OF PHILOSOPHY

in the Department of Chemistry

We accept this dissertation as conforming to the required standard

The Synthesis and Characterization of Lanthanide Complexes with Phenalenide and Aromatic-Fused Cyclopentadienyls as Ligands

By

Jianlong Sun

BSc, Shandong University, China, 2001

Supervisory Committee

Dr. David J. Berg, (Department of Chemistry)

Supervisor

Dr. Reginald H. Mitchell, (Department of Chemistry)

Departmental Member

Dr. Peter Wan, (Department of Chemistry)

Departmental Member

Dr. Barbara J. Hawkins, (Department of Biology)

Outside Member

Dr. Josef Takats, (University of Alberta, Chemistry)

External Examiner

Supervisory Committee

Dr. David J. Berg, (Department of Chemistry)

Supervisor

Dr. Reginald H. Mitchell, (Department of Chemistry)

Departmental Member

Dr. Peter Wan, (Department of Chemistry)

Departmental Member

Dr. Barbara J. Hawkins, (Department of Biology)

Outside Member

Dr. Josef Takats, (University of Alberta, Chemistry)

External Examiner

ABSTRACT

The synthesis of yttrium phenalenide complexes **129-132** was achieved by salt metathesis reactions between ligand anions and YCl_3. Ytterbium phenalenide complexes **133-137** were synthesized by protonolysis reactions between neutral ligands and $Yb[N(SiMe_3)_2]_2(THF)_2$. The solid state structure of $(Pn^{tBu})_2Yb(THF)$ **136** reveals a unique η^3 bonding pattern, however the electrons of the phenalenide ligand remain delocalized even when bonded to the metal center.

Mono-alkyl complexes $(PCp^R)_2Y(CH_2SiMe_3)(THF)$ **147-149** (R = Me, Ph, H) and bis-alkyl complexes $(PCp^*)Y(CH_2SiMe_3)_2(THF)$ **150** and $(sCp)Y(CH_2SiMe_3)_2(THF)$ **152** were synthesized by direct protonolysis reactions between $Y(CH_2SiMe_3)_3(THF)_2$ and neutral ligands. When treated with phenylsilane, complex **148** generated the crowded hydride dimer $[(PCp^{Ph})_2Y(\mu\text{-}H)]_2$ **161**.

Complexes **150** and **152** undergo acid-base, metallation, insertion reactions and polymerization of small substrates. A variable temperature ^{1}H NMR study of **150** and **152** at low temperature reveals an equilibrium between **150/152-THF** and **150/152**. The THF-free complexes, **150/152-THF**, appear to undergo inversion of a pyramidal ground state structure to generate a C_{2V} symmetric intermediate. The X-ray structures of **136**, **147**, **150**, **152**, (sCp)Y(CH_2SiMe_3)$_2$(bipy) **154**, **161**, [PCp*Y($CCSiMe_3$)(THF)]$_2$(μ^2-$CCSiMe_3$)$_2$] **167**, acetylide cluster **169** and bis-(Me_3Si)$_2$Cp yttrium chloride dimer **176** were determined and structural features discussed.

Table of Contents

List of Tables

List of Graphs

List of Figures

List of Schemes

List of Abbreviations

bipy	2,2'-bipyridine
COSY	correlation spectroscopy
Cp	cyclopentadienyl
Cp*	pentamethylcyclopentadienyl
DAD	diazadiene
DIBAL	diisobutylaluminium hydride
DME	dimethoxyethane
Flu	fluorenyl
Ind	indenyl
Ln	lanthanoid: Y, La-Lu
MMA	methyl methacrylate
NMR	nuclear magnetic resonance
ppm	parts per million
PTSA	p-toluenesulfonic acid
py	pyridine
TFA	trifluoroacetic acid
THF	tetrahydrofuran
tmeda	N,N,N',N'-tetramethylethylenediamine
VT	variable temperature

List and Code Number of Synthesized Ligands

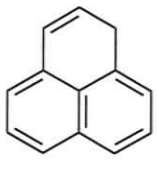

PnH **101**

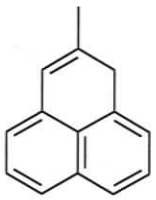

(Pn^{Me})H **102**

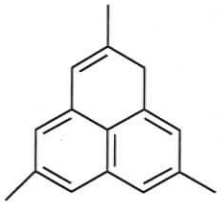

(Pn^{Me})H **103**

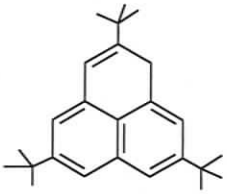

(Pn^{tBu})H **104**

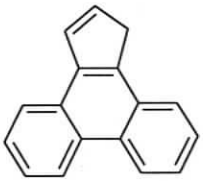

(PCp)H **105**

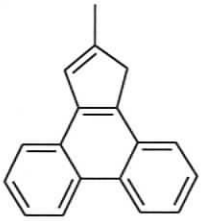

(PCp^{Me})H **106**

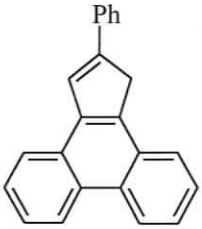

(PCp^{Ph})H **107**

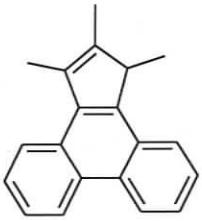

(PCp*)H **108**

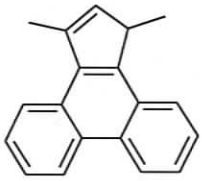

(PCp')H **109**

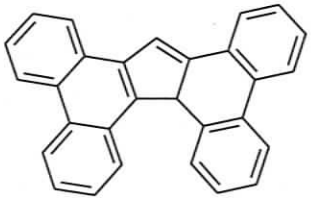

(sCp)H **110**

List and Code Number of Synthesized Complexes

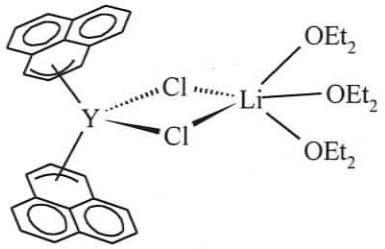

129

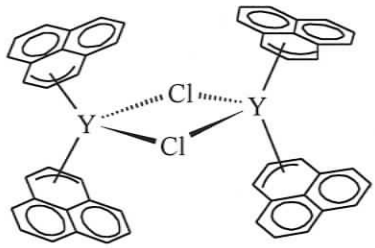

130

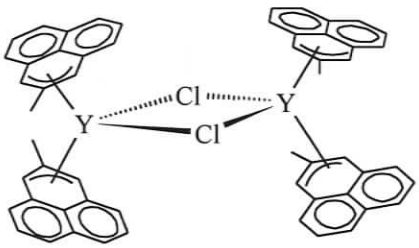

131

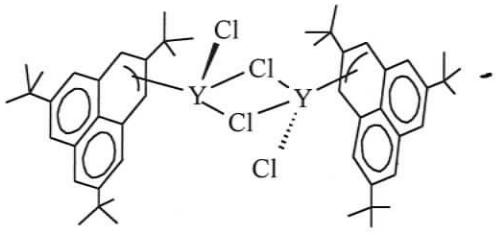

132

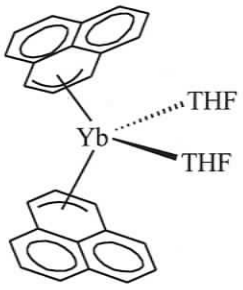

133

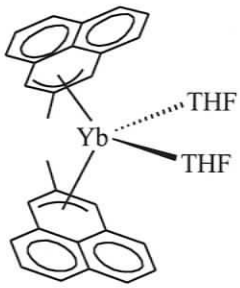

134

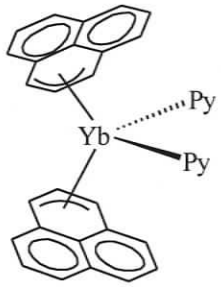

135

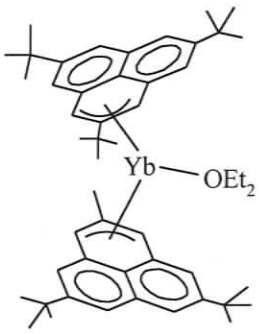

136

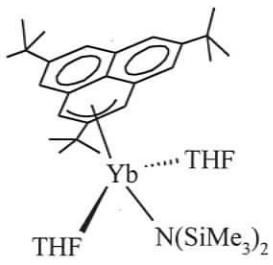

137

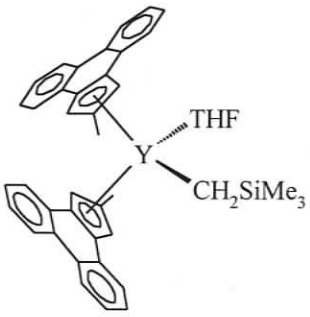

147

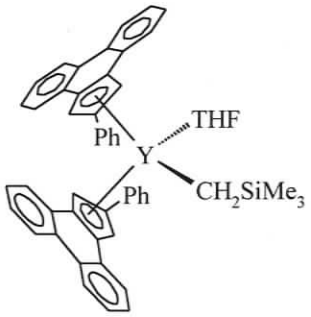

148

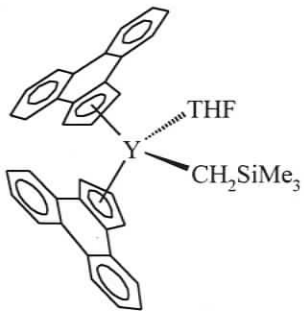

149

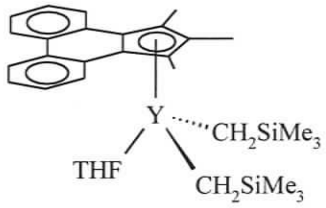

150

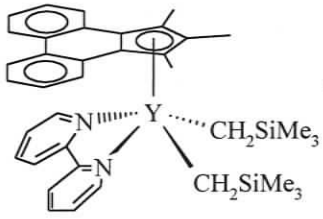

151

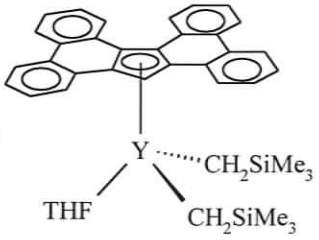

152

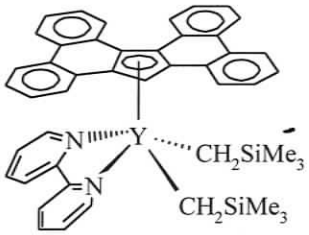

154

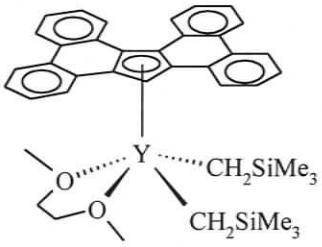

155

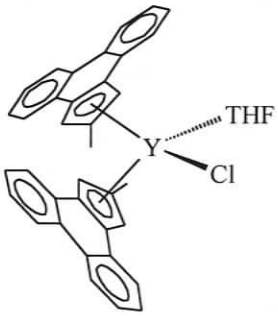

156

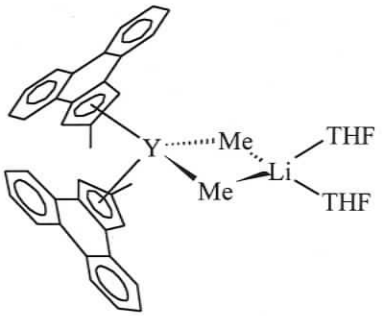

157

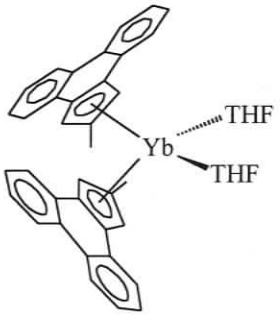

158

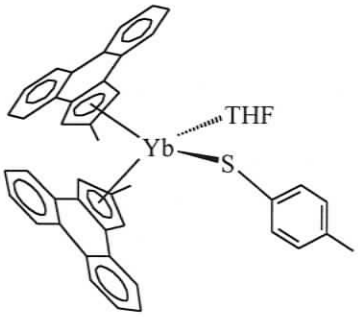

159

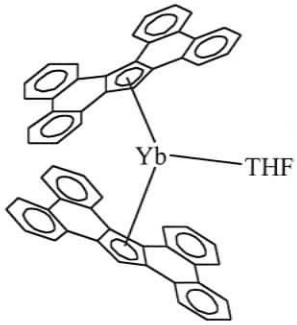

160

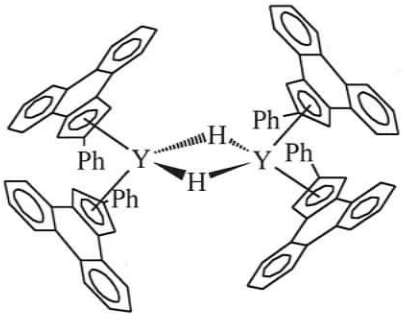

161

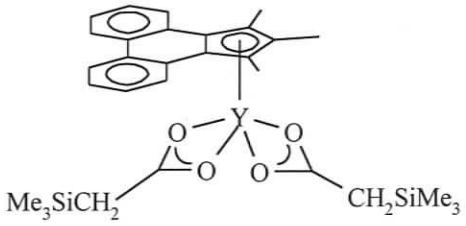

162

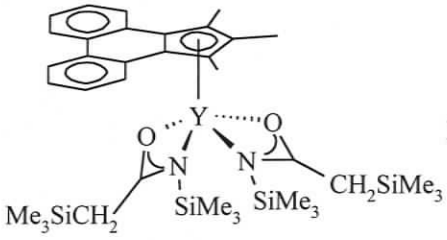

163

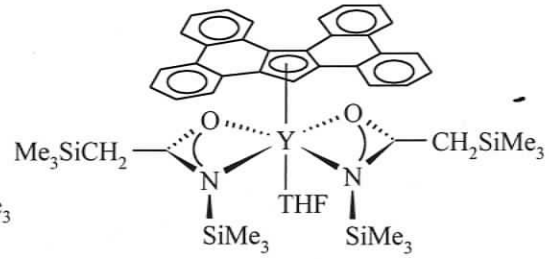

164

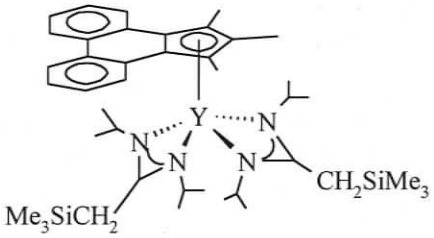

165

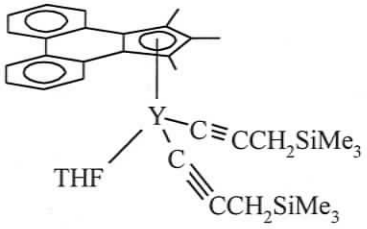

166

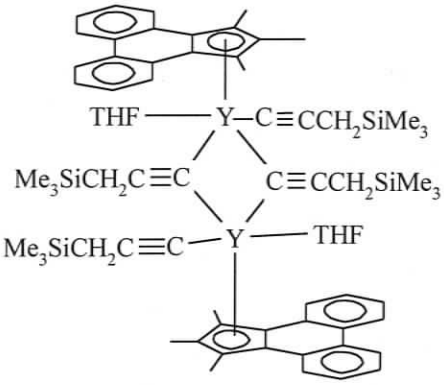

167

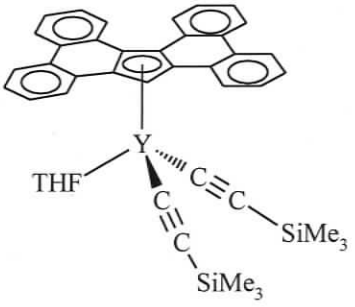

168

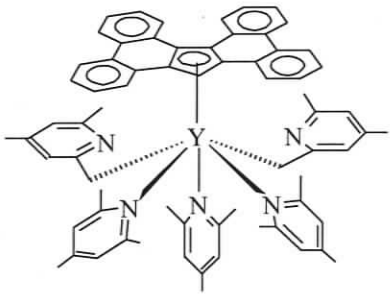

170

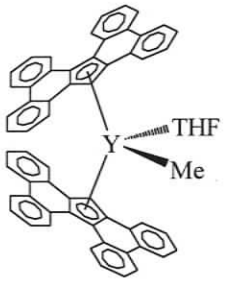

171

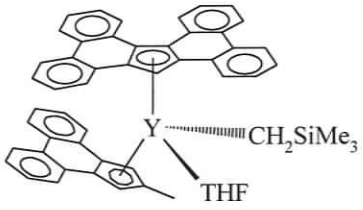

174

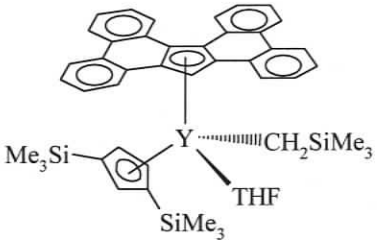

175

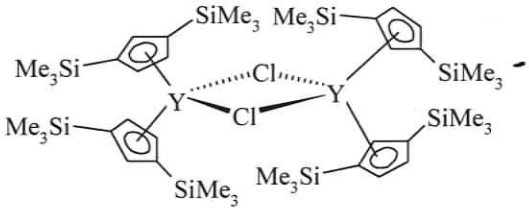

176

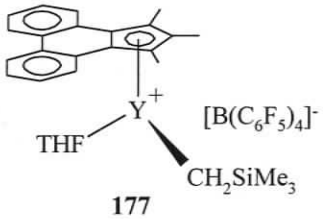

177

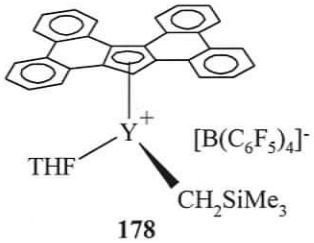

178

Acknowledgements

I would like to thank my supervisor Dr. David J. Berg for his guidance, encouragement and patience during the course of this work. Also, I would like to thank Dr. Paul O'Connor for his help and other members of the Berg group: Dr. Wei Fan, Dr. Chuanjian Zhou, Karen Button, Pengrong Zhang, Jin Zou for their help and cooperation.

I would like to thank Dr. Brendan Twamley for solving all of my crystal structures and Ms. Chris Greenwood for recording many of the NMR spectra for me. Finally, I would like to thank all the staff of the Chemistry Department for their support and help during my graduate study and the department for making UVic a great place to work and learn.

To my wife

who traveled from the other side of the earth to Victoria

to stay with me and to support me

and my parents

who raised me and educated me to be a better person

with their unconditional love

Chapter One. Introduction

1.1 Historical Development

The discovery of ferrocene in 1951 is considered to be the start of organometallic chemistry.[1,2] The use of cyclopentadienyl (Cp) as a ligand was expanded rapidly to other transition metals. Tris(cyclopentadienyl) lanthanide complexes, the first Cp lanthanide complexes, were reported in 1956 by Birmingham and Wilkinson.[3] In the next twenty years, lanthanide chemistry mainly focused on salt metathesis reactions (**Scheme 1.1**) by starting with a lanthanide halide and an alkali salt of the ligand, and modification of the complexes with various groups.[4] Due to the small size of the Cp ligand, the preparation of Cp lanthanide complexes can easily afford "ate" complexes (negatively charged species formed by addition rather than salt elimination, eg. $Na^+[YbCp_3]^-$), especially for early lanthanide metals with larger ionic radii. To resolve the problem of "ate" complexes, two strategies were applied to lanthanide chemistry: increase the ligand bulk and develop acid-base reactions by starting with neutral protic ligands (**Scheme 1.1**).

$$3L^+M^- + LnX_3 \longrightarrow LnL_3 + 3MX$$

$$3LH + LnR_3 \longrightarrow LnL_3 + 3RH$$

L = ligand; Ln = Sc, Y, La-Lu; R = alkyl, amide; M = alkali metal; X = halides

Scheme 1.1. Protonolysis and salt metathesis reactions

As a result of the ionic bonding in lanthanide complexes,[4] the structural configuration adopted is mainly controlled by steric effects, so increasing the ligand

bulk should bring dramatic structural changes and therefore affect chemical reactivity. Pentamethylcyclopentadienyl (Cp*), linked Cp and indenyl were investigated under this assumption and did show some interesting changes as expected.[5-7] To avoid solvation and "ate" complexes completely, lanthanide tris(alkyl) precursors such as $Ln[CH(SiMe_3)_2]_3$ and $Ln(CH_2SiMe_3)_3(THF)_2$ were developed to react with neutral Cp ligands (CpH) to give halide-free complexes.[8,9] Although the development of lanthanide chemistry prior to 1980 was very fundamental, the basic foundation was firmly built during this period.

After 1980, lanthanide Cp chemistry expanded rapidly and developed in two distinctive but correlated directions: (i) synthesis and characterization of novel complexes possessing interesting ligands or properties; and (ii) the development of lanthanide complexes focusing on specific catalytic reactivity. Protonolysis of lanthanide alkyl or amide precursors were developed into an important route for the preparation of lanthanide complexes, while salt metathesis reactions remained viable for some preparative routes. Although bulky amide or diamide lanthanide complexes have attracted growing interest in the last decade, Cp chemistry shows more diversity and remains central to organolanthanide synthesis and reactivity.

1.2 Lanthanide Complexes Bearing Cp Units

The Cp ligand represents the earliest stage of organolanthanide chemistry with numerous papers published based on the parent Cp ligand or simple modifications. Cp* (C_5Me_5) **1**, Cp with bulky substituents **2**, aromatic-fused Cp ligands **3**, Cp with

constrained geometry **4** and linked ansa-Cp **5** and have all been well studied over the last two decades in lanthanide chemistry (**Fig 1.1**). Many complexes possessing unique structures and properties were developed. Although the Cp ligand itself may show a great deal of diversity by different substituents on the Cp ring, lanthanide chemistry with different Cp ligands remains relatively similar to Cp*, so a more detailed discussion of the Cp* ligand system is given in the next section.

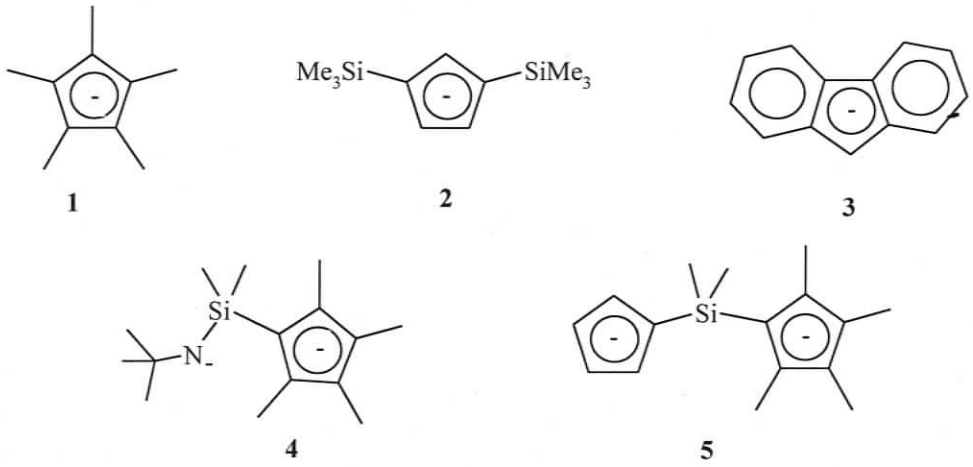

Figure 1.1. Interesting ligands bearing the Cp unit.

1.2.1 Cp* Lanthanide Chemistry

Divalent metallocenes of Sm, Eu and Yb based on the Cp* ligand form a very exciting class of low oxidation state lanthanide complexes (E°_{ox} (vs. SCE): Sm, 1.55V; Yb, 1.15V; Eu, 0.43V).[4] A number of papers report the synthesis of divalent metallocenes by reacting different lanthanide halides with an alkali metal salt of Cp*.[10-14] In addition, reductive routes including metal vapor reactions are unique. Europium, with the most stable divalent oxidation state, forms a divalent metallocene directly in the reaction of $EuCl_3$ with three equivalents of NaCp*.[11] In this case, Cp^{*-}

acts as the reducing agent for Eu(III) and is oxidized to Cp* radical. The metal vapor routes use the lanthanide metals alone as a reducing agent for Cp*H with generation of hydrogen gas and metallocene formation.[12] The coordinating solvent in solvated $Cp^*_2LnL_x$ complexes could sometimes be removed by heating to form Cp^*_2LnL or sublimation to form solvent-free Cp^*_2Ln.[14,17] Stronger electron donors could also replace Et_2O or THF by ligand exchange (**Scheme 1.2**).[15,16]

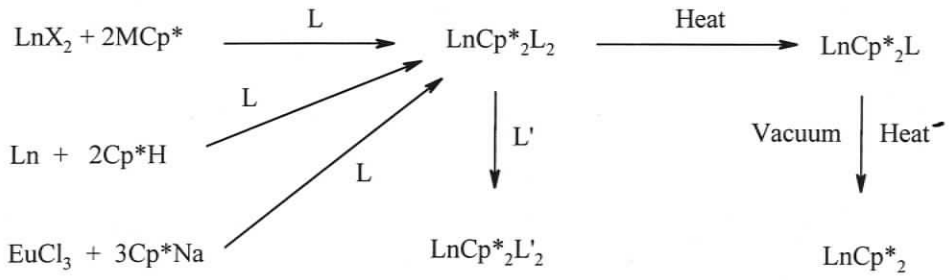

Ln= Sm, Yb, Eu; X= Cl, Br, I; M= Li, Na, K; L= Et_2O, THF; L'= Py

Scheme 1.2. Reaction routes for divalent lanthanide metallocenes

X-ray structural studies on $YbCp^*_2(THF)$ **6** showed a monomeric structure,[11] unlike $Yb(MeCp)_2(THF)$ **7**,[18] which was determined by X-ray to exist as a chain polymer structure. The average Yb-C and Yb-O bonding distances in **6** are both shorter than those in **7**. Thus, the great impact imposed by the bulky Cp* ligand can be seen clearly. Also, X-ray structural studies showed that unsolvated $LnCp^*_2$ (Ln = Sm, **8**; Yb, **9**) adopt bent structures, possibly due to weak van der Waals attractive forces between the ligand Cp* rings.[19,20]

$Cp^*_2Sm(THF)_2$ **10** and unsolvated $SmCp^*_2$ **8** showed extremely high reactivity towards substrates containing multiple bonds, including N_2, various alkenes and large aromatic hydrocarbons. The first lanthanide dinitrogen complexes **11** was obtained by

slow evaporation of $SmCp^*_2$ solution under N_2 and showed unusual dinitrogen side-on coordination to two $SmCp^*_2$ units.[21] The reaction with styrene yields a binuclear Sm(III) complex **12** bonded to a reduced hydrocarbon through η^2:η^4 bonding (**Scheme 1.3**).[22] The presence of a Sm(III) metal center can be seen by the significantly shorter Sm-Cp* (2.4-2.5Å) distances compared with those in Sm(II)-Cp* (2.8Å).[17] Remarkably, this reaction with styrene can be reversed to starting materials with simple addition of THF.[23] Similarly, the reaction with diphenylacetylene generates a Sm(III) metal center and $(PhCCPh)^{2-}$ with an η^2:η^2 bonding mode.

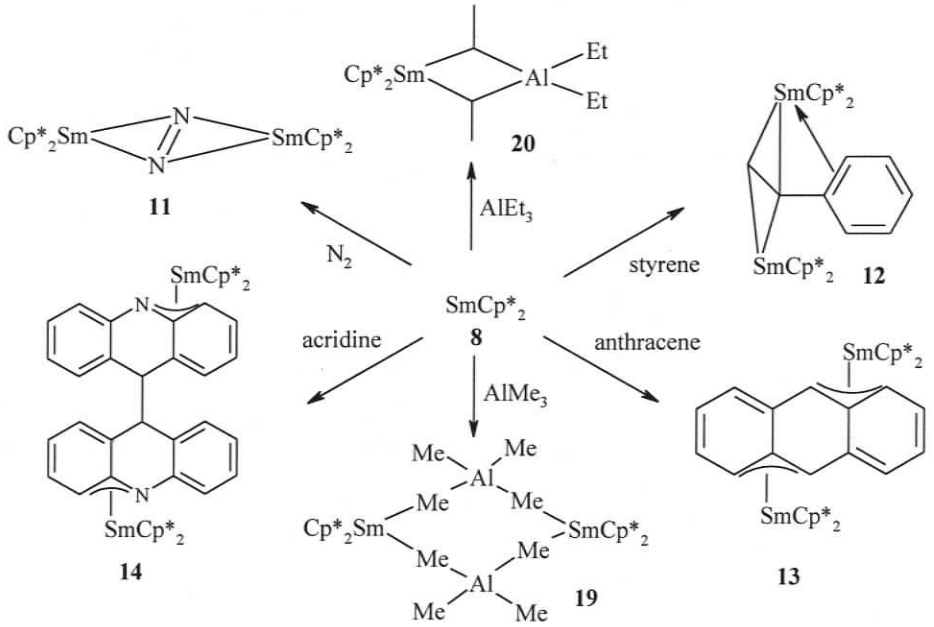

Scheme 1.3. Reactions of $SmCp^*_2$ with various substrates

The reactivity of $SmCp^*_2$ **8** with polycyclic aromatic hydrocarbons was also studied in detail. $SmCp^*_2$ reacted with anthracene or acridine to afford trivalent complexes **13** or **14** in which the Sm(III) metal centers were bonded with the aromatic hydrocarbons through an η^3-allyl or azaallyl unit. Interestingly, reductive dimerization

was observed in the acridine case (**Scheme 1.3**).[24] The dimerization product, with the η^3:η^3 bonding mode, was also found for the reaction between 1,3-butadiene and $SmCp^*_2$ **8**.[25] The reaction with bispyridylethene (pyCH=CHpy) gave two products which could undergo interconversion to each other. Sm(II) reduces pyCH=CHpy to form the radical, which could then either react with another $SmCp^*_2$ to generate $(SmCp^*_2)_2(\mu\text{-}\eta^2\text{:}\eta^2\text{-pyCHCHpy})$ **15** or dimerize to form $(SmCp^*_2)_2[\mu\text{-}\eta^3\text{:}\eta^3\text{-py}_4(CH)_4]$ **16**.[26]

These interesting reactions are all due to the high reducing power of Sm(II) for the Sm(II)/Sm(III) couple. Compared with the divalent samarium metallocenes, the chemistry of $YbCp^*_2$ **9** with π-ligand is not well developed, and no simple alkene adducts were made successfully, except for one stable π-adduct of divalent ytterbium with an electron rich ethylene coordinated to a platinum center.[27,28] In case of alkynes, $YbCp^*_2(\eta^2\text{-MeCCMe})$ showed weak coordination of the alkyne with the Yb center remaining in the divalent oxidation state.[29] The coordination of various heterocyclic nitrogen bases to **9** was also studied and showed various features depending on coordination ability of the bases.[32] Similarly to the Sm analogue,[30] $YbCp^*_2$(bipy) **17** is paramagnetic and contains a bipyridyl radical anion.[31]

Given their high oxidation potentials, divalent Sm and Yb complexes can be oxidized to trivalent complexes by a variety of oxidizing reagents. $LnCp^*_2(THF)_2$ can be oxidized by traces of oxygen, pyridine-N-oxide or N_2O to form $(\mu\text{-O})(LnCp^*_2)_2$ **18**.[33,34] Reductive cleavage of E-E bonds (ie, Ph_2E_2) is an elegant route to prepare trivalent Ln-E (Ln= Yb, Sm; E= S, Se, Te) (ie, $LnCp^*_2EPh$) complexes.[35,36] Cp

lanthanide fluoride can be prepared by oxidation of divalent complex by perfluoroalkenes.[37] Remarkably, **8** can reduce trimethylaluminium to Al metal and form the trivalent cyclic dimer **19** (**Scheme 1.3**, p5).[38] Similarly, reaction with triethylaluminium gave a monomer $Cp^*_2Sm(\mu\text{-}Et)_2AlEt_2$ **20** (**Scheme 1.3**).[39] Similar reaction with $Cp^*_2Yb(THF)$ yields an Yb(II) adduct $Cp^*_2Yb(\mu\text{-}Et)AlEt_2(THF)$ **21** with an interesting μ-Et coordination mode.[40]

Unlike divalent chemistry which is essentially restricted to Sm, Yb and Eu, trivalent chemistry involves all lanthanide metals and has mainly focused on the preparation and reactivity of lanthanide alkyls and hydrides. Cp^*_2LnR itself is catalytically active and behaves as a precursor for a potentially more active lanthanide hydride. A typical procedure for the preparation of lanthanide hydrocarbyls and hydrides starts with bis-Cp* lanthanide halides and the alkali salt of the hydrocarbyl ligand. Once isolated, the lanthanide hydrocarbyl may be reacted with hydrogen gas to generate a lanthanide hydride.

The THF adducts $LnCp^*_2Me(THF)$ (Ln =Sc, Y, Sm, Yb, Lu) are all thermally stable, and can form "ate" complexes $[LnCp^*_2(\mu\text{-}Me)_2]^-Li^+$ in presence of excess organolithium reagents.[41] A monomeric scandium methyl complex can be prepared from $ScCp^*_2Cl$ and MeLi.[42] The larger lanthanides yield dimeric $[Cp^*_2Ln(\mu\text{-}Me)]_2$ (Ln= Y, **22**; Lu, **23**) in a similar reaction.[43,44] Oxidation of divalent metal centers (Yb or Sm) can be used to prepare lanthanide hydrocarbyls, such as $[Cp^*_2Yb(\mu\text{-}Me)]_2$ **24** and $Cp^*_2SmPh(THF)_2$ **25** by oxidation of the appropriate $LnCp^*_2$ with methylcopper or $HgPh_2$, respectively.[38, 45]

The lanthanide methyl complexes mentioned above can afford the corresponding hydrides by hydrogenolysis and they are highly reactive in C-H activation of bezene, pyridine, or $SiMe_4$ by methane elimination (**Scheme 1.4**).[43,44] More remarkably, C-H bonds in $^{13}CH_4$ can be activated by methyl lanthanides possibly through a fulvene lanthanide complex as intermediate. Fulvene complexes have also been shown to form in the thermal decomposition of $LnCp^*_2Me(THF)$.[46,48] CO and CO_2 can readily insert into the Ln-C bond to afford the corresponding acyls and carboxylates, respectively.[47]

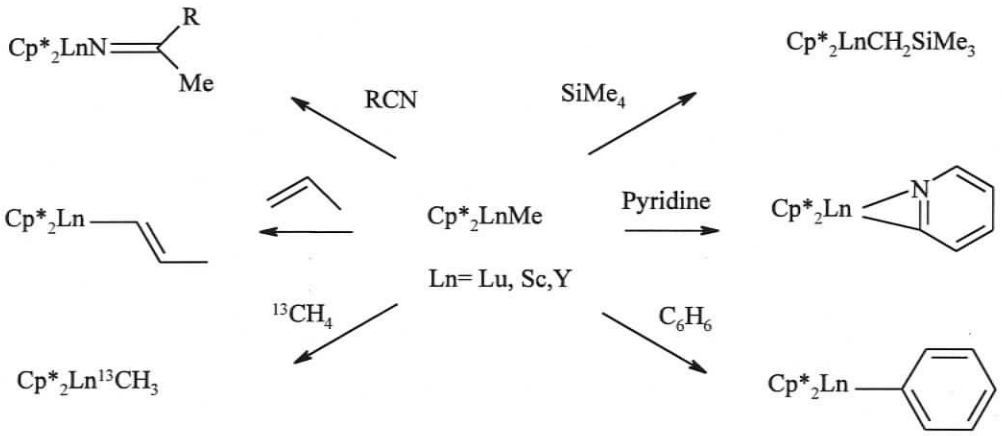

Scheme 1.4. Reactions of Cp^*_2LnMe with various small substrates

Lanthanide bis(trimethylsilyl)methyl, $CH(SiMe_3)_2$, complexes are very important among the hydrocarbyls, because they form solvate free complexes due to the steric effects of the two trimethylsilyl groups. The X-ray structure of $Cp^*_2YCH(TMS)_2$ **26** shows α-C-H--Y and γ-H-C--Y agostic interactions.[49] Similarly, $Cp^*_2LnCH(TMS)_2$ (Ln = Nd, **27**; Ce, **28**) exhibit α-C-H--Ln and β-Me-Si--Ln agostic interactions. The presence of agostic interactions is due to the electronic and

coordinative unsaturation of the metal center, which can be seen clearly from the relatively short Ln--H and Ln--C distances.[50,51]

The reactivity of $Cp^*_2LnCH(TMS)_2$ is quite similar to, but the rate of reaction is somewhat slower than the lanthanide methyl complexes in insertion reactions with nitriles, CO_2, and in the activation of C-H bonds of pyridine or alkynes.[52,53] Lanthanide alkyls show varying reactivity with different ketones. When treated with acetone, the alkyl is able to form aldolates, but enolates form when the alkyl is treated with diethyl ketone. Also, lanthanide alkyls fail to react with di-t-butyl ketone for steric reasons (**Scheme 1.5**).[54] The thermal decomposition of $Cp^*_2LnCH(TMS)_2$ proceeds via a fulvene intermediate, $Cp^*Ln(C_5Me_4CH_2)$, and forms a complex with metal centers bridged by a $CH_2C_5Me_3CH_2$ unit.[55]

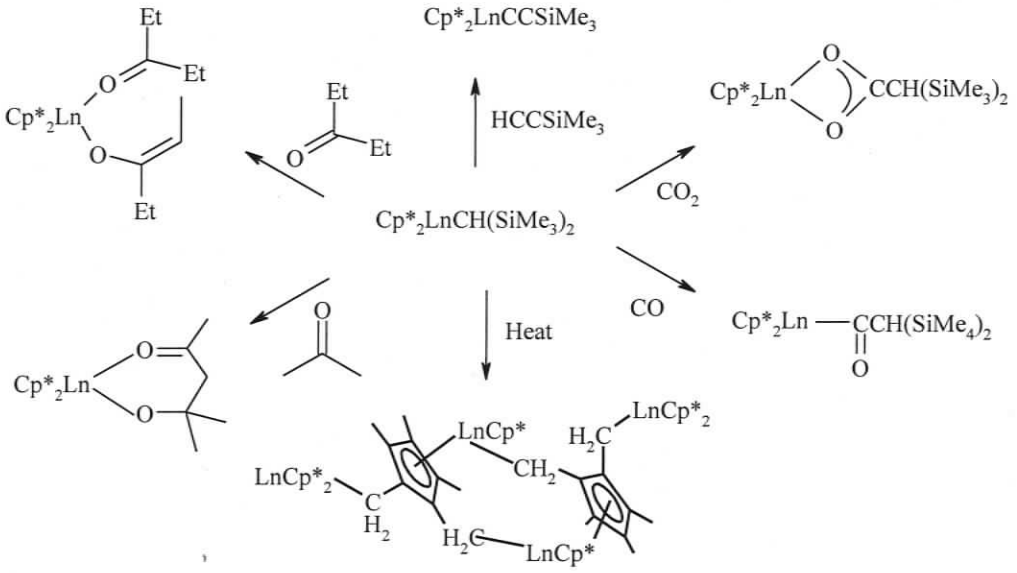

Scheme 1.5. Reactions of $Cp^*_2LnCH(TMS)_2$ with various substrates

The dimeric hydrides $[Cp^*_2Ln(\mu\text{-}H)]_2$ **29** are prepared from corresponding hydrocarbyl by hydrogenation.[15,16,43,51,60,61] Similar to lanthanide hydrocarbyls, thermal decomposition of hydrides lead to formation of fulvene complexes.[62,63] Lanthanide hydrides can activate small molecules such as CO, ethylene, benzene, pyridine, furan and even $SiMe_4$.[43,44,48,64] η-Allyl complexes can be prepared from insertion of allene, or reaction with alkenes, which involves insertion of hydride to alkenes followed by hydrogen abstraction.[48]

Mono-Cp* lanthanide chemistry is not developed as well as bis-Cp* lanthanide complexes, because mono-ring species can normally undergo redistribution (ligand exchange) to form more sterically or electronically saturated complexes. Although characterized by NMR and X-ray crystallography, $Cp^*La[CH(SiMe_3)_2]_2(THF)$ **30** decomposed in two hours to $Cp^*_2LaCH(SiMe_3)_2$ **31**, $CH_2(SiMe_3)_2$ and other products.[56] Surprisingly, THF-free **31** shows higher stability than its THF adduct. Both complexes show two methyne resonances at -90°C, indicating restricted rotation of the trimethylsilyl groups at low temperature.[56] Prepared from $Cp^*Y(OAr)_2$ and $LiCH(SiMe_3)_2$, $Cp^*Y(OAr)CH(SiMe_3)_2$ **32** (Ar = *o*-2,6-di-t-butylC_6H_3) showed high stability and formed the hydride dimer $[Cp^*Y(OAr)\mu\text{-}H]_2$ **33** by hydrogenolysis, which afforded only the single insertion product with terminal alkenes.[57] $Cp^*Lu(CH_2SiMe_3)_2(THF)$ **34** was prepared from direct protonolysis of $Lu(CH_2SiMe_3)_3(THF)_2$ by Cp*H and remained relatively stable, presumably due to smaller radii of Lu(III) compared with other Ln(III).[58] DME and 2,2'-bipyridyl can replace THF easily to form corresponding complexes. $Cp^*Lu(CH_2SiMe_3)_2(bipy)$ **35**

reacts with one or two equivalent of H_2NAr (Ar = 2,6-diisopropylphenyl) to afford the corresponding amide products. Reaction with phenylacetylene can afford a bridged acetylide, in which the bridge can be broken to generate terminal acetylide by simple addition of THF.[58] The outstanding stability of these complexes is due to coordination of the bipy ligand that helps to saturate the metal center. A neutron diffraction study carried out on $Cp^*_2LaCH(SiMe_3)_2$ **31** and $Cp^*Y(OAr)CH(SiMe_3)_2$ **32** revealed that β-Si-C-Y agostic interactions predominate, instead of α-C-H or γ-C-H interactions observed in other systems. This conclusion is based on no enlongation of the corresponding C-H bonds, but significant enlongation of the C-Si bond.[59]

1.2.2 Cp or Cp* Complexes Modified with Bulky Substituents

By adding bulky groups like t-butyl or trimethylsilyl to the Cp or Cp* core, complexes can be prepared in more desirable ways and many possess some particularly unique properties; for example, an ability to avoid "ate" complex formation or to form stable mono-Cp complexes. The majority of this chemistry follows Cp* chemistry, including the preparation and modification of the complexes; however, several distinctive cases below are sufficient to show the important impact imposed by the bulky groups.

Compared with Cp^*_2Yb **9** and $[(1,3\text{-}Me_3Si)_2(C_5Me_3)]_2Yb$ **36**, $[(1,3\text{-}tBu)_2(C_5Me_3)]_2Yb$ **37** is the simplest ytterbocene from a structural perspective. This complex is monomeric in the solid state with no intermolecular interactions between units. However, intramolecular interactions are evident from two short Yb--C

distances of 3.09(1) Å and 3.20(2)Å with methyl carbons on two different t-butyl groups of the same Cp ring. For **9** and **36**, the intermolecular interaction is obvious from the short Yb—Me contact distance between a methyl group on a Cp* or $SiMe_3$ group and the metal center in another unit. Although both t-butyl and trimethylsilyl groups provide extra bulk for the Cp* ring, the significant distance difference between the C-C bond (1.53Å) in a t-butyl group and the Si-C bond (1.88Å) in a $SiMe_3$ fragment results in different interactions for these two compounds. Compared with a C-C bond, the long Si-C bond lengths makes the distance between the metal center and the methyl group relatively longer and this leads to no intramolecular interaction.[65]

$[RMe_2Si(C_5Me_4)]Y(CH_2SiMe_3)_2(THF)$ **38** (R= Me, Ph), prepared successfully by the protonolysis reaction between $Y(CH_2SiMe_3)_3(THF)_2$ and the neutral protic ligand, failed to form any characterizable insertion products or polymerize hexene and styrene. Hydrogenation failed to afford the desirable dihydride complexes, possibly due to scrambling problems.[66] $(2\text{-}FurylMe_2SiC_5Me_4)Y(CH_2SiMe_3)_2(THF)$ **39** reacts with BPh_3 to afford a stable mono-alkyl cationic species. Surprisingly, replacement of 2-furyl with 5-methylfuryl has a huge impact on the chemistry as the bis-alkyl yttrium complex obtained in this case undergoes the furyl-ring-opening and dimerizes by losing one THF molecule.[67]

Compared with lanthanide mono hydride complexes, lanthanide dihydrides are very rare. Early attempts to prepare these complexes through hydrogenolysis with $[RMe_2Si(C_5Me_4)Y(CH_2SiMe_3)_2(THF)$ **38**, $Cp^*Lu(CH_2SiMe_3)_2(THF)$ **34** and

$Cp^*Lu[CH(SiMe_3)_2]_2(THF)$ **40** all failed.[66,68] A series of lanthanide polyhydride clusters have attracted much interest for their uniqueness. When $[Me_3Si(C_5Me_4)]Lu(CH_2SiMe_3)_2(THF)$ **41** is treated with one equivalent of $PhSiH_3$, a hydride dimer $\{[Me_3Si(C_5Me_4)]Lu(CH_2SiMe_3)(THF)(\mu\text{-}H)\}_2$ **42** was formed as a stable intermediate. Treating the intermediate with a further equivalent of $PhSiH_3$ in hexanes afforded the polyhydride cluster $\{[Me_3Si(C_5Me_4)]LuH_2\}_4$.[69] The polyhydride cluster can react with benzonitrile or styrene to afford polynuclear complexes.[70,71]

1.2.3 Aromatic-fused Cp Lanthanide Chemistry

Cp ligands fused to an aromatic system offer potentially more diverse bonding patterns than simple η^5 bonding between the lanthanide metal centers and a Cp unit, since the fused aromatic group may also interact directly with the metal center. In addition, they can provide extra bulk to help avoid "ate" complex formation so frequently observed in single Cp systems. Numerous papers have been published on the basic chemistry of lanthanide indenyl (Ind) **43** and fluorenyl (Flu) **44** complexes, including the preparation of Ind_2Ln, Ind_3Ln, Ind_2LnX, Flu_2Ln, Flu_2LnX (X = halides).[72-78]

The first indenyl yttrium hydride dimer $(2,4,7\text{-}Me_3IndYH)_2$ **45** was prepared by hydrogenolysis of the corresponding $Ind_2YCH(SiMe_3)_2$ **46**. The hydride can behave as a catalyst for dimerization for various α-olefins and can tolerate substituents containing sulfur and oxygen.[79] $Flu_2Yb(THF)_2$ **47** can be prepared by reacting $(C_{10}H_8)_2Yb(THF)_2$ ($C_{10}H_8$ = naphthalene) with the neutral ligand (Flu)H or by a

regular salt metathesis reaction. $Flu_2Yb(THF)_2$ **47** reacts with diazadiene (DAD) tBuN=CH-CH=NtBu to form trivalent ytterbium complexes.[80] Interestingly, the ytterbium metal center remains divalent after $Flu_2Yb(THF)_2$ reacts with ArN=CH-CH=NAr and ArN=CMe-CMe=NAr. Moreover, the reaction undergoes more than simple coordination to form unexpected products. In the ArN=CH-CH=NAr case, the product **48** not only shows an unprecedented coupling between fluorenyl and diazadiene, but also migration of two protons forms an NH-CH_2 unit, and the fluorenyl bonding mode changes from η^5 to η^3 (**Scheme 1.6**). In the ArN=CMe-CMe=NAr case, the fluorenyl anion deprotonates one of the methyl groups of the diazadiene to give (Flu)H and the product possessing η^1: η^1 bonding between the deprotonated diazadiene and the metal center in **49**.[81]

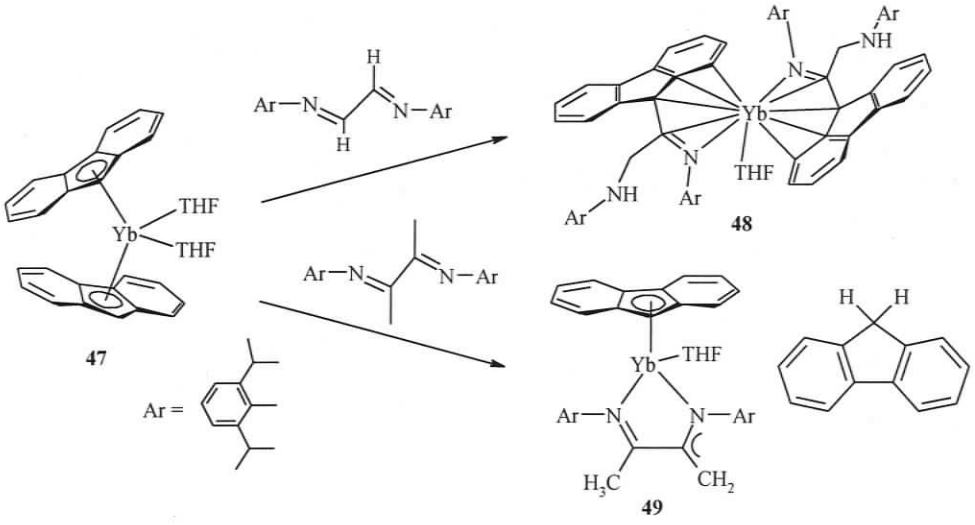

Scheme 1.6. Reactions of $Flu_2Yb(THF)_2$ with diazadiene

When treated with $AlMe_3$ or $AlEt_3$, $(Me_3SiFlu)_2Sm(THF)_2$ **50** undergoes a haptotropic rearrangement to form an η^6-bonded complex **51** in which the Sm center is bonded to the six-membered ring; the reaction can be reversed by addition of THF.

Treatment of $(Me_3SiFlu)_2Yb(THF)_2$ **52** with $AlMe_3$ leads to formation of a complex **53** with both η^6 and η^5 bonding, while addition of THF forms $(Me_3SiFlu)Yb(THF)_4AlMe_4$ **54** (**Scheme 1.7**).[73]

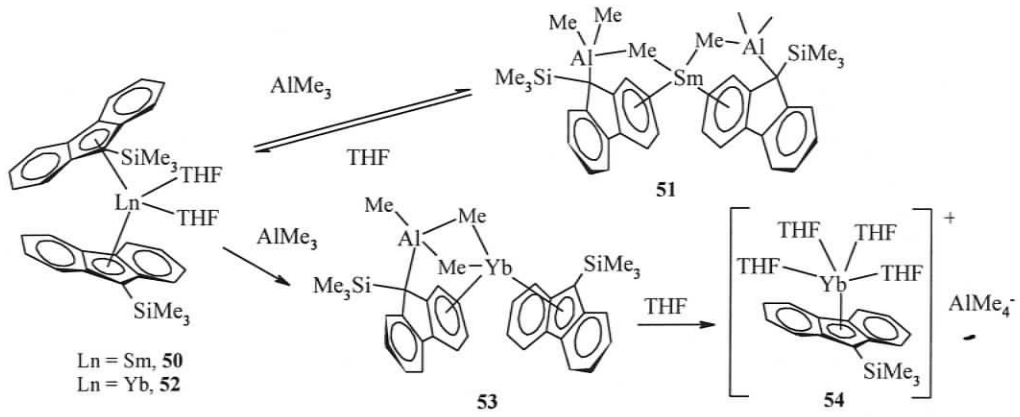

Scheme 1.7. Reactions of $(SiMe_3Flu)_2Ln(THF)_2$ with AlR_3

1.2.4 Mono-Cp or Cp* Ligands with Constrained Geometry

Compared with regular bis-Cp, Cp* and indenyl complexes, donor-linked half metallocenes normally possess sterically and electronically less saturated metal centers and are expected to show more unique reactivity. Although there is only one alkyl or amido group available for functionalization, linked half metallocenes can potentially avoid the scrambling problems by incorporating amido or phosphido bonds. Also, protonolysis reactions are the dominant preparative route for alkyl complexes with these ligands, rather than salt metathesis.

Hydrogenolysis of $[(Me_3CN)Me_2Si(C_5Me_4)]Y(CH_2SiMe_3)(THF)$ **55** afforded the dimeric hydride complex **56**.[66] At 50°C, the ^1H NMR spectrum only shows one triplet for the hydride resonances, indicating fast interconversion between two asymmetrical

isomers. However, at -40°C, two triplets for the hydride resonances are visible with 4:1 ratio as a result of slow interconversion (**Scheme 1.8**).[66] The ytterbium and lutetium hydride dimers were prepared in the same way.[82] The dimeric yttrium hydride complex **56** can not polymerize styrene, but did form a single insertion product **57** and **58** with1-hexene and styrene, respectively (**Scheme 1.8**).

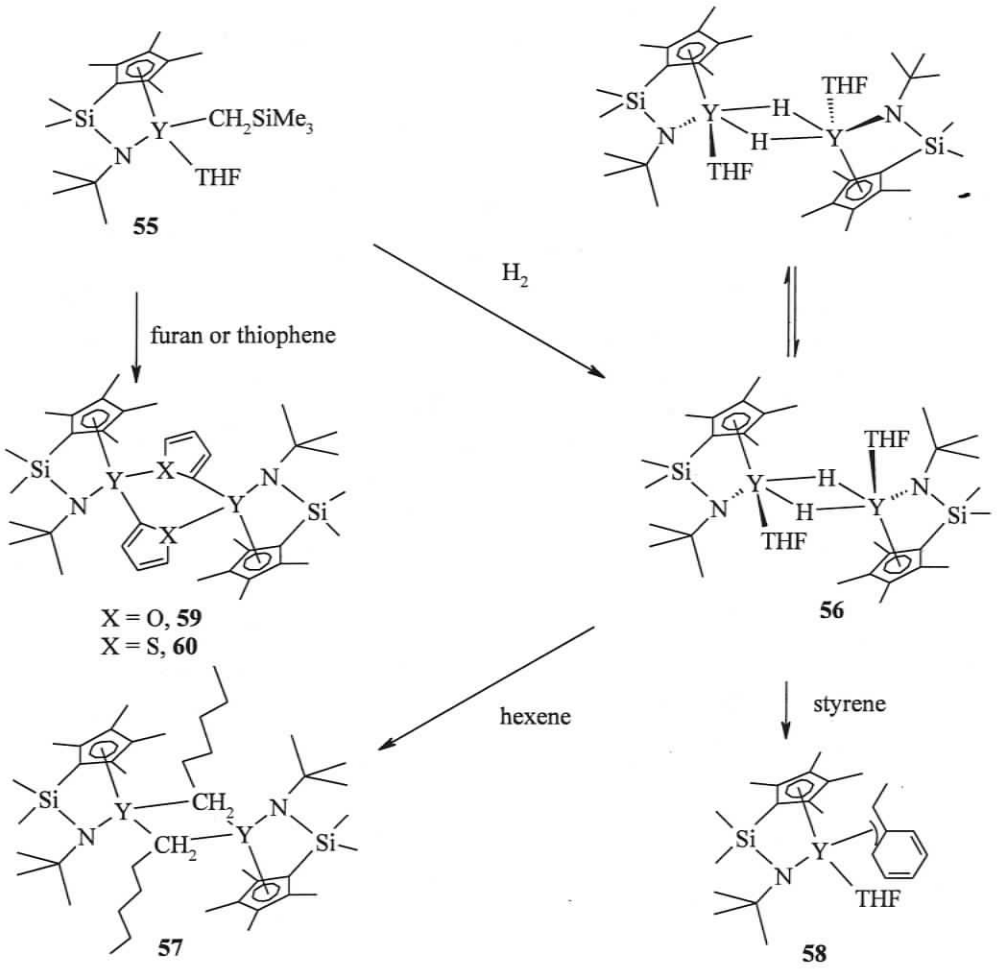

Scheme 1.8. Reactions of lanthanoid half metallocenes

It was first believed that the dimeric insertion product, **57**, initiated the polymerization of styrene due to loss of coordinated THF during the insertion process.[83] However, a more detailed study showed that a THF-solvated monomer,

formed from **57**, initiates the polymerization based on the lability of THF. Neither dimer **57**, nor the styrene insertion product **58** initiates the polymerization, because of the low electrophilicity and fluxionality of the η^3 unit blocking the insertion. The lability of THF is crucial for initiating polymerization because this provides an open coordination site for incoming substrate.[84] The yttrium alkyl complex **55** also reacts with furan and thiophene to afford 2-furyl **59** and 2-thienyl **60** complexes by $SiMe_4$ elimination.[85,86]

$[Me_2NCH_2CH_2NSiMe_2(C_5Me_4)]Y(CH_2SiMe_3)$ **61** (**Fig 1.2**), synthesized by a salt metathesis reaction, reacts with dihydrogen gas to cleanly give a hydride dimer. This hydride dimer also forms a single insertion product with styrene, but fails to polymerize this substrate.[87] $[(Me_3CN)Me_2SiCH_2(C_5Me_4)]Y(CH_2SiMe_3)(THF)$ **62** and $[(Me_3C)NSiMe_2(C_5H_3)CH_2CH_2NMe_2]Sc(CH_2SiMe_3)$ **63** have also been prepared (**Figure 1.2**).[88,89]

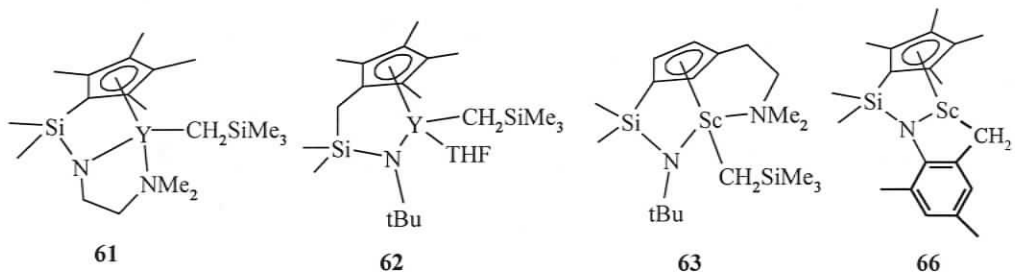

Figure 1.2. Linked amido half metallocenes

The complex $[ArN(Me_2Si)CH_2(C_5Me_4)]Ln(CH_2SiMe_3)(THF)$ (Ln = Yb, Ar = phenyl, **64**; Lu, Ar = 2,4,6-trimethylphenyl, **65**) react with phenylacetylene to give very stable dimeric acetylide complexes, and the bridges remain intact even in the

presence of THF at high temperature.[90] Given their excellent stability, these dimeric alkynide complexes can serve as a unique type of catalyst for dimerization of terminal alkynes. The reaction of the ytterbium complex **64** with $PhSiH_3$ affords the hydride dimer, but the ligand spans over both metal centers. Surprisingly, the reaction of the lutetium complex with $PhSiH_3$ formed a metallation product **66** (**Fig 1.2**, p17) with the ortho-methyl group via σ-bond metathesis with the Lu-H bond. [90]

Phosphido-linked half metallocenes also show some unique features. Compared with amido complexes, phosphido alkyls $[(\mu\text{-PPh})Me_2Si(C_5Me_4)Ln(CH_2SiMe_3)]_2$ (Ln = Y, **67**; Yb, **68**; Lu, **69**) and $[(\mu\text{-PR})Me_2Si(C_5Me_4)Ln(CH_2SiMe_3)]_2$ (R = cyclohexyl, Ln = Y, **70**; Yb, **71**) were formed as dimers by protonolysis reactions from lanthanide tri-alkyl precursors and neutral ligands (**Fig 1.3**).[91] Salt metathesis reactions, known to break the Si-P bond, are not suitable for the preparation of phosphido alkyls. Complexes **67**, **68** and **69** react with $PhSiH_3$ to give a hydride dimer with two metal centers bonded with two hydride ions and one phosphorus. A tetranuclear hydride complex was obtained when treating complex **70** with $PhSiH_3$. Formed as a bisalkyl complex, $[(ArP\boldsymbol{H})Me_2Si(C_5M_4)]Y(CH_2SiMe_3)_2(THF)$ **72** (Ar = 2,4,6-$tBu_3C_6H_2$) still possesses one active P*H* proton due to the extremely crowded Ar group. However, generation of a hydride by reaction with $PhSiH_3$ enables the active P-H bond to react with one alkyl group resulting in a hydride dimer.[91]

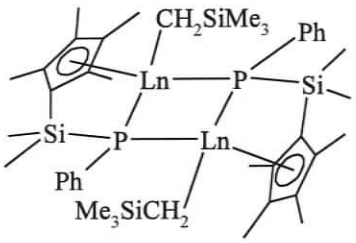

Ln = Y, **67**; Yb, **68**; Lu, **69**

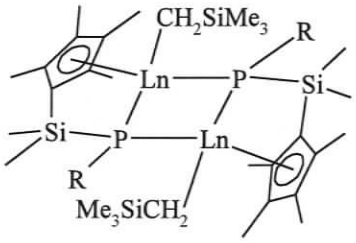

R = cyclohexyl

Ln = Y, **70**; Yb, **71**

Figure 1.3. Structures of phosphido-linked half metallocenes

$\{[(2,6\text{-}tBu_2Flu)SiMe_2N(CMe_3)]Y(\mu\text{-}H)\}_2$ **73,** prepared by treatment of the corresponding hydrocarbyl with $PhSiH_3$, undergoes 1,4-insertion with pyridine, rather than ordinary metallation, to afford $(\eta^5{:}\eta^1\text{-}2,6\text{-}tBu_2FluSiMe_2NCMe_3)Y(NC_5H_6)py_2$ **74** (**Fig 1.4**). It is surprising to find that the insertion product shows an η^5 bonding mode between the fluorenyl ligand and metal center in **74**, compared with the η^3 bonding in the hydrocarbyl complex. Because pyridine is a stronger base, reduced hapaticity was expected for the insertion product **74** with two pyridine molecules coordinated to the metal center.[92,93]

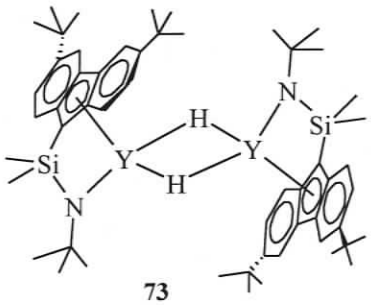

73

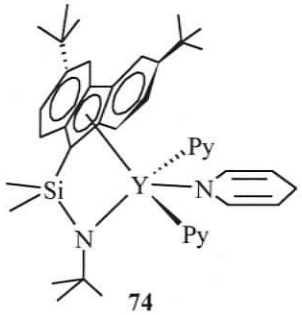

74

Figure 1.4. Structures of fluorenyl half-metallocenes

1.2.5 Ansa-metallocenes

The early motivation to prepare linked Cp lanthanide complexes was to avoid serious bridging problems encountered with simple Cp as ligand. It was also found that the ansa-bridge makes the metal coordination sphere more open and accessible for substrates to attack, thus increasing the catalytic activity. The linked ligand can be prepared from Cp, Cp*, indenyl or fluorenyl ligands. Subtle changes such as varying the length of the linker or the functional groups on the Cp ring can result in dramatic changes in the chemistry of the derived lanthanide complexes. Among the numerous ligands reported, linked ligands with silicon chains are the dominant ones and most easily accessible for preparation of lanthanide alkyls or hydrides.

$[Me_2Si(C_5Me_4)_2LnH]_2$ (Ln = Nd, **75**; Sm, **76**; Lu, **77**), prepared by hydrogenolysis of the corresponding hydrocarbyls, can polymerize ethylene, and oligomerize propene or 1-hexene.[94] Compared with regular Cp* lanthanide complexes, the more open metal sphere can be seen by the smaller Cp*-Ln-Cp* angle, indicating a larger wedge angle between the two Cp* ligands in these ansa-metallocenes. The reactivity for polymerization of alkenes was measured to be 10 times that of $[Cp^*_2Ln(\mu\text{-}H)]_2$, which is obvious proof for the profound effect of the bridged ligand.

Lanthanide hydrocarbyls $Me_2Si(C_5H_4)(C_5Me_4)LuCH(SiMe_3)_2$ **78** were prepared by salt metathesis reactions. These alkyls can initiate ethylene polymerization and afford dihydride complexes $[Me_2Si(C_5H_4)(C_5Me_4)Lu(\mu\text{-}H)]_2$ **79** by hydrogenolysis. The lutetium hydride reacts slowly and reversibly with ethylene to form a single insertion product $[Me_2Si(C_5H_4)(C_5Me_4)Lu]_2(\mu\text{-}H)(\mu\text{-}CH_2CH_3)]$ **80**, which is inactive

for alkene polymerization. (**Scheme 1.9**) The reversibility can be seen from the broadening, coalescence and sharpening of the diasterotopic methylene resonanaces by VT NMR as the temperature is raised from -45°C to 75°C.[95]

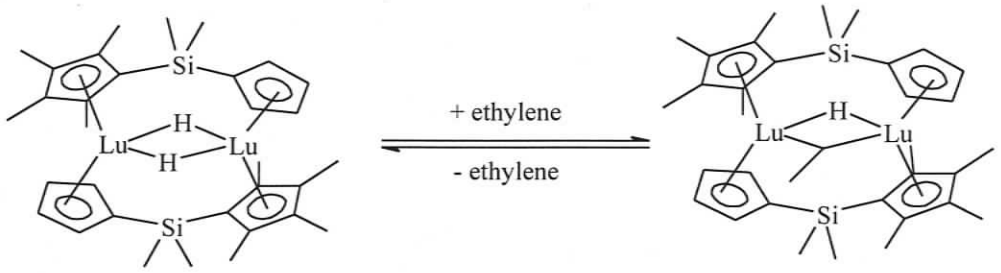

79 **80**

Scheme 1.9. Equilibrium of ethylene insertion

A homochiral hydride dimer [rac-$Me_2Si(2\text{-}SiMe_3\text{-}4\text{-}tBu\text{-}C_5H_2)_2YH]_2$ **81** with D_2 symmetry was synthesized from the corresponding hydrocarbyl, and showed a remarkably high degree of isotacticity for polymer formed from 1-butene, 1-pentene or 1-hexene.[96] As an extension of this work, a more complicated ligand system was developed to synthesize an enantiopure yttrocene. It was found that the lanthanide hydride complexes dimerize immediately after hydrogenolysis of enantiopure lanthanide hydrocarbyl leading to formation of a 1:1 ratio of two isomers: heterochiral isomer (R,S)-(BnBp)Y(μ-H)$_2$-(S,R)-(BnBp) **83** and homochiral isomer (R,S)-(BnBp)Y(μ-H)$_2$-(R,S)-(BnBp) **84** [BnBp = $(OC_{10}H_6C_{10}H_6O)Si(2\text{-}Me_3Si\text{-}4\text{-}Me_3C\text{-}C_5H_2)_2$], of which the heterochiral one is thermodynamically disfavored due to the repulsion between the bulky tBu groups (**Scheme 1.10**). The heterochiral isomer **83** can undergo rearrangement to the thermodynamically favored homochiral **84**. Hydride dimer **81** was also found to be formed in the same way from meso-isomer **82**. The

transformation process was monitored by the changes with two hydride triplet resonances of the two isomers.[97] The insertion of alkene into the Y-H bond of **81** favors the transition state with minimum steric interaction between the ligand (especially bulky groups) and substrate; despite this, the product shows low levels of enantiomeric preference.[98]

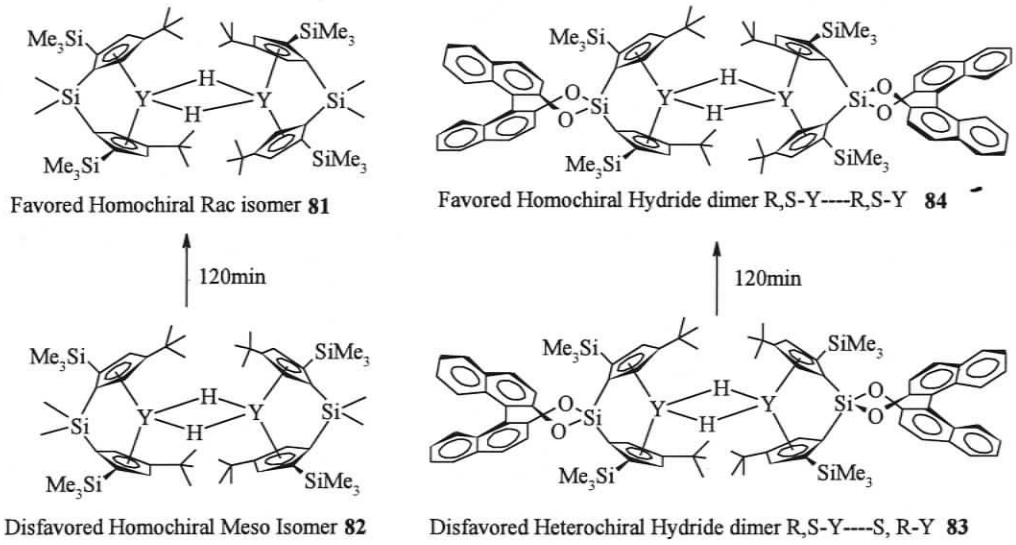

Scheme 1.10. Transformation of hydride dimer isomers

In contrast to the normal preparation of ansa-metallocenes by salt metathesis reactions, aromatic fused ansa-metallocene **85** rac-[{Me_2Si(2-Me-$C_{14}H_{10})_2$}Ln{$N(SiHMe_2)_2$}] and **86** rac-[{Me_2Si(2-Me-$C_9H_5)_2$}Ln{$N(SiHMe_2)_2$}] were prepared by protonolysis reactions starting with neutral protic ligands and $Ln[N(Si\boldsymbol{H}Me_2)_2]_3(THF)_2$. This method takes advantage of the ability of the less bulky $N(Si\boldsymbol{H}Me_2)_2$ to react more quickly and completely with some neutral ligands compared with the more bulky $N(SiMe_3)_2$ group. The new ansa-metallocenes possess a strong Si-H-Ln interaction which remains intact in the temperature range of -90°C to

130°C. (**Fig 1.5**) The strong bond can be observed clearly in the crystal structure by an elongated Si-H bond.[99] Unlike regular hydrogenolysis of lanthanide hydrocarbyls to afford lanthanide hydrides, the lanthanide hydride rac-[{Me_2Si(2-Me-C_9H_5)$_2$}Ln(μ-H)]$_2$ **87** could also be prepared by treatment of lanthanide silylamide precursor **86** with DIBAL at ambient temperature.[100] The mechanism involves the coordination of DIBAL to the metal center, followed by elimination of tBu_2Al N($SiHMe_2$)$_2$ to form the hydride dimer.

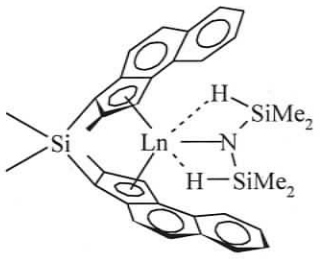

85

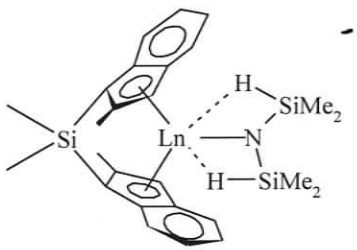

86

Figure 1.5. Strong Si-H-Ln bonds in ansa-metallocenes

The fluorenyl group can also be applied in ansa-metallocene chemistry. Lanthanide silylamides complexes with fluorenyl-linked ligands **88** and **89** were synthesized by salt metathesis reactions and show reactivity for methyl methacrylate (MMA) polymerization.[101,102] By applying different bulky groups on the Cp ring, ansa-metallocenes **90-95** with various linked ligands could be generated that show some interesting features (**Fig 1.6**).[103-109] Particularly, lanthanide complexes binding a chiral ligand **96**, containing a (+)-neomenthyl group on the Cp ring, show relatively high stereoselectivity for hydrogenation and hydrosilylation reactions.[110-112]

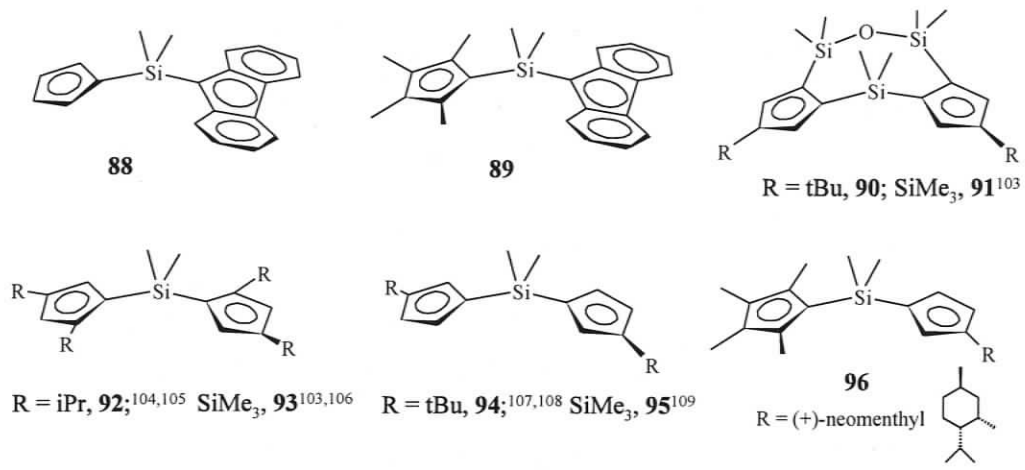

Figure 1.6. Various types of ansa-metallocenes

1.3 Homogeneous Catalysis

With a d^0 electron configuration, lanthanide metal centers are highly electrophilic and exhibit with a more ionic rather than covalent nature; consequently, the structural configuration mainly depends on the steric effects of the ligand, which contributes to the unique reactivity of lanthanide complexes. The key step for homogenous catalysis is the insertion of multiple bonds into lanthanide alkyl, amide or hydride bonds. Mostly, the insertion step is extremely exothermic and irreversible. For some substrates, the insertion product can also undergo further insertion to polymerize the substrates, or undergo self-insertion to produce cyclic products.

1.3.1 Polymerization

Polymerization of olefins, such as ethylene and styrene, is the general method to test the catalytic activity of the lanthanide hydrocarbyl or hydride complexes. The olefin polymer propagation proceeds via continuous addition of olefins and

termination by β-hydride or β-alkyl elimination. Polar substrates such as MMA can also be easily polymerized by lanthanide complexes, such as $[Cp^*_2Sm(\mu\text{-}H)]_2$ **29** and even divalent complexes $Cp^*_2Sm(THF)_2$ **10** and $Cp^*_2Yb(THF)_2$ **6**.[113] The catalytic activity was found to decrease with the increasing bulk for divalent yttrium complexes (Cp > MeCp > Cp*).[114] Ring opening polymerization of lactones is of great interest for generating biodegradable polyesters and can be achieved even with lanthanide halides.[115] The cation alkyl species generated from bis-alkyl complex and $[Ph_3C]^+[B(C_6F_5)_4]^-$ can also show reactivity towards olefin polymerization.[116]

Trivalent lanthanide complexes normally cannot act as homogenous catalysts to initiate the polymerization of 1,3-butadiene because they can form a stable η^3 allyl complex with this substrate. However, it was found that lanthanide metallocenes $Cp^*_2Ln[(\mu\text{-}Me)AlMe_2(\mu\text{-}Me)]_2Cp^*_2Ln$ **97** with $[Ph_3C]^+[B(C_6F_5)_4]^-$ or co-catalyst AlR_3 can initiate the polymerization of 1,3-butadiene to give polymer with 1,4-trans or cis microstructure depending on the R group.[117] For the ring opening polymerization of lactones, it was found that $Cp^*_2LnMe(THF)$ (Ln = Yb, Sm) initiates the living polymerization of lactones such as ε-caprolactone and δ-valerolactone to give polymer with high molecular weight and narrow polydispersity (**Eq 1.1**). But $Cp^*_2LnMe(THF)$ can form a stable six-membered ring complex with β-propiolactone (**Eq 1.2**), and as a result, it cannot initiate the ring-opening polymerization of this substrate. In contrast to lanthanide alkyls, Cp* lanthanide alkoxides show good catalytic activity for polymerization of all three lactones.[118] Co-

polymerization of 1-olefins with polar monomers such as ε-caprolactone and MMA was also carried out with linked lanthanide hydrides as catalyst.[119]

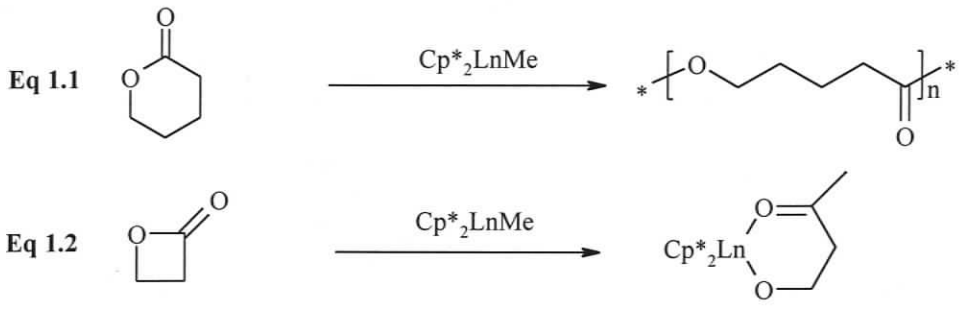

1.3.2 Hydrogenation

The hydrogenation process involves σ-bond metathesis to generate lanthanide hydrides. Olefin insertion into the Ln-H bond is exothermic and normally irreversible.[120-122] The last step is σ-bond metathesis with hydrogen gas to regenerate lanthanide hydride and to release the final hydrogenation product. The reaction rate is proportional to the concentration of lanthanide catalyst and pressure of hydrogen gas, indicating a rapid Ln-H/olefin insertion and rate limiting σ-bond metathesis between lanthanide hydrocarbyl and hydrogen gas in the last step (**Scheme 1.11**).[123]

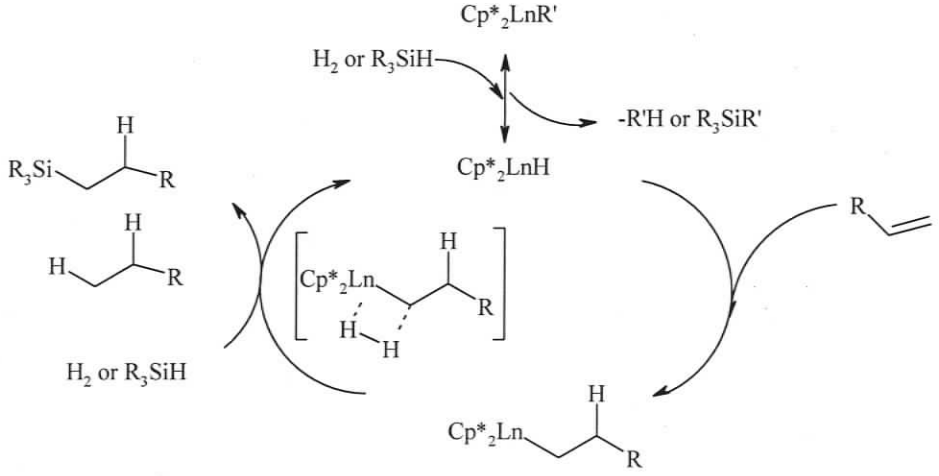

Scheme 1.11. Catalytic cycle for hydrogenation and hydrosilylation reactions

$Cp^*_2YMe(THF)$ shows similar reactivity towards the hydrogenation of mono-substituted alkenes, 1,2-disubstituted or 1,1-disubstituted alkenes and also shows impressive selectivity for the double bonds of dienes containing oxygen, possibly because a stable chelate can be formed with coordination of oxygen that inhibits the catalytic process (**Eq 1.3**).[124] The catalysts $Cp^*_2LnCH(SiMe_3)_2$ show high regioselectivity in avoiding bulky groups and the size effects decrease dramatically with longer distance between the double bond and the bulky substituents.[125]

Eq 1.3

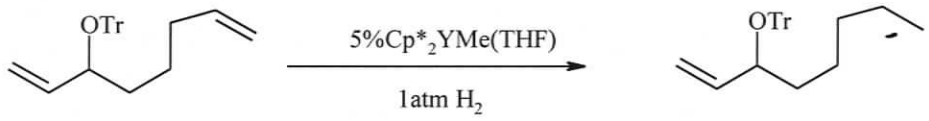

1.3.3 Hydrosilylation

Hydrosilylation provides a very easy and economical way to prepare hydrosilanes, which can be transformed into the corresponding alcohols by oxidation reactions.[126,127] Similarly to hydrogenation reactions, hydrosilylation processes involve generation of a lanthanide hydride, insertion of alkene or alkyne, followed by slow rate-determinating σ-bond metathesis to afford the hydrosilylation product and regenerate the catalyst (**Scheme 1.11**). [123, 128]

Compared with hydrogenation, hydrosilylation of alkenes required prolonged reaction time at temperatures of about 80 °C.[129,130] The use of linked ligands such as $Me_2SiCp^*_2$ and larger lanthanide metal centers results in the formation of more branched organosilanes for 1-decene, compared with $Cp^*_2LnCH(SiMe_3)_2$ (Ln = Yb, Lu) complexes that afford almost 100% of terminal organosilanes.[128,131] Among various lanthanide hydrocarbyls, $Cp^*_2YCH(SiMe_3)_2$ shows relatively high efficiency

and selectivity for the synthesis of hydrosilanes, as well as the tolerance for halide, ether and acetal functional groups.[132] Despite being less effective for hindered alkenes, hydrosilylation with $Cp^*_2YCH(SiMe_3)_2$ shows high selectivity toward dienes with different subsititution patterns, such as selective and complete hydrosilylation of terminal alkenes over untouched disubstituted alkenes (**Eq 1.4**).[132] By simply using Sm, which has a larger ionic radius, $Cp^*_2SmCH(SiMe_3)_2$ can catalyze hydrosilylation of highly substituted alkenes.[125]

Eq 1.4

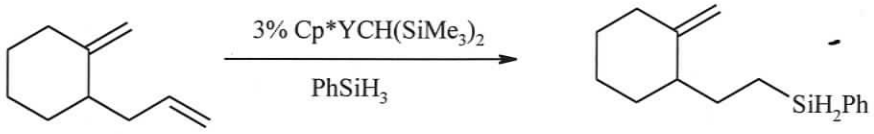

Although terminal alkynes were able to form metallation products with lanthanide hydrocarbyls or hydrides via an acid-base reaction, internal alkynes can undergo hydrosilylation to give corresponding organosilanes. For linear alkynes, two hydrosilylation products can be obtained with relatively low regioselectivity. For unsymmetrical alkynes with bulky groups at one side, lanthanide hydrocarbyls show high regioselectivity.[133]

1.3.4 Hydroamination

Since new carbon-nitrogen bonds can be generated by insertion of alkenes or alkynes into lanthanide amide complexes,[134] hydroamination of aminoalkenes can provide a very powerful way to generate nitrogen containing heterocycles. A lanthanide amide complex is generated by protonolysis of a lanthanide hydrocarbyl

with an amine, and the resulting amide then undergoes intramolecular insertion of the alkene function into the Ln-N bond to form the heterocycle after protonolysis by an incoming amine (**Scheme 1.12**).

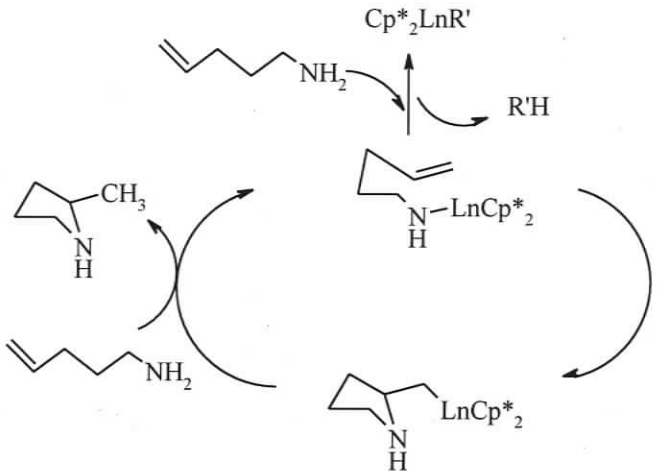

Scheme 1.12. Catalytic cycle for hydroamination reactions

Transformation of aminoalkenes to five, six and seven-membered ring heterocycles by $Cp^*_2LaCH(SiMe_3)_2$ gives impressively high yields (**Eq 1.5**).[135] A more powerful catalyst $[(Me_3SiCp)_2Ln(\mu\text{-}Me)]_2$ enhances the reactivity to a higher level by hydroamination of various 1,1-disubstituted alkenes, such as formation of monocyclic amines, fused bicyclic systems and bridged bicyclic systems.[136] This type of catalyst also shows high reactivity for double hydroamination to form fused heterocycles.

Similar to hydroamination of alkenes, hydroamination of aminoalkynes by $Cp^*_2SmCH(SiMe_3)_2$ is capable of forming five, six, or seven-membered heterocycles, despite the greater acidity of the terminal alkyne protons relative to the primary amine(**Eq 1.6**). This is because coordination of the amine to the lanthanide metal

facilitates the deprotonation of the amine group by lowering the amine N-H pKa.[137] Sequential bicyclization of polyunsaturated molecules can also be achieved by hydroamination and cyclization for some suitable substrates. This process provides a valuable strategy to afford bi-heterocycles.[138] Besides alkenes and alkynes, allenes can also undergo intramolecular hydroamination to form heterocycles and prefer to form six-membered rings over seven- and five-membered rings.[139] Intermolecular hydroamination can also proceed, but the rate is much slower than intramolecular hydroamination.[140]

Eq 1.5

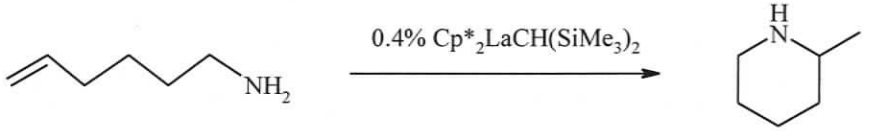

Eq 1.6

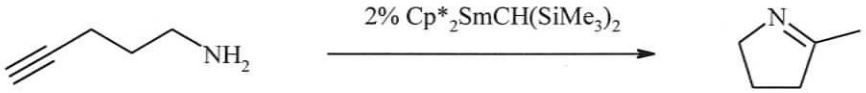

1.3.5 Cyclization

Based on the polymerization of olefins by lanthanide complexes, polyunsaturated systems are expected to undergo cyclization to form cyclic molecules. The most important requirement for cyclization is that the rate of cyclization should be more rapid than termination; in other words, intramolecular insertion should be faster than β-hydride elimination or σ-bond metathesis in the last step. Otherwise, the insertion product would be transformed into hydrogenation or hydrosilylation products.

The cyclization can be terminated by β-hydride elimination, hydrogen gas or organosilanes. Termination by organosilanes was studied in great detail because of the

ease of transforming silanes into other functional groups. Intermolecular insertion between lanthanide complexes and substrate diene shows selectivity for less substituted multiple bonds over more hindered ones (**Eq 1.7**).[141] For hydrogenation termination, direct hydrogenation of double bonds is very common, especially for rigid carbon chains, which makes it difficult to form the transition state for intramolecular insertion.[142] In contrast, substrates without a rigid structure can undergo cyclization quantitatively.[143]

Eq 1.7

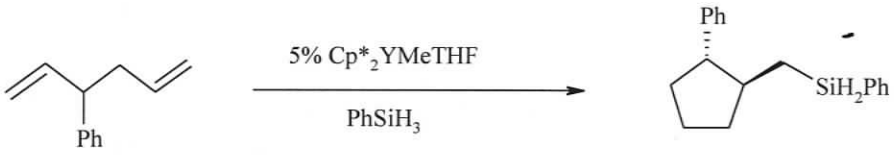

1.4 Scope of Our Work

The evolution of Cp, Cp* and ansa-metallocene complexes clearly shows that progress in lanthanide chemistry has been greatly stimulated by problems encountered in ligand design. Because of the small size of the simple Cp ligand, lanthanide complexes based on simple Cp can form "ate" complexes readily that have very low solubility in hydrocarbons and are difficult to purify. The use of Cp* as ligand clearly enhances the solubility of lanthanide complexes and avoids the formation of "ate" complexes to some extent. Therefore, Cp* lanthanide chemistry expanded rapidly and showed good reactivity towards small substrates. However, bis-Cp* lanthanide complexes possess a larger Cp*-Ln-Cp* angle compared with bis-Cp complexes, indicating a smaller wedge angle for complexes bearing the Cp* ligand. This means the metal centers are less open for small substrate attack, due to the bulk of the methyl

group and the smaller wedge angle between the two Cp* ligands. Ansa-Cp ligand systems in lanthanide chemistry can open up the metal center by use of a short chain to link the two Cp ligands, and this results in increased reactivity towards polymerization of alkenes. A more open metal center can also be achieved by the use of Cp or Cp* ligands with constrained geometry (**Fig 1.7**). With only one Cp or Cp* ligand bonded to the metal center, half metallocene complexes possess a much more open metal center than other ligands in this general family. The chain with electron donor chelate and bulky groups such as t-butyl and $SiMe_3$ can help saturate the metal centers sterically and electronically.

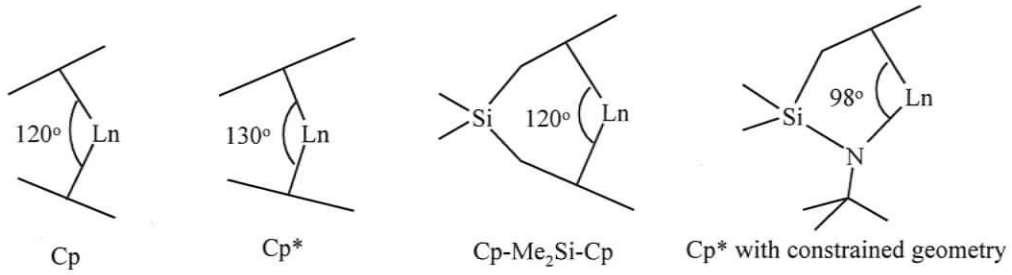

Figure 1.7. Bend angles of various ligands

One major problem encountered in lanthanide chemistry is the tendency to form bridging interactions, especially for lanthanide hydrides; this makes the reactivity decrease dramatically and can possibly lead to redistribution of the ligand. The bulk size of Cp* ligand was proven to be insufficient in prohibiting bridging interactions in many cases. With more open metal centers, ansa-metallocenes still allow the formation of bridging interactions, even with extra bulky groups such as t-butyl or $SiMe_3$. This bridging tendency is so great that the ligand itself often spans two lanthanide metal centers. In this case, the Cp-Me_2Si-Cp unit was bent nearly flat to

adjust the hydride bridges between two metal centers in **87** and **98**, indicating that regular Cp-Me_2Si-Cp is not rigid enough to hold the wedge structure (**Fig 1.8**). This is also true for half metallocenes with constrained geometry as they have even more open metal centers.

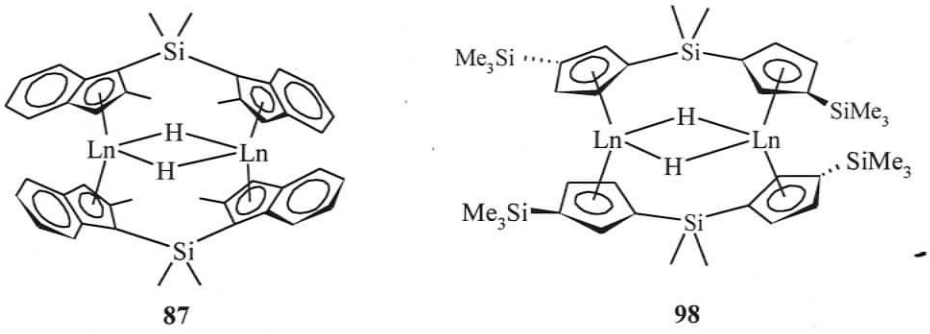

87 **98**

Figure 1.8. Structure of hydride dimers for ansa-metallocenes

Although numerous interesting complexes were obtained from ligands with bulky groups such as t-butyl, $SiMe_3$ and ^{i}Pr, these groups failed to block the bridging interaction. Moreover, these groups can rotate freely and reach into the wedge area between the two Cp units. Consequently, the free space inside the wedge is partially occupied by these bulky groups and access for small substrate entry is blocked significantly, thus limiting the reactivity of the lanthanide complexes. This is clearly demonstrated by the space-filling model of the structure of $Sm(C_5{}^{i}Pr_4H)_2$ **99**,[144] in which four iPr groups occupy the space of the wedge and block access to the metal center (**Fig 1.9**). In contrast, $Sm(Flu)_2$ **100** possesses an open wedge and access to the metal center is much better than in $Sm(C_5{}^{i}Pr_4H)_2$ **99**.[145] The open metal center of $Sm(Flu)_2$ **100** clearly benefited from the rigidity of the fluorenyl (**2-D**) planar skeleton, compared with the (**3-D**) bulk of $C_5{}^{i}Pr_4H$. Inspired by this sharp contrast, we aim to

synthesize complexes with substantially larger rigid ligands possessing (**2-D**) bulk at the ligand periphery in order to block bridging interactions (**Fig 1.9**).

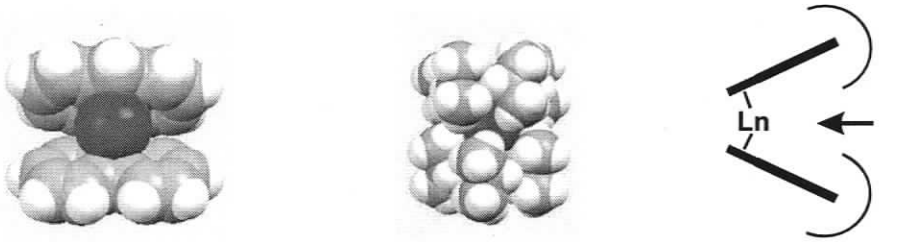

2-D bulk $Sm(Flu)_2$ **100** **3-D** bulk $Sm(C_5{}^iPr_4H)$ **99** Desired model

Figure 1.9. Complexes with 2-D and 3-D bulk and desired model

Indenyl and fluorenyl lanthanide chemistry have been well investigated and still allow the formation of bridging interactions. However, polycyclic aromatic systems with larger rigid skeletons have not been studied yet in organolanthanide chemistry and can possibly solve the problems met by other ligand systems. The combination of bulk and rigidity from the aromatic decks should limit the formation of bridging interactions. Unlike (**3-D**) substituents such as t-butyl, $SiMe_3$ and ^iPr, the aromatic decks do not project into the metallocene wedge area. Thus, the metal center remains open for attack by small substrates. Considering the above criteria, the initial candidates for our research are phenalenes **101-104**, phenanthrenyl-fused $(PCp^R)H$ **105-107**, (PCp*)H **108**, (PCp')H **109** and tetrabenzofluorene (sCp)H **110** (**Fig 1.10**).

Phenalenyl has been studied in transition metal chemistry,[146] and shows interesting bonding patterns and dynamic processes in solution. Although it is not a Cp ligand, the phenalenyl anion meets all the criteria of the fused aromatic Cp system and is an interesting target to explore. Also it would be interesting to understand the

bonding pattern between lanthanide ions and the phenalenyl anion. The PCp^R **105-107**, PCp* **108**, PCp' **109** and sCp **110** ligands possess a large aromatic polycycle that can provide the bulk and rigidity required to block the possible bridging interactions, although there is a possibility that twisting of the ligands in bis-ligand complexes may avoid steric hindrance between the two ligands and partially reduce their bulk. Due to their large size, these polycyclic aromatic systems should also form mono-ligand lanthanide complexes that possess electronically and sterically unsaturated metal centers, leading to greater and unique reactivity.

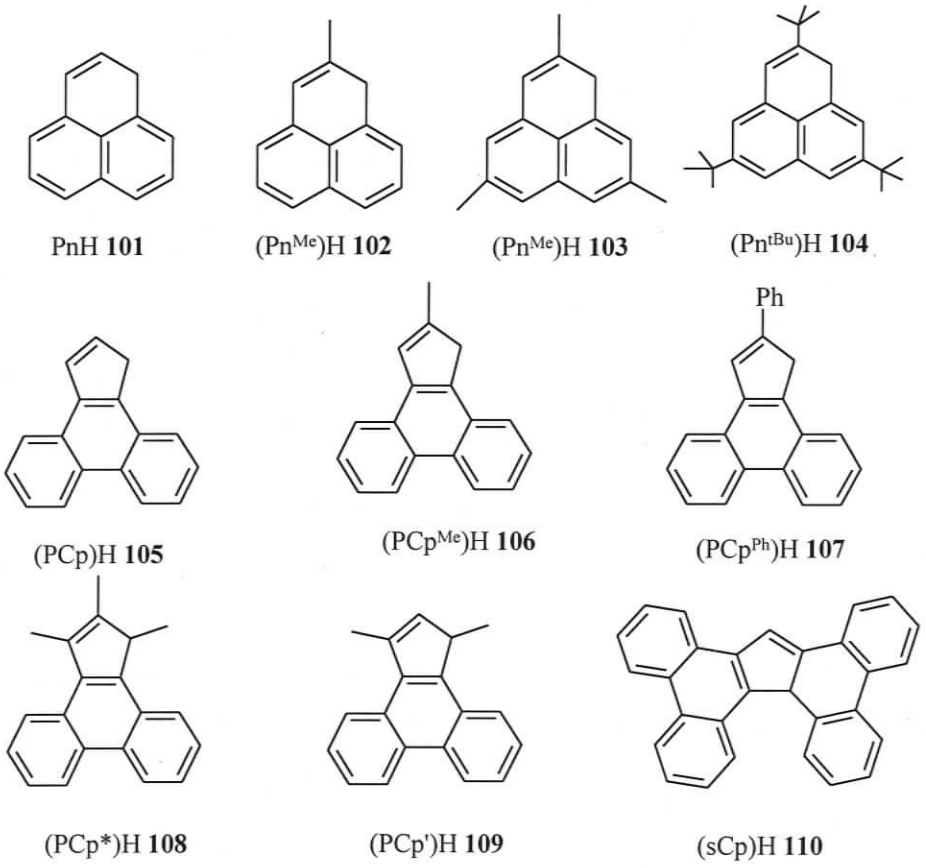

Figure 1.10. Ligand candidates for our research

One major concern regarding these ligands is the degree of electronic delocalization and consequent reduction of charge in the five-membered Cp ring core. Since the bonding in lanthanides is viewed as being almost entirely ionic, lower charge density on the five Cp carbons would be expected to lead to less coulombic attraction to the metal center, weaker binding and the potential for easy ligand loss. However, the five-membered rings of indenyl and fluorenyl ligands also possess lower electron density than simple Cp due to partial delocalization of the electrons into the fused aromatic rings, and yet these ligands still bind very effectively to lanthanide ions. For the ligands which possess additional fused aromatic rings, substantially lower electron density in the Cp ring than in indenyl and fluorenyl is a concern. However, simple extended Hückel calculations show that the electron density on the carbons of the five-membered rings in these ligands is not significantly lower than in indenyl and fluorenyl. With two remotely fused aromatic rings, PCp^R **105-107**, PCp* **108** and PCp' **109** anion possess 93% of the electron density of indenyl. Similarly, the four more remotely fused aromatic rings in sCp **110** only result in a 5% reduction in the electron density on the carbons of the five-membered ring compared to fluorenyl (**Fig 1.11**). These results, also replicated at higher level of theory, indicate that the electron density of the Cp ring is only significantly reduced by direct aromatic ring fusion, and addition of further aromatic rings more remote from the Cp ring has little effect.

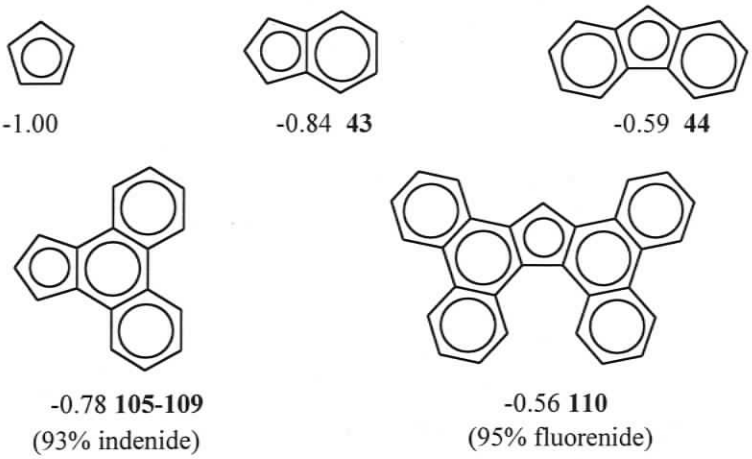

Figure 1.11. Electron density of five-membered rings for various ligands

This thesis discusses the synthesis, characterization and reactivity of Pn **101** and its derivatives **102-104** (**Chapter 2**) and PCp^R **105-107**, PCp* **108**, PCp' **109** and sCp **110** (**Chapter 3**) complexes of the lanthanides (yttrium and ytterbium). The broad range of ligands investigated was designed to allow some comparison in their ability to form stable complexes, to prevent bridges and to allow unique reactivity. The reactions investigated with each ligand system were similar to allow comparison, but the reactivity studies are not exhaustive at this point. Nevertheless, this work points out interesting and promising ligand systems for further studies.

Chapter Two.

Organolanthanide Complexes with Phenalenide as Ligand

2.1 Introduction

Phenalenyl possesses a nonbonding molecular orbital as an odd alternant hydrocarbon.[148,149] Since the non-bonding molecular orbital can be doubly occupied, singly occupied or vacant, the corresponding three-oxidation states of phenalenyl, anion, radical and cation are all stable. The pKa of phenalene (PnH) **101** was reported as 19.45 in DMSO, and is about 3 units more acidic than fluorene and one unit less acidic than indene,[150] which indicates that the phenalenide anion could act as potential ligand in lanthanide chemistry, like Cp, Cp* and fluorenide. Charge density in the phenalenide anion is equally distributed over the six α-carbon positions consistent with the symmetrical nature of the HOMO (**Fig 2.1**).

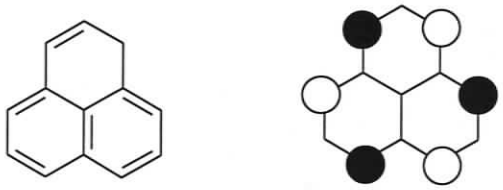

PnH **101** Homo of Pn^-

Figure 2.1. Structure of phenalene and the HOMO of its anion

Prior to our work, only a few phenalenyl metal complexes were reported, including complexes of the phenalenyl cation, radical, the phenalenide anion and neutral phenalene.[151-155] Among those complexes, the phenalenide anion type is of interest to us for their similarity to complexes of the Cp* anion. The first X-ray

structure of a phenalenide complex was reported in 1978 and showed a η^3 bonding pattern between platinum and the phenalenide ligand.[146] However, there was no evidence for any dynamic process. Eight years later, Ichiro Murata isolated a phenalenide palladium complex and observed threefold fluxionality in solution (**Fig 2.2**).[147] In this complex, the palladium moiety is bonded to a phenalenyl unit through an a η^3 bonding pattern but migration of the metal around the phenalenide skeleton takes place on the NMR time scale at elevated temperature.

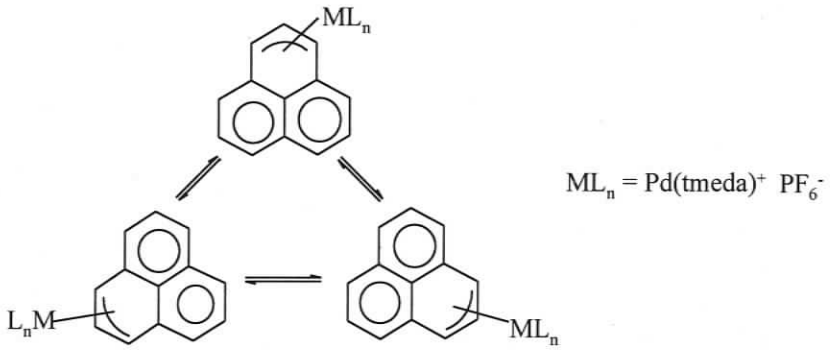

Figure 2.2. Haptotropic rearrangement of a phenalenide palladium complex

Lanthanide-ligand bonds possess more ionic than covalent character, because 4f electrons are extensively shielded by the filled 5s and 5p orbitals due to the greatly contracted 4f orbitals.[156] The ionic nature of lanthanide metal centers theoretically enable them to bond with the phenalenide anion in several different ways including η^6 bonding to the six α-carbons bearing the most electron density (see the HOMO of Pn^- shown in **Fig 2.1**), or η^3 bonding to the allylic part of one six-membered ring. Regarding the η^3 bonding, the metal can either bond tightly without any motion in solution or migrate rapidly along the face of the phenalenide skeleton. Given the

unusual bonding possibilities, we felt it would be very interesting to understand the bonding mode between a lanthanide metal center and a phenalenide anion.

The rigidity of the phenalenide ring can also help us understand if the outer sphere is large enough to block bridging interactions. Both an η^6 or η^3 bonding pattern enable bis-ligand complexes to form a clear metallocene-like wedge. Other phenalenide derivatives based on 2-methylphenalene ($Pn^{Me}H$) **102**, 2,3,5-trimethylphenalene ($Pn^{3Me}H$) **103** and 2,3,5-tri-t-butylphenalene ($Pn^{tBu}H$) **104** are also interesting targets (**Fig 2.3**). Despite the additional alkyl substituents, the added bulk is on the outer edge of the phenalenide skeleton and projection into the wedge should be very minimal. Moreover, the alkyl substituents can help block the bridging interaction and help us understand the effect of different substituents on the properties of the complexes. Both acid-base and salt metathesis reactions will be attempted to prepare these complexes. Additionally, the properties and reactivity of the resulting complexes can help determine if the phenalenide ligand is a suitable substitute for the Cp* ligand in organolanthanide chemistry.

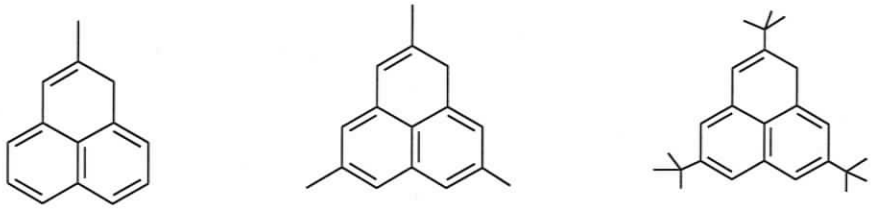

(Pn^{Me})H **102** (Pn^{3Me})H **103** (Pn^{tBu})H **104**

Figure 2.3. Phenalene derivatives used in this work

2.2 Synthesis and Characterization of Lanthanide Complexes

2.2.1 Synthesis of the Ligands

Among PnH **101**, (Pn^{Me})H **102** and (Pn^{tBu})H **104**, (Pn^{tBu})H **104** was the most difficult one to prepare and the overall yield was only about 3%. All the ligands were synthesized with some modification of the original literature. For the synthesis of PnH **101** and (Pn^{Me})H **102** (**Scheme 2.1**),[157] after the decarboxylation of the diacid **113** at 180°C, the propanoic acid **114** was treated in a one pot procedure with $SOCl_2$ in CH_2Cl_2 to form the acid chloride followed by a Friedel-Crafts reaction using $AlCl_3$ to generate the phenalanone **115**. Reduction of **115** followed by dehydration afforded **101** or **102**. The overall yield for these two ligands was about 15%.

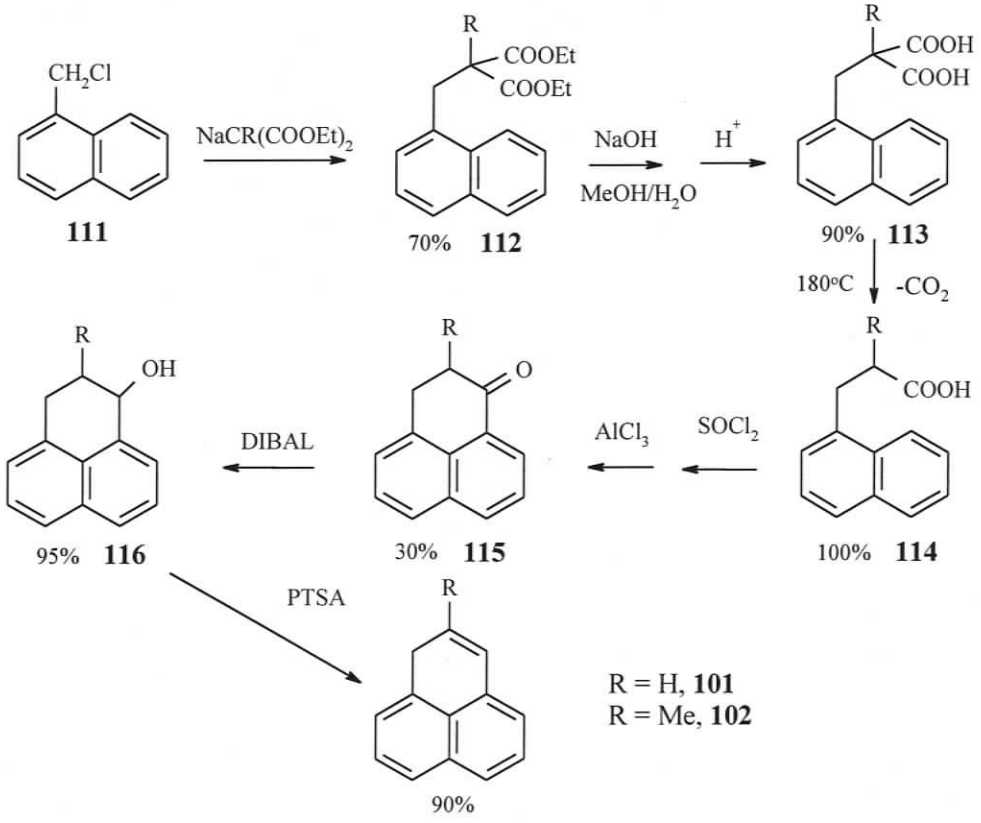

Scheme 2.1. Synthesis of PnH and (Pn^{Me})H

Another good way to synthesize PnH **101** was to reduce *phenalenone* by diisobutylaluminium hydride in one step.[158] At room temperature, $(Pn^{Me})H$ **102** showed more stability than PnH, which decomposed slowly even in the glovebox over a long period of time.

For the synthesis of $(Pn^{tBu})H$ **104** (**Scheme 2.2**),[159] the phenalanone **123** was directly synthesized by addition of four equivalents of BCl_3 to methyl ester solution;[160] this step greatly simplified the preparation reported in the original literature that included transformation of the ester to a carboxylic acid, then a carboxylic halide and finally to the ketone.

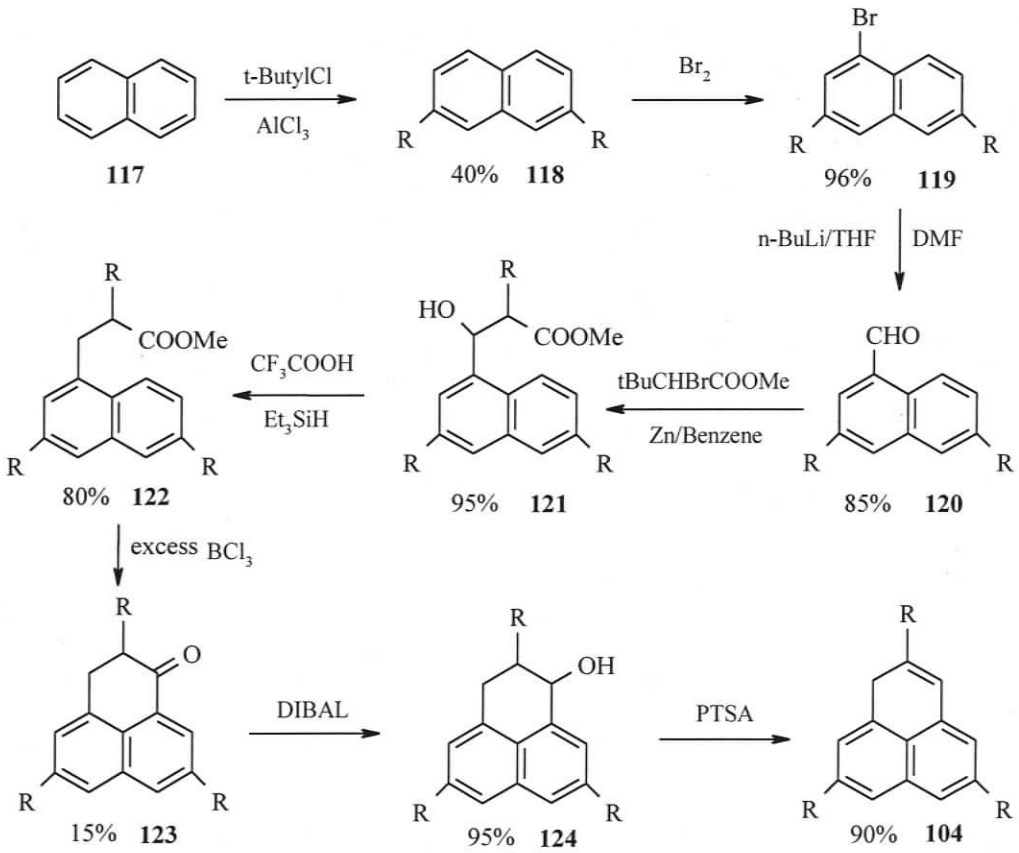

Scheme 2.2. Synthesis of $(Pn^{tBu})H$ 104 (R = t-butyl)

Attempts to prepare (Pn^{3Me})H **103** were not successful because of difficulties with two steps (**Scheme 2.3**). Chloromethylation gave a much lower yield (15%) than the literature claimed (75%),[161] and reductive debromination, though reported in the literature, failed to proceed in our hands. With development of the research, complexes made from PnH, (Pn^{Me})H and (Pn^{tBu})H ligands provided enough information to understand the reactivity and the bonding mode, so the synthesis of (Pn^{3Me})H was not further pursued.

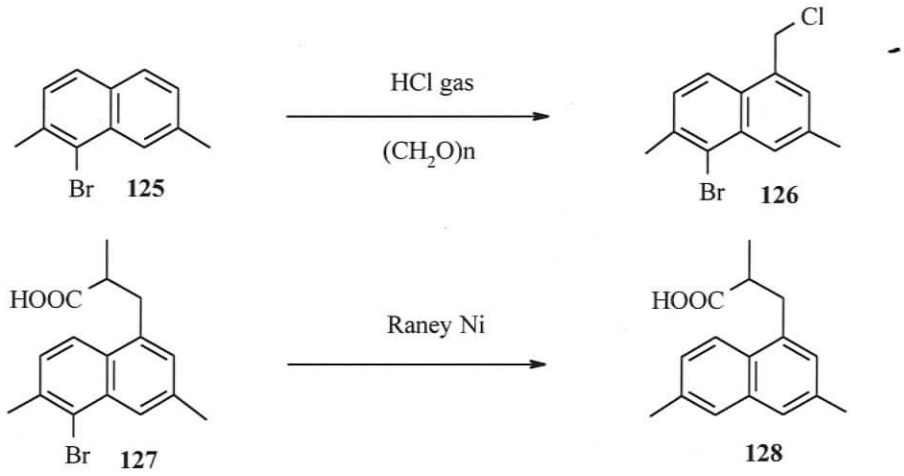

Scheme 2.3. The problematic steps in the synthesis of (Pn^{3Me})H

2.2.2 Yttrium Complexes by Salt Metathesis

Salt metathesis starting with anhydrous lanthanide chlorides is the well-established route to lanthanide complexes by reacting the metal halide with an alkali metal salt of a ligand. In this project, the phenalenide Pn **101** and Pn^{Me} anion **102** were made by deprotonating the neutral ligand with an excess of n-BuLi in hexanes. The advantage of generating the anion in hexanes over THF or ether was that it afforded greater purity since the ligand anion precipitates out and any unreacted neutral ligand

or extra n-BuLi can be washed away easily by hexanes. Among several metal halides (YCl_3, $YbCl_3$ and $ZrCl_4$) tried with the ligand anion, yttrium chloride proved to be the only metal to afford clean product in relatively high yield. Also, diethyl ether proved to be a better solvent than THF for salt metathesis, because the reaction in diethyl ether gave a cleaner and more crystalline product than in THF.

After 2:1 stoichiometry of Pn anion and YCl_3 was stirred overnight in ether, the reaction mixture was filtered and concentrated to a smaller volume by vacuum, then cooled at –10 °C overnight in the fridge. A dark brown solid of crude $[Y(Pn)_2(\mu\text{-}Cl)_2Li(Et_2O)_3]$ (**129**) was isolated. The solid was redissolved in toluene, filtered to remove some insoluble solid and the solvent was removed to yield a dark brown powder of $[Y(Pn)_2(\mu\text{-}Cl)]_2$ (**130**) (**Eq 2.1**).

Salt metathesis reactions are known to form $[LnL_2(\mu\text{-}Cl)_2Li(THF)_2]$ 'ate' complexes easily.[162,163] In the absence of a crystal structure, the formula of complex **129** was established by comparing the integration of the aromatic protons with that of coordinated diethyl ether. The presence of three ether molecules in **129** (**Fig 2.4**) suggests that **129** is an 'ate' complex because it is very unlikely the yttrium center could accommodate three Et_2O molecules in a simple species such as $Y(Pn)_2Cl(OEt_2)_3$.[164] After dissolving in toluene, **129** transforms into **130** by losing Et_2O and LiCl, as shown by disappearance of the Et_2O resonances in the ^1H NMR spectrum. It is also reasonable to assume that the structure of **130** is dimeric, not monomeric; otherwise, there would be a vacant coordination site, which has not yet been seen for other Cp or Cp* lanthanide halide complexes. Also, **130** can dissolve in

THF, but not in Et_2O, indicating that chloride bridges in **130** can only be cleaved by the strong donor THF. This process is consistent with the cleavage of chloride bridge of dimer **130** by THF to form a monomer as observed in other cases.[165,166] The ^1H NMR spectrum of **130** clearly shows two resonances in the aromatic region at 5.58 and 6.28ppm with a 7.5Hz coupling constant, indicating C_{2V} symmetry in solution given the ligand rotates freely at room temperature. The ^1H NMR spectrum of **129** in C_6D_6 shows aromatic resonances with the same chemical shift and coupling constants as **130**, further suggesting that **129** transforms into **130** spontaneously when dissolved in toluene or benzene by loss of diethyl ether and LiCl salt. The resonances of **129** in the ^1H NMR spectrum (**Fig 2.4**) are the simple combination of **130** and three equivalents of free diethyl ether molecules (assigned by their chemical shift).

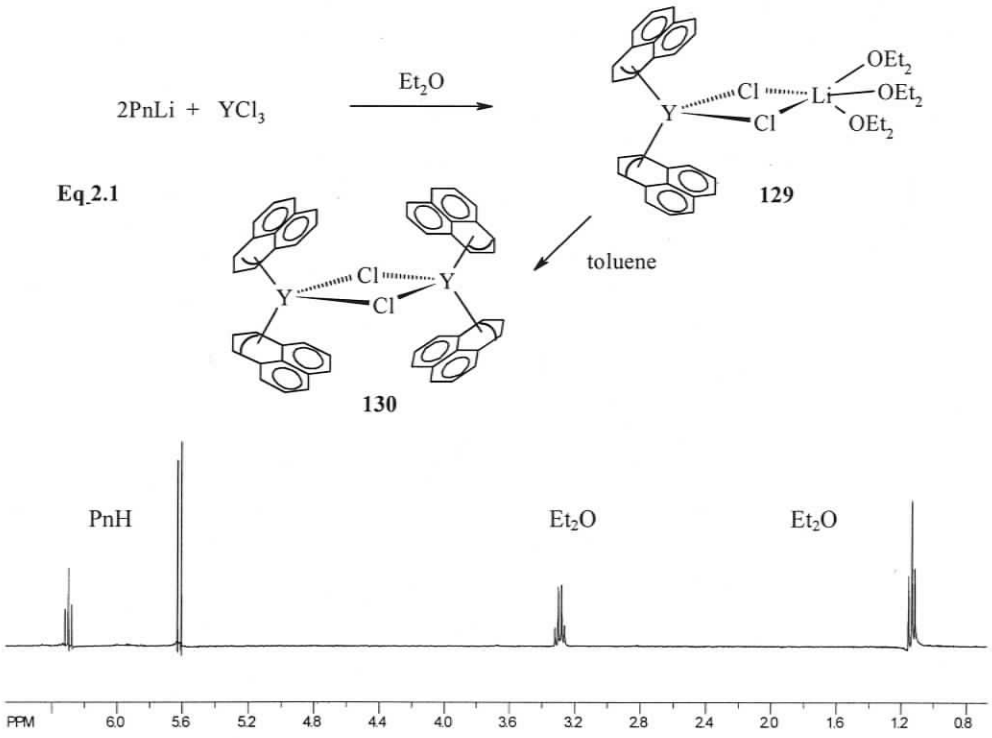

Figure 2.4. ^1H NMR spectrum (300 MHz, C_6D_6) of 129

When $(Pn^{Me})Li$ was reacted with YCl_3 in Et_2O, instead of forming the lithium chloride adduct analogous to **129**, the dimer $[Y(Pn^{Me})_2(\mu\text{-}Cl)]_2$ (**131**) was obtained directly from crystallization of the reaction mixture at -10°C (**Eq 2.2**). A dimeric structure for **131** is suggested by the absence of resonances for Et_2O and its high solubility in toluene. The ^1H NMR spectrum of **131** shows four sharp resonances in the aromatic region (**Fig 2.5**), indicating **131** also possesses high symmetry in solution. Direct formation of **131** is attributed to the steric effect of the methyl group on Pn^{Me} that helps block formation of an "ate" complex.

Eq 2.2 $2Pn^{Me}Li + YCl_3 \xrightarrow{Et_2O}$ 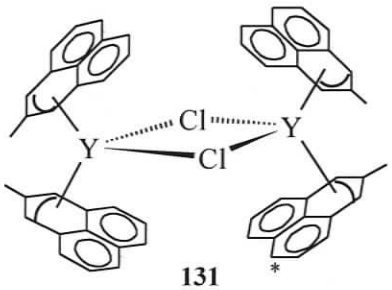

131

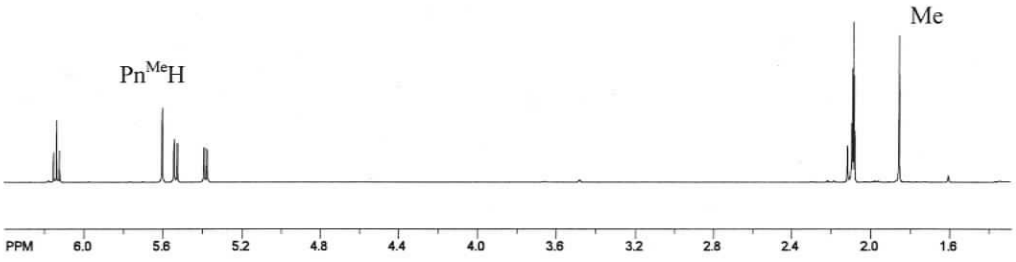

Figure 2.5. ^1H NMR spectrum (500 MHz, C_7D_8*) of 131

(* = NMR solvent residue. This applies to the other spectra as well)

The Pn^{tBu} anion is obtained as a deep red-orange precipitate from n-BuLi and the neutral ligand $(Pn^{tBu})H$ **104** in hexanes. The Pn^{tBu} anion is not soluble in hexanes which enables us to separate clean product; however, $(Pn^{tBu})Li$ is very sensitive to moisture and can decompose even in THF freshly distilled from Na/benzophenone.

As a result, the reaction of (Pn^{tBu})Li with metal salts can only be carried out in toluene. When (Pn^{tBu})Li and three equivalents of YCl_3 were mixed and the resulting suspension stirred for three days in toluene, [Y(Pn^{tBu})(μ-Cl)Cl]$_2$ (**132**) was obtained. All attempts to convert **132** to the bis-(Pn^{tBu}) yttrium complex by treatment with one more equivalent of (Pn^{tBu})Li failed (**Eq 2.3**). During the three-day reaction period, the reaction mixture changed from deep red-orange to dark brown. The chemical shift of the aromatic protons in **132** is 6.02 ppm compared to 5.65 ppm for (Pn^{tBu})Li, so the reaction process can be monitored easily by NMR spectroscopy (**Fig 2.6**), confirming that three days or more are required for the reaction to reach completion. In the absence of comparative integration standards, there is the possibility of **132** being a bis-Pn^{tBu} complex. However, given the slowness of this reaction, stepwise formation of the bis-Pn^{tBu} complex from an intermediate mono-Pn^{tBu} complex seems likely. Three resonances for (Pn^{tBu})Li, mono-Pn^{tBu} and bis-Pn^{tBu} complex are therefore expected; however, only two resonances were observed during the three day reaction period. Thus, a bis-Pn^{tBu} structure can be ruled out.

Normally, mono-Cp lanthanide complexes show a strong tendency to increase the coordination number of the metal atom by coordination of solvent molecules and/or incorporation of alkali metal halide.[166-168] Considering that no coordinating solvent is available in this reaction, a mono-Pn^{tBu} yttrium complex is expected to be unstable due to its coordination vacancy; consequently, **132** is generated most likely as a dimer. Further binding of more units to form larger clusters is probably not feasible because of the presence of the three bulky t-butyl groups on the Pn skeleton.

Eq 2.3 $Pn^{tBu}\text{-}Li^{+} + YCl_3 \xrightarrow{\text{toluene}}$ 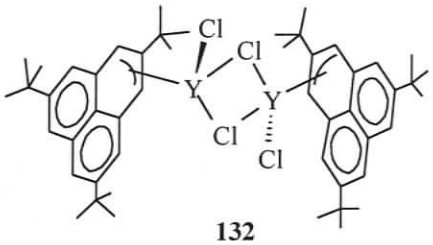

132

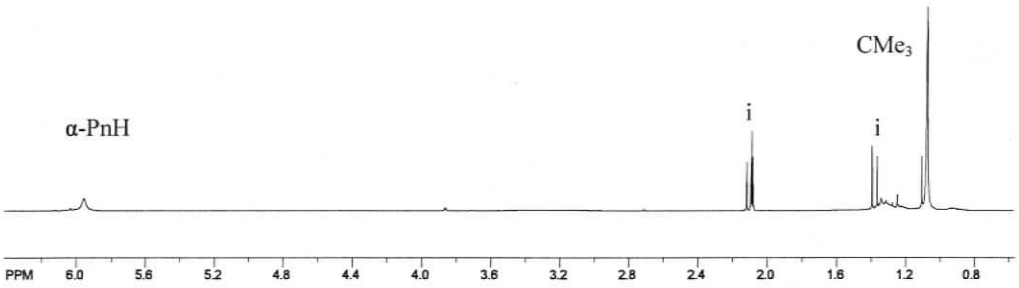

Figure 2.6. ^{1}H NMR spectrum (500 MHz, C_7D_8) of 132

(i = impurity; this applies to other spectra as well)

Complexes **130**, **131** and **132** were expected to be important precursors to $(Pn)_2YR$ or $(Pn^{tBu})YR_2$ (R= amide, alkyl, H) type complexes that should be accessible by salt metathesis. Reaction of **130** with $LiCH(SiMe_3)_2$, $NaN(SiMe_3)_2$, NaH, NaOAr and MeLi were investigated to generate $(Pn)_2YR$ type complexes. However, these reactions either resulted in Pn ligand loss, or failed to give any tractable solids or useful NMR information (**Eq 2.4**). Similarly, complex **132** failed to afford any products by salt metathesis with LiR. Ligand loss can be easily distinguished by precipitation of the toluene-insoluble Pn salt. After being hydrolyzed, the ^{1}H NMR spectrum of the Pn salt hydrolyzate only shows resonances due to the neutral ligand PnH, indicating that only the Pn salt precipitates.

Eq 2.4 **2** + $LiCH_2SiMe_3$ ⟶✕ $(Pn)_2YCH_2SiMe_3$

+ $NaN(SiMe_3)_2$ ⟶✕ $(Pn)_2YN(SiMe_3)_2$

2.2.3 Ytterbium Complexes by Protonolysis

Since salt metathesis reactions did not afford any alkyl, amide or hydride complexes from the halide precursor, the focus was shifted to direct acid-base reactions between the neutral PnH ligands and easily prepared lanthanide alkyl or amide complexes: $Y[N(SiMe_3)_2]_3$, less bulky $Y[N(HSiMe_2)_2]_3(THF)_2$, $Y(CH_2SiMe_3)_3(THF)_2$, $Y[CH(SiMe_3)_2]_3$ and $Yb[N(SiMe_3)_2]_2(THF)_2$.[8,9,169,170] Protonolysis reactions of $Y[N(SiMe_3)_2]_3$ and $Y[N(HSiMe_2)_2]_3(THF)_2$ with neutral PnH ligands did not proceed at all, even when the reaction mixture was heated. $Y(CH_2SiMe_3)_3(THF)_2$ and $Y[CH(SiMe_3)_2]_3$ appeared to react with the neutral ligands very slowly; however this reaction was not practical, because both tris(alkyl) precursors are thermally sensitive and can decompose easily over time at room temperature.[171] $Yb[N(SiMe_3)_2]_2(THF)_2$ turned out to be the only lanthanide precursor capable of reacting with neutral PnH ligands cleanly.

Although salt metathesis reaction involving $YbCl_3$ and YbI_2 did not work, the protonolysis reaction between PnH and $Yb[N(SiMe_3)_2]_2(THF)_2$ to generate ytterbium complexes worked very well. A 2:1 stoichiometry of PnH **101** or $(Pn^{Me})H$ **102** with $Yb[N(SiMe_3)_2]_2(THF)_2$ in hexane afforded a red-brown toluene-soluble precipitate of $(Pn)_2Yb(THF)_2$ (**133**) or $(Pn^{Me})_2Yb(THF)_2$ (**134**) in about 60% yield (**Eq 2.5**, P51). Both **133** and **134** are quite soluble in toluene and benzene, but not soluble in hexanes. Both complexes are stable at room temperature in the solid state or in solution, but decompose easily when heated. Unfortunately, X-ray quality crystals were not obtained to characterize solid-state structures. As a better electron donor, pyridine can

replace THF to afford $(Pn)_2Yb(py)_2$ (**135**) as a dark brown powder; however, crystallization of complex **135** also failed to give X-ray quality crystals.

The aromatic protons of **133** show two broad resonances at 6.32 and 5.61 ppm (**Fig 2.7**). Complex **134** shows broad resonances at similar chemical shifts. Despite some broadening, the resonances still clearly show a coupling constant of 6.7Hz between the α and β protons for **133**. The broad resonances for **133** and **134** are somewhat surprising, because sharp resonances are expected for diamagnetic, divalent ytterbium. One possible explanation for the ^1H spectra of **133** and **134** is that these complexes undergo a fluxional process and are near the coalescence temperature. However, variable temperature spectra carried out at higher and lower temperature failed to show any sharpening of these resonances. Although this does not necessarily rule out a dynamic process, the system cannot simply be close to coalescene at room temperature. Contamination of the sample by a trace amount of paramagnetic ytterbium (III) complexes is not convincing either, because both complex **133** and **134** are quite stable at room temperature and don't show any decomposition. In addition, solvent resonances are sharp ruling out a significant paramagnetic impurity. The reasons for broadening of the spectra for **133** and **134** remain unknown.

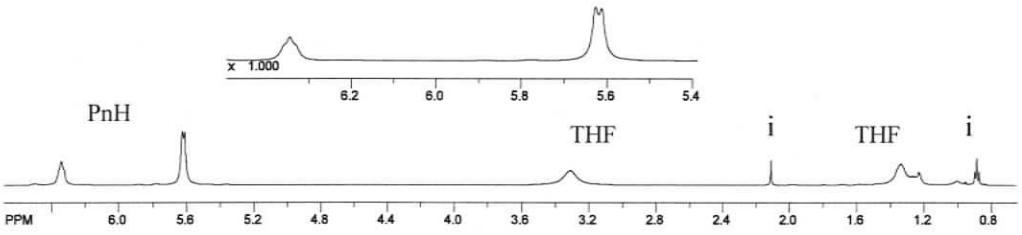

Figure 2.7. ^1H NMR spectrum (500 MHz, C_6D_6) of 133

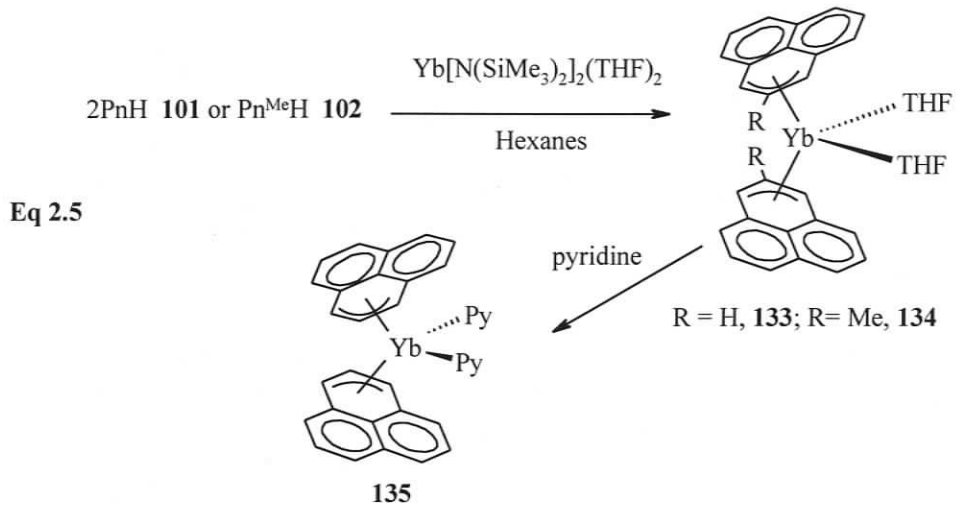

Eq 2.5

Compared with the smaller PnH ligands, $Pn^{tBu}H$ reacted much more slowly with $Yb[N(SiMe_3)_2]_2(THF)_2$. After heating at 80 °C in hexanes for 8 days followed by cooling in the fridge, the reaction mixture afforded a dark red solid $(Pn^{tBu})_2Yb(THF)$ (**136**) (**Eq 2.6**, P53). $(Pn^{tBu})_2Yb(Et_2O)$ was produced in some batches due to the use of $Yb[N(SiMe_3)_2]_2(Et_2O)_2$ as starting material. Complex **136** is soluble in hexanes and very soluble in toluene and benzene. The aromatic protons only show one sharp resonance at 5.63 ppm (**Fig 2.8**). Complex **136** is quite stable in either the solid state or solution, as indicated by the robust method needed to prepare it. Crystallization of **136** from hexanes afforded dark red plate crystals suitable for X-ray crystallography and the structure shows two coordinated THF molecules. However, a ^1H NMR spectrum of **136** shows only one THF molecule, indicating **136** loses one THF when exposed to vacuum for a long time.

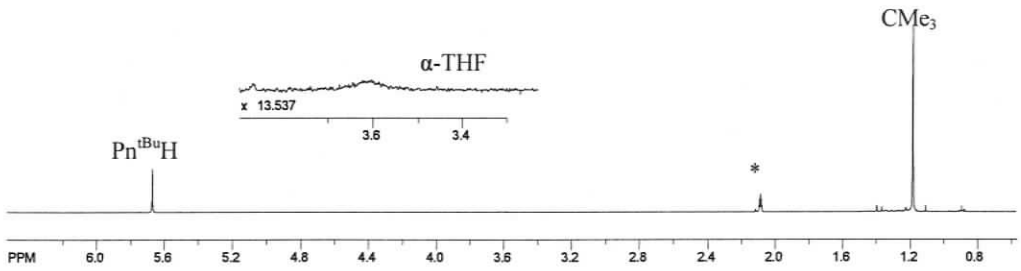

Figure 2.8. ^{1}H NMR spectrum (500 MHz, C_7D_8) of 136

When monitoring the slow reaction to give **136** by ^{1}H NMR, one resonance with almost identical chemical shift to **136** was always observed in the reaction mixture. This most likely indicates the presence of the mono-Pn^{tBu} ytterbium complex, especially considering the extremely long reaction period for the formation of **136**. A 1:1 stoichiometry reaction between $Pn^{tBu}H$ with $Yb[N(SiMe_3)_2]_2(THF)_2$ was attempted to prepare the mono-ligand complex. ^{1}H NMR shows complete conversion of neutral ligand to complex $(Pn^{tBu})Yb[N(SiMe_3)_2](THF)_2$ (**137**) as an oily, dark-red solid after overnight heating at 70°C (**Eq 2.6**, **Fig 2.9**). Compared to complex **136**, **137** is more interesting from a chemical point of view because this complex includes a readily replaceable $N(SiMe_3)_2$ group and thus can serve as an excellent precursor to other complexes. Also, **137** shows great stability both in the solid state and solution, and does not show any sign of redistribution or decomposition over a long period of time.

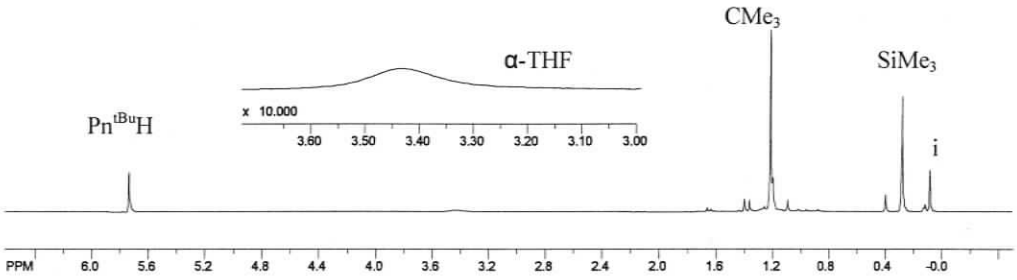

Figure 2.9. ^{1}H NMR spectrum (300 MHz, C_6D_6) of 137

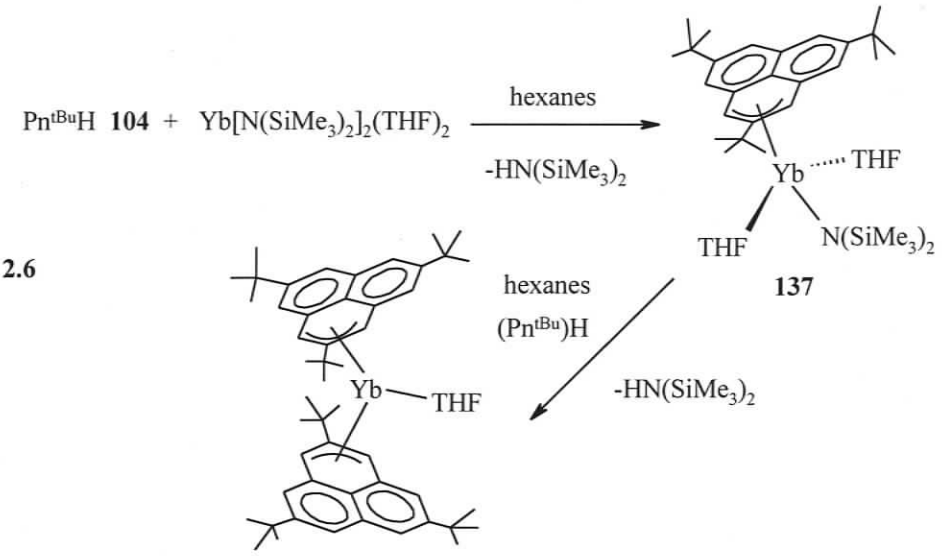

Eq 2.6

Since ytterbium has two stable oxidation states, (II) and (III), and the oxidation potential of Yb(II) to Yb(III) is +1.15 V,[172] it was of some interest to generate Yb(III) complexes from Yb(II) precursors by oxidation. Oxidation of divalent ytterbium complexes to the trivalent state by alkyl halides, p-tolyldisulfide and $HgCl_2$ were attempted. However, all of these oxidation reactions resulted in formation of intractable products or decomposition of the ytterbium complex and formation of neutral PnH ligand derivatives as indicated by discharge of the deep solution color. For example, oxidation of **133** by t-butylCl was expected to give Pn_2YbCl; instead, ^1H NMR shows the formation of neutral ligand PnH. Although reaction of **133** with $HgCl_2$ and p-tolyldisulfide did show signs of oxidation, no useful NMR information could be obtained to characterize the products. Given the difficulty of preparation and separation of complex **136**, oxidation reactions were not carried out on this complex in light of the failure of complex **133** to oxidize cleanly. Also, loss of ligand during oxidation of **136** is expected to be easier because the difficulty in preparing **136** with

the bigger Yb(II) center suggests that bis-(Pn^{tBu}) Yb(III) with the smaller radius of Yb(III) than Yb(II) will be even less stable.

Unlike simple oxidation of the complexes **133**, **134** and **136**, complex **137** possesses a replaceable amide group for further modification. Attempts to carry out further acid-base reactions on **137** with 2,6-di-t-butylphenol, phenylacetylene and hydrogen gas afforded neutral $Pn^{tBu}H$ ligand, instead of the desired product. Treating **137** with $AlMe_3$ in hexanes afforded a brown toluene-soluble precipitate. The ^1H NMR spectrum shows a huge broad resonance near 0 ppm, a possible indication of extensive $AlMe_3$ adducts. Crystallization and further characterization of this product also failed due to its easy decomposition in solution even at very low temperature.

That $Yb[N(SiMe_3)_2]_2(THF)_2$ reacts more readily with phenalene ligand than the tris-alkyl yttrium complexes, i.e. $Y(CH_2SiMe_3)_3(THF)_2$, is surprising because $CH_2(SiMe_3)_2$ and $CH_3(SiMe_3)$ have much higher pKa 's (~45) than $HN(SiMe_3)_2$ (~30).[173] Since the acid-base reaction between ligand and tris-alkyl yttrium complex must be thermodynamically favorable, the kinetics of this reaction are apparently too slow. During the process of protonolysis, the ligand and lanthanide precursor have to form a four-center transition state (**Fig 2.10**), the stability of which depends on the size of metal, the steric effects of the neutral ligand and those of other ligands in the lanthanide precursor. The ionic radii of Y(III) and Yb(II) are about 0.90 Å and 1.02 Å,[172] respectively, so Yb(II) provides less crowded transition state for protonolysis. In addition, $Yb[N(SiMe_3)_2]_2(THF)_2$ has only two silyl amide ligands while the yttrium precursors possess three bulky CH_2SiMe_3 or $CH(SiMe_3)_2$ groups. The extra steric

effects of the alkyl substituents in $Pn^{Me}H$ and $Pn^{tBu}H$ make them even more difficult to react with these relatively unreactive precursors compared to the simple PnH ligand. This explanation is strongly supported by the fact that the reaction process to form **136** was very slow. As a result, large amounts of $Yb(Pn^{tBu})[N(SiMe_3)_2](THF)_2$ **137** formed as a stable intermediate. In contrast, the reaction between PnH or $Pn^{Me}H$ with $Yb[N(SiMe_3)_2]_2(THF)_2$ produced only **133** and **134** at room temperature with no sign of formation of the intermediate $(Pn)Yb[N(SiMe_3)_2](THF)_2$ complexes.

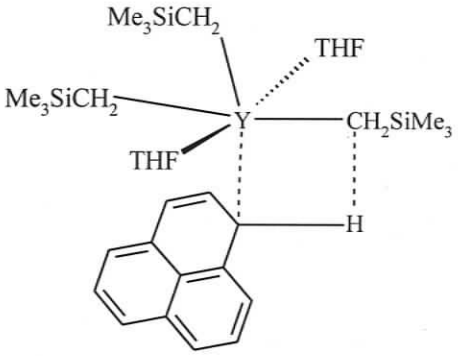

Figure 2.10. Transition state for the protonolysis reaction

Ansa-phenalenide complexes are of interest because they should possess a more open metal coordination sphere. Dimethylsilyl linked $Me_2Si(Pn^{Me}H)_2$ **138** was prepared from PnLi and dimethyldichlorosilane in THF (**Eq 2.7**). However, the reaction progress for both protonolysis and salt metathesis were very slow and we were unable to separate clean product. Given the difficulties in modifying **129-137**, further investigation of this ligand was not pursued.

Eq 2.7 $2(Pn^{Me})Li + Me_2SiCl_2 \longrightarrow$ 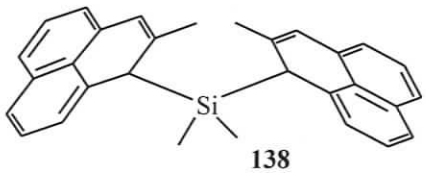

138

2.2.4 Bonding Pattern of Phenalenide Anions

The ^{1}H NMR spectra of complexes **129-132** and **136-137** show simple, sharp resonances, ruling out the possibility of tight η^3 bonding between the metal center and phenalenide anion. A static structure with the metal sitting over the center of the phenalenide ring and equally bonded to the six α-carbons could explain the high symmetry observed in solution. Alternatively, a dynamic process in which the metal center is bonded to one six-membered ring by η^3-allyl bonding and migrates rapidly from one ring to another on the NMR time scale at room temperature could also explain the observed spectra. In a covalent bonding model, the symmetrical static structure is not possible because the d (or f) orbitals of most metals are not sufficiently large to span the whole ring system. However, in an ionic bonding picture, placing the metal symmetrically over the center of the ring is not prohibited. On the other hand, a simple calculation of the coulombic attraction in an η^6 versus η^3-bonding model suggests that the latter is more favorable, mainly because the Yb-C bond distances are calculated to be much longer in the η^6-bonding (**Fig 2.11**). If this is correct, the simple ^{1}H NMR spectra suggest that rapid migration of the metal around the phenalenide π-system is occurring.

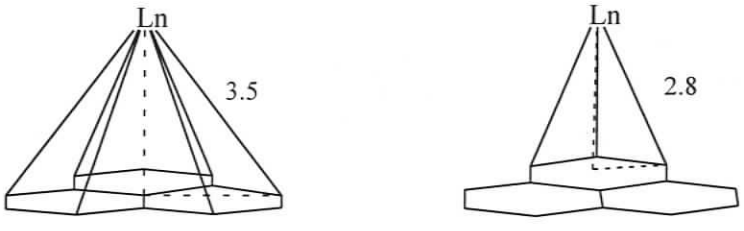

Figure 2.11. Possible bonding patterns between Yb and phenalenides (Å)

Generally, aromatic rings π-bonded to metals rotate very rapidly and it is not possible to distinguish individual protons by NMR. For example, in Cp compounds, all five Cp protons are normally equivalent. However, the energy barrier for migration of metal fragments *between* rings should be large enough for low temperature NMR detection. This is exactly the case for $[Pd(\eta^3\text{-Phenalenyl})tmeda]^+PF_6^-$ that possesses an energy barrier of about 22 kcal mol^{-1} for migration (**Fig 2.2**).[147] Considering the different bonding model for late transition metals (covalent) and lanthanides (ionic), a lower coalescence temperature might be expected for our system since there are no orbital considerations in an ionic system. Various sets of low temperature VT NMR spectra on different complexes were therefore obtained to investigate this possibility. Although several of the compounds precipitate out of solution at lower temperature, the spectra did show broadening of the phenalenide resonances, indicating a rapid migration. Fortunately, due to extremely high solubility of $(Pn^{tBu})_2Yb(THF)$ **136** in toluene, decoalescene of **136** appears to start at about 190K, just before the complex precipitates from solution (**Fig 2.12**).

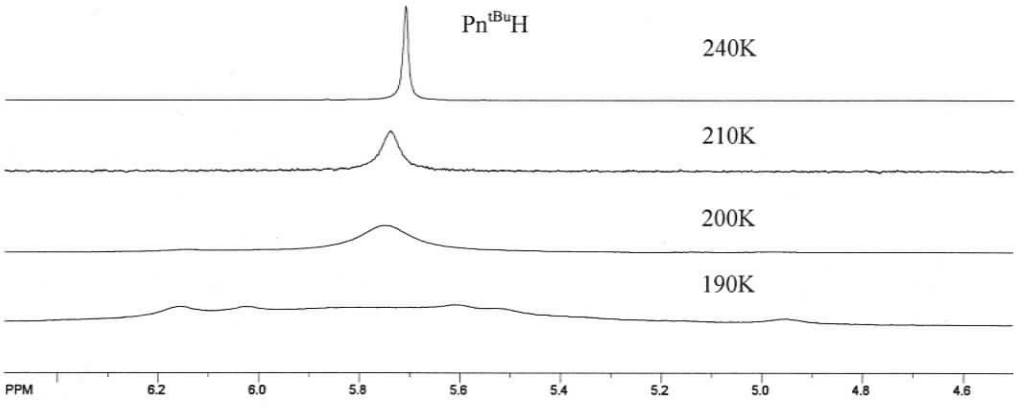

Figure 2.12. VT ^1H NMR spectra (500 MHz, C_7D_8) of 136 at low temperature

Unfortunately, the low temperature limiting spectrum still could not be reached due to insolubility below about 180K. Although VT NMR did not show conclusive evidence for a migration process, it does strongly suggest that the ground state structure is lower symmetry and rapid migration of the metal center along the phenalenide skeleton occurs at very low temperature.

The average chemical shifts of the phenalenide protons observed in the ^{1}H NMR spectra of **129-137** are remarkably far upfield and very similar to the α-allylic protons (5.45-6.04 ppm) observed in the slow exchange spectra of known group 10 η^3-phenalenyl complexes.[146] The chemical shifts of naphthalene (7.4-8.0 ppm) protons differ from allylic protons by at least 1.9 ppm. Moreover, the average α-proton was observed at 7.32 ppm in $[Pd(\eta^3\text{-phenalenyl})(tmeda)]^+PF_6^-$.[147] Thus, the chemical shifts of electron localized naphthalene unit in previously reported transition metal complexes are unable to provide a reasonable reference for calculation of energy barrier for rapid migration in **136** because the chemical shifts for delocalized naphthalene unit of **136** can not be estimated accurately (the details will be discussed in **Section 2.3**).

An intermolecular dynamic process can be ruled out because no changes in coalescence temperature or line widths were observed when the solvent was changed from d_8-toluene to d_8-THF or when the concentration of the complex was varied by a factor of three. This supports an intramolecular fluxional process because such a process should show no dependence on complex concentration or solvent donor ability. Additionally, mixing **133** and **134** or **130** and **131** together in D_8-toluene

produced no change in the ^{1}H NMR spectra of either complex, strongly suggesting that intermolecular ligand exchange does not take place on the NMR timescale.

2.3 Solid State Structure

After many attempts, crystals of complex **136** were obtained from hexanes solution and crystallographically characterized; significant bond distances and angles are given in **Table 2.1** and an Ortep3 drawing is shown in **Fig 2.13**. As the Ortep3 drawing clearly shows, the bonding pattern is not η^6, but more like η^3. The bond distances of Yb(II)-C for regular bis-Cp ytterbium complexes range from 2.60 to 2.85 Å.[174-176] The Yb-C bond distances in complex **136** range from 2.789 to 2.886 Å which puts them at the long end of the Yb(II)-C bond distance range. Also, the Yb-C distances in **136** are at the long end of the range found in symmetrically bonded, 8-coordinate lanthanoid allyls (2.682–2.839 Å).[177] In a strict formal sense, **136** is a 6-coordinate complex but using this definition, then the Yb-C bond distances observed in **136** fall well past the normal range. Even regarding **136** as an 8-coordinate complex, the ytterbium metal center is clearly more sterically crowded than most lanthanoid allyls as a result of the 'fused' naphthalene group. This crowding is obvious from the long Yb–O distances (2.435(2) and 2.436(2) Å) compared to 8-coordinate, ytterbium indenyl complexes (2.348–2.431 Å)[178] and the observation that **136** readily loses one THF molecule on exposure to vacuum.

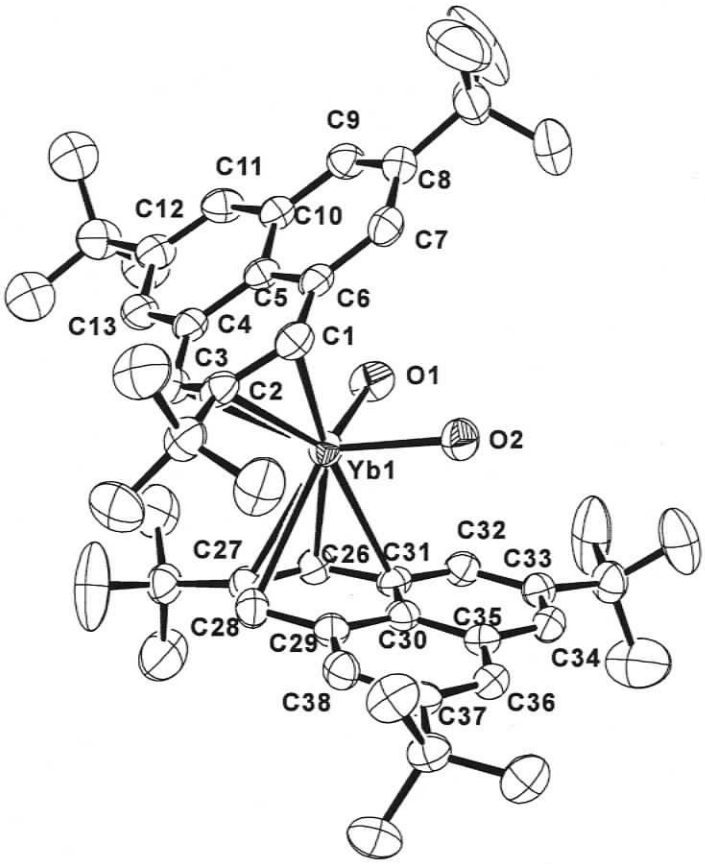

Figure 2.13. Ortep3[179] diagram (thermal ellipsoid 50% probability) of 136

Carbons on THF and hydrogen atoms omitted for clarity

Table 2.1. Selected bond lengths (Å) and angles (deg) for 136

C(1)-Yb(1)	2.817(3)	C(2)-Yb(1)	2.838(3)	C(3)-Yb(1)	2.808(3)	C(4)-Yb(1)	2.996(3)
C(5)-Yb(1)	3.049(3)	C(6)-Yb(1)	2.955(3)	C(26)-Yb(1)	2.789(3)	C(27)-Yb(1)	2.869(3)
C(28)-Yb(1)	2.864(3)	C(29)-Yb(1)	3.022(3)	C(30)-Yb(1)	3.013(3)	C(31)-Yb(1)	2.886(3)
C(1) - C(2)	1.390(4)	C(2) - C(3)	1.399(4)	C(3) - C(4)	1.435(4)	C(1) - C(6)	1.436(4)
C(26)-C(27)	1.396(4)	C(27)-C(28)	1.393(4)	C(28)-C(29)	1.437(4)	C(26)-C(31)	1.437(4)
O(2) - Yb(1)	2.436(2)	O(1) - Yb(1)	2.435(2)	torsion angle	96.4		
O(1)-Yb(1)-O(2)	94.73(8)			Pn(A)-Yb(1)-Pn(B)	144.6		

Torsion angle is defined as the angle between C(2)-Cp(cent) and C(2)'-Cp(cent)' in bis-indenyl complexes where Cp(cent) and Cp(cent)' are the centroid of the five-membered rings. In this case, the torsion angel is for C(2)-Pn(A)-Pn(B)-C(27). Pn(A)= centroid C(1)-C(6), Pn(B)= centroid C(26)-C(31).

As is apparent from the structure, the bonding modes of the two ligands are somewhat different. One of them bonds to metal center via η^3 bonding while the other is more like η^4 bonding. The different bonding modes show the possible inequivalence of the two ligands and asymmetry of this complex. However, the C-C bonding patterns of both ligands are very similar (**Fig 2.14**), indicating that the different bonding modes between ytterbium and the two ligands have no substantial effect on the ligands themselves. Considering the presence of six bulky t-butyl groups, it is most likely that the difference is due to the slight shift of the metal center caused by steric effects of the t-butyl groups. This can be seen clearly from crowding of the two allylic units where the t-butyl groups on the two allylic units approach very close to one another; while the repulsion between them can be observed from the 96.4° torsion angle and large Pn(A)-Yb(1)-Pn(B) angle (144.6°) between the two phenalenide ligands. Thus, combining the highly symmetrical NMR spectrum in solution, the equivalence of the two phenalenide ligands can be established despite their apparently different bonding modes in the solid state.

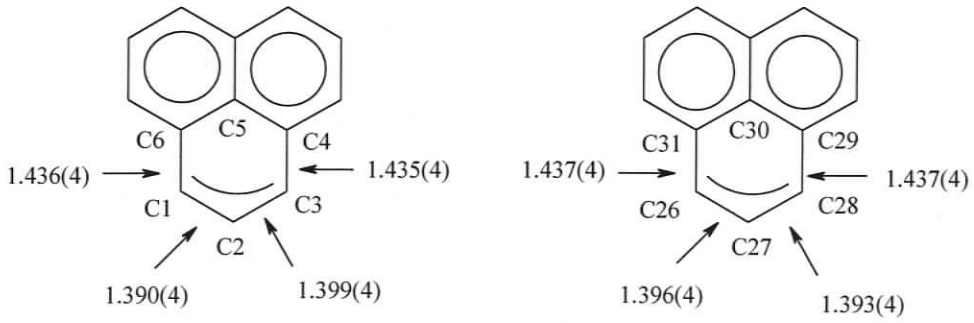

Figure 2.14. Bond distances within the Pn^{tBu} ligands from the structure of 136

The fold angles between the allyl and six-membered ring in previously reported Yb(II) indenyl complexes range from 1.4° to 6.8°,[180-186] significantly smaller than that in η^3 transition metal complexes (20-40°).[8,187-191] As a result, there is no substantial difference among Yb-C bond distances (0.019-0.140 Å) between the five-membered ring and the metal center. However, the difference between metal-carbon bond distances in η^3 transition metal indenyl complexes is more substantial and typically ranges from 0.5 to 0.9 Å longer between the metal and the allyl versus ring fusion carbons. This suggests that the electrons on the five-membered ring are still delocalized for the Yb(II) indenyl complexes, but much more localized over allylic unit in η^3 transition metal indenyl complexes. These facts clearly demonstrate the bonding pattern between indenyl and Yb(II) as η^5.

The fold angles in **136** (12.0, 12.6°) are slightly bigger than those (1.4-6.8°) in Yb(II) indenyl complexes, resulting in a larger difference between the Yb(II)-C distances to the allylic unit and adjacent non-bonded Yb(II)-C distances of 0.14Å. However, the C-C bond distances within the bonded ring only show a difference of 0.04Å between the C-C bonds of the allylic (C1-C2, C2-C3) unit and other C-C bonds in this bonded six-membered ring (C1-C6, C4-C3) (**Fig 2.14**). Also, the naphthalene subunit of the phenalenide does not show a similar bond alternation pattern to that found in naphthalene or its derivatives in electron localized system (**Fig 2.15**),[192-194] indicating that electrons of the naphthalene subunit in the phenalenide ligand are still delocalized over the whole phenalenide skeleton. In sharp contrast to **136**, the fold angle is significantly bigger in $[(\eta^3\text{-}(4\text{–}6)\text{-}1\text{-ethoxyphenalenyl})Pt(PPh_3)_2]^+BF_4$

(30.1°).[146] This leads to localization of electrons in the naphthalene unit as indicated by the long C-C bond distances (1.484, 1.517 Å) connecting the allyl and naphthalene units, and a large difference (0.8 Å) between Pt-C bond distances to the allylic unit and non-bonded Pt-C distances to ring fusion carbons.

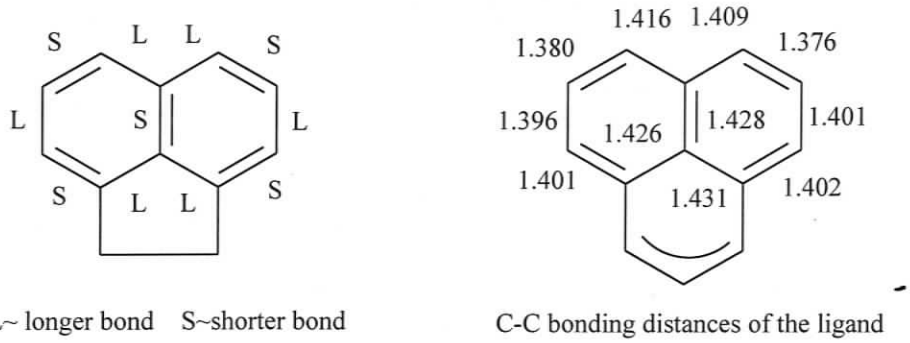

L~ longer bond S~shorter bond C-C bonding distances of the ligand

Figure 2.15. Naphthalene units in electron localized and delocalized systems

The similarity in Yb-C and C-C bond distances and fold angles between **136** and Yb(II) indenyl complexes does not necessarily mean their bonding is similar; in other words, the clear η^5 bonding pattern for Yb(II) indenyl complexes cannot help determine the bonding pattern of **136**, although they are helpful to understand electron delocalization over the phenalenide ligand when bonded to the metal. This is because charge density in phenalenide is equally distributed over the six α-carbons with little on other carbons. Electron delocalization keeps the phenalenide skeleton nearly planar and brings the metal close to non-bonded carbons, resulting in only minor differences between between the Yb(II)-C distances to the allylic unit and adjacent non-bonded carbons.

In summary, the bonding patterns in the ytterbium phenalenide system possesses several distinctive features compared to yttrium indenyl complexes and

typical η^3-bonding complexes: i) very small fold angles similar to Yb(II) indenyl complexes that possess an η^5 bonding pattern; ii) insignificantly longer distances between the metal center and non-bonded carbons and significant electron delocalization of the whole aromatic system even when bonded; iii) weaker bonding as indicated by longer Yb-C bond distances compared to that in Yb(II) indenyl complexes. Although there is no conclusive evidence to rule out the possibility that the longer Yb-C bond distances in **136** are only a function of crowding from the t-butyl groups, the similarity in dynamic behaviour and chemical shifts between **136** and **133** or **134** with much less bulky Pn ligands makes this assumption unlikely. These features show the uniqueness of the phenalenide system when bonded to lanthanides and also helps to explain the easy loss of the ligand during reactions because the electron density within the allylic bonding unit is relatively low due to electron delocalization over the rest of the phenalenide skeleton. Consequently, the lanthanide metal can migrate freely with a low energy barrier over the entire phenalenide skeleton.

We attribute this unique behavior to the ionic nature of lanthanide metals, because these metals are not restricted to the 18 electron rule and can accept more ligands if sterically allowed. The short non-bonded distances between the metal center and ring fusion carbons of the Pn ligand show that additional interactions between the metal center and the non-bonded part of phenalenide are possible. Also the similar chemical shifts of **129-137** indicate that similar bonding patterns are very likely to occur in other phenalenide complexes.

Chapter Three.

Synthesis and Properties of Organolanthanide Complexes with Aromatic-Fused Cyclopentadienyls as Ligands

3.1 Introduction

The lanthanide phenalenide complexes discussed in Chapter two possess interesting dynamic behaviour due to delocalization of electron density over the entire phenalenide skeleton; this delocalization is possibly responsible for the easy loss of the phenalenide ligand. Compared to the electron delocalized phenalenide anion, the electron densities in aromatic-fused cyclopentadienyl ligands are calculated to be similar to the parent indenide and fluorenide anions, indicating that further delocalization of electrons by fusion of more aromatic rings does not occur. Thus, ligand loss is not expected to be a major concern for these ligands.

Although indenyl and fluorenyl lanthanide complexes have been studied extensively, larger systems have not been investigated yet. The fusion of additional aromatic rings not only allows more possible bonding patterns, it can also provide the bulk and rigidity to block bridging interactions. Moreover, these ligands should form mono-Cp bis-alkyl complexes possessing two alkyl groups for modification. Despite lacking electron donors to stabilize the metal center, bis-alkyl complexes with our ligands should be very stable by taking advantage of the large and rigid ancillary ligands.

Various levels of aromatic fusion on the Cp ring can provide access to either mono or bis-alkyl complexes (**Fig 3.1**). The synthesis and characterization of lanthanide complexes with these large ligands can help understand the effect of aromatic fusion on the reactivity of these complexes. The fundamental reactivity patterns of alkyl complexes, such as insertion, polymerization and acid-base reactions will be explored; moreover, the uniqueness of the reactivity and solid state structure of these complexes will be discussed.

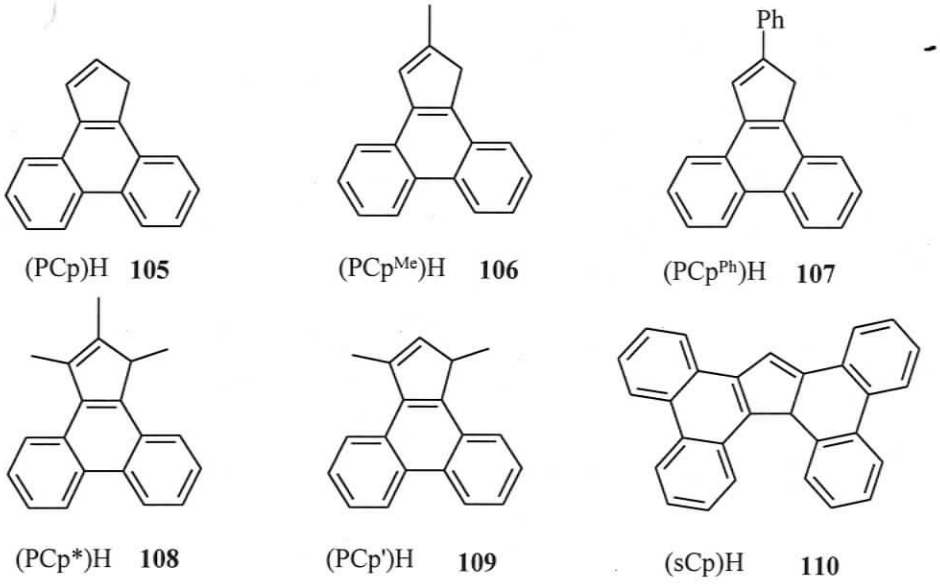

Figure 3.1. Targeted ligands for investigation

3.2 Synthesis and Characterization of Lanthanide Complexes

3.2.1 Synthesis of the Ligands

The ligands (PCp^{Me})H **106** and (PCp^{Ph})H **107** can be synthesized from commercially available 9,10-phenanthroquinone **139** and ethyl acetoacetate with modifications of a literature procedure involving treatment of the condensation

product **140** from the first step with Zn/acetic acid,[195,196] followed by addition of MeMgBr or PhMgBr and dehydration of the alcohol with p-toluenesulfonic acid (PTSA) to afford clean (PCp^{Me})H **106** or (PCp^{Ph})H **107** (**Scheme 3.1**). Compared to the original literature, Zn/acetic acid gave a much cleaner product than aqueous HI. However, for the synthesis of (PCp)H **105**, dehydration attempts by various methods failed to afford (PCp)H readily. A modification made by Bertil Eliasson resolved this problem by using the Shapiro reaction (**Scheme 3.1**).[197,198]

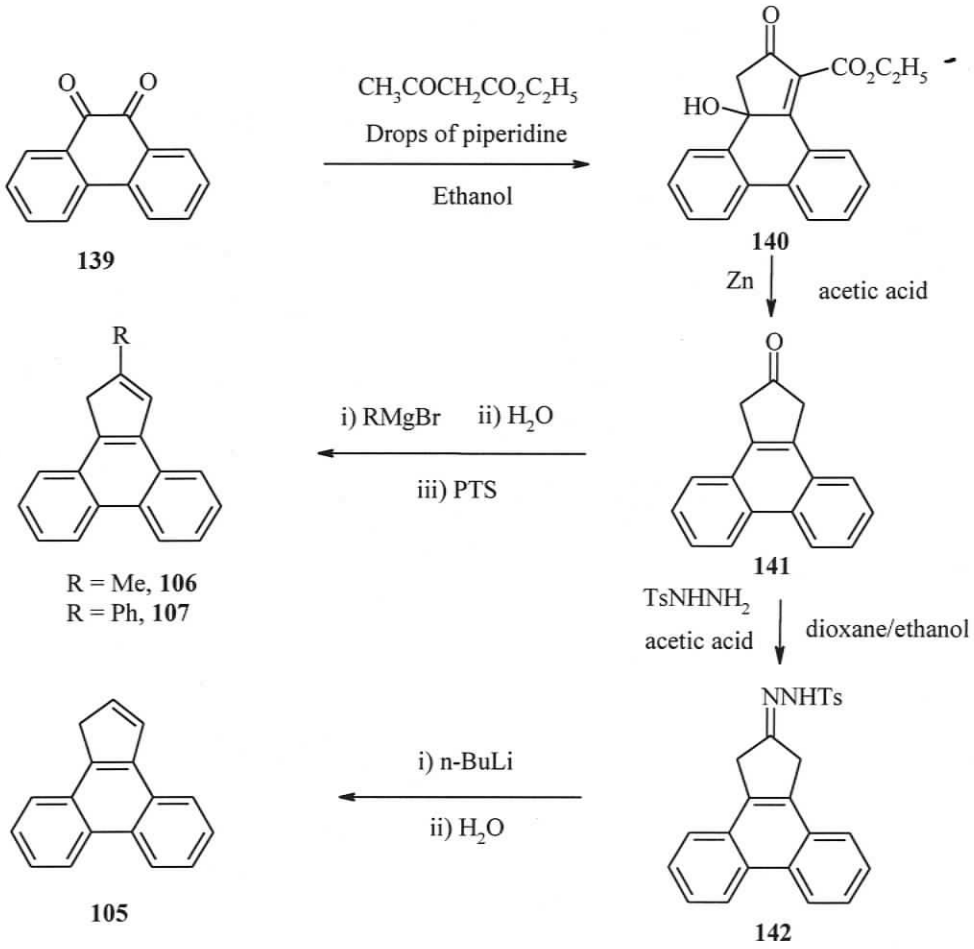

Scheme 3.1. Synthesis of mono-substituted PCp ligands

The ligands (PCp*)H **108** and (PCp')H **109** were prepared by the base-catalyzed condensation of phenanthroquinone **139** with 3-pentanone followed by reduction of the condensation product **143** with zinc and acetic acid, treatment with MeMgBr (for (PCp*)H **108**) or $LiAlH_4$ ((PCp')H **109**), respectively, and dehydration with pyridine and trichlorophosphine oxide (**Scheme 3.2**).[199] The ligand (sCp)H was synthesized starting from 9-bromophenanthrene **145** via a Grignard reaction with methyl formate, followed by dehydration and cyclization of **146** with trifluoroacetic acid (**Scheme 3.3**).[200]

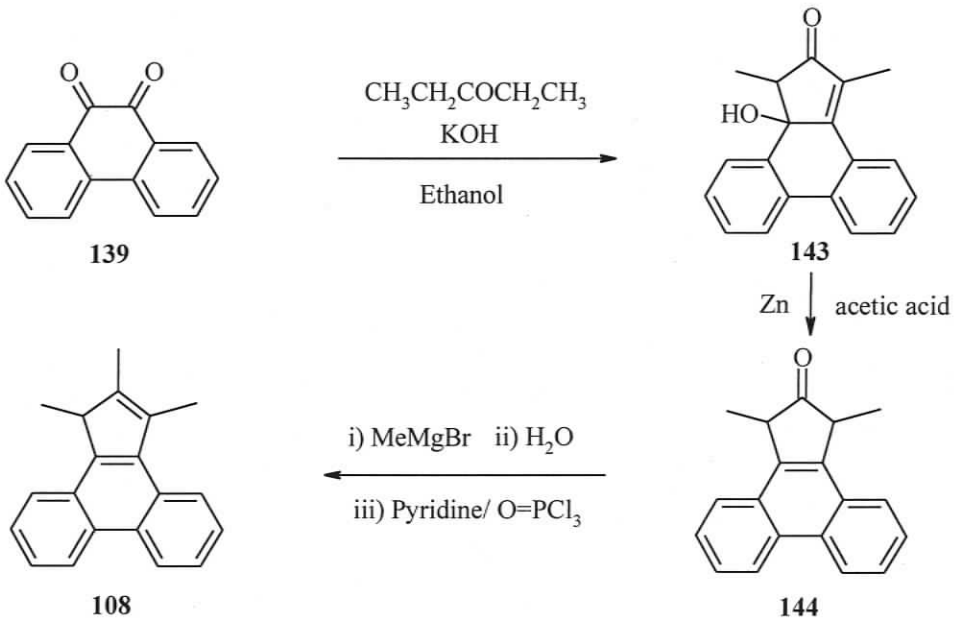

139 **143** **144** **108**

Scheme 3.2. Synthesis of (PCp*)H

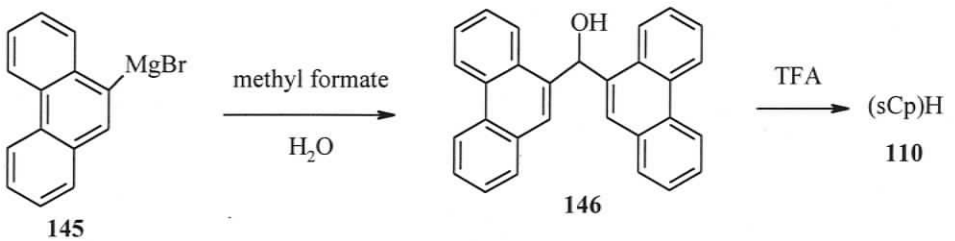

145 **146** **110**

Scheme 3.3. Synthesis of (sCp)H

3.2.2 Yttrium Mono and Bis-alkyl Complexes by Protonolysis

Reaction of the ligand (PCp^{Me})H **106** or (PCp^{Ph})H **107** with half an equivalent of the yttrium tris(alkyl) precursor, $Y(CH_2SiMe_3)_3(THF)_2$, in toluene, followed by extraction with hexanes, afforded the yttrium alkyl complexes $(PCp^{Me})_2Y(CH_2SiMe_3)(THF)$ (**147**) or $(PCp^{Ph})_2Y(CH_2SiMe_3)(THF)$ (**148**) as pale yellow powders in 88% and 90% yield, respectively (**Eq 3.1**). $(PCp)_2Y(CH_2SiMe_3)(THF)$ (**149**) was synthesized by a similar route to **147** and **148** in 85% yield, but **149** shows relatively low solubility in hexanes, so extraction of **149** with hexanes is not a feasible way to remove unreacted ligand. Substitution at the *2*-position of PCp seems to have little effect on formation of bis versus mono-Cp complex, since incorporation of phenyl and methyl substituents gave analogous complexes. Attempts to synthesize a mono-PCp^{Me} complex by using 1:1 stoichiometry of (PCp^{Me})H and yttrium tris(alkyl) also afforded the bis-PCp^{Me} complex **147**, suggesting that the mono-PCp^{Me} is unstable to redistribution in solution.

Eq 3.1

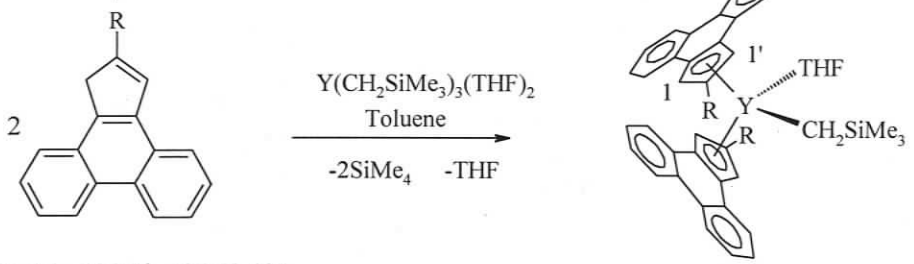

R= Me, **106**; Ph, **107**; H, **105**

R= Me, **147**; Ph, **148**; H, **149**

The ^1H and ^{13}C NMR spectra of complex **147** show the CH_2SiMe_3 resonance at -0.62 ppm ($^2J_{YH}$=3.7Hz) and 31.0 ppm ($^1J_{YC}$= 45 Hz), respectively, in the normal range for Y-CH_2SiMe_3 groups compared to previously reported examples.[201-203] The

THF resonances can be observed at 1.95 ppm (α-protons) and 0.57 ppm (β-protons) (**Fig 3.2**). Also, the protons and carbons in the *1* and *1'* positions on the PCp^{Me} ring show different resonances in the ^{13}C and ^{1}H NMR spectra, while the ^{13}C DEPT spectrum shows ten resonances for the aromatic carbons including the two of the Cp ring. These results indicate the two ligands remain chemically equivalent, but all carbons and protons on each ligand are themselves inequivalent consistent with C_S symmetry in solution. The two chemically inequivalent protons show long range coupling with a coupling constant of 2 Hz providing more proof for a C_S symmetry complex. Complex **148** and **149** show similar NMR spectra to **147**, indicating that they have similar symmetry in solution.

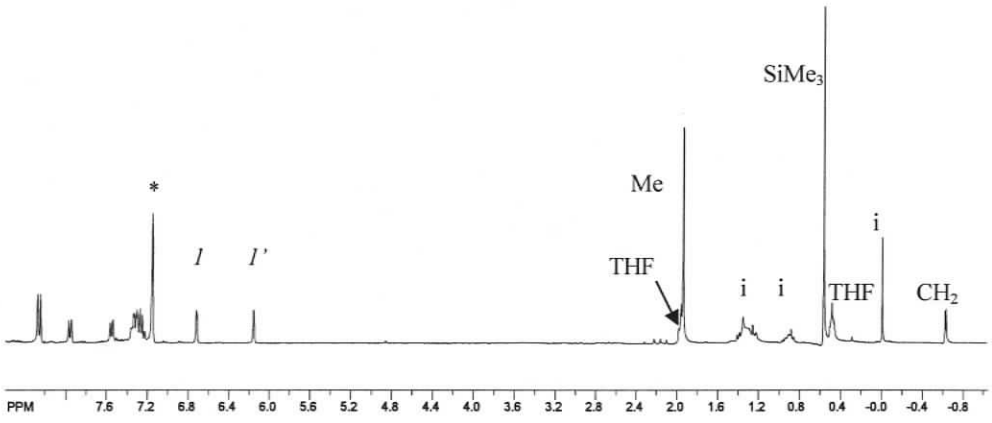

Figure 3.2. ^{1}H NMR spectrum (500 MHz, C_6D_6) of 147

A 2:1 stoichiometry reaction between (PCp*)H **108** and the yttrium tris(alkyl) precursor was tried on both preparative and NMR tube scale. In all cases, a significant amount of ligand remained in solution, even after extended periods of time. Attempts to force the reaction by heating were not feasible because of the thermal instability of $Y(CH_2SiMe_3)_3(THF)_2$. From this we conclude that the mono-ligand complex is stable

and that formation of a bis-ligand complex is kinetically slow, probably for steric reasons. Reaction of yttrium tris(alkyl) with one equivalent of (PCp*)H **108** in toluene overnight, followed by extraction with hexanes and crystallization, afforded very pale yellow plate crystals of (PCp*)Y(CH_2SiMe_3)$_2$(THF) (**150**) in 25% yield (**Scheme 3.4**). The low yield is due to difficulty in separating unreacted **108** from **150** and the high solubility of **150** in hexanes. Based on the substitution pattern for the PCp type ligands, it seems that substitution at the *1* and *3*-positions plays a more important role in formation of mono-PCp yttrium complexes than does substitution at the *2*-position.

The resonances of coordinated THF in **150** are at 2.52 ppm (α-protons) and 0.60 ppm (β-protons). The alkyl group resonances are observed at 0.26 ppm for $SiMe_3$ and -0.60 ppm for CH_2 ($^2J_{YH}$=3.2Hz, YCH_2), respectively (**Fig 3.3**). These proton resonances are similar to the complexes reported previously and bis-PCp^R complexes **147-149**. The equivalence of the two α-protons on each alkyl, as indicated by the simple doublet for YCH_2SiMe_3, indicates that rapid dissociation of THF from (PCp*)Y(CH_2SiMe_3)$_2$(THF) **150** and inversion at the metal center of (PCp*)Y(CH_2SiMe_3)$_2$ is possibly occurring in solution at room temperature (see **Section 3.5** for details).

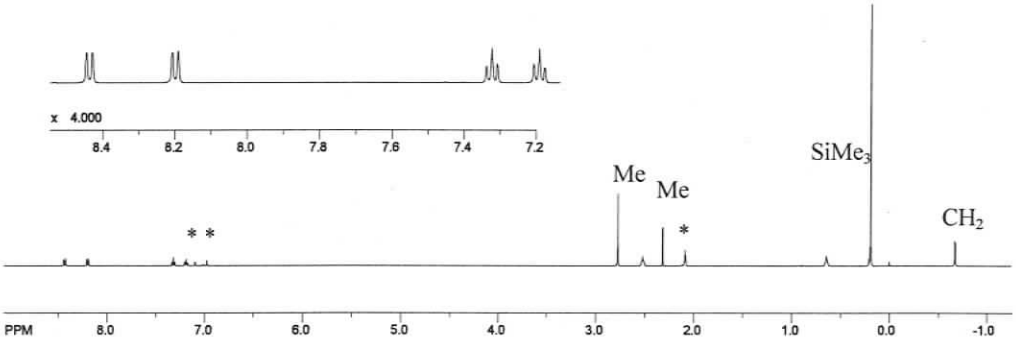

Figure 3.3. ^{1}H NMR spectrum (500 MHz, C_7D_8) of 150

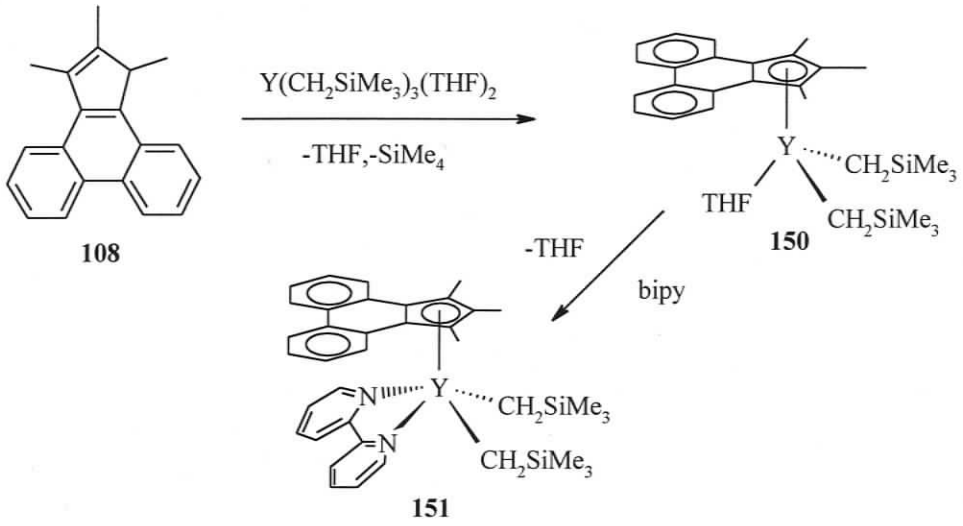

Scheme 3.4. Synthesis of mono-PCp* complex 150 and its bipy adduct 151

Complex **150** reacts with one equivalent of 2,2'-bipyridine (bipy) to give (PCp*)Y(CH_2SiMe_3)$_2$(bipy) (**151**) cleanly in NMR tube scale reactions (**Scheme 3.4**). Replacement of THF by bipy not only results in dramatic chemical shift changes for the aromatic protons of the PCp* ligand, but also results in two separate doublet of doublets for the α-protons at -0.23 and -0.44 ppm ($^2J_{YH}$=3.0Hz, $^2J_{HH}$=11.4Hz). This clearly shows that bipy is more strongly coordinated to the yttrium metal center and does not undergo a rapid dissociation process like THF in **150**. The equivalence of both halves of the bipy ligand is consistent with a C_S symmetry, pseudo-square pyramidal structure.

Both 2:1 and 1:1 stoichiometry reactions between (PCp')H **109** and yttrium tris(alkyl) were attempted. Surprisingly, information based on NMR spectroscopy is not conclusive for formation of either a bis or mono-PCp' complex. The ^{1}H NMR spectra showed dramatic changes with several resonances visible in the reaction

mixture in C_6D_6 overnight, possibly indicating ongoing redistribution processes. This observation seems to contradict the trend of analogous ligands because the two methyl groups on the five-membered ring fail to show a substantial effect on the formation of mono or bis-Cp complexes. On the other hand, (PCp')H **109** is less bulky than (PCp*)H **108**, but more bulky than (PCp^{Me})H **106**; thus, redistribution between bis and mono-PCp' complexes might be expected given its intermediate bulk.

Reaction of $Y(CH_2SiMe_3)_3(THF)_2$ with one equivalent of (sCp)H **110** proceeded smoothly in toluene overnight. Removal of toluene followed by extraction of the crude product with hexanes yielded (sCp)$Y(CH_2SiMe_3)_2$(THF) (**152**) as a pale yellow powder in 60% yield (**Eq 3.2**). Similarly to **150**, the ^1H and ^{13}C NMR spectra of **152** show resonances for the YCH_2SiMe_3 group at -0.98 ppm ($^2J_{YH}$ = 3.1Hz) and 37.92 ppm ($^1J_{YC}$ = 45 Hz), respectively (**Fig 3.4**), indicating rapid dissociation of THF and inversion at the metal center at room temperature. The resonances of coordinated THF were observed at 2.54 ppm (α-protons) and 0.59 ppm (β-protons).

Eq 3.2

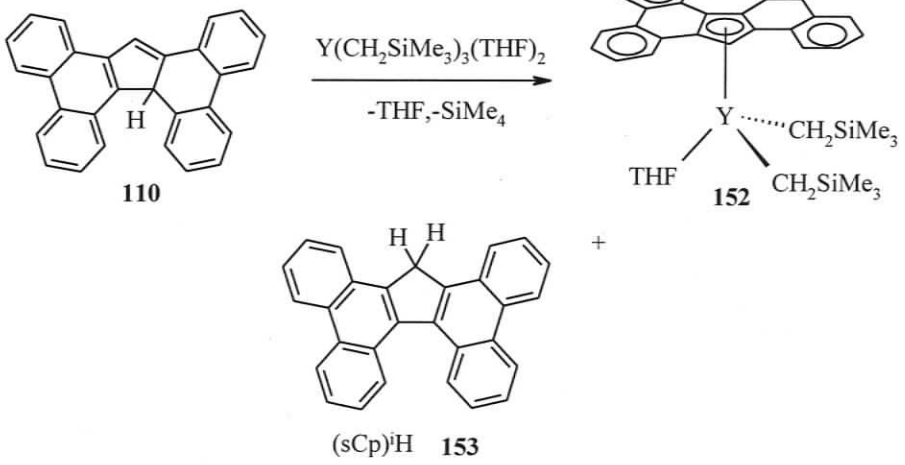

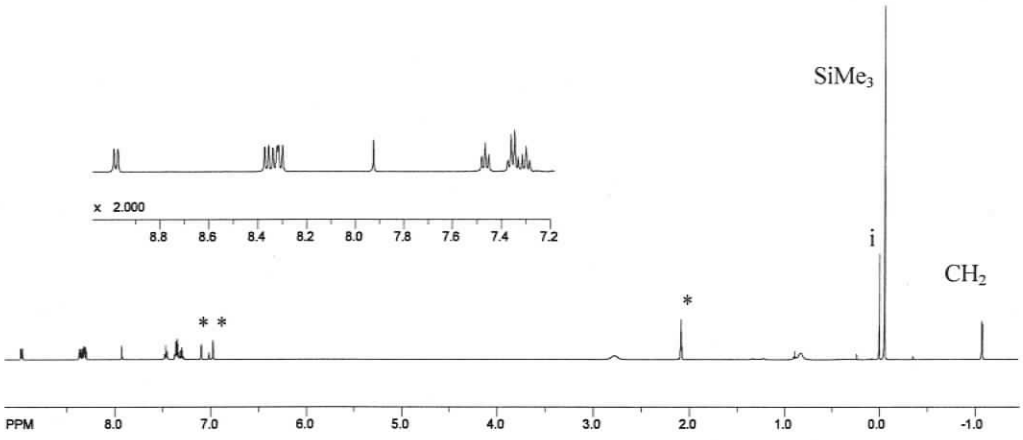

Figure 3.4. ^{1}H NMR spectrum (500 MHz, C_7D_8) of 152

The ^{13}C NMR DEPT spectrum shows nine different resonances for the aromatic carbons. Considering that there are seventeen C-H groups on the aromatic ligand, including one on the five-membered ring, this indicates that the sCp ligand has mirror plane symmetry in solution even though the ligand itself is known to be helically distorted in the solid state.[204] This indicates that rapid racemization of the sCp ligand occurs in solution at room temperature as shown schematically by the cartoon in **Eq 3.3**. X-ray suitable crystals were obtained from hexanes solution under -40˚C and confirmed the non-flat and rigid structure of this ligand (see **Fig 3.17**). Complex **152** shows good solubility in toluene and mediocre solubility in hexanes. It is quite stable in solution or the solid state but decomposes to a red solution with precipitate formation at 60˚C without any sign of a metallation product.

Eq 3.3

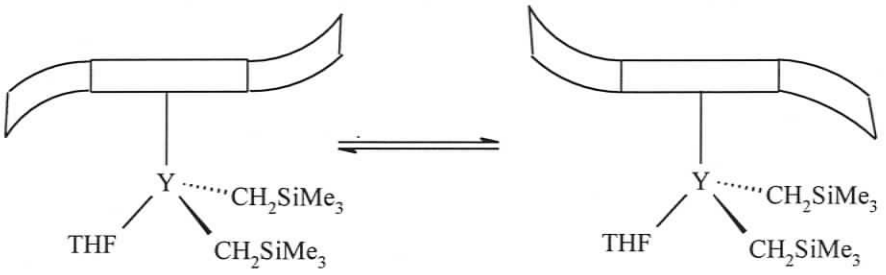

The isomer of the (sCp)H ligand, $(sCp)^{i}H$ **153** (see **Eq 3.2**), formed as a byproduct in the reaction between (sCp)H **110** and $Y(CH_2SiMe_3)_3(THF)_2$, could be separated from **152** and unreacted tris(alkyl) easily due to its low solubility in hexanes. $(sCp)^{i}H$ **153**, intentionally prepared from $(sCp^{-})Li^{+}$ and water, does not show any sign of reaction with yttrium tris(alkyl) over two days. This is consistent with the observation from the original reaction where yttrium tris(alkyl) and $(sCp)^{i}H$ **153** co-exist after long periods of time. A simple extended Hückel calculation reveals that the heat of formation (ΔH_f) of $(sCp)^{i}H$ **153** is about 10 kJ mol^{-1} lower than (sCp)H **110**, indicating that $(sCp)^{i}H$ **153** is the thermodynamically more stable isomer. Since it is highly unlikely that $(sCp)^{i}H$ **153** possesses a pKa larger than 45 (pKa of $SiMe_4$), the failure of $(sCp)^{i}H$ **153** to react with the tris(alkyl) must be due to slow kinetics of the σ-bond metathesis process.

Similarly to complex **151**, the bipy adduct $(sCp)Y(CH_2SiMe_3)_2(bipy)$ (**154**) was formed by addition of bipy to a C_6D_6 solution of **152**. Complex **154** shows relatively poor solubility in C_6D_6 and X-ray suitable crystals of **154** were obtained directly from the reaction mixture. The replacement of THF in **152** by bipy in **154** shows the same effect as in the related **151/150** pairing: dramatic chemical shift changes in the

aromatic region and two doublets of doublet resonances for the Y-CH_2 groups due to C_S symmetry in **154**. DME adduct (sCp)Y(CH_2SiMe_3)$_2$(DME) (**155**) was prepared in similar fashion (**Scheme 3.5**). Surprisingly, the CH_2SiMe$_3$ resonances do not show any significant chemical changes from replacement of THF by DME and remain a simple doublet indicating that rapid dissociation of DME molecule occurs at room temperature.

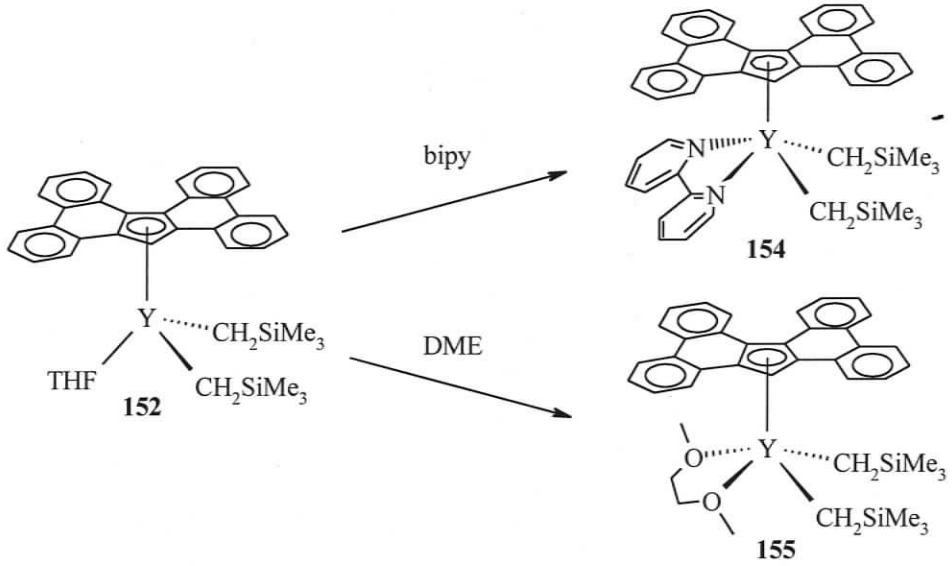

Scheme 3.5. Synthesis of bipy adduct 154 and DME adduct 155

3.2.3 Yttrium Complexes by Salt Metathesis

Although protonolysis reactions between neutral ligands and yttrium tris(alkyl) were quite successful, salt metathesis reactions were attempted as an alternate way to synthesize the alkyl complexes. Also, Y-Cl bonds can provide more potential for future functionalization. Salt metathesis reactions are the most common and important routes to synthesize lanthanide halide precursors. However, the disadvantage of this

route is the formation of alkali salt adducts in presence of coordinating solvent (anionic 'ate' complexes), and the adducts complicate product characterization and are very difficult to remove once formed.

Reaction of $(PCp^{Me})^{-}Li^{+}$, generated as an insoluble precipitate by reacting neutral ligand $(PCp^{Me})H$ **106** and n-BuLi in toluene, with YCl_3 in THF overnight afforded $(PCp^{Me})_2YCl(THF)$ (**156**) in 63% yield. Although the ^1H NMR spectrum of **156** was broad and not completely clean, the most distinctive feature of this complex, similar to **147** with C_S symmetry, was the observation of two separate resonances for the *1* and *1'* protons on the five-membered ring at 6.64 and 6.48 ppm. Treatment of **156** with excess MeLi in THF afforded $(PCp^{Me})_2Y(\mu\text{-}Me)_2Li(THF)_2$ (**157**) in 43% yield (**Scheme 3.6**). The ^1H NMR spectrum of **157** shows only one resonance for the *1* and *1'* protons on the five-membered ring with a simple ^{13}C resonance for the corresponding carbons consistent with an overall C_{2V} symmetry. Despite the fact that the $^2J_{YH}$ coupling is missing from the broad resonances at -2.25 ppm for the Y-Me groups, a $^1J_{YC}$ coupling constant of 50 Hz confirms the structure of **157**. Although **156** and **157** were prepared successfully by salt methathesis, the difficulty of purification limited further investigation of their reactivity.

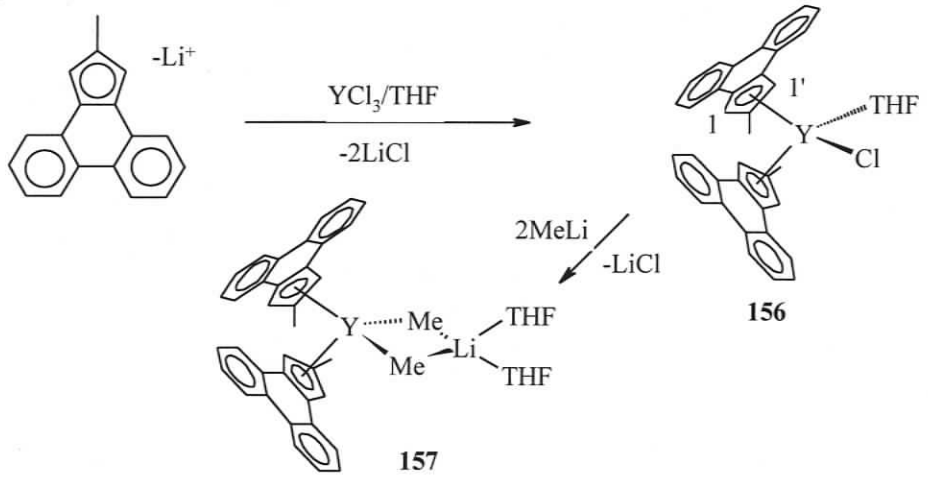

Scheme 3.6. Preparation of 156 and 157 by salt metathesis reactions

$(sCp)^-Li^+$ was prepared by treating (sCp)H **110** in THF with one equivalent of n-BuLi, followed by removal of the solvent. Surprisingly, the salt metathesis reaction between YCl_3 and $(sCp)^-Li^+$ afforded neutral product $(sCp^i)H$ **153** with either THF or toluene as solvent. Similarly, reaction of $(sCp)^-Li^+$ with YbI_2 afforded $(sCp)^iH$ **153** and several more attempts gave the same results. The reason for the generation of neutral ligand in the salt metathesis reactions remains unknown, but this meant that the salt metathesis route could not be investigated further.

3.2.4 Ytterbium Complexes by Protonolysis

When $(PCp^{Me})H$ ligand and $Yb[N(SiMe_3)_2]_2(THF)_2$ were stirred overnight in 2:1 ratio, they afford $(PCp^{Me})_2Yb(THF)_2$ (**158**) as a red powder in 74% yield. Complex **158** is very soluble in toluene or benzene, but insoluble in hexanes. The bis-PCp^{Me} structure of **158** can be confirmed by the absence of $N(SiMe_3)_2$ resonances, a single

resonance of CpC*H* at 6.32 ppm and the resonances of aromatic protons at 7.15-8.26 ppm.

Since Yb(II) is a good reducing agent, it was of some interest to see if **158** could reduce a suitable substrate. Aryldisulphides have been reduced in the past by $Cp^*_2Yb(OEt_2)$ to afford lanthanide thiolates, $Cp^*_2Yb(SAr)(OEt_2)$, that can serve as suitable precursors to lanthanide alkyls.[35] Two oxidation experiments were attempted between **158** and p-tolyldisulfide or bromobutane. Oxidation of **158** by p-tolyldisulfide in C_6D_6 gave a deep purple solution of $(PCp^{Me})_2Yb(S\text{-tolyl})(THF)$ (**159**) (**Scheme 3.7**). The dramatic change in color and the paramagnetic ^1H NMR resonances at 90 to -100 ppm are consistent with formation of an ytterbium thiolates similar to those made before.[35,205,206] Oxidation of **158** with bromobutane afforded neutral ligand and failed to give the expected Yb(III) complex.

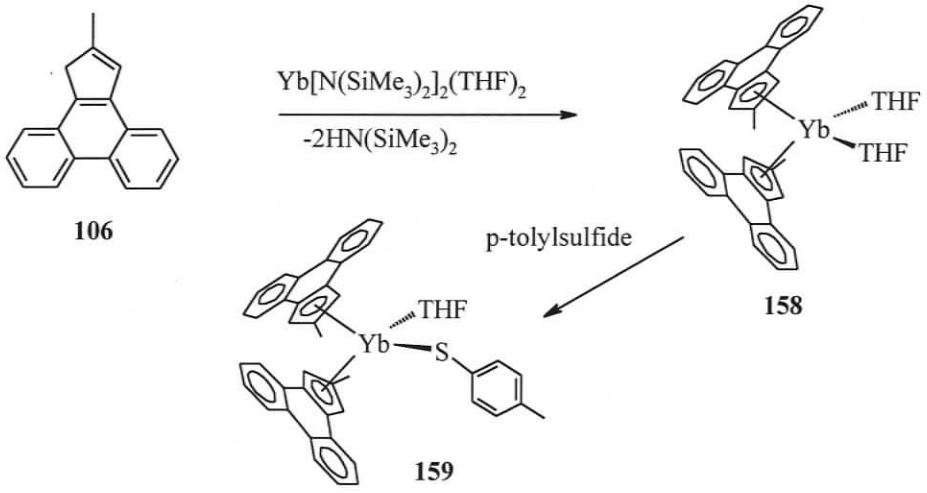

Scheme 3.7. Synthesis of ytterbium complexes 158 and 159

Reaction of $Yb[N(SiMe_3)_2]_2(THF)_2$ with two equivalents of (sCp)H in toluene overnight afforded a red-brown powder $(sCp)_2Yb(THF)$ (**160**) (**Eq 3.4**). The ^1H NMR of the crude product clearly shows the formation of neutral ligand isomer $(sCp)^iH$. Similar to **158**, the resonances of $N(SiMe_3)_2$ were not observed from the ^1H NMR spectrum, indicating that **160** is a bis-sCp complex. Recrystallization of the crude product gave red crystals of **160** in 46% yield. By comparison of the integrations for the THF and aromatic sCp ligand, only one THF molecule is coordinated to the metal center in **160**, clearly due to steric effects of the sCp ligands. The resonances of the THF molecule (1.47 ppm for α-THF CH_2) are very far upfield compared to **158**, indicating that an increased shielding from having two large aromatic systems takes place. The ^1H NMR spectrum of **160** also shows only nine resonances for the protons in the sCp **110** ligand (**Fig 3.5**), indicating that rapid racemization of the sCp **110** ligands take place in solution. This also means that the two chemically equivalent sCp **110** ligands do not interfere with each other sterically and formation of a bis-sCp complex does not have any substantial effect on ligand racemization.

Eq 3.4

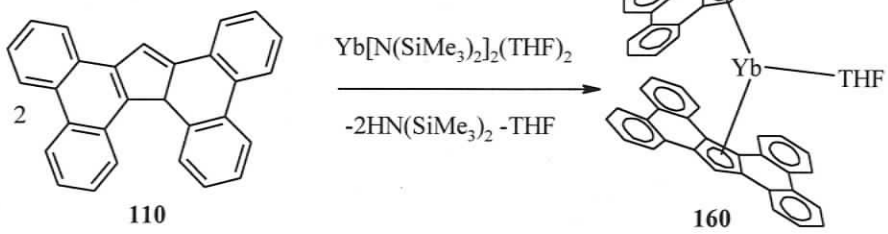

110 **160**

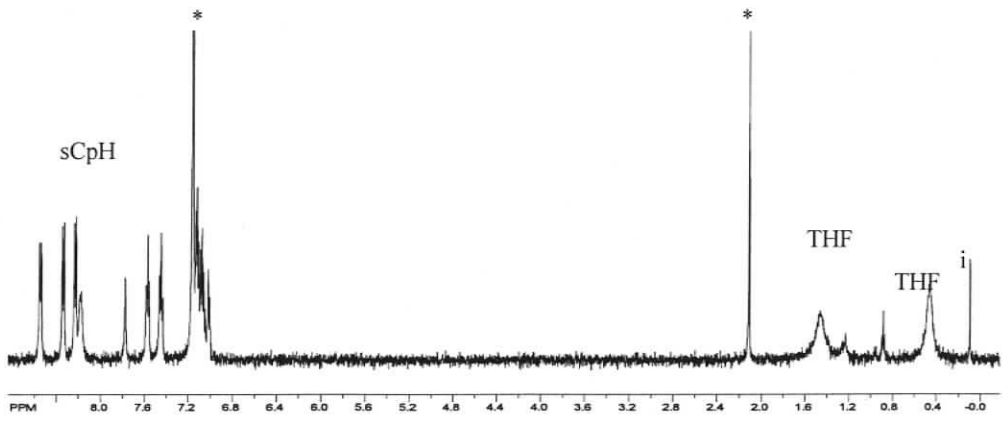

Figure 3.5. ^{1}H NMR spectrum (500 MHz, C_6D_6) of 160

Because both **160** and (sCp)^{i}H **153** are very soluble in toluene, it is quite difficult to separate clean **160** from this byproduct. Thus, the chemistry of this complex was not investigated in detail, except for the simple oxidation reaction with p-tolyldisulfide. The bright red color of **160** fades immediately after addition of p-tolyldisulfide. However, the ^{1}H NMR spectrum was not clean enough to characterize the product. Also, tiny bright yellow crystals that grew on the wall of the NMR tube were found to be an organic compound because no heavy metal atom was detected by X-ray crystallography. This indicates that loss of ligand from the extremely crowded Yb(III) metal center, formed after oxidation of Yb(II), takes place. We suspect that this organic compound is tetrabenzofluorenone because fluorenone was known to be bright yellow crystalline powder. Attempts to generate a mono-sCp complex using a 1:1 stoichiometry between $Yb[N(SiMe_3)_2]_2(THF)_2$ and (sCp)H **110** also produced bis-sCp complex **160** and (sCp)^{i}H **153**. This observation indicates that the mono-sCp intermediate $(sCp)YbN(SiMe_3)_2(THF)$ during formation of **160** is unstable and can readily react with a further equivalent of (sCp)H to generate **160**, consistent with the

larger ionic radii of the Yb(II) metal center in **160**. This can provide larger space for the second sCp ligand to bind compared with the smaller Y(III) metal center in **152**.

3.3 Reactivity Studies

3.3.1 Hydride Chemistry

Addition of phenylsilane to a hexane solution of **148** afforded a light orange-brown precipitate overnight. Although the ^{1}H NMR spectrum of the product was relatively messy, the triplet at 3.50 ppm (^{89}Y 100% natural abundance, I = ½; $^{1}J_{YH}$ = 34.5 Hz) indicated formation of a dimeric yttrium hydride $[(PCp^{Ph})_2Y(\mu\text{-}H)]_2$ (**161**) (**Eq 3.5**). Although X-ray quality crystals were obtained by crystallization of **161** from a toluene/hexane solution, the large scale preparation of clean **161** proved to be very difficult; making a detailed investigation of the chemistry of **161** impractical. However, **161** generated *in situ*, failed to show any catalytic activity towards the polymerization of ethylene. Reaction of **147** and **149** with dihydrogen gas or phenylsilane in hexanes and toluene afforded toluene or THF insoluble products, which could be hydride cluster complexes, since the ^{1}H NMR of the toluene-soluble residue did not show any signs of free ligand.

Eq 3.5

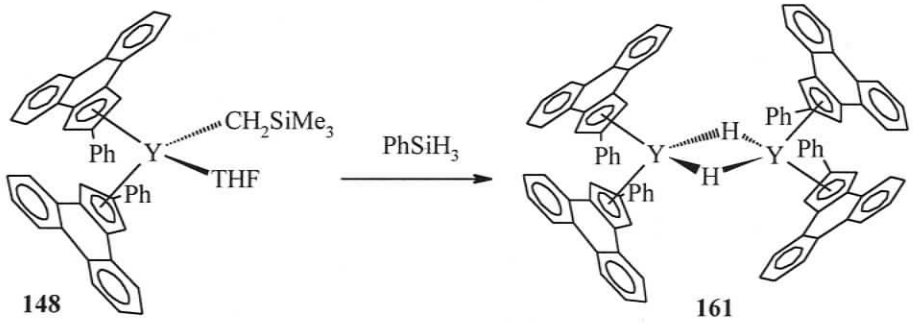

148 **161**

Reaction of **150** with phenylsilane in hexanes afforded a toluene-soluble red-brown powder; however, the ^{1}H NMR spectra was unable to provide any useful information to characterize this product. Moreover, crystallization of this product from toluene failed. In comparison, reaction of **150** with dihydrogen gas afforded only neutral ligand. Similar reactions were also attempted for **152** with both phenylsilane and dihydrogen gas. Both reactions afforded toluene and THF-insoluble but bromobenzene-soluble red-brown powders. Unfortunately, this product was unable to be characterized by the ^{1}H NMR spectrum and crystallization. Hydrolysis of these red-brown powders by a drop of water did afford neutral ligand and $SiMe_4$, and this process also generated a gas, assumed to be H_2. This suggests the presence of sCp, hydride and CH_2SiMe_3 ligand in what is possibly an oligomeric or polymeric product. Attempts to polymerize ethylene with these products failed but this is not surprising if the complexes contain extensive and strong hydride or alkyl bridges.

3.3.2 Insertion Chemistry

Complex **150** reacts with CO_2 gas overnight in hexanes to give a hexane-insoluble white precipitate of $(PCp^*)Y(O_2CCH_2SiMe_3)_2$ (**162**) (**Eq 3.6**). The ^{1}H and ^{13}C NMR spectra show disappearance of the CH_2 resonance at -0.60 ppm and appearance of a new CH_2 singlet at 1.10 ppm which shows no coupling to ^{89}Y (**Fig 3.6**). The ^{13}C NMR spectrum also shows a distinctive carboxylate carbon resonance at 185.4 ppm. A singlet resonance for CH_2SiMe_3 clearly shows the equivalence of the two α-protons and overall C_{2V} symmetry for **162**. This indicates that two equivalents

of CO_2 have inserted into the Y-CH_2 bonds. Moreover, this also indicates formation of either a four carboxylate-bridging dimer or a monomeric form of **162** because both of these two structures possess equivalent α-protons. No resonances for coordinated THF are visible in the spectrum consistent with a monomeric pseudo square pyramidal structure. Crystals obtained from toluene solution lose solvent rapidly and proved unsuitable for X-ray crystallography. Complex **152** also reacts with CO_2 but in this case a toluene and THF-insoluble product is formed which may be an oligomer containing bridging oxygen atoms of the carboxylate groups.

Eq 3.6

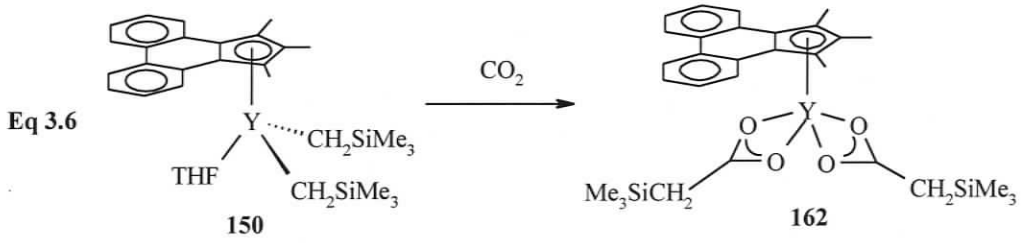

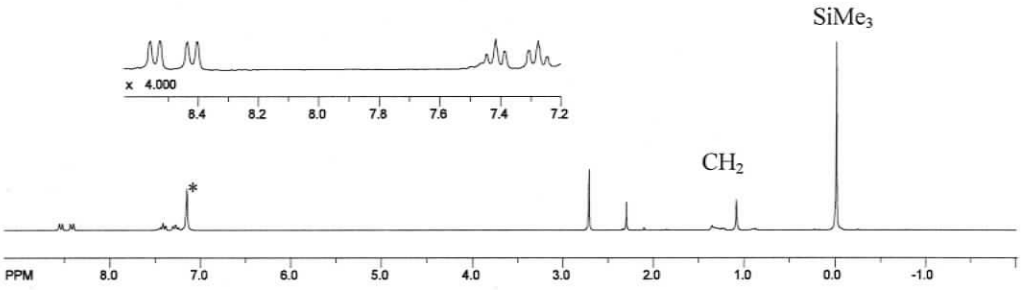

Figure 3.6. ^{1}H NMR spectrum (500 MHz, C_6D_6) of 162

Complex **150** also reacts with excess trimethylsilylisocyanate (Me_3SiNCO) to give an off-white powder of (PCp*)Y[κ^2-(N,O)-(Me_3SiNCO)CH_2SiMe_3]$_2$ (**163**). Similar to complex **162,** complex **163** shows significant shifting for the CH_2SiMe_3 protons from -0.60 to 1.65 ppm with disappearance of Y-H and Y-C coupling.

Complex **163** only shows a single resonance for each trimethylsilyl group consistent with either a cis (C_S) or trans (C_2) arrangement of the iminoacyl groups in a pseudo square pyramidal geometry. The α-protons of C-bonded CH_2SiMe_3 are expected to be inequivalent for both isomers. However, since a singlet resonance for these CH_2SiMe_3 protons is observed, this indicates that a rapid fluxional process occurs to make them equivalent. This could include dissociation of an Y-O bond followed by rotation around the C(acyl)-CH_2 bond and Y-N bond and reformation of the κ^2-(N,O)-iminoacyl (**Scheme 3.8**).

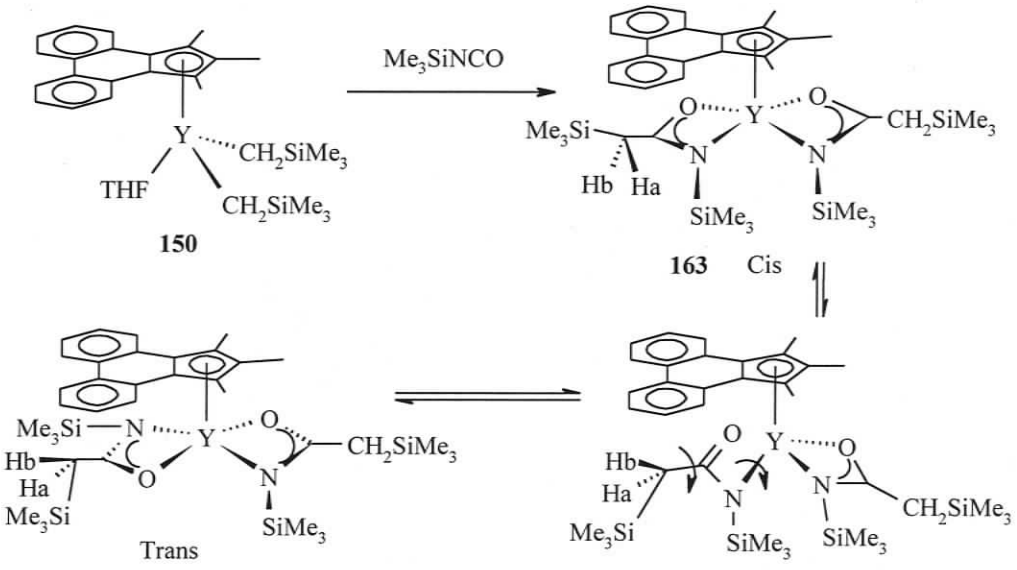

Scheme 3.8. Synthesis of 163 and its dynamic behaviour

Trimethylsilyl isocyanate also reacts with **152** in toluene overnight to afford an oily yellow-brown residue of (sCp)Y[κ^2-(N,O)-(Me_3SiNCO)CH_2SiMe_3]$_2$(THF) (**164**) in quantitative yield. Similar to **163**, formation of clean **164** can be seen by disappearance of Y-CH_2 coupling and a dramatic shift of the CH_2SiMe_3 resonance

from -0.98 ppm to 1.50 ppm. The resonances of THF are observed clearly at 2.99 ppm (α-THF CH_2) and it is very likely that **164** adopts pseudo-octahedral geometry with THF trans to the sCp ligand to minimize the steric effects. Thus, the coordination of THF has no substantial effect on the symmetry of **164** compared to **163**. The singlet for the CH_2SiMe_3 and $NSiMe_3$ resonances indicates that rapid Y-O bond dissociation and rotation is occurring at room temperature in order to generate the high symmetry environment observed (**Scheme 3.9**).

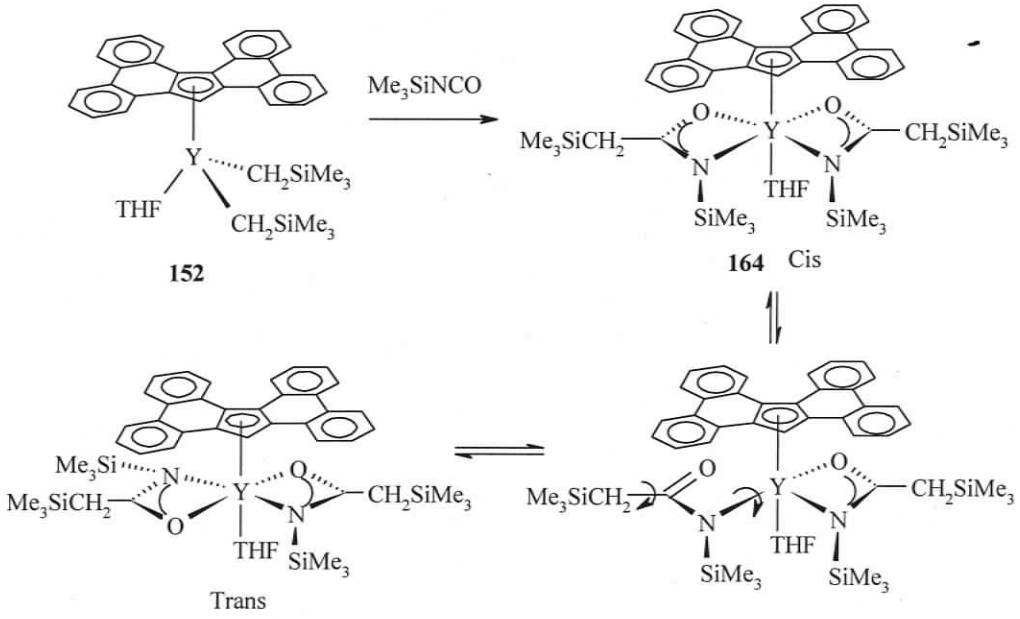

Scheme 3.9. Synthesis of 164 and its dynamic behaviour

The insertion of diisopropylcarbodiimide into **150** results in similar shift from -0.60 ppm to 1.83 ppm for the CH_2SiMe_3 resonance in (PCp*)Y[κ^2-(N,N)-iPrN(CH_2SiMe_3)CN(i-Pr)]$_2$ (**165**) (**Eq 3.7**). However, the insertion reaction of this diimide with **152** affords a much more complicated spectrum with two inequivalent isopropyl and trimethylsilyl groups, indicating a low symmetry insertion product.

More surprisingly, this product possesses one equivalent of sCp ligand to four equivalents of diisopropylcarbodiiminate from the relative integration of the sCp and i-Pr protons. Unfortunately, attempts to crystallize this product all failed and the exact structure of this product has not been ascertained at this point.

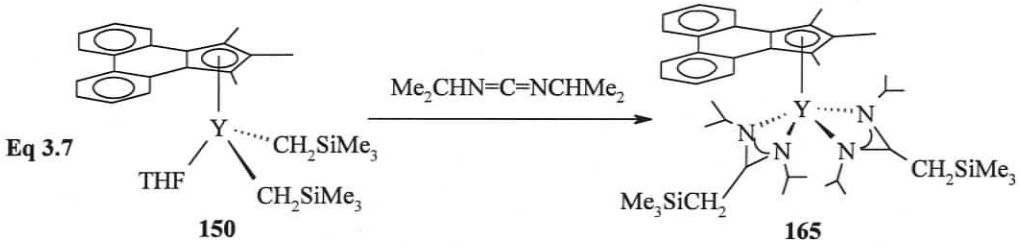

Eq 3.7

150 **165**

Insertion reaction between **150** or **152** and other small substrates, such as t-butylisocyanide (t-butylNC), t-butylnitrile (t-butylCN) and carbon monoxide (CO), were also attempted; however, these reactions failed to afford clean materials. This is not surprising since these initial insertion products are all bonded as monodentate ligands and the metal center is sterically unsaturated, possibly leading to complicated bridging interactions. Moreover, further insertion is possible which complicates the analysis of the reaction mixture. In contrast, complexes **162-165** all involve bidentate insertion products which help stabilize the metal center sterically and electronically, and further insertion of **162-165** was not observed.

3.3.3 Acid-Base Reactions

When complex **150** is treated with an excess amount of phenylacetylene (PhCCH), generation of a deep red-brown solution and disappearance of the CH_2SiMe_3 resonances is observed indicating complete protonation of the alkyl groups

to form a di-acetylide complex. However, the ^{1}H NMR spectrum was not very clean for this product, even with addition of D_8-THF to break any possible bridging interactions. Fortunately, complex **150** also reacts with two equivalents of the more bulky trimethylsilylacetylene (Me_3SiCCH) in toluene/THF mixtures to generate a toluene-soluble complex, $(PCp^*)Y(CCSiMe_3)_2(THF)$ (**166**) (**Scheme 3.10**). The ^{1}H and ^{13}C NMR spectra of **166** show only one resonance for the trimethylsilyl group, suggesting a structure with terminal acetylides in solution (**Fig 3.7**). Since lanthanide acetylide complexes were known to form dimers through the α-C,[207,208] it is quite straightforward to distinguish the dimeric and monomeric forms of the complex by chemical shifts and coupling constants for the Y-α-C bond. The presence of terminal acetylide is confirmed by the ^{13}C NMR spectrum in C_6D_6 solution that shows only one simple doublet at 171.2 ppm ($^{1}J_{YC}$= 55.5 Hz) for the yttrium-alkynide carbon at room temperature. In the solid state, **166** exists as an acetylide-bridged dimer $[PCp^*Y(CCSiMe_3)(THF)]_2(\mu\text{-}CCSiMe_3)_2$ (**167**) (**Scheme 3.10**) as shown by X-ray crystallography. Thus, an equilibrium between monomeric **166** and dimeric **167** occurs for this complex and the dimeric form **167** is preferred in the solid state. This observation is somewhat surprising because previously reported amido acetylide complexes possess very stable alkynide bridging interactions in solution and distinct, non-exchanging resonances for both terminal and bridging acetylides were observed.[209]

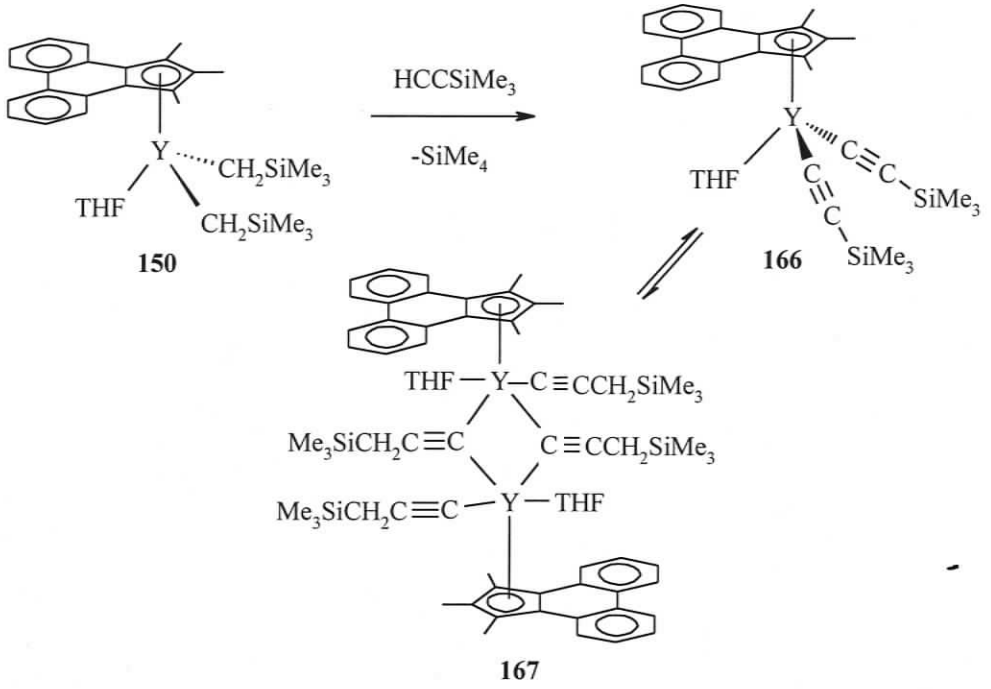

Scheme 3.10. Synthesis of acetylide complexes 166 and 167

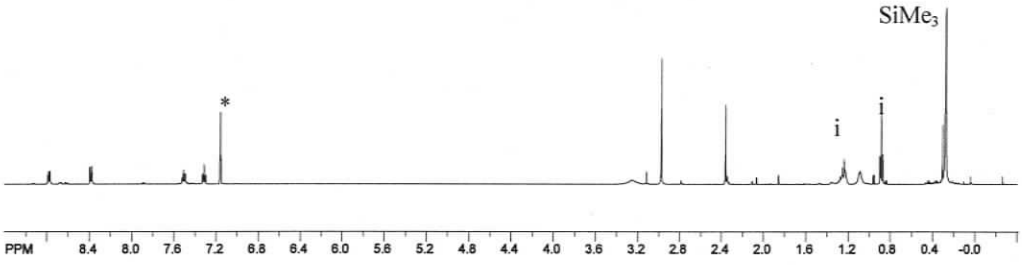

Figure 3.7. ^{1}H NMR spectrum (500 MHz, C_6D_6) of 166

Trimethylsilylacetylene also reacts with **152** in hexanes overnight to give a pale yellow toluene-insoluble powder. Addition of several drops of THF to the suspension of precipitate in toluene helps dissolve the product. The ^{1}H and ^{13}C NMR spectra confirm the formation of the acetylide complex (sCp)Y(CCSiMe$_3$)$_2$(THF) (**168**) (**Eq 3.8**). In the ^{13}C NMR spectrum, this complex shows a doublet at 172.46 ppm ($^{1}J_{YC}$= 47.8Hz) and a doublet at 111.95 ppm ($^{2}J_{YC}$= 8.8Hz, β-C) (**Fig 3.8**), as well as only one resonance for the SiMe$_3$ groups, supporting a monomeric complex in solution. This

reaction was also carried out in toluene to understand the effect of different solvents, but the same result was obtained. The white-grey precipitate formed in first stage was possibly an oligmer bonded through the α-carbon of the acetylides; after addition of strongly coordinating THF, the bridging acetylide bonds presumably break to generate the monomeric form of **168**, similar to the acetylide chemistry of previously reported $Cp^*Lu(CH_2SiMe_3)_2(THF)$.[58]

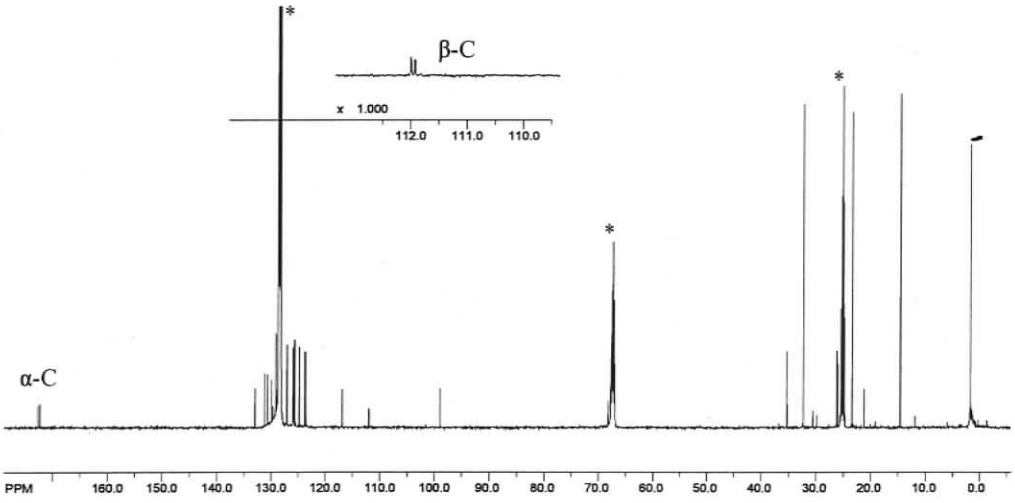

Figure 3.8. ^{13}C NMR spectrum (125 MHz, D_8-THF/C_6D_6) of 168

Eq 3.8

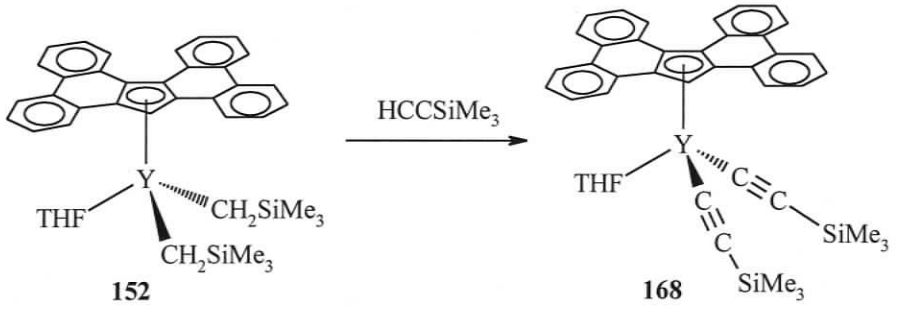

152 **168**

Crystallization of **168** from toluene afforded a very small amount of acetylide cluster **169** with three yttrium metal centers (see **Fig 3.19**, P116), consistent with the observation in **167** that the acetylide bridging interactions are preferred in the solid

state. Surprisingly, the structure was determined to contain one $sCpY(CCSiMe_3)_2$ unit and two $Y(CCSiMe_3)_3$ units in a tri-nuclear cluster. Since the protonolysis reaction of sCpH ligand with yttrium tris(alkyl) is not 100% complete, the unreacted yttrium tris(alkyl) left in solution may react with excess amount of $HCCSiMe_3$ to generate a $Y(CCSiMe_3)_3$ species. Considering the formation of **167** at -40 °C, the cluster **169** is also favored at low temperature.

Reactions were also attempted with various other substrates such as phenylphosphine, diphenylphosphine and t-butylphosphine. Unfortunately, these reactions failed to give clean products for characterization, even though in all cases the substrate indeed reacted with the bis-alkyl complexes.

3.3.4 Metallation Reactions

Pyridine and pyridine N-oxide react with both **150** and **152** as indicated by the disappearance of CH_2SiMe_3 resonances and dramatic color change, although none of these reactions gave clean characterizable products. In view of this, 2,4,6-trimethylpyridine (collidine), a much bulkier pyridine derivative, was reacted with **152** and afforded a red-orange powder, shown to be $(sCp)Y[\kappa^2\text{-}(N,C)\text{-}CH_2\text{-}(C_5H_2N\text{-}4,6\text{-}Me_2)]_2(collidine)_3$ (**170**) (**Eq 3.9**) in 50% yield. The ^1H NMR spectrum of **170** clearly shows two types of collidine groups coordinated to the metal center. A single resonance is observed at 6.43 ppm for aromatic C*H* protons on N-coordinated collidines while two resonances are observed at 5.77 ppm and 5.33 ppm for the two inequivalent aromatic C*H* protons on the metallated collidines (**Fig 3.9**). Although the

distinct doublet carbon and doublet of proton resonances for the Y-CH_2 groups were not observed, possibly due to a rapid dynamic process of **170** in solution, a broad singlet resonance at 1.62 ppm in the ^{1}H NMR showed a C-H correlation with a weak resonance at 50.13 ppm in the ^{13}C NMR spectrum. The chemical shift of these proton and carbon resonances are consistent with previously reported metallation products and clearly shows the presence of Y-CH_2 groups in **170**.[210] Relative integration shows the presence of two metallated and three coordinated collidines in this complex.

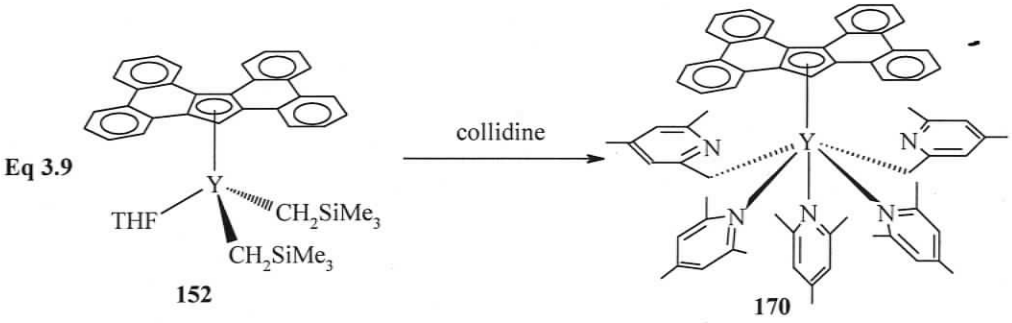

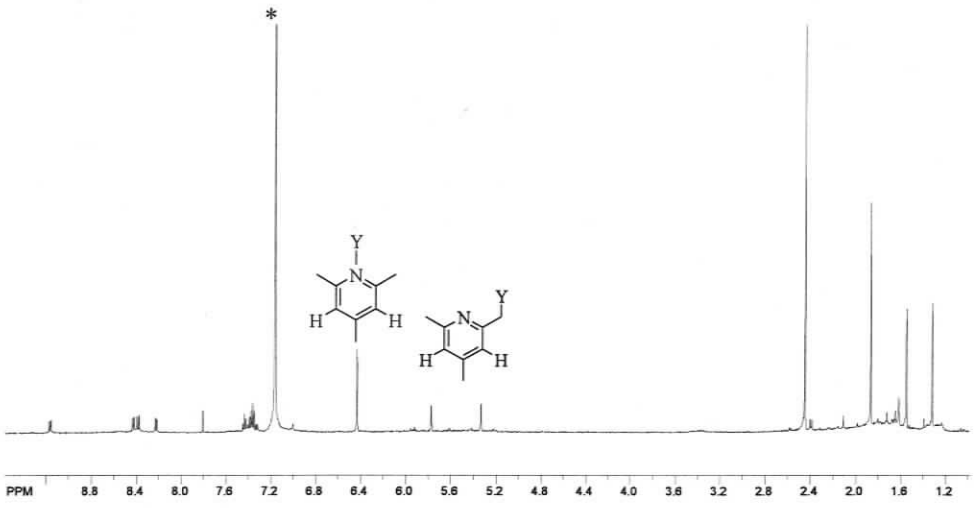

Figure 3.9. ^{1}H NMR spectrum (500 MHz, C_6D_6) of 170

The bonding pattern in **170** is somewhat surprising because the coordination sphere appears to be very crowded with five bulky collidines, especially given the fact

that the two metallated collidines can also possibly possess extra N-coordination. Moreover, the equivalence of all three N-coordinated collidines in **170** indicates an ongoing rapid exchange of coordinated collidine, because the observed symmetry is far higher than any possible static structure of **170**. Although pyridine is known to be a stronger Lewis base than THF and does not usually undergo any dissociation process as observed in complexes **151** and **154**, the extremely crowded metal center in **170** and the bulkier nature of collidine clearly overcomes the strong Y-N coordination bond leading to rapid exchange. Moreover, a possible hapacity shift for sCp from η^5 to η^3 may help to stabilize the crowded metal center, although this is a speculation in the absence of a solid state structure.

3.3.5 Reactions with Tri-alkyl Aluminum Reagents

Reaction of complex **150** with a large excess of $AlMe_3$ in toluene or hexane overnight gave a hexane-soluble product that failed to provide clean NMR information for characterization. In contrast, **152** reacted with $AlMe_3$ under the same condition to give a toluene-insoluble white grey precipitate. Addition of drops of THF to the suspension of this precipitate in toluene, followed by removal of the solvent and washing with hexanes, gave a pale yellow powder of $(sCp)_2YMe(THF)$ (**171**) in 15% yield (**Scheme 3.11**). The ^1H NMR spectrum of **171** shows a Y-CH_3 doublet resonance at -2.80 ppm (d, $^2J_{YH}$ = 2 Hz) with the correct integration relative to the aromatic ligand resonances (**Fig 3.10**). The ^{13}C DEPT spectrum shows seventeen

resonances for the carbons of the sCp ligand. This provides proof of an asymmetric structure for the two halves of the sCp ligand and formation of a bis-ligand complex.

In the first stage, the precipitate in C_6D_6/D_8-THF shows the same resonances as the final product **171**, as well as an additional resonance at -0.45 ppm [(THF)(Al*Me*$_3$)], which can be washed away by hexanes (**Fig 3.10**). This indicates that there is only a single type of methyl group associated with aluminum. As a strong Lewis base, THF breaks any bridging methyl bonds between the $AlMe_3$ unit and the metal center to form a ($AlMe_3$)(THF) which is readily washed away by hexanes. Thus, the spectrum of the original precipitate is actually complex **171** with the presence of (THF)($AlMe_3$) adduct. However, there is still the question of the step at which redistribution involving the sCp ligand occurs: i) redistribution takes place in the original reaction mixture after formation of (sCp)Ln[(μ-Me)$_2$AlMe$_2$]$_2$ **172** as an initial product (**Scheme 3.11**); ii) redistribution occurs after breaking of the bridge bonding between Al-Me-Y by THF to form a (THF)($AlMe_3$) adduct, and (sCp)YMe$_2$(THF) that redistributes to **171**. Two $AlMe_3$ units are expected for the second route; however only one $AlMe_3$ unit is observed in the precipitate as indicated by a 3:1 NMR integration of (THF)($AlMe_3$) relative to Y-Me (**Fig 3.10**), indicating that redistribution takes places by the first route. Compared to the stable, previously reported Cp*Ln[(μ-Me)$_2$AlMe$_2$]$_2$ **173**,[211] the redistribution process to form **171** is somewhat surprising because sCp is a bulkier ligand than Cp* and the intermediate (sCp)Ln[(μ-Me)$_2$AlMe$_2$]$_2$ **172** in this reaction is expected to be more stable.

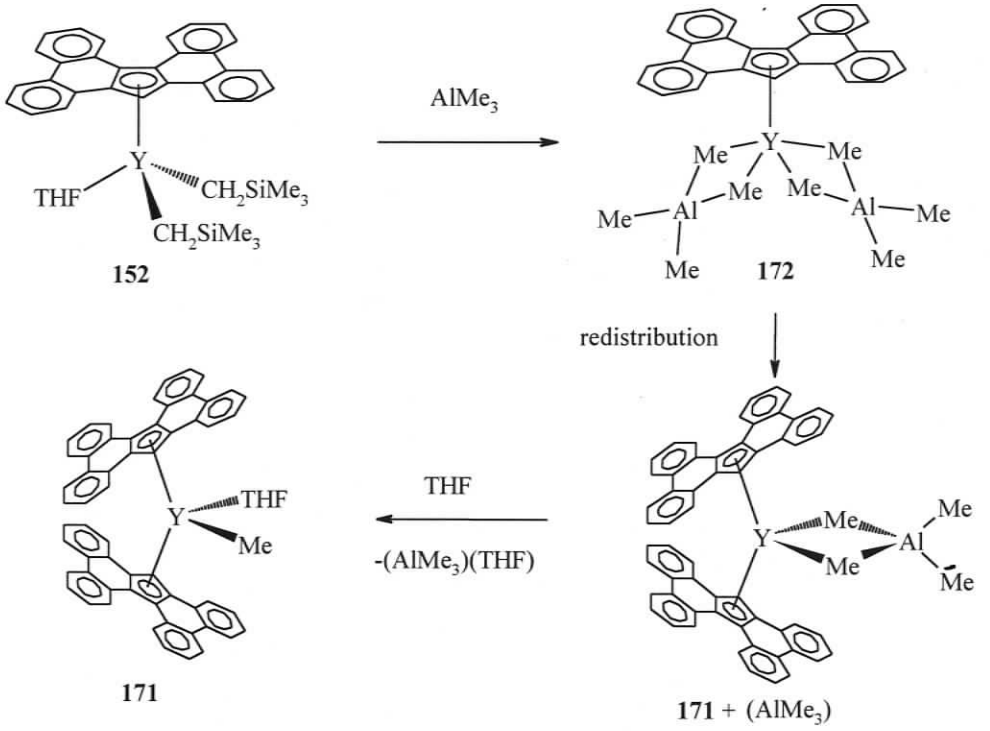

Scheme 3.11. Synthesis of 171

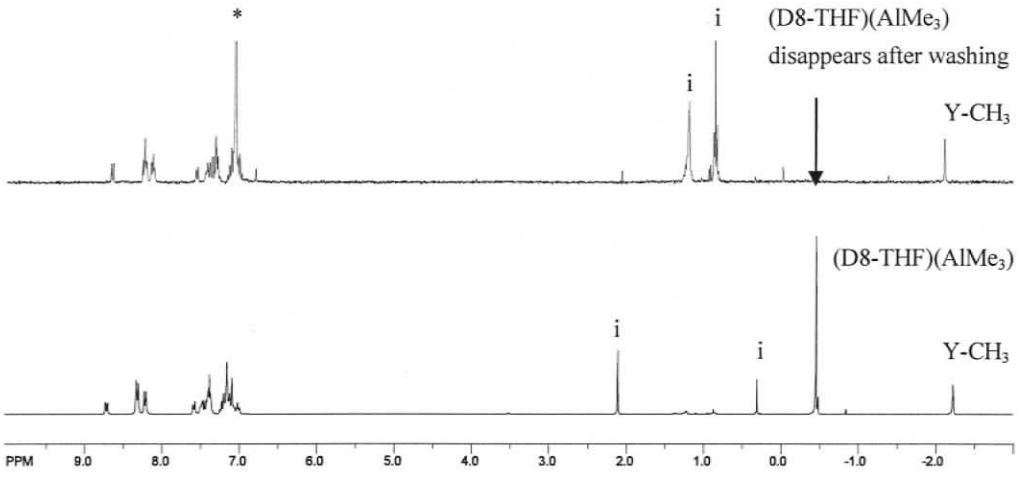

Figure 3.10. ^{1}H NMR spectrum (300 MHz, C_6D_6) of 171 formed from 172 by treatment with D_8-THF: before (bottom) and after (top) washing with hexanes.

As mentioned above, **171** possesses two asymmetric halves for the sCp ligand. There are two possible ways to generate asymmetry for the sCp ligand: i) the small ionic radius of yttrium results in close interaction between the two large sCp ligands,

leading to slow racemization of the sCp ligand thus generating a chiral metal center or ii) simple asymmetric bonding caused by THF and Me groups, as in complexes **147-149** in which the metal centers bind CH_2SiMe_3 and THF. A combination of these two factors is also possible (**Fig 3.11**). In the case of (ii), this implies that THF dissociation or inversion at yttrium is slow on the NMR time scale. Depending on the bending direction of the sCp ligand, two meso-isomers still possess C_S symmetry leading to equivalence of the two sCp ligands with two asymmetric halves, which is the combination of the chirality of the sCp ligands and the asymmetric bonding of Me and THF. The racemic mixture of two enantiomers does not possess any symmetry, leading to 33 (2*16+1) resonances in the ^{13}C DEPT NMR spectrum, inconsistent with the 17 (16+1) resonances observed. Therefore, a single meso isomer is the only structure that matches the observations for a slow racemization process. However, such a static structure is very unlikely because the meso isomers are clearly more crowded than the enantiomeric pair and it also seems unlikely that only the meso isomer would form in the reaction. Therefore, we favor slow exchange of THF and rapidly racemizing sCp ligands as the explanation for the observed solution behaviour.

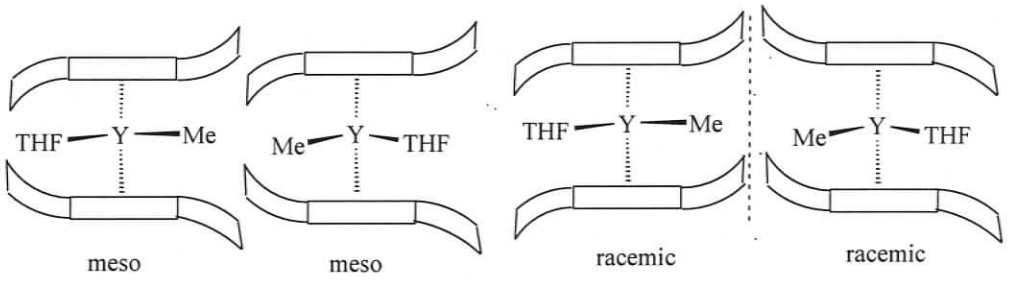

Figure 3.11. Isomers for sCp ligand in a slow racemization process in 171

Given the low yield (15%) of **171**, the remaining toluene-soluble residue from the reaction mixture was also investigated. However, the NMR information is much more complicated than that of **171**, so we were unable to fully characterize this residue. Addition of THF, followed by washing with hexanes, afforded a product with a simpler, but similar, spectrum to **171**. Presumably this indicates a similar structure to **171** after any bridging bonds are broken by coordinating THF. Crystallization of **171** and this residue failed to give X-ray quality crystals.

3.3.6 Mixed Ligand Complexes

Synthesis of mixed Cp ligand complexes is often a challenge because the complexes normally undergo redistribution to form more stable homoleptic Cp complexes. Interestingly, reaction of $(PCp^{Me})H$ ligand with **152** in toluene cleanly afforded the mixed Cp complex $(PCp^{Me})(sCp)Y(CH_2SiMe_3)(THF)$ (**174**) as a yellow-brown solid in quantitative yield (**Eq 3.10**). The complex is chiral at the metal because of the four different ligating groups. The slow dissociation of THF can be seen from the upfield resonances at 1.35 ppm (α-THF CH_2) for the THF molecule. The two α-protons of the Y-CH_2SiMe_3 group each show a doublet of doublet resonance with $^2J_{HH}$ = 10 Hz and $^2J_{YH}$ = 3.7 Hz. The protons of THF also show an asymmetric pattern with four different resonances, an indication of two chemically inequivalent protons on the α and β carbons respectively. Although the two Cp ligands are very bulky and rigid, THF still can rotate freely to simplify the pattern of resonances. This is clear because rotation about the Y-O bond results in exchange of

H_1 with H_4 and H_2 with H_3 on the NMR timescale (**Eq 3.11**). Only one carbon resonance for the α and β carbons further proves that the rotation about Y-O bond is rapid but on/off dissociation/reassociation by THF is slow on the NMR timescale at room temperature.

Eq 3.10

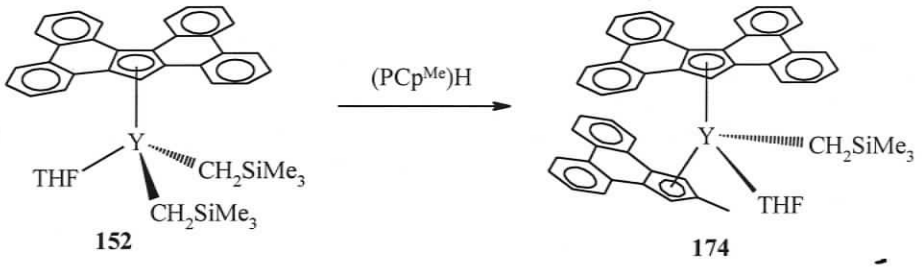

Eq 3.11

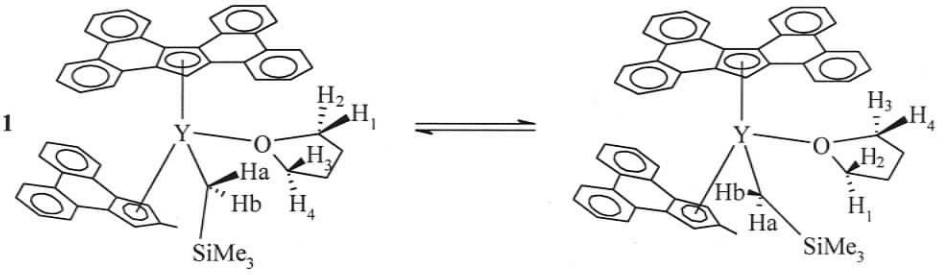

Preparation of the mixed ligand complexes from **152** was also attempted with CpH, Cp*H, $(Me_3Si)CpH$ and $(Me_3Si)_2CpH$; however, only $(Me_3Si)_2CpH$ gave a clean product, $[(Me_3Si)_2Cp](sCp)YCH_2SiMe_3(THF)$ (**175**) (**Eq 3.12**). All other reactions either afforded a product with a very complicated spectrum or appeared to decompose in solution over time, both phenomena possibly indicating ongoing ligand redistribution. Similar to **174**, the ^1H NMR of **175** shows two doublet of doublet resonances for the CH_2SiMe_3 protons and separate triplets for the α-protons of THF, indicating the formation of a mixed ligand complex. The inequivalent halves for $(Me_3Si)_2Cp$ can be observed clearly from three C-H resonances at 6.19, 5.66 and 4.61

ppm. Although two inequivalent Me_3Si groups of $(Me_3Si)_2Cp$ should also be observed, five carbon resonances of Me_3Si possibly indicate slow rotation of the Me_3Si-C bond in **175**, clearly due to steric effects of two bulky ligands. This complex is quite stable in both solution and the solid state, as indicated by observation of a clean NMR spectrum over a period of a month with no sign of redistribution or decomposition.

Eq 3.12

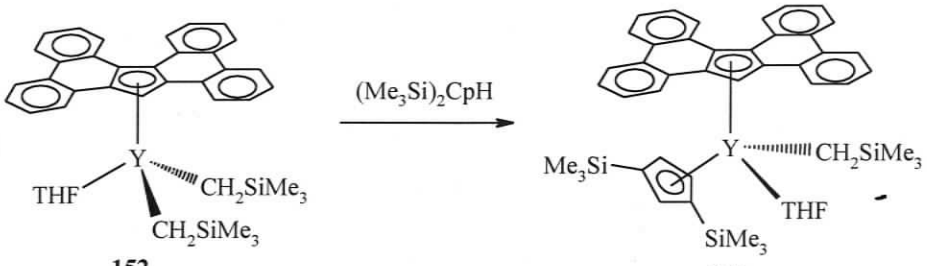

152 **175**

Recrystallization of **175** afforded very small amount of colourless plates suitable for X-ray crystallography; surprisingly, the structure of the crystals was determined to be $\{[(Me_3Si)_2Cp]_2Y(\mu\text{-}Cl)\}_2$ (**176**), which has been previously synthesized by the salt metathesis reaction between $(Me_3Si)_2Cp^-$ anion and metal halide. Exess neutral $(Me_3Si)_2CpH$ would react with yttrium tris(alkyl) (left over from reaction of yttrium tri(alkyl) with sCpH to give **175** to give the expected alkyl complex, but this does not explain the presence of chloride. The formation of chloride dimer can be explained by: i) the sCp ligands in **175** redistribute and bind free YCl_3 being present in the yttrium tris(alkyl) or ii) a small portion of $Y(CH_2SiM_3)_2Cl(THF)_2$ crystallized with the yttrium tris(alkyl) and then reacted with $(Me_3Si)_2CpH$ to form the dimeric yttrium chloride **176**. Considering the excellent stability of **175** in solution or the solid state, route ii) seems more likely despite the absence of conclusive evidence.

3.3.7 Polymerization Chemistry

Although a bis-PCp yttrium cation is not expected to be active for olefin polymerization due to a lack of an yttrium alkyl unit, structures of this type are still very interesting because of their rareness. Addition of one equivalent of $[Ph_3C]^+[B(C_6F_5)_4]^-$ or $B(C_6F_5)_3$ was used to generate the cation from complex **147** by alkyl abstraction in toluene. Reaction of $B(C_6F_5)_3$ with **147** afforded an oily residue that was sparingly soluble in THF or bromobenzene. The disappearance of the CH_2SiMe_3 resonances and the formation of an oil are consistent with other lanthanide cations that have been prepared with $[Ph_3C]^+[B(C_6F_5)_4]^-$ or $B(C_6F_5)_3$, although crystalline cationic species were obtained by other regeants and methods.[212,225]

Bis-alkyl complexes **150** and **152** can be converted to the cationic mono-alkyl derivatives by reaction with one equivalent of $[Ph_3C]^+[B(C_6F_5)_4]^-$ in toluene. The slow addition of $[Ph_3C]^+[B(C_6F_5)_4]^-$ to **150** or **152** is essential, because excess $[Ph_3C]^+[B(C_6F_5)_4]^-$ can potentially form the dicationic species that is inactive for polymerization. Although the cation of **150** generated on either preparative or NMR scale did not afford any clean NMR spectra in either C_6D_6 or C_6D_5Br, this cation $[(PCp^*)YCH_2SiMe_3(THF)]^+[B(C_6F_5)_4]^-$ (**177**) (**Eq 3.13**) does show moderate ethylene polymerization activity on the order of 21 kg $mol^{-1}bar^{-1}h^{-1}$ at room temperature with an induction time of 90 minutes. Complete generation of cation **177** from **150** can be easily distinguished by a color change of the reaction mixture from bright red to very pale yellow. A relatively long induction period is necessary because the reaction

mixture did not show any catalytic activity after 30 minutes reaction under the same conditions.

In contrast to $[Ph_3C]^+[B(C_6F_5)_4]^-$, the reaction mixture generated from $B(C_6F_5)_3$ and **150** did not show any catalytic activity for the polymerization of ethylene even after two hours. This is not surprising because the cation generated from $B(C_6F_5)_3$ and **150** may form bridging interactions between the partially abstracted CH_2SiMe_3 group of $[B(C_6F_5)_3(CH_2SiMe_3)]^-$ and the metal center leading to incomplete generation of a true yttrium alkyl cation center. This results in low electrophilicity of the metal center and the absence of a coordination site for olefins, consequently leading to lack of catalytic activity.

Eq 3.13

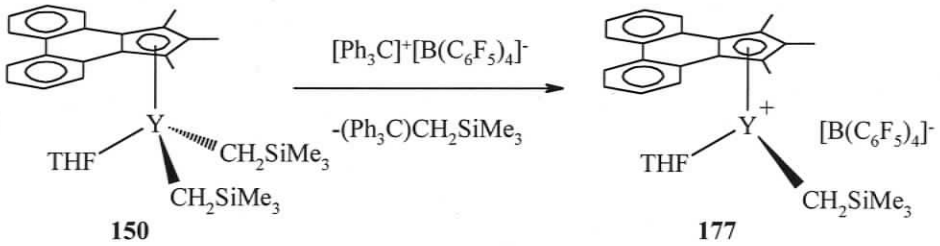

150 **177**

In toluene, the reaction mixture of **152** and $[Ph_3C]^+[B(C_6F_5)_4]^-$ changed from orange-red to pale yellow in 30 minutes, indicating a complete reaction to generate $[(sCp)YCH_2SiMe_3(THF)]^+[B(C_6F_5)_4]^-$ (**178**) (**Eq 3.14**). The ^1H NMR spectrum in C_6D_6 shows significant changes in chemical shifts for all protons, but especially for the CH_2SiMe_3 group (-0.98 ppm to -0.82 ppm) and the proton on the five-membered ring (8.0 ppm to 7.61 ppm). The freshly generated cation shows moderate ethylene polymerization catalytic activity of 36 kg mol^{-1} $bar^{-1}h^{-1}$. Surprisingly, this cation fails to catalyze the polymerization of ε-caprolactone, but does show low activity towards

the polymerization of styrene. Similar to **150**, the cation generated from $B(C_6F_5)_3$ did not show any catalytic activity for ethylene polymerization, although the formation of an oil suggests that partial alkyl abstraction by boron has occurred.

Eq 3.14

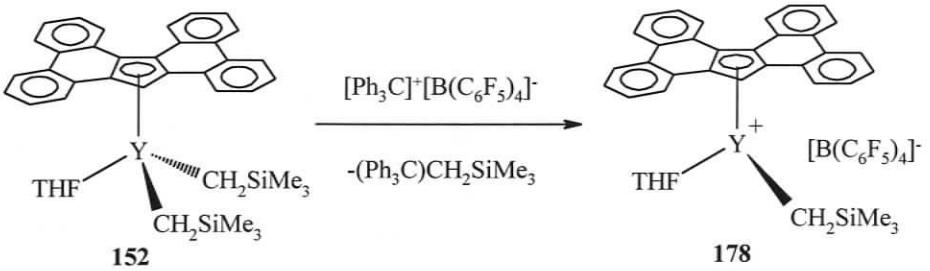

152 **178**

Interestingly, yellow plate crystals, obtained after placing the sealed NMR tube containing **178** outside of the glovebox for two weeks, turned out to be sCp ligand dimer **179** (**Fig 3.12**). This may be due to the presence of trace oxygen leaking into the NMR tube and oxidizing the sCp anion to the radical which dimerizes to form the ligand dimer.

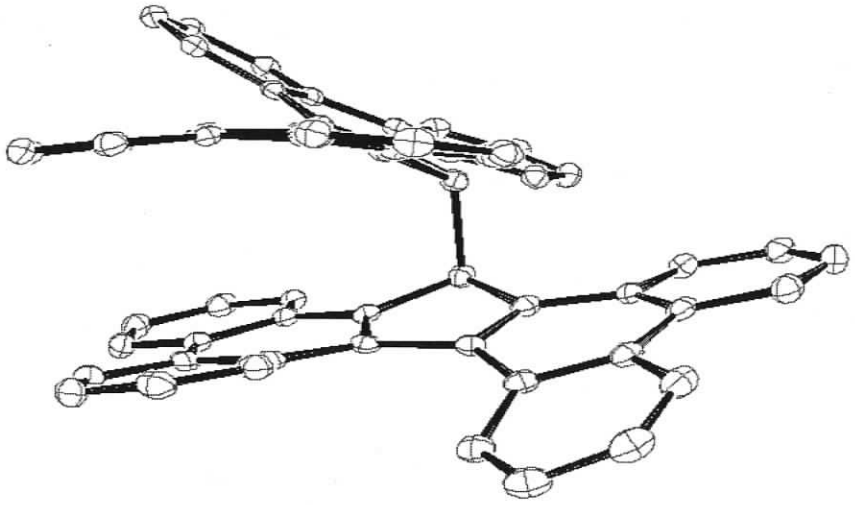

Figure 3.12. Ortep3 drawing (thermal ellipsoid 50% probability) of 179

3.4 Solid State Structures

3.4.1 X-ray Structures of PCp^R Complexes 147 and 161

Complex **147** was characterized by single crystal X-ray diffraction and its structure is shown in **Figure 3.13**. Only one of two molecules in the asymmetric unit is shown in this figure. Complex **147** adopts a pseudo-tetrahedral geometry with THF positioned in the twisted wedge formed by the two PCp^{Me} ligands and the CH_2SiMe_3 group projecting outside the wedge to avoid steric interactions with the fused phenanthrene skeleton. The PCp^{Me}(cent)-Y-PCp^{Me}(cent) angle of **147** (133.6°) is similar to the Cp*-Y-Cp* angles reported previously,[213,214] including those in $Cp^*_2YCl(THF)$ and $Ind^*_2YCl(THF)$ (**Table 3.1**).[215,216] The Y-CH_2SiMe_3 (Y-C(41)) bond distance of **147** (2.398 (6) Å) is also similar to those previously reported in yttrium Cp* alkyl complexes. The C-C bond lengths within the central six-membered ring are significantly longer than in the other two rings, i.e., C(12)-C(13) (1.454(9) Å) compared to C(11)-C(12) (1.415(9) Å). These data are consistent with localized 6π electron rings and localization of electron density on the five-membered ring as calculated in Chapter One. The torsion angle between the two ligands is 117.0°. This indicates a significant twist between the two ligands, essentially due to the steric effects of phenanthrene fusion. Most of the yttrium indenyl complexes are ansa-metallocene complexes where there is linkage between ligands so they are not comparable to complex **147**. An yttrium chloride complex with heptamethylindenyls as ligands (Ind*) shows a similar Ind*-Y-Ind* angle, but a much smaller torsion angle of 40°.[215] The huge difference in torsion angle between our complexes and previous

ones shows that the size and shape of the ligand have a substantial effect on the structure of the complex.

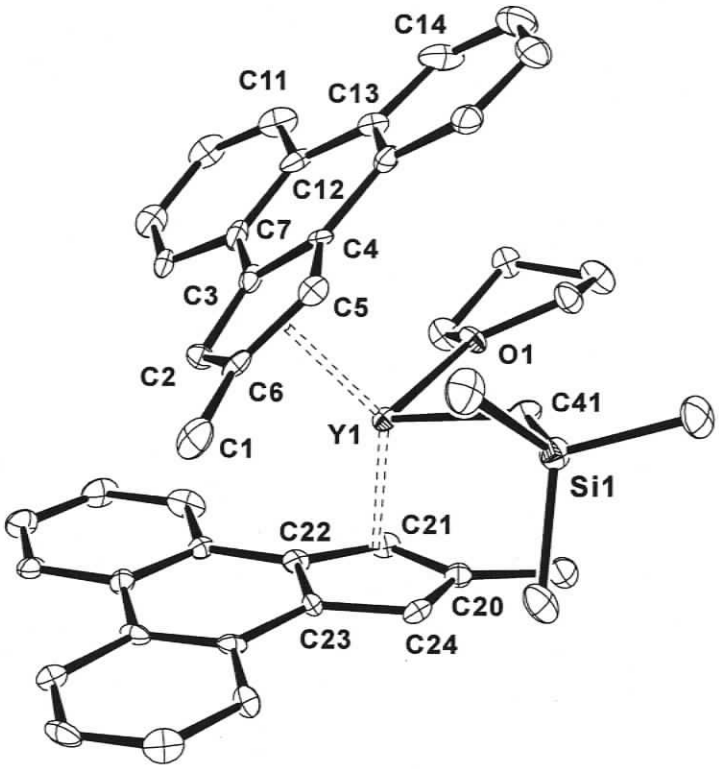

Figure 3.13. Ortep3 diagram (thermal ellipsoid 50% probability) of 147

Table 3.1. Selected bond lengths (Å) and angles (deg) for 147

C(2)-Y(1)	2.661(6)	C(3)-Y(1)	2.680(6)	C(4)-Y(1)	2.676(5)
C(5)-Y(1)	2.670(6)	C(6)-Y(1)	2.666(6)	C(20)-Y(1)	2.669(6)
C(21)-Y(1)	2.706(6)	C(22)-Y(1)	2.725(5)	C(23)-Y(1)	2.708(5)
C(24)-Y(1)	2.649(6)	O(1)-Y(1)	2.360(4)	C(41)-Y(1)	2.398(6)
PCp^{Me}(A)-Y(1)	2.383	PCp^{Me}(B)-Y(1)	2.407	C(12)-C(13)	1.454(9)
PCp^{Me} (A)-Y(1)-C(41)	104.8°	PCp^{Me} (B)-Y(1)-C(41)	108.7°	PCp^{Me} (A)-Y(1)-O(1)	107.7°
PCp^{Me} (B)-Y(1)-O(1)	101.8°	PCp^{Me}(A)-Y(1)-PCp^{Me}(B)	133.6°	torsion angle	117.0°

A = centroid C(2)-C(6), B = centroid C(20)-C(24)

X-ray quality crystals of **161** were obtained by crystallization from mixed toluene hexanes solvent, and several toluene molecules appear in the unit cell of this structure. As indicated by the triplet for the hydride resonances in the ^{1}H NMR, this complex is dimeric in the solid state (**Fig 3.14**). The PCp^{Ph}(cent)-Y-PCp^{Ph}(cent) angle in **161** (131.4˚) is similar to **147** (133.6˚) and to that in an indenyl yttrium hydride dimer $[(Ind^*)_2Y(\mu\text{-}H)]_2$ **45** (132.0˚).[79] However, the torsion angle between the two PCp^{Ph} ligands on each metal center of **161** (164.0˚) shows a 50˚ difference from that in **147**, but is similar to the torsion angle in $[(Ind^*)_2Y(\mu\text{-}H)]_2$ **45**.[79] The Y-H bond lengths of Y(1)-H(1Y), 2.10(2) Å and Y(1)-H(2Y), 2.14(3) Å are equal within experimental error and are consistent with the previously reported $[(Ind^*)_2Y(\mu\text{-}H)]_2$ **45**.

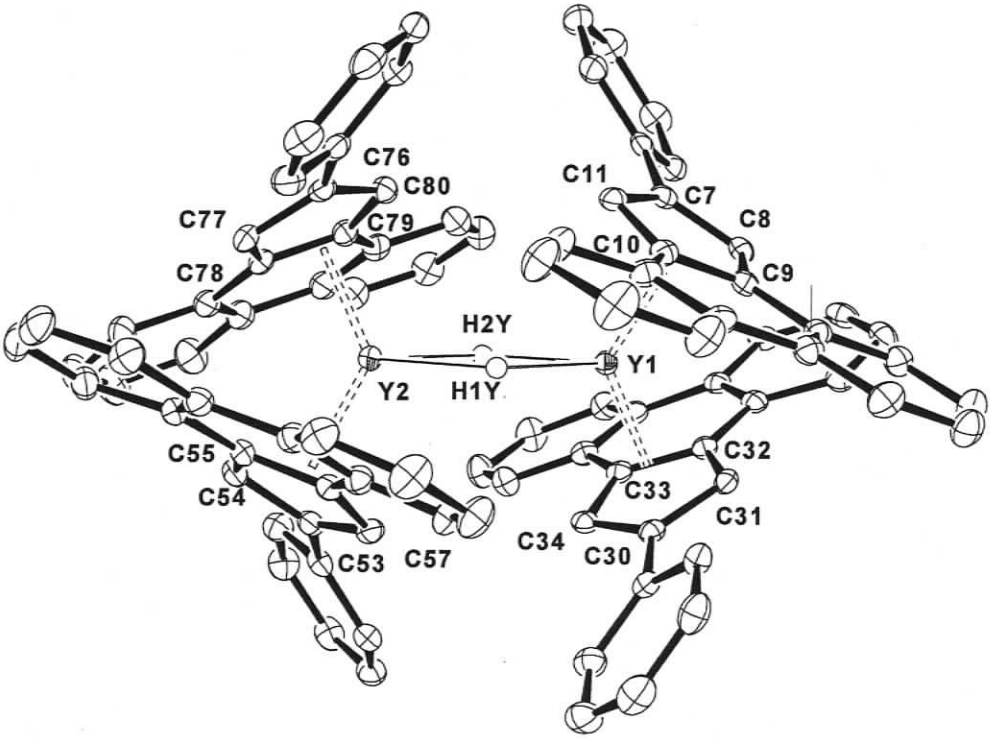

Figure 3.14. Ortep3 diagram (thermal ellipsoid 50% probability) of 161

Table 3.2. Selected bond lengths (Å) and angles (deg) for 161

C(7)-Y(1)	2.650(2)	C(30)-Y(1)	2.620(2)	C(53)-Y(2)	2.657(2)	C(76)-Y(2)	2.636(2)
C(8)-Y(1)	2.633(2)	C(31)-Y(1)	2.599(2)	C(54)-Y(2)	2.641(2)	C(77)-Y(2)	2.589(2)
C(9)-Y(1)	2.715(2)	C(32)-Y(1)	2.686(2)	C(55)-Y(2)	2.704(2)	C(78)-Y(2)	2.667(2)
C(10)-Y(1)	2.712(2)	C(33)-Y(1)	2.711(2)	C(56)-Y(2)	2.691(2)	C(79)-Y(2)	2.697(2)
C(11)-Y(1)	2.664(2)	C(34)-Y(1)	2.660(2)	C(57)-Y(2)	2.658(2)	C(80)-Y(2)	2.665(2)
Y(1)-H(1Y)	2.10(2)	Y(1)-H(2Y)	2.14(3)	Y(2)-H(2Y)	2.10(3)	Y(2)-H(1Y)	2.16(2)
H-Y-H	67.5(9)	Y-H-Y	113.1(9)	torsion angle 164.0°			

The Y-C bond lengths between the carbons at the *1*, *2* and *3* positions of the five-membered rings and the metal center are in the range 2.589(2)-2.664(2) Å (**Table 3.2**). In comparison, the bond lengths between the *4* and *5* carbons and yttrium are in the range of 2.667(2)-2.715(2) Å. Thus, **161** shows a clear distortion toward η^3 bonding between the five-membered ring and the metal center compared to **147**; however, the five-membered rings of **161** do not show the substantial bending associated with more η^3 bonding character. The four PCp^{Ph}(cent)-Y distances are in the range of 2.361(2)-2.385(2) Å and do not show a significant difference between yttrium hydride **161** and alkyl complex **147**. The H-Y-H angle (67.5(9)°) and Y-H-Y angle (113.1(9)°) are consistent with previously reported hydride dimers. In one of the central rings (C(9)-C(12)-C(17)-C(18)-C(23)-C(10)), bond lengths C(9)-C(12), C(17)-C(18) and C(23)-C(10) fall in the range of 1.447(3)-1.473(3) Å; in contrast, bond lengths for C(12)-C(17), C(18)-C(23) and C(10)-C(9) are in the range of 1.410(3)-1.419(3) Å. The significant difference between these two types of C-C bond lengths

in the central six-membered ring indicates some electron localization in the three 6π electron systems, and the central ring possesses much less aromaticity than other true 6 electron π systems. Similar to **147**, this also strongly supports the calculation made in Chapter One that remote fusion does not show a substantial effect on electron density in the Cp ring.

The solid state structure of **161** shows that yttrium complexes even with large rigid ligands still allow hydride bridging interactions. The clear wedge usually formed by regular bis-Cp* complexes can not exist in this case, simply due to the PCp^{Ph} ligands rotation to avoid steric repulsion with each other. More significantly, the tendency to form a hydride dimer is so strong that the ligands can adopt a torsion angle close to 180° to avoid unfavourable steric interactions.

3.4.2 X-ray Structures of PCp* Complexes 150 and 167

The structure of **150** also adopts a pseudo-tetrahedral geometry, with a THF molecule positioned underneath the phenanthrene skeleton and the two alkyl groups projecting away from the phenanthrene unit (**Fig 3.15**). Similar to **147** and **161**, the PCp* ligand consists of three isolated 6 electron π systems, this is evident from the shorter C-C bond lengths for the outer three rings compared with the central six-numbered ring (**Appendix Table A.8**). Interestingly, the X-ray structure shows shorter bond lengths for C(4)-Y(1) (2.631 (2) Å) and C(5)-Y(1) (2.630(2) Å) than for C(1)-Y(1) (2.675(2) Å), C(2)-Y(1) (2.695 (2) Å) or C(2)-Y(1)(2.679(2) Å) (**Table 3.3**). This is a very strange case because regular indenyl systems normally show a

bonding pattern with yttrium closer to the outer three (allylic type) carbons of the five-membered ring with longer bond distances to the two carbons fused to the aromatic ring. The 20° difference between the angles O(1)-Y(1)-C(26) (112.10(5)°) and O(1)-Y(1)-C(22) (93.30(5)°) is quite significant compared to other bis-alkyl Cp complex in which these two angles are very similar.[58] This clearly indicates the steric effect imposed by the phenanthrene fusion in **150**. Compared to an α-agostic interaction with a distance of 2.53 Å between Y and the α-proton observed in $Cp^*_2YCH(SiMe_3)_2$,[49] no agostic interactions are evident from the relevant distances in **150** (2.819 Å) (**Table 3.3**).

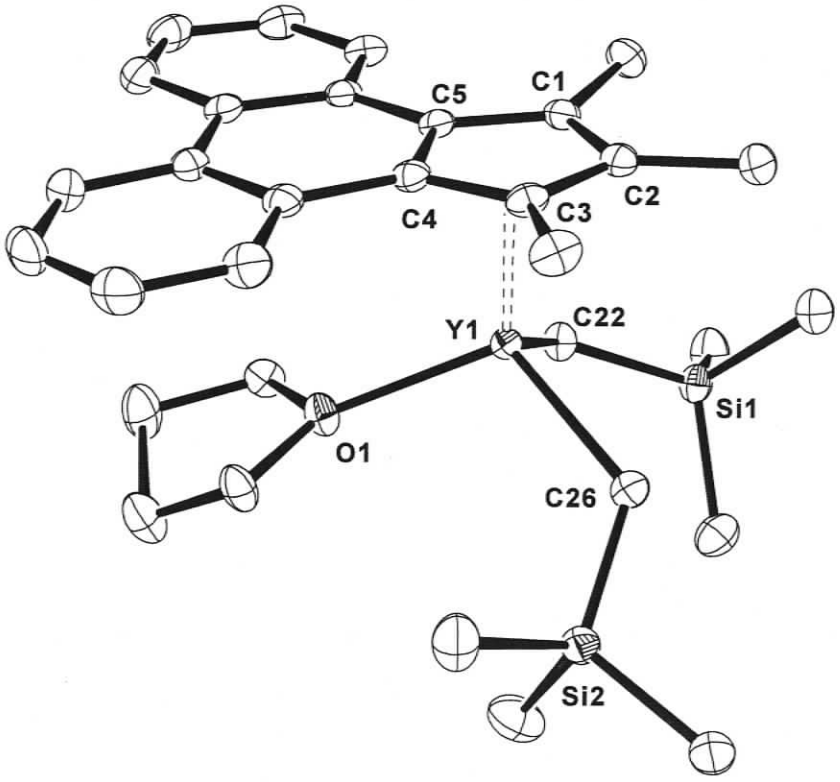

Figure 3.15. Ortep3 diagram (thermal ellipsoid 50% probability) of 150

Table 3.3. Selected bond lengths (Å) and angles (deg) for 150

C(1)-Y(1)	2.675(2)	C(2)-Y(1)	2.695(2)	C(3)-Y(1)	2.679(2)
C(4)-Y(1)	2.631(2)	C(5)-Y(1)	2.630(2)	C(26)-Y(1)	2.383(2)
C(22)-Y(1)	2.390(2)	PCp*(cent)-Y(1)	2.370	O(1)-Y(1)	2.324(2)
Y-α-C-H	2.819- 2.834	Si(1)-C(22)-Y(1)	123.76(9)	Si(2)-C(26)-Y(1)	125.92(9)
O(1)-Y(1)-C(26)	112.10(5)	O(1)-Y(1)-C(22)	93.30(5)	C(26)-Y(1)-C(22)	107.75(6)
PCp*(cent)-Y-O(1)	115.1	PCp*(cent)-Y-C(26)	138.6	PCp*(cent)-Y-C(22)	116.0

X-ray quality crystals were also obtained from a toluene solution of **166**. Surprisingly, the X-ray crystallography structure reveals the centro-symmetric dimeric form of **167** (**Fig 3.16**). The structure also reveals the asymmetry of the bridging acetylide groups as noted from the 45° difference in angle between C(27)-C(26)-Y(1) (105.8(2)°) and C(27)-C(26)-Y(2) (151.2(2)°), even though the difference in bond length between Y(1)-C(26) (2.507 (3) Å) and Y(2)-C(26) (2.517(3) Å) is insignificant. There is a significant Y-C bond distance difference between the terminal Y(1)-C(21) (2.412(3) Å) and bridging Y(1)-C(26) (2.507(3) Å), Y(1)-C(60) (2.521(3) Å) acetylides; but no significant difference between the C-C triple bond distances for the terminal and bridging acetylides. The values for these parameters fall in the ranges for structurally characterized lanthanide dimers.[207-209] The distances between the metal centers and β-carbons C(27) and C(61) are about 3.0 Å and beyond the range for a possible π-bond.

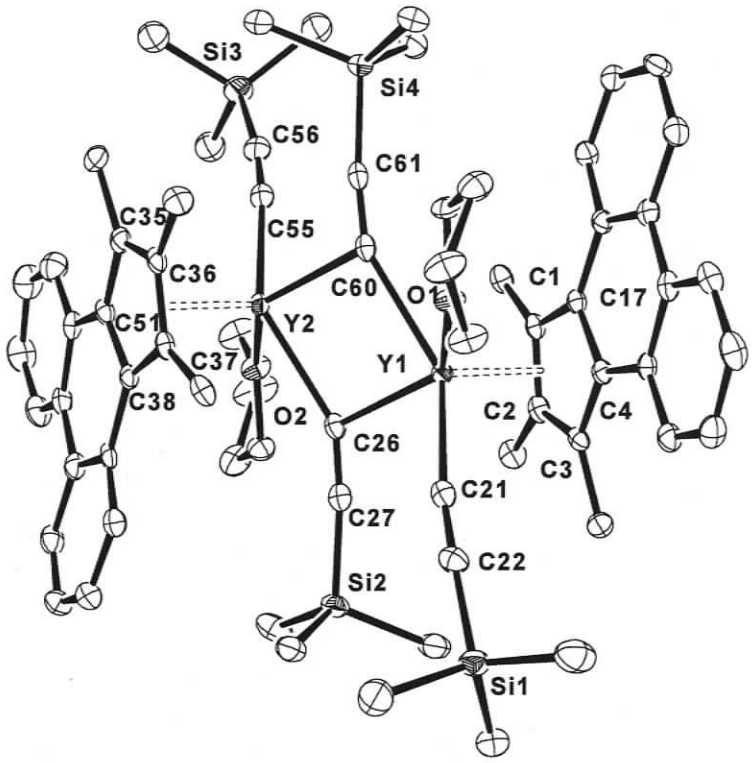

Figure 3.16. Ortep3 diagram (thermal ellipsoid 50% probability) of 167

Table 3.4. Selected bond lengths (Å) and angles (deg) for 167

C(1)-Y(1)	2.670(3)	C(2)-Y(1)	2.713(3)	C(3)-Y(1)	2.693(3)
C(4)-Y(1)	2.637(3)	C(17)-Y(1)	2.657(3)	C(35)-Y(2)	2.698(3)
C(36)-Y(2)	2.718(3)	C(37)-Y(2)	2.672(3)	C(38)-Y(2)	2.663(3)
C(51)-Y(2)	2.634(3)	C(21)-Y(1)	2.412(3)	C(26)-Y(1)	2.507(3)
C(26)-Y(2)	2.517(3)	C(55)-Y(2)	2.397(3)	C(60)-Y(2)	2.499(3)
C(60)-Y(1)	2.521(3)	C(61)-Y(2)	3.007	C(27)-Y(1)	3.073
PCp*(cent)-Y(2)	2.388	PCp*(cent)-Y(2)	2.384	Y(1)-(O1)	2.361(2)
Y(2)-(O2)	2.380(2)	C(27)-C(26)-Y(1)	105.8(2)	C(27)-C(26)-Y(2)	151.2(2)
C(61)-C(60)-Y(1)	154.9(2)	C(61)-C(60)-Y(2)	102.2(2)	C(60)-Y(2)-C(26)	79.17(10)
C(26)-Y(1)-C(60)	78.94(10)	Y(1)-C(60)-Y(2)	100.98(11)	Y(1)-C(26)-Y(2)	100.85(10)

Since the dimer **167** has a coordination number of 7, additional steric repulsion between the Me_3Si groups and the PCp* ligand should be greater resulting in longer PCp*(cent)-Y distances than observed in formally 6-coordinate **150**. Surprisingly, compared to **150**, no change of bonding mode or longer PCp*(cent)-Y bond distances were observed in **167** after dimerization (**Table 3.4**), possibly due to minimization of the steric repulsion by the closely parallel position of the YCCSi groups relative to the PCp* ligands.

3.4.3 X-ray Structures of sCp Complexes 152 and 154

The X-ray quality crystals of **152** were obtained from hexanes solution. The sCp ligand twists dramatically by 48° due to strong H---H repulsions between the back aromatic rings resulting in a chiral complex in the solid state (**Fig 3.17**). However, the protons on C(16) and C(28) can pass by one another in solution easily so the sCp skeleton can racemize rapidly to give symmetrical NMR spectra. The bond distances between yttrium and carbons in the five-membered ring are similar to those in **147**, **150**, **161** and **167**, except for the significantly longer distance for C(4)-Y(1) (2.765(3) Å), possibly due to the distortion of the whole sCp skeleton (**Table 3.5**). Similarly to **147** and **150**, the electrons of **152** are localized on the five-membered ring and outer six-membered rings, as indicated by the longer C-C bond distances for the two central six-membered rings compared to the other terminal rings. The O(1)-Y(1) (2.307(2) Å) in **152** and (2.324(2) Å) in **150** are shorter than the Y-O (2.360(4) Å) distance in **147** due to the lower coordination number in **150** and **152** (6) compared

to **147** (8). Thus, there is no strong correlation between the dynamics of THF in solution and the solid state structure. Moreover, there is no significant difference between the two O-Y-C_α angles in **152** (7˚) compared to **150** (20˚). Similar to **150**, the long distances (2.762-2.778 Å) between the metal center and α-CH_2 protons of the alkyls rule out the possibility of an α-agostic interaction.

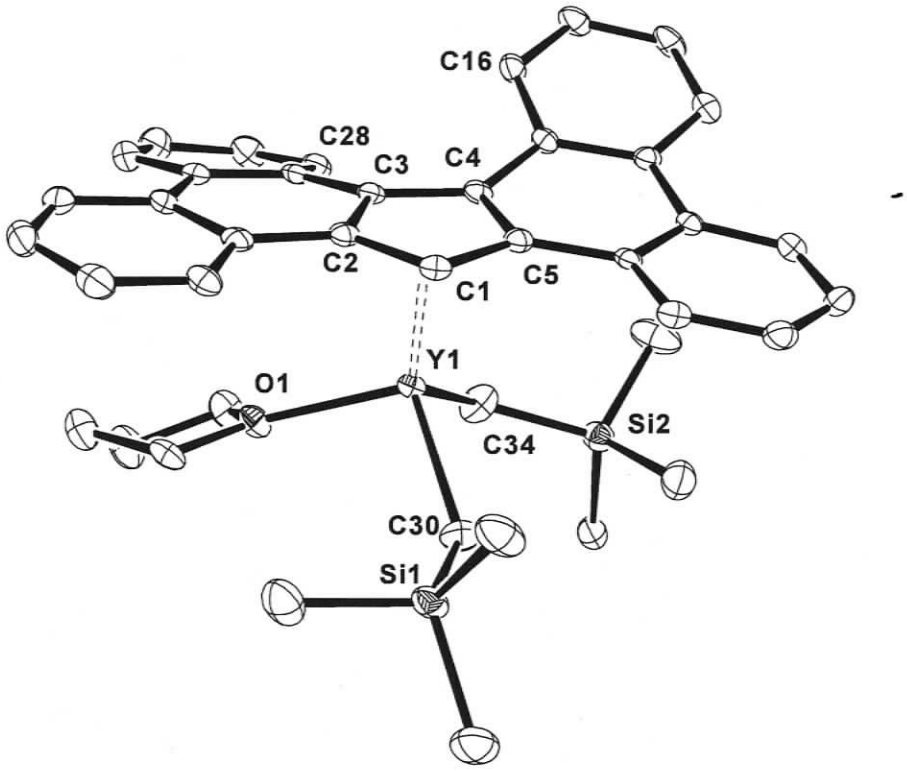

Figure 3.17. Ortep3 diagram (thermal ellipsoid 50% probability) of 152

Table 3.5. Selected bond lengths (Å) and angles (deg) for 152

C(1) - Y(1)	2.641(3)	C(2) - Y(1)	2.645(3)	C(3) - Y(1)	2.667(3)
C(4) - Y(1)	2.765(3)	C(5) -Y(1)	2.699(3)	sCp(cent)-Y(1)	2.396
C(30) - Y(1)	2.360(3)	C(34) -Y(1)	2.353(3)	O(1) - Y(1)	2.307(2)
O(1)-Y(1)-C(34)	95.28(10)	O(1)-Y(1)-C(30)	102.76(9)	C(34)-Y(1)-C(30)	103.93(11)
sCp(cent)-Y(1)-O(1)	113.9	sCp(cent)-Y(1)-C(30)	119.5	sCp(cent)-Y(1)-C(34)	117.9
Y(1) -C(34)- Si(2)	129.3(2)	Y(1)-C(30)-Si(1)	135.4(2)	Y(1)-α-C-H	2.762-2.778

The X-ray quality crystals of **154** were obtained directly from the reaction mixture of **152** and bipy in toluene. **154** adopts a pseudo-square pyrimidal geometry with the bipy unit and one alkyl group positioned under the sCp ligand, with the other alkyl group projecting outside of the sCp skeleton (**Fig 3.18**). Similar to **152**, the N-Y-C_α angles of **154** are very symmetrical. The twist angle between two back terminal rings is 40°. The long distance between the metal center and α-CH_2 protons of the alkyls (2.732-2.894 Å) again rules out the presence of any agostic interactions. This is not surprising given that the metal center is even more saturated with bidentate bipy coordination as further shown by the significant differences between Y-C bond distances: C(1)-Y(1) (2.640(2) Å), C(2)-Y(1) (2.689(2) Å), C(29)-Y(1) (2.721(2) Å), C(15)-Y(1) (2.804(2) Å), C(16)-Y(1) (2.780(2) Å) (**Table 3.6**). The significantly longer Y-C bond distances for C(16) and C(15) show a favorable η^3 bonding pattern between the metal center and the sCp ligand in **154**, compared to the η^5 bonding mode in **152**. A longer sCp(cent)-Y(1) distance (2.443 Å) in **154** compared to **152** (2.396 Å) shows the significant effect caused by a change in coordination number.

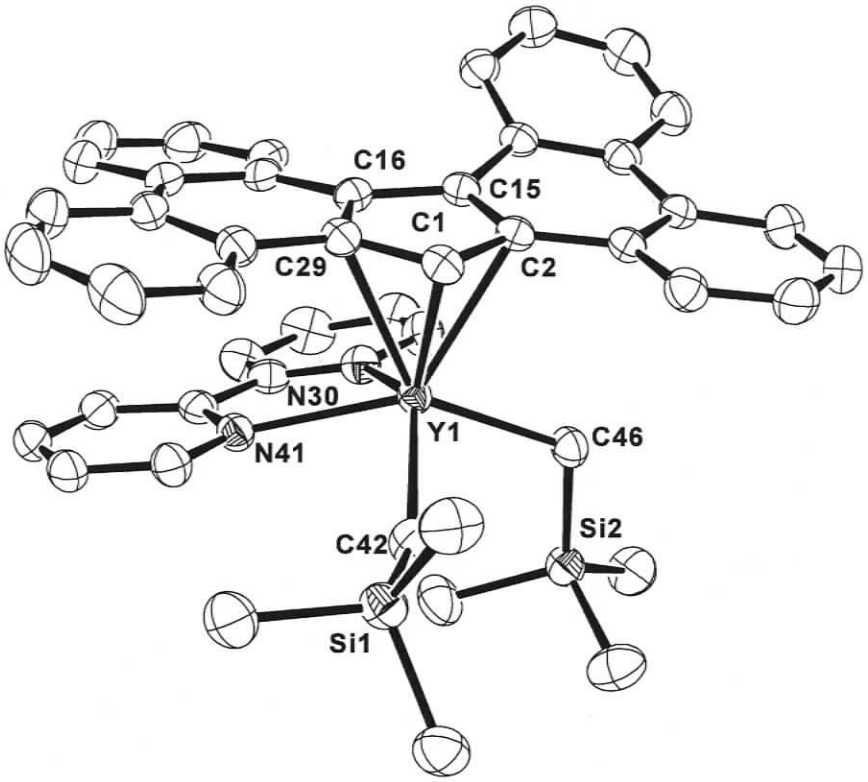

Figure 3.18. Ortep3 diagram (thermal ellipsoid 50% probability) of 154

Table 3.6. Selected bond lengths (Å) and angles (deg) for 154

C(1)-Y(1)	2.640(2)	C(2)-Y(1)	2.689(2)	C(15)-Y(1)	2.804(2)
C(16)-Y(1)	2.780(2)	C(29)-Y(1)	2.721(2)	sCp(cent)-Y(1)	2.443
C(46)-Y(1)	2.423(2)	C(42)-Y(1)	2.396(2)	N(41)-Y(1)	2.469(2)
N(30)-Y(1)	2.519(2)	C(42)-Y(1)-N(41)	87.48(7)	C(46)-Y(1)-N(41)	134.28(7)
C(42)-Y(1)-N(30)	136.11(7)	C(46)-Y(1)-N(30)	85.69(7)	N(41)-Y(1)-N(30)	64.49(6)
C(42)-Y(1)-C(46)	92.24(8)	sCp(cent)-Y(1)-C(42)	117.3	sCp(cent)-Y(1)-C(46)	113.0
sCp(cent)-Y(1)-C(41)	107.5	sCp(cent)-Y(1)-C(46)	103.6		

3.4.4 X-ray Structures of Acetylide Cluster 169

Crystallization of the acetylide cluster **169** from toluene afforded a few pale yellow crystals suitable for single crystal X-ray crystallography. The geometry about Y(1) is pseudo-octahedral with the centroid of the sCp five-membered ring, the three μ^2- and one μ^3-bridged acetylide groups and one THF molecule forming the coordination sphere (**Fig 3.19**). Besides the significant twist between the two back rings, the two front rings of the sCp ligand also show a twist angle by 27.3° compared to 6.5° in **152**, presumably due to the steric repulsion from the Me_3Si groups caused by the octahedral geometry of **169**. Moreover, the bonding mode between Y(1) and the sCp ligand slips to a unique side η^3-bonding mode as a result of increasing the coordination number to 7 in presence of bulky Me_3Si groups.

The main framework of this cluster is a triangle formed by the three yttrium metal centers with very different bonding modes. In constrast to Y(1), Y(2) is bound to one μ^3-acetylide, two μ^2-acetylides (one each with Y(1) and Y(3)), and two terminal acetylides. Similarly, Y(3) is also bonded to five acetylides with the same bonding modes but with an additional coordinated THF molecule. Overall, the cluster consists of three terminal acetylide groups (C(49), C(54), and C(69)), four μ^2-bridged acetylide groups (C(59), C(30), C(35), C(44)) and one μ^3-bridged acetylide group (C(64)). Interestingly, the μ^2-bridged acetylide groups (C(44)-C(45), C(35)-C(36)) also show some π-bonding character between the C-C triple bonds and the metal centers (Y(3), Y(2)), this is evident from the relative short bond distances between the metal center and β-carbons in acetylides (C(36)-Y(2) 2.85(2) Å, C(45)-Y(3) 2.87 (2)

Å) (**Table 3.7**). Compared to the μ^3-bridged acetylide groups (C(64)-Y(2) 2.66(2) Å), the μ^2-bridged (C(30)) shows a strong interaction towards Y(2) as indicated by a bond distance of C(30)-Y(2) (2.79(2) Å).

As the very minor product, NMR characterization of this cluster was not carried out. Despite the unique structure of this cluster, the bond distances and angles are not very reliable due to the significant deviation of the data and poor quality of the crystals. Thus a more detailed discussion on specific crystallographic data will not be carried out; however, this solid state structure represents the first μ^3-bridged acetylide lanthanide complex.

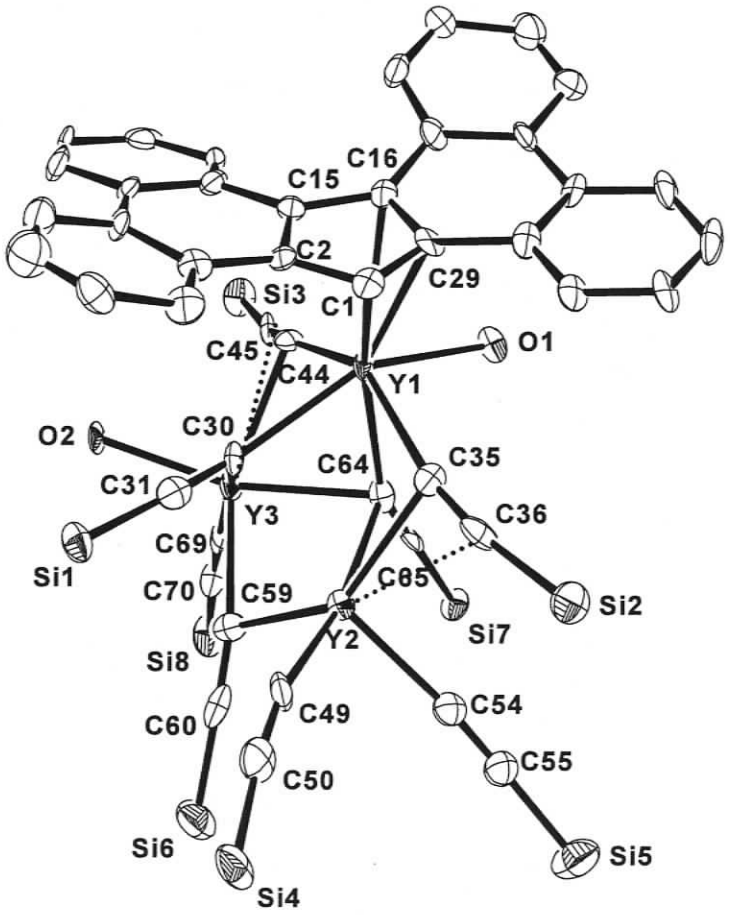

Figure 3.19. Ortep3 diagram (thermal ellipsoid 50% probability) of 169

Carbons on Me_3Si groups and THF omitted for clarity

Table 3.7. Selected bond lengths (Å) and angles (deg) for 169

C(1)-Y(1)	2.657(11)	C(2)-Y(1)	2.791(11)	C(15)-Y(1)	2.773(11)	C(16)-Y(1)	2.721(11)
C(29)-Y(1)	2.610(11)	sCp(cent)-Y(1)	2.426	C(30)-Y(1)	2.500(13)	C(30)-Y(3)	2.668(12)
C(30)-Y(2)	2.789(12)	C(35)-Y(1)	2.463(13)	C(35)-Y(2)	2.552(12)	C(36)-Y(2)	2.849(12)
C(44)-Y(3)	2.515(12)	C(44)-Y(1)	2.530(14)	C(45)-Y(3)	2.873(12)	C(49)-Y(2)	2.340(14)
C(59)-Y(3)	2.400(13)	C(59)-Y(2)	2.517(13)	C(64)-Y(3)	2.504(12)	C(64)-Y(1)	2.563(13)
C(64)-Y(2)	2.656(12)	C(69)-Y(3)	2.364(14)	Y(2)-C(54)	2.394(13)	O(1)-Y(1)	2.350(8)
O(2)-Y(3)	2.285(7)	Y(1)-Y(3)	3.570(2)	Y(1)-Y(2)	3.730 (2)	Y(2)-Y(3)	3.637(2)
Y(3)-Y(1)-Y(2)	59.71(3)	Y(1)-Y(3)-Y(2)	62.33(3)	Y(3)-Y(2)-Y(1)	57.95(3)		

3.4.5 Bis-$(Me_3Si)_2Cp$ Complex 176

X-ray quality crystals of $\{[(Me_3Si)_2Cp]_2Y(\mu\text{-}Cl)\}_2$ **176** were obtained from the solution of **175** in toluene (**Figure 3.20**). The most significant feature of **176** is a torsion angle of 177.6° which minimizes steric repulsion from the Me_3Si groups. The angle Cp(cent)-Y(1)-Cp(cent) in **176** (130.2°) is similar to **147** (133.6°), **161** (131.4°) and Cp*-Y-Cp* angles reported previously (**Table 3.8**). Several lanthanide complexes with similar structure have been reported,[217-219] so the details of **176** will not be discussed further.

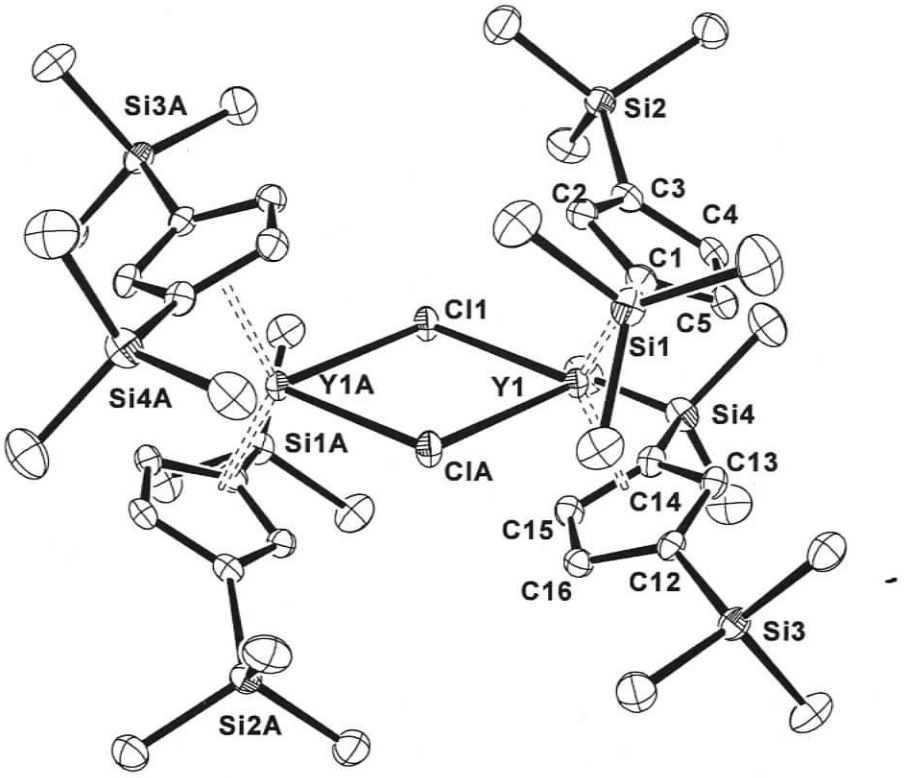

Figure 3.20. Ortep3 diagram (thermal ellipsoid 50% probability) of 176

Table 3.8. Selected bond lengths (Å) and angles (deg) for 176

C(1)-Y(1)	2.640(2)	C(2)-Y(1)	2.689(2)	C(3)-Y(1)	2.666(2)
C(4)-Y(1)	2.616(2)	C(5)-Y(1)	2.613(2)	Cp($C_{1\text{-}5}$cent)-Y(1)	2.349
C(12)-Y(1)	2.651(2)	C(13)-Y(1)	2.644(2)	C(14)-Y(1)	2.657(2)
C(15)-Y(1)	2.636(2)	C(16)-Y(1)	2.637(2)	Cp($C_{12\text{-}16}$cent)	2.353
Y(1)-Cl(1)-Y(1A)	100.4	torsion angle	177.6	Cl(1)-Y(1)-Cl(1A)	79.6
Cp(cent)-Y(1)-Cp(cent)	130.2			Cp(cent)-Y(1)-Cl(1)A	107.2

3.5 Dynamic Behaviour of Yttrium Alkyl Complexes in Solution

3.5.1 Dynamic Behaviour of $(PCp^{Me})_2Y(CH_2SiMe_3)(THF)$ 147

Non-THF alkyl complexes are expected to be much more reactive, because the metal center is more open for substrate attack. A large excess of Et_2O at 40 °C was therefore used to establish an equilibrium between Et_2O and THF coordination to the metal in complex **147** with the goal of replacing THF by Et_2O after several cycles. However, this method failed to remove THF and eventually led to decomposition of the complex. This result may not be surprising, since the chemical shift of the THF resonances are far upfield (1.95 ppm for the α-protons, 0.57 ppm for the β-protons) compared with previously reported alkyl complexes (α-proton > 2.8ppm), [66,67,89,220] suggesting that THF is tightly bound at room temperature. To test this further, five equivalents of free THF were added to **147** in C_6D_6 solution at room temperature and separate resonances for the free and coordinated THF were observed which clearly proves that THF exchange is slow for **147** at room temperature. The VT ^{1}H NMR spectra of **147** from 25 to 75°C were taken in order to study the dynamic behaviour of THF exchange. At room temperature, two separate resonances for the protons on the Cp ring indicate two inequivalent protons in the *1* and *1'* positions due to the C_S symmetry of **147**. These resonances start to broaden at elevated temperature and eventually coalesce at 65 °C; a new broad resonance appears at 6.4 ppm at 75°C (**Fig 3.21**). This indicates that fast exchange of THF occurs at this temperature and the complex adopts averaged C_{2V} symmetry without the coordinated THF molecules (**Eq**

3.14). Note, the two α-protons in CH_2SiMe_3 group remain equivalent regardless of whether a slow or fast exchange process is operational (**Fig 3.22**).

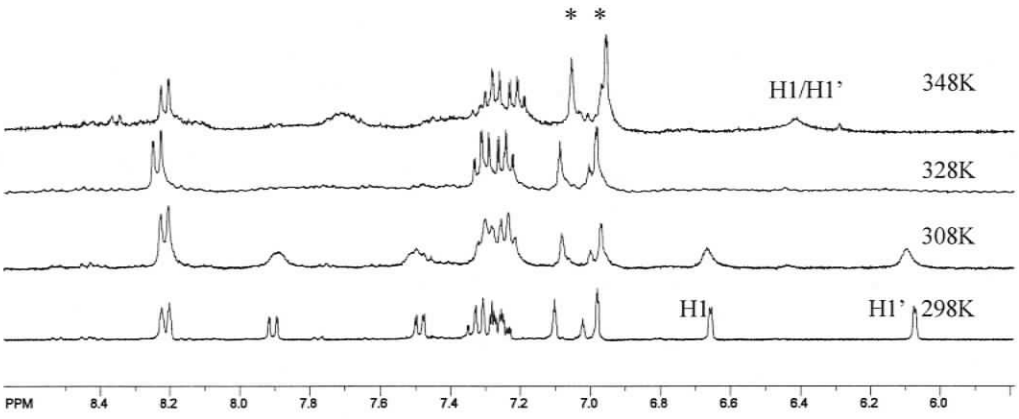

Figure 3.21. VT ^{1}H NMR spectra (360 MHz, C_7D_8) of 147

Complex **147** adopts a pseudo-tetrahedral geometry with coordinated THF and only possesses C_S symmetry with freely rotating PCp^{Me} at room temperature (**Fig 3.22**). Since it is very likely that the PCp^{Me} ring rotates rapidly at 65 °C, the higher symmetry of **147-THF** in the fast exchange spectra involves two possible mechanisms: i) if a pyramidal or pseudo-pyramidal geometry is maintained as the minimum energy state after dissociation of THF (**Fig 3.22 i**), rapid inversion at the yttrium metal center must occur; or ii) if a trigonal planar geometry is the minimum energy state (**Fig 3.22 ii**), then rapid relaxation of the alkyl group from a pyramidal to a trigonal planar geometry occurs after THF dissociation. A pyramidal geometry might be favoured if an agostic interaction takes place for **147-THF**. However, the α-CH_2 coupling constant at high temperature is not observed due to the decomposition of **147**. Similar to mono-alkyl complexes reported previously,[221,222] the 102 Hz coupling constant observed at room temperature for **147** is not convincing evidence

for an α-agostic interaction compared with the 84 Hz observed in agostic $Cp^*_2YCH(SiMe_3)_2$.[49] The small reduction (16 Hz) in $^1J_{CH}$ compared to the regular sp^3 C-H coupling constant (118 Hz) is most likely caused by the electronic effect of the yttrium metal center. Moreover, X-ray crystallographic data do not support any agostic interaction in the solid state. Thus, the absence of an agostic interaction suggests that a pyramidal geometry is unlikely to be maintained after THF dissociation, leading to a less crowded trigonal planar geometry as the ground state structure.

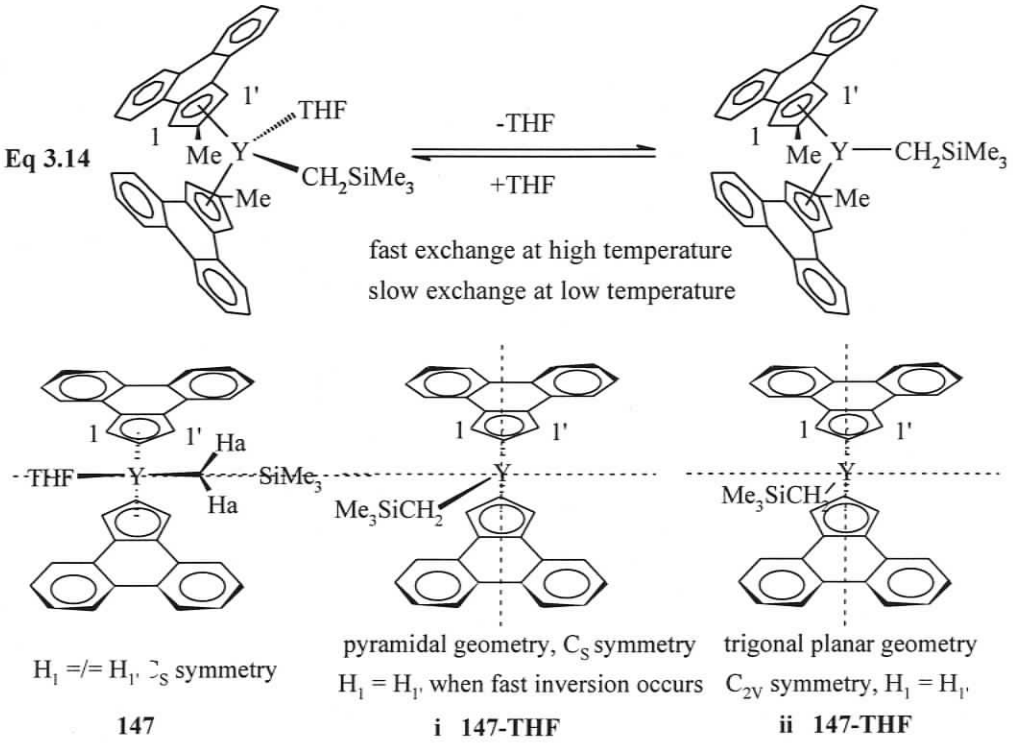

Figure 3.22. Symmetry of 147 and 147-THF

From the coalescence temperature shown in **Figure 3.21**, the activation energy for THF dissociation is calculated to be 63.7 kJ mol^{-1} from the two-site, equal population equation $\Delta G^{\#} = (1.912*10^{-2})(Tc)[9.972+ \log(Tc/\delta\nu)]$, where $\delta\nu$ is the

separation of the resonances for the protons in the *1* and *1'* positions in Hz and Tc is the coalescence temperature (328K).[224] However, the ground state energy difference, ΔG°, for the dissociation process can not be obtained from the chemical shifts of the THF resonances. At room temperature where slow exchange of THF occurs, the equilibrium between **147** and **147-THF** favors **147**, and the equilibrium does not shift significantly with elevated temperature in the slow exchange range, since no free THF was observed. At high temperature, the equilibrium constant at fast exchange also can not be obtained from the continuously shifting THF resonances, because **147** decomposes easily at higher temperature and the spectra above the coalescence temperature do not provide enough data for calculation of binding entropy and enthalpy.

3.5.2 Dynamic Behavior of Mono-ligand Bis-alkyl Complexes 150 and 152

Both complex **150** and **152** possess C_S symmetry and adopt a pseudo-tetrahedral geometry in the solid state; this indicates the absence of symmetry between the two α-protons of the CH_2SiMe_3 groups (illustrated for **150** in **Fig 3.24**). However, the ^1H NMR shows a single α-proton resonance as indicated by a simple doublet due to Y-H coupling for both **150** and **152** (**Fig 3.24**). This clearly indicates ongoing dynamic behaviour for both complexes in solution at room temperature, leading to higher symmetry. This dynamic behaviour is believed to be due to rapid exchange of THF at room temperature which is evident from a single set of resonances for THF when excess THF is added.

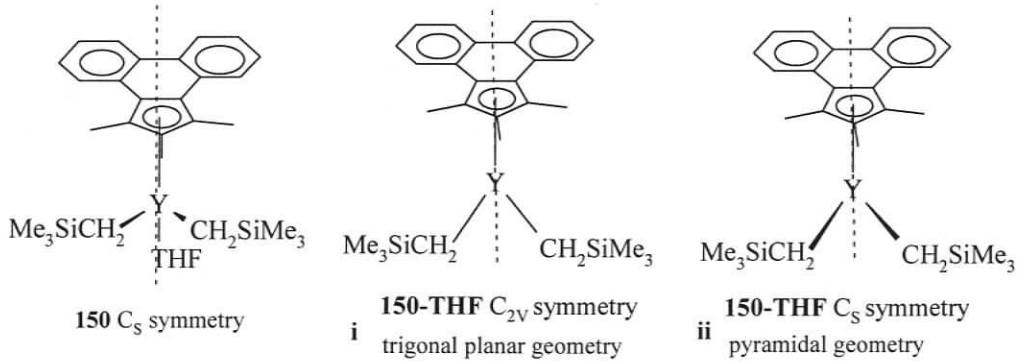

Figure 3.23. Symmetry of 150 and 150-THF

Three important changes for the resonances of **150** at lower temperature were observed (**Fig 3.24**): i) the resonances of the aromatic protons shift dramatically at lower temperature, ii) the resonances of THF remain as a broad singlet and shift upfield continuously with declining temperature (**Graph 3.1**), iii) the resonance of CH_2SiMe_3 shifts downfield from -0.66 ppm at 300K and splits into two doublet of doublets at -0.46 and -0.38 ppm at 190K with a coupling constant of $^2J_{HH} = 9.3$ Hz.

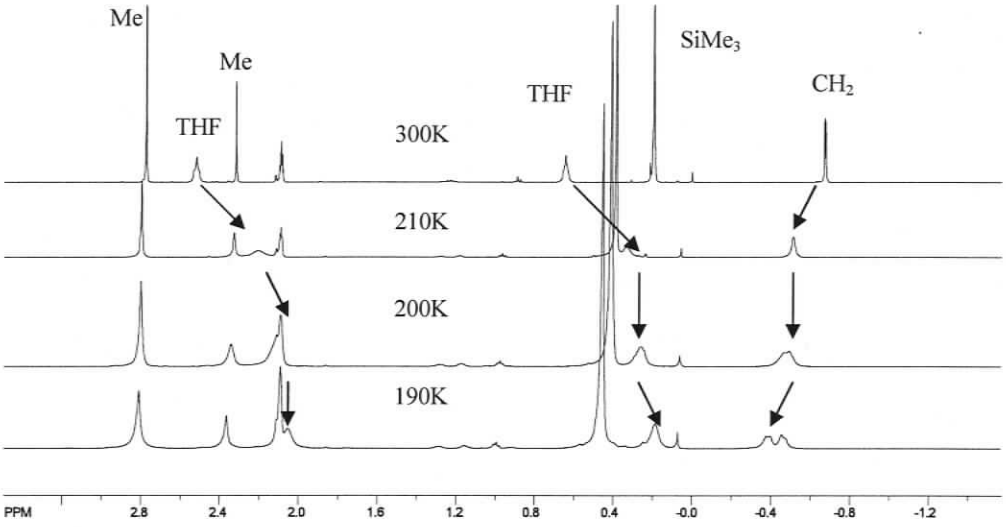

Figure 3.24. VT ^{1}H NMR spectra (500 MHz, C_7D_8) of 150

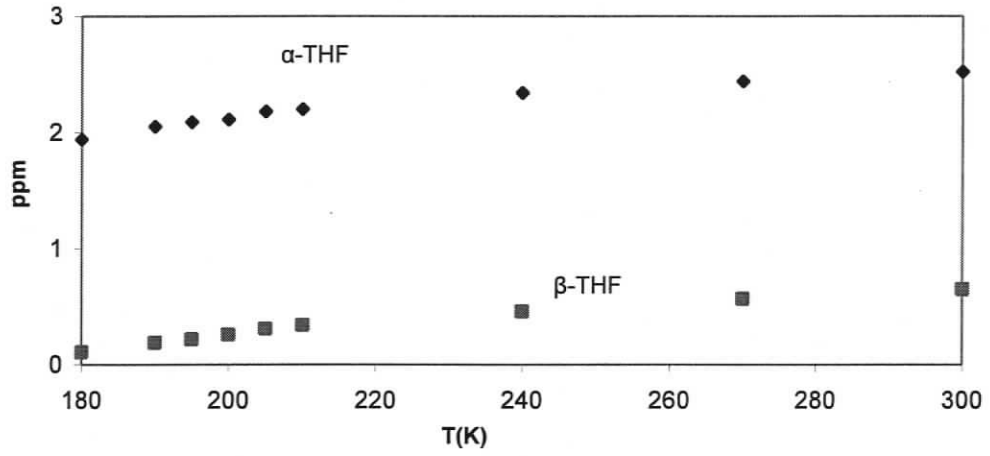

Graph 3.1. Chemical shifts of the resonances of THF in 150

A continuous upfield shift of the THF resonances indicates an ongoing rapid dynamic equilibrium between **150** and **150-THF**, assuming that the temperature has no significant effect on the chemical shift of one specific type of resonance. If slow exchange of THF was observed, we would expect two different resonances for the α-THF protons, representing the free and coordinated THF. However, these distinctive features for a slow exchange process were not observed, so we conclude a fast exchange occurs at all temperatures in the range 300K to 180K. Moreover, the chemical shift of the α-protons for free THF molecule is 3.57 ppm in C_6D_6, so considering the continuous upfield shifting, the chemical shift of THF can act as an indicator for the mole fraction of coordinated THF in the fast exchange process. The greater the mole fraction of coordinated THF, the more upfield the resonances shift. Continuous upfield shifting clearly indicates that the equilibrium is shifting from **150-THF** to **150** with decreasing temperature.

The observation that the CH_2 α-protons become inequivalent at low temperature but the two $SiMe_3$ groups do not indicates that the molecular symmetry has been lowered from average C_{2V} to C_S. Assuming **150-THF** adopts a trigonal planar ground state (**Fig 3.23 i**), this can be explained by restricted rotation about the PCp*-Y bond where the preferred rotamer has C_S symmetry. In fact, at high temperature, the rotation of PCp* ligand is very rapid to generate the equivalence between the two α-protons. At low temperature, the least crowded rotamer which places neither CH_2SiMe_3 group under the fused phenanthrene portion of the PCp* ligand dominates and leads to inequivalence between the two α-protons. However, to the best of our knowledge, slow rotation of Cp* or other aromatic-fused Cp ring has not been observed in organolanthanide chemistry, suggesting the low possibility of slow rotation of the PCp* ligand in a trigonal planar geometry of **150-THF**.

An alternative explanation could be that the ground state structure of **150-THF** is actually pyramidal or pseudo-pyramidal (**Fig 3.23 ii**), not trigonal planar, and the low temperature dynamic process represents inversion at the metal center. At high temperature, the inversion is fast enough to generate average C_{2V} symmetry (**Scheme 3.12**). In contrast, the inversion slows down to disrupt the equivalence of the two α-protons at low temperature and **150-THF** maintains pyramidal geometry. For the inversion mechanism, an agostic interaction between the alkyl and the metal center would be the most logical reason why **150-THF** might maintain the pyramidal geometry in the ground state. Similar to **147**, the α-C-H coupling constant of 102 Hz does not provide convincingly proof that an α-agostic interaction exists in solution for

this complex. The absence of any agostic interaction (α, β or γ) is also confirmed by the solid state structure of **150**. However, this does not rule out the possibility of an agostic interaction for pure **150-THF** because the previously reported bis-alkyl complex $Cp^*La(CHSiMe_3)_2$ possesses a strong β-Si-C-Y agostic interaction.[49] The inversion mechanism was also suggested for a previously reported yttrium alkyl-alkene complex without concrete evidence for an agostic interaction.[223] In our opinion, the inversion at the metal center is more likely and explains the whole dynamic behaviour of **150** and **152** more reasonably.

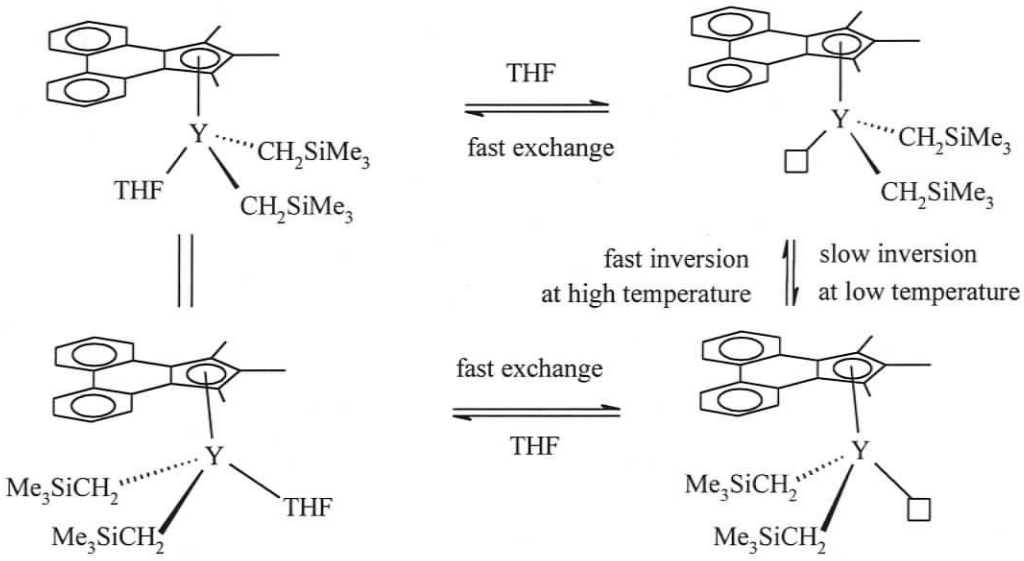

Scheme 3.12. Inversion of the metal center in 150

The activation energy for this process was calculated by the equal population, two-site exchange equation to be 42 kJ mol^{-1}. The binding energy of THF to the metal center can be estimated from the equilibrium between **150-THF** and **150**. The chemical shift of free α-THF protons is 3.57 ppm in C_6D_6; however, the chemical shift for the static, coordinated THF is unknown, since we were unable to reach the

100% coordination before the precipitation of **150** at low temperature. An approximate estimation for this shift of 1.7 ppm can be made from complexes **147-149** which possesses 100% coordinated THF with chemical shifts ranging from 1.75-1.99 ppm and the observation of a large 0.11 ppm upfield shift from 190K (2.05 ppm) to 180K (1.94 ppm).

$$\delta = 3.57x + 1.7(1-x) \qquad x = (\delta - 1.7)/(3.57 - 1.7)$$

δ - chemical shifts observed, x - mole fraction of free THF

chemical shift of α-protons in free THF = 3.57 ppm

chemical shift of α-protons in coordinated THF = 1.7 ppm

From the above equation, the equilibrium constants at different temperatures can be estimated, and ΔH° and ΔS° can be obtained from a Van't Hoff plot as 19 kJ mol^{-1} and 45 J mol^{-1} K^{-1} (**Graph 3.2**). The positive entropy and enthalpy are consistent with the THF dissociation process, similar to previously reported alkyl complexes $RMe_2Si(C_5Me_4)Y(CH_2SiMe_3)_2(THF)$ **180** and $[(Cp)Me_2C(Flu)]Y(CH_2SiMe_3)(THF)$ **181**.[66,220]

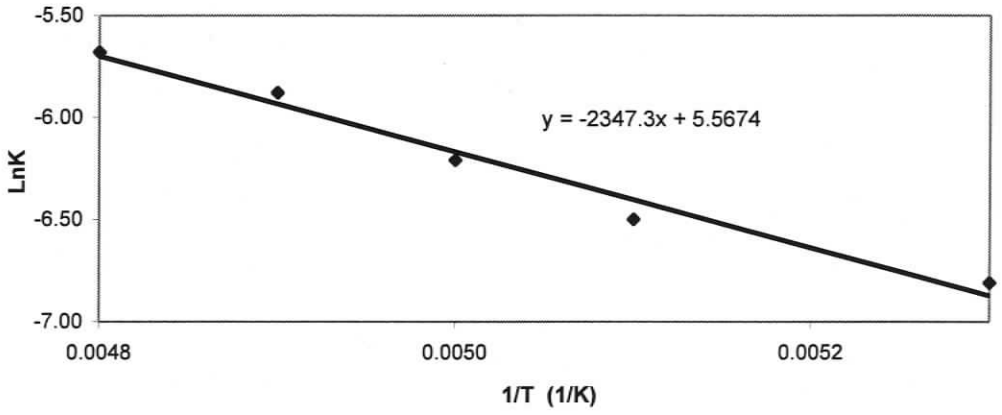

Graph 3.2. Van't Hoff plot for the equilibrium of THF dissociation in 150

Interestingly, addition of four equivalents of THF to a D_8-toluene solution results in quite different dynamic behaviour for **150**. The resonances of the α-protons in the CH_2SiMe_3 groups remain as a broad singlet from 240K to 190K and slow exchange between free and coordinated THF is clearly observed at 195K with the resonances for the α-protons of the coordinated THF at 3.18 ppm compared to 2.09 ppm in **150** (**Fig 3.25**). This is clearly inconsistent with the formation of **150** but indicates formation of a bis-THF complex **150+THF** possessing C_{2V} symmetry in the slow exchange limit (**Eq 3.15**). The relative integration ratio of 2:1 for the coordinated THF α-protons versus the CH_2 singlet supports a bis-THF species. Surpringly, **150** was not observed during this process indicating that in presence of excess THF complete generation of **150+THF** must occur at higher temperature where the dynamic process is still very fast; consequently, **150** was not observed during the whole process. Moreover, if slow rotation about PCp*-Y bond does take place in **150-THF**, the PCp* ligand should also rotate slowly on the NMR timescale in **150+THF** to generate the C_S symmetry and the inequivalence of the two α-protons. However, this is clearly inconsistent with the observation in **Fig 3.25**.

Eq 3.15

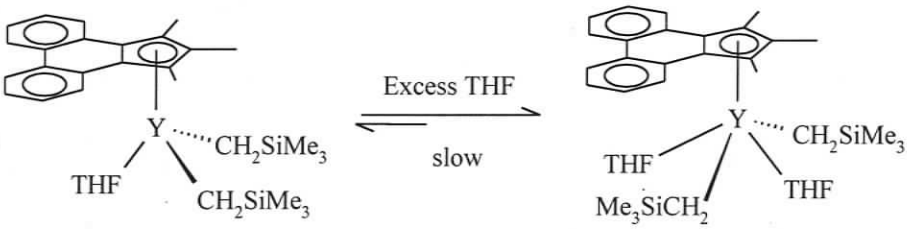

150 **150+THF**

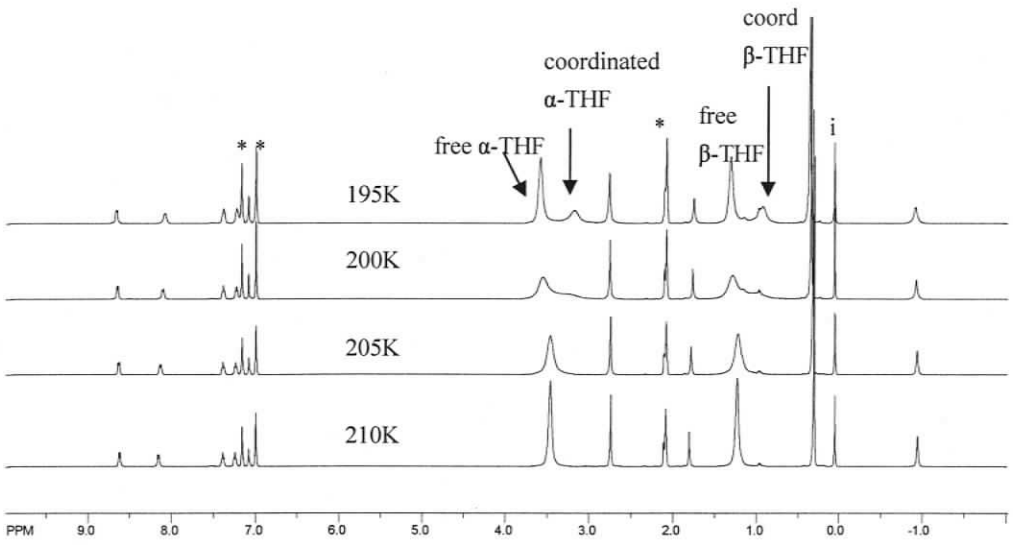

Figure 3.25. VT ^{1}H NMR spectra (500 MHz, C_7D_8) of 150 with excess THF

Similar to the VT NMR spectra of **150**, complex **152** in the temperature range 220K-300K shows similar chemical shifts for the protons of the THF and CH_2SiMe_3 groups, with two distinctive doublet of doublet resonances at 230K (**Fig 3.26**). This indicates a similar dynamic process for complex **150** and **152**. The equilibrium constants at different temperature can also be calculated from the chemical shifts of the α-protons in THF and ΔH° and ΔS° for the dissociation of THF molecule can be also obtained from a Van't Hoff plot as 14 kJ mol^{-1} and 9 J mol^{-1} K^{-1} (**Graph 3.3**), respectively. Addition of five equivalents of THF also generated the bis-THF species **152+THF** at 210K, as indicated by the separate resonance at 3.04 ppm for the α-protons of the coordinated THF molecule (**Fig 3.27, top spectrum**).

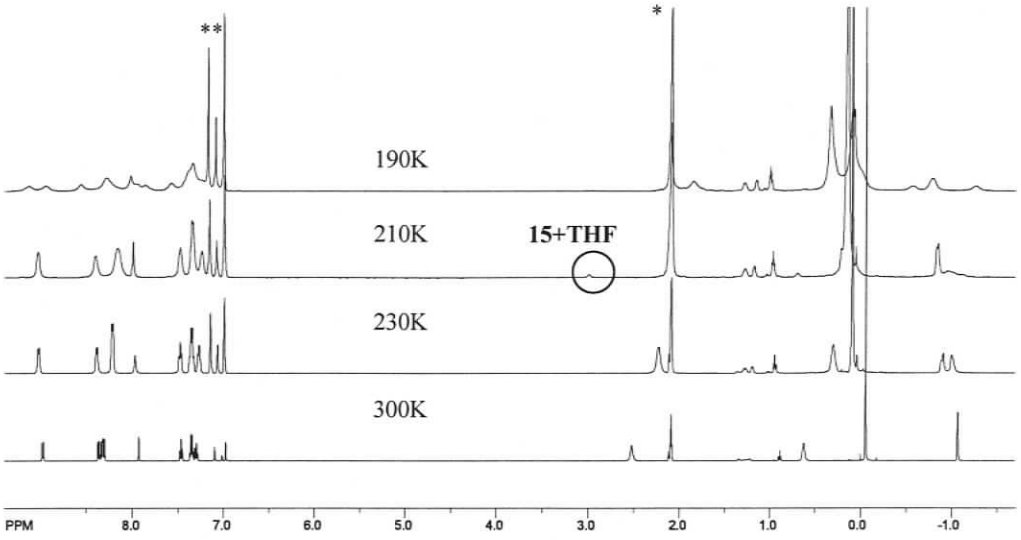

Figure 3.26. VT ^{1}H NMR spectra (500 MHz, C_7D_8) of 152

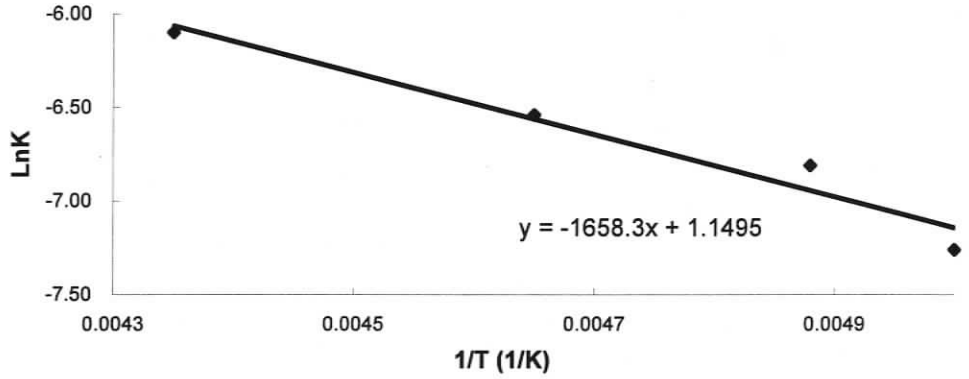

Graph 3.3. Van't Hoff plot for the equilibrium of THF dissociation in 152

Surprisingly, at lower temperature, the resonances of the α-protons in the CH_2SiMe_3 groups show a more complicated pattern. New resonances at 3.00 ppm and -1.12 ppm appear simultaneously (**Fig 3.27, bottom spectrum**) and show great similarity to **152+THF** generated with excess THF, suggesting the formation of some **152+THF** even without the addition of excess THF. A repeat experiment with a more pure sample of **152** still gave these two resonances (**Fig 3.26**), although less was present as indicated by the relative integration. Although this result was originally

very distracting, it provides convincing evidence for a slow THF association/dissociation process for the **152/152+THF** pair at 210K. This also explains the downfield chemical shift for the α-protons of THF at 2.84 ppm at room temperature (2.54 ppm for very clean samples) and the larger amount of **152+THF** in the first VT NMR experiment (**Fig 3.27, bottom spectrum**) because THF molecules associated with the impurities participate in the fast THF exchange process at room temperature and provide the required THF to generate more **152+THF** than a cleaner sample (**Figure 3.26**).

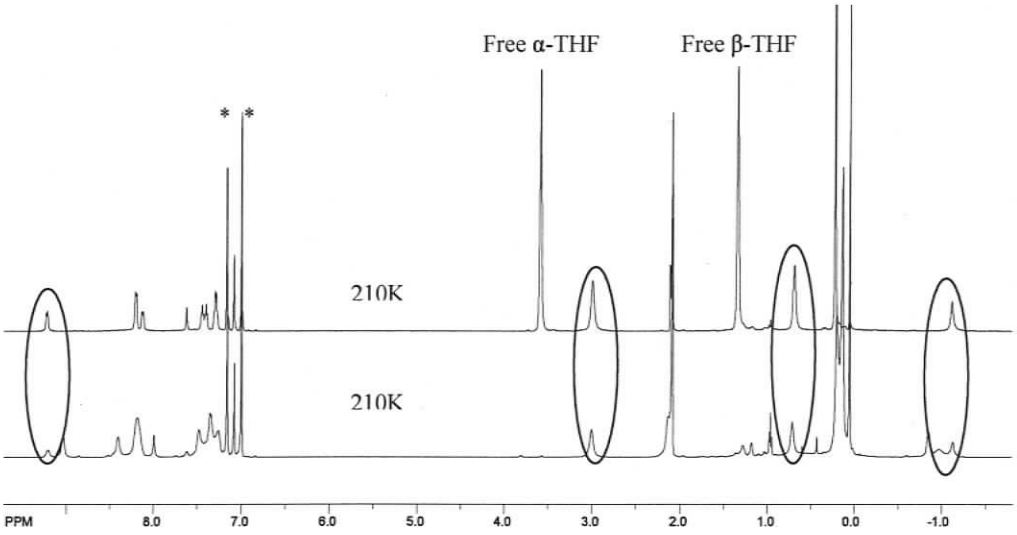

Figure 3.27. Comparison between clean 152+THF generated with excesss THF (top) and the smaller amount of 152+THF generated from impurities in the attempt without excess THF (bottom).

The complexity of the dynamic processes for **152** can also be seen from the three α-CH_2SiMe_3 proton resonances and the two sets of aromatic resonances at 190K (**Fig 3.25**). However, this is not seen for **150** at 190K and the possibility of this being due to a **152+THF** species can be ruled out. One possible explanation is slow

racemization of the sCp ligand. Since the racemization of the sCp ligand is not essentially related to the dynamics of THF exchange, the amount of THF should not have a significant effect on the racemization rate. Thus, if slow racemization does occur, the symmetry of **152+THF** should be lowered and a complicated pattern for the α-protons of CH_2SiMe_3 and aromatic protons should be observed even in the presence of excess THF. However, this is clearly not the case because the spectrum of **152** with excess THF at 190K does not show substantial difference to the spectrum at 210K (**Fig 3.27 top spectrum**).

Another possible explanation, which seems more likely, is that dimerization of **152-THF** occurs at low temperature. The two sCp ligands are chemically equivalent but each half of a given sCp ligand and two $SiMe_3$ groups are inequivalent due to the asymmetric bonding pattern, consistent with the observation of two sets of resonances for sCp ligands and $SiMe_3$ groups. Dimerization can also lead to inequivalence of the α-protons in CH_2SiMe_3 and the three resonances can be explained by accidental overlap between two of the α-protons. This is not observed in the presence of a large excess of THF because the large amount of THF disrupts the dynamics of dimerization.

More surprisingly, when the VT NMR of **152** was carried out in a 1:1 mixture of D_8-toluene and D_8-THF, a new dynamic process was discovered which clearly involves slow generation of a new species from **152+THF** on the NMR timescale. This can be observed from the new resonances for aromatic protons and CH_2SiMe_3 groups (**Fig 3.28**, **circled**). The simple resonance for the α-protons in CH_2SiMe_3

indicates C_{2V} symmetry for the new species and this dynamic process certainly depends on the amount of THF in solution because this was not observed when only five equivalents of THF were added (**Fig 3.27, top spectrum**). Thus, the most likely explanation is the generation of a **152+2THF** species possessing a pseudo-octahedral geometry (**Eq 3.16**), since racemization and dimerization certainly do not match the observation.

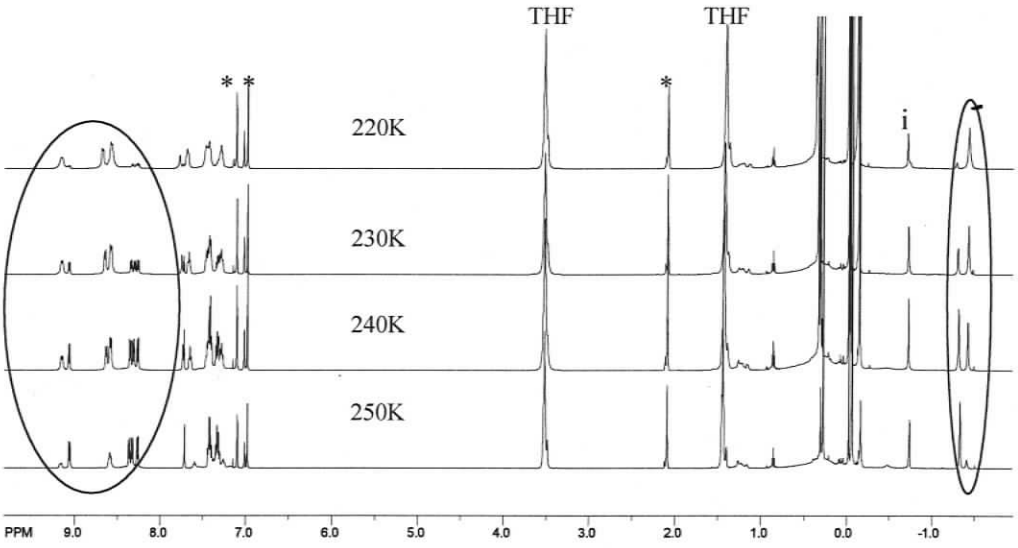

Figure 3.28. VT ^{1}H NMR spectra (500 MHz, 1:1 D_8-THF/C_7D_8) of 152+THF

Eq 3.16

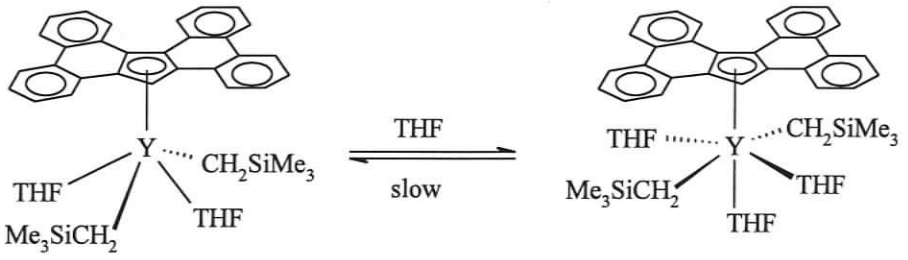

152+THF **152+2THF**

The equilibrium can be established between **152+THF** and **152+2THF** according to the relative integration between these two species. Moreover, the THF

association entropy ΔS° and enthalpy ΔH° can be obtained from Van't Hoff plot as -236 J mol^{-1} K^{-1} and -52 kJ mol^{-1} (**Graph 3.4**). Compared to the entropy of THF dissociation for **150** and **152**, the entropy of a third THF binding is substantially larger possibly due to the highly organized octahedral geometry. However, the significantly larger value of ΔH° is unreasonable compared with **150**, **152** and previously reported examples, because the bond between the metal center and the third coordination THF is expected to be very weak due to the crowding of the metal center. A convincing answer to this dynamic behaviour is still unkown.

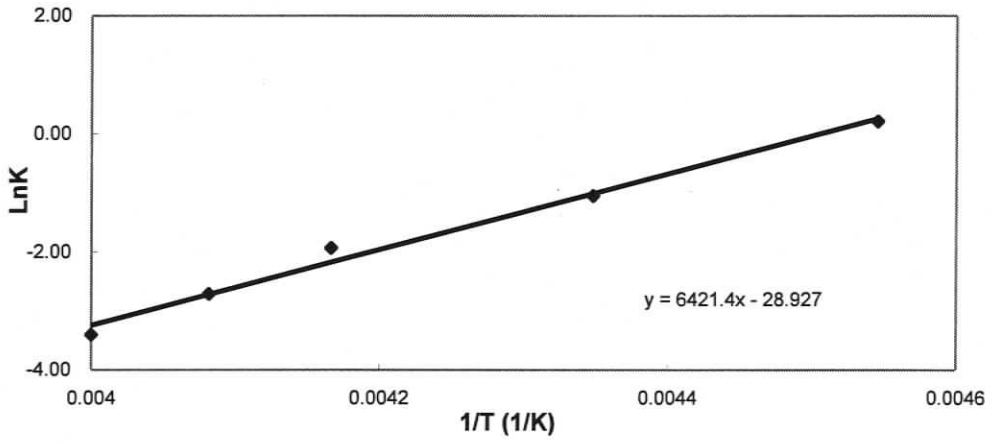

Graph 3.4. Van't Hoff plot for the equilibrium between 152+THF and 152+2THF

Chapter Four

Conclusion and Future Directions

4.1 Phenalenide Chemistry

Lanthanide phenalenide complexes were synthesized successfully by both salt metathesis and protonolysis reactions and demonstrated a more rapid dynamic process than group 10 metal complexes. The solid state structure of **8** revealed that the phenalenide ligand is bonded to the lanthanide metal by a unique η^3-bonding mode. The further modifications of these complexes mostly failed due to the weak bonding between the phenalenide and the metal center. We attribute the easy ligand loss of phenalenide complexes to the strong electron delocalization even after the phenalenide is bonded to the metal. If the aromaticity is disrupted it might be possible to generate an η^3 complex with relatively strong bonds between the metal center and the ligand.

*Meso*benzanthrene (mBzH) **182** possesses a similar structure to phenalene, and the fusion of another six-membered ring disturbs the aromaticity of the phenalenyl ring after deprotonation. Therefore, mBzH **182** is a quite good candidate for further research on phenalenyl derivatives. Preliminary experiments were attempted to understand its reactivity. Surprisingly, mBzH **182** can only react with one equivalent of $Yb[N(SiMe_3)_2](THF)_2$ to generate $(mBz)YbN(SiMe_3)_2(THF)_2$ **183** (**Eq 4.1**), even after long periods of heating, despite the fact that this ligand is not that large. The VT NMR at low temperature did not show a significant change, ruling out the possibility

of a migration process but indicating that the metal center is indeed strongly bonded to a single ring. There are several possible bonding patterns between the ligand and ytterbium metal center (**Fig 4.1**). Bonding patterns (iii) and (iv) are the most likely ones because they possess three aromatic six-membered rings. However, a combination of various NMR experiments was not sufficient to determine the exact structure of this complex. Future work will focus on characterization of this type of complex by incorporation of different substituents so that a full study of their reactivity can take place. The easy loss of the *meso*benzanthrenyl ligand should be very unlikely as indicated by the great stability of this mono-ligand complex at high temperature. Given the stability of ytterbium amide complexes, yttrium alkyl complexes should also be very stable and easily accessible.

Eq 4.1

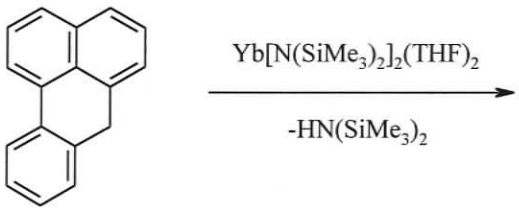

182 **183**

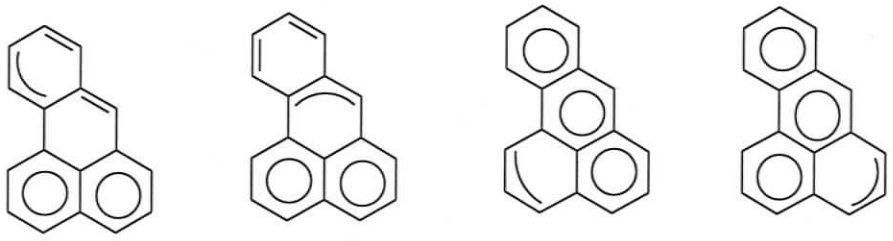

i ii iii iv

Figure 4.1. Four possible bonding modes between a metal center and mBz

4.2 Phenanthrene-Fused Cyclopentadienyl Chemistry

Both bis and mono-alkyl complexes were synthesized by direct protonolysis between neutral ligands and yttrium tris(alkyl) precursors. The bis-alkyl complexes show diverse reactivity, including insertions, acid-base reactions, metallations and polymerization of some small substrates. Moreover, dynamic studies on bis-alkyl complexes **150** and **152** reveal that several equilibra take place between **152/152-THF**, **150/152** and **150/152+THF** and that inversion of the metal center may play a role in the fast THF exchange process. In contrast, the study of mono-alkyl **147** shows the dependence of THF dissociation on temperature. The solid state structures of **147** and **161** also show that large rigid ligands are unable to form the clear 'V'-shaped wedge to block bridging interactions due to the steric repulsion by the fused aromatic groups. Although compared to previously reported mono-alkyl complexes, the chemistry of bis-alkyl complexes **150** and **152** do not show a fundamental difference, our work did provide very valuable information on the reactivities of bis-alkyl Cp complexes, such as the importance of bulky substrates for the acid-base reaction, the use of bidentate substrates for insertion reaction, conditions which can lead to redistribution of the ligands and complicated dynamic behaviours with or without excess THF.

This work shows that rigid steric bulk itself is insufficient to block potential bridging interactions without control of ring orientation. The use of regular silicon-linked ansa-metallocenes also fails to block the bridging interactions because the silicon link is not strong enough to hold the wedge when lanthanide hydrides dimerize and the wedge is also twisted when the ansa link is made of the synthetically more

accessible *1*-position of the five membered rings (**Fig 4.2 i**). Thus, ordinary silicon linked PCp ligands show no substantial advantage over PCp ligands. An alternate silicon link at the *2*-position as shown in **Fig 4.2 ii** should provide a clear wedge, and the usage of a phenyl ring (**Fig 4.2 iii**) might provide the rigidity for ansa-metallocenes which is lacking for a silicon link. Additionally, ligands **ii** and **iii** possess a higher symmetry leading to easier characterization of the complexes. However, the synthesis of these ligands will be a challenge.

The chirality of **152** observed in the solid state is not maintained in solution. However, additional substituents on the carbon skeleton of the sCp ring (**Fig 4.2 iv**) will lock the racemization in solution and generate chiral metal complexes which can be applied in chiral catalysis. Some progress toward synthesis of this ligand has been made, but no suitable synthetic scheme to iv exits at this stage. This is certainly an area for future effort.

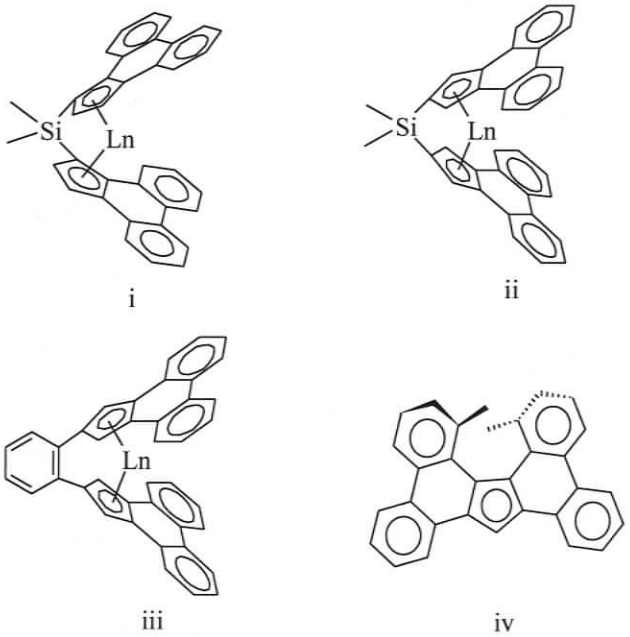

Figure 4.2. Potential ligands for future study

This thesis has broadened the range of aromatic anions used in Group 3 and lanthanide organometallic chemistry and established the basis for a more detailed study. Future work to prepare derivatives with greater control over the orientation of the fused aromatic bulk and to explore the reactivity of these metal complexes in detail can now move forward.

Chapter Five. Experimental

5.1 General Procedures and Instrumentation

All the manipulations of metal complexes were carried out under an argon or nitrogen atmosphere using standard glovebox (Braun, MB150-GH) or Schlenk techniques, with rigorous exclusion of oxygen and water. THF, diethyl ether, hexane and toluene were obtained directly from the solvent purification system or dried by distillation from Na/benzophenone under argon prior to use. Lanthanide precursors $Yb[N(SiMe_3)_2]_2(THF)_2$ and $Y(CH_2SiMe_3)_3(THF)_2$ were prepared as reported in the literature.[9,169] YbI_2 was prepared from ytterbium metal chips and NH_4I in liquid ammonia. The ligands PnH **101**, $(Pn^{Me})H$ **102**,[157] $(Pn^{tBu})H$ **104**,[159] (PCp)H **105**,[197] $(PCp^{Me})H$ **106**, $(PCp^{Ph})H$ **107**,[195,196] (PCp*)H **108**, (PCp')H **109**,[199] (sCp)H **110** [200] were synthesized by following the literatures with minor modifications. All other chemicals were purchased from Aldrich and directly used in reactions.

The ^1H NMR spectra for detailed characterization and dynamic study were mainly recorded on a Bruker AVANCE 500 spectrometer at 500.13 MHz, using the residual solvent resonance for calibration. The ^1H NMR spectra for routine study were recorded on a Bruker AMX 360 at 360.13 MHz or a Bruker AC 300 at 300.13 MHz. The ^{13}C NMR spectra were recorded at 125.77 or 75.47 MHz, using the solvent resonance for calibration. The spectra of ligand anions and metal complexes were recorded at room temperature, unless otherwise specified, in either C_6D_6, D_8-toluene or C_6D_5Br dried over activated 4 Å molecular sieves, or in D_8-THF dried over

Na/benzophenone under argon. Melting points were determined on a Reichert 7905 melting point apparatus and are uncorrected. X-ray crystallographic details for all the metal complexes are given in the Appendix. Elemental analyses were performed by Canadian Microanalytical Services Ltd., Vancouver, B.C. Attempts to obtain Masspec all failed due to rapid decomposition of complexes in the regular procedure. Attempts to obtain very clean crystalline samples for elemental analysis mostly failed, except specified in experimental procedure.

5.2 NMR Data of Ligands and Minor Modification of Procedure

PnH (101)

^{1}H NMR (250 MHz, $CDCl_3$): δ 7.50-6.92 (6H, m, *PnH*), 6.56 (dd, 1H, *alkenylH*), 6.00 (s, 1H, *alkenylH*), 3.95 (s, 2H, PnCH_2).

PnH **101**

(Pn^{Me})H (102)

^{1}H NMR (250 MHz, $CDCl_3$): δ 7.46-6.82 (6H, m, *PnH*), 6.28 (s, 1H, *alkenylH*), 3.82 (s, 2H, PnCH_2), 1.84 (s, 3H, CH_3).

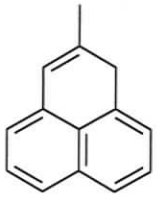

(Pn^{Me})H **102**

(Pn^{tBu})H (104)

^{1}H NMR (270 MHz, $CDCl_3$): δ 7.40 (d, 1H, Pn*H*), 7.33 (d, 1H, Pn*H*), 7.24 (d, 1H, Pn*H*), 6.96 (d, 1H, Pn*H*), 6.40 (t, 1H, *alkenylH*), 3.96 (br, 2H, PnCH_2), 1.31 (s, 9H, CMe_3), 1.30 (s, 9H, CMe_3), 1.15 (s, 9H, CMe_3).

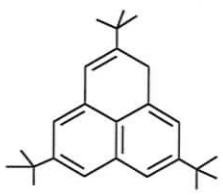

(Pn^{tBu})H **104**

tri-*tert*-butylphenalanone (123)

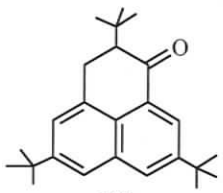

123

Four equivalents of BCl_3 (2.32 g , 20 mmol) were added to the propanate **122** (1.85 g, 5 mmol) in 30 mL dichloromethane while stirring at 0˚C. 10 mL distilled water was added to the mixture after stirring overnight. The organic layer was separated, dried by $MgSO_4$ and evaporated to give brown residue. After the separation by column chromatography, clean **123** was obtained as an off-white powder of 0.27 g in 15% yield.

(PCp)H (105)

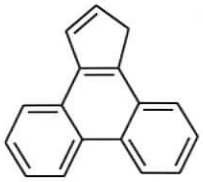
(PCp)H **105**

^{1}H NMR (250 MHz, $CDCl_3$): δ 8.80-8.70 (m, 2H, *arylH*), 8.30-8.00 (m, 2H, *arylH*), 7.80-7.50 (m, 5H, *arylH* and *alkenylH*), 6.80-6.70 (m, 1H, *alkenylH*), 3.86 (t, 3H, $CpCH_2$).

(PCp^{Me})H (106)

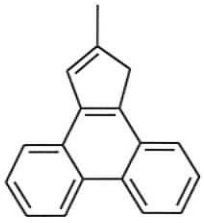
(PCp^{Me})H **106**

^{1}H NMR (250 MHz, $CDCl_3$): δ 8.75-8.68 (m, 2 H, *arylH*), 8.13-8.10 (m, 1 H, *arylH*), 7.96-7.93 (m, 1 H, *arylH*), 7.65-7.53 (m, 4 H, *arylH*), 7.07 (s, 1 H, *alkenylH*), 3.74 (s, 2 H, $CpCH_2$), 2.31 (s, 3 H, *Me*).

(PCp^{Ph})H (107)

^{1}H NMR (600 MHz, $CDCl_3$): δ 8.72 (d, 1H, *arylH*), 8.68 (d, 1H, *arylH*), 8.20 (d, 1H, *arylH*), 8.02 (d, 1H, *arylH*), 7.79 (s, 1H, *alkenylH*), 7.75 (d, 2H, *PhH*), 7.66-7.56 (m, 4H, *arylH*), 7.42 (t, 2H, *PhH*), 7.29 (t, 1H, *PhH*), 4.20 (s, 2H, CpCH_2).

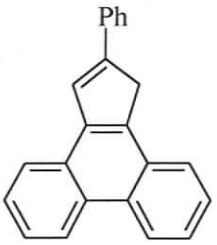

(PCp^{Ph})H **107**

(PCp*)H (108)

^{1}H NMR (90 MHz, $CDCl_3$): δ 8.90-7.30 (m, 8H, *arylH*), 3.77 (m, 1H, MeC*H*), 2.50 (s, 3H, *Me*), 2.05 (s, 3H, *Me*), 1.37 (d, 3H, *Me*).

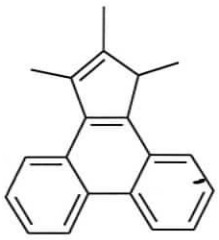

(PCp*)H **108**

(PCp')H (109)

^{1}H NMR (90 MHz, $CDCl_3$): δ 8.85-7.30 (m, 8H, *arylH*), 6.34 (m, 1H, *alkenylH*), 3.77 (m, 1H, CH_3CH), 2.65 (t, 3H, *Me*), 1.42 (d, 3H, *Me*)

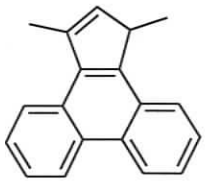

(PCp')H **109**

(sCp)H (110)

^{1}H NMR (250 MHz, $CDCl_3$): δ 8.81-8.76 (2H, m, *arylH*), 8.28-7.08 (m, 15H, *arylH*), 5.39 (s, 1H, Cp*CH*)

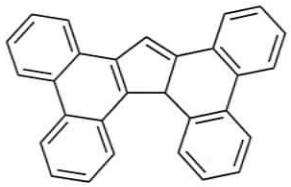

(sCp)H **110**

5.3 Synthesis and Characterization of New Complexes

$Y(Pn)_2(\mu\text{-}Cl)_2Li(Et_2O)_3$ (129) and $[(Pn)_2Y(\mu\text{-}Cl)]_2$ (130)

A solution of n-BuLi (1.6 M, 1.9 mL, 3.0 mmol) in hexane was added dropwise to a solution of phenalene (0.50 g, 3.0 mmol) in 20 mL diethyl ether at 0°C. The mixture turned deep red immediately. After stirring for 30 min at 0°C and 2 hours at room temperature, the deep red solution was transferred by cannula to a stirring suspension of YCl_3 (0.30 g, 1.5 mmol) in 10 mL diethyl ether. After overnight stirring, the mixture turned dark brown-red and was filtered through Celite. The mixture was concentrated by vacuum to 10 mL and stored in the fridge (-10°C) overnight. The mother solution was transferred by cannula to leave a dark brown-red solid. The solid **129** was evaporated under vacuum and taken into the glovebox. ^{1}H NMR (300 MHz, C_6D_6): δ 6.26 (t, 6H, $^3J_{HH}$ = 7.8Hz, β-Pn*H*), 5.58 (d, 12H, $^3J_{HH}$ =7.5Hz, α-Pn*H*), 3.35 (q, 12H, OC*H*$_2$CH$_3$), 1.04 (t, 16H, OCH$_2$C*H*$_3$). The solid product was washed twice with 5 mL hexane and dissolved in toluene; the solution was filtered through Celite, and evaporated to dryness to afford 0.46 g of **130** as a dark brown powder. Yield: 68%. Mp 223°C (decompose). ^{1}H NMR (500 MHz, C_6D_6): δ 6.28 (t, 12H, $^3J_{HH}$ = 7.8Hz, β-Pn*H*), 5.58 (d, 24H, $^3J_{HH}$ = 7.5Hz, α-Pn*H*); ^{13}C NMR (125.7MHz, C_6D_6): δ 139.72 (quaternary Pn*C*), 132.93 (β-Pn*C*), 109.61 (α-Pn*C*).

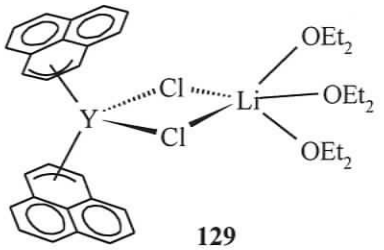

129

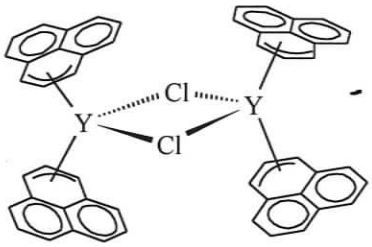

130

$[Y(Pn^{Me})_2(\mu\text{-}Cl)]_2$ (131)

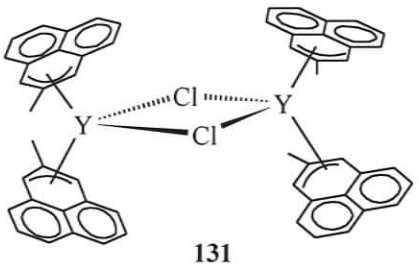

131

A solution of n-BuLi (1.6 M, 0.69 mL, 1.1 mmol) in hexane was added dropwise to a solution of (Pn^{Me})H (0.20 g, 1.1 mmol) in 15 mL diethyl ether at 0˚C. The mixture turned deep red immediately. After stirring one half hour at 0˚C and 2 hours at room temperature, the deep red solution was transferred by cannula to a stirring suspension of YCl_3 (0.11 g, 0.56 mmol) in 10 mL diethyl ether. After overnight stirring, the mixture turned dark brown-red and was filtered through Celite. The mixture was evaporated under vacuum to a dark brown solid and this was taken into the glovebox. The solid product was washed twice with 5 mL hexane and then dissolved in toluene. The resulting solution was filtered through Celite, and evaporated to afford 0.12 g of **131** as a dark brown powder. Yield: 46%. Mp 190˚C (decompose). ^{1}H NMR (500 MHz, C_6D_6): δ 6.14 (t, 4H, $^3J_{HH}$ = 7.7Hz, β-Pn*H*), δ 5.61 (s, 4H, α-Pn^{Me}*H*), 5.54 (d, 4H, $^3J_{HH}$ = 7.7Hz, α-Pn*H*), 5.39 (d, 4H, $^3J_{HH}$ = 7.7Hz, α-Pn*H*); ^{13}C NMR (125.7 MHz, C_6D_6): δ 141.48, 140.00 (quaternary Pn*C*), 132.91 (β-Pn*C*), 111.98, 107.96, 107.13 (α-Pn*C*), 21.69 (*Me*).

Pn^{tBu} $^-Li^+$

A solution of n-BuLi (1.6 M, 1.0 mL, 1.6 mmol) in hexane was added to a solution of (Pn^{tBu})H (0.40 g, 1.2 mmol) in 10 mL hexane. The mixture turned red immediately. After overnight reaction, a red suspension was formed. In the glovebox, the red

suspension was filtered on a sintered glass frit and washed with 5 mL hexane, followed by drying under vacuum to afford 0.26 g of the lithium salt as a toluene-soluble red powder. Yield: 65%. ^{1}H NMR (250 MHz, C_6D_6): δ 5.69 (s, 6H, α-Pn*H*), 1.19 (s, 27H, *CMe*$_3$); ^{13}C NMR (62.9 MHz, C_6D_6): δ 153.03 (quaternary Pn*C*), 141.89 (β-Pn*C*), 101.51 (α-Pn*C*), 34.45 (*C*Me$_3$), 30.63 (C*Me*$_3$).

[Y(Pn^{tBu})(μ-Cl)Cl]$_2$ (132)

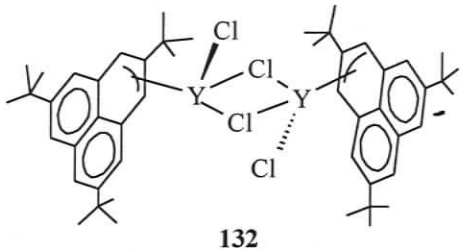

132

A solution of Pn^{tBu}–Li$^+$ (20 mg, 0.059 mmol) in 2 mL toluene was added to a suspension of YCl_3 (23 mg, 0.12 mmol) in 5 mL toluene. After stirring over three days, the mixture changed from red to dark red and was filtered through Celite, followed by removal of solvent under vacuum to afford 24 mg of **132** as a dark red powder. Yield: 81%. Mp 232°C (decompose). ^{1}H NMR (300 MHz, C_6D_6): δ6.02 (s, 12H, α-Pn*H*), 1.09 (s, 54H, C*Me*$_3$); ^{13}C NMR (75.0MHz, C_6D_6): δ 154.56 (quaternary Pn*C*), 138.60 (β-Pn*C*), 109.22 (α-Pn*C*), 34.66 (*C*Me$_3$), 30.19 (C*Me*$_3$).

(Pn)$_2$Yb(THF)$_2$ (133)

PnH (100 mg, 0.60 mmol) was dissolved in 15 mL hexane in a 50 mL Erlenmeyer flask, and Yb[N(SiMe$_3$)$_2$]$_2$(THF)$_2$ (195 mg, 0.30 mmol) in 10 mL hexane was added. The color of reaction mixture changed

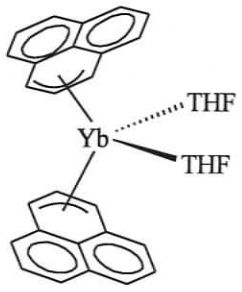

133

rapidly from light red to dark red. The mixture was stirred rapidly overnight to afford a brown-red precipitate. The precipitate was filtered on a sintered glass frit and washed twice with a total volume of 10 mL hexane, followed by drying under vacuum to give 125 mg of **133** as a brown-red powder. Yield: 63%. Mp 86°C (decompose). ^{1}H NMR (300 MHz, C_6D_6): δ 6.32 (br, 6H, β-Pn*H*), 5.61 (br, 12H, α-Pn*H*), 3.26 (br, 8H, α-THF C*H*$_2$), 1.31 (br, 8H, β-THF C*H*$_2$). ^{13}C (125.7MHz, C_6D_6): δ 142.47 (β-Pn*C*), 106.42 (α-Pn*C*), 70.49, 26.03 (THF). A satisfactory elemental analysis could not be obtained despite repeated attempts.

$(Pn^{Me})_2Yb(THF)_2$ (134)

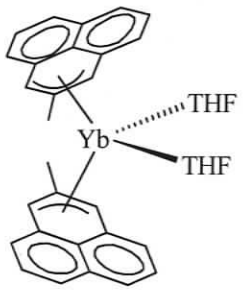

134

(Pn^{Me})H (30 mg, 0.17 mmol) was dissolved in 10 mL hexane in a 50 mL Erlenmeyer flask and Yb[N(SiMe$_3$)$_2$]$_2$(THF)$_2$ (53 mg, 0.085 mmol) in 5 mL hexane was added. The color of the reaction mixture changed rapidly from light red to dark red. The mixture was stirred rapidly overnight to afford a brown-red precipitate. The precipitate was filtered and washed twice with a total volume of 5 mL hexane and dried under vacuum to give 40 mg of **134** as a brown-red powder. Yield: 71%. Mp 81°C (decompose). ^{1}H NMR (300 MHz, C_6D_6): δ 6.33 (br, 4H, β-Pn*H*), 5.59-5.52 (br, 12H, α-Pn*H*), 3.28 (br, 8H, α-THF C*H*$_2$), 1.86 (s, 6H, C*H*$_3$), 1.33 (br, 8H, β-THF C*H*$_2$); ^{13}C NMR (125.7MHz, C_6D_6): δ 142.50 (β-Pn*C*), 109.21, 106.18, 104.53 (α-Pn*C*), 70.11, 26.04 (THF), 22.22 (Pn*Me*); Anal. Calcd. for $C_{36}H_{38}YbO_2$: C 63.99; H 5.67; found C 62.60, H, 5.27.

$(Pn)_2Yb(py)_2$ (135)

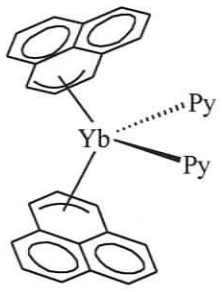

135

1 mL of dry pyridine was added to 20 mg of **133** in 10 mL toluene solution resulting in a color change from deep red to dark brown immediately. After stirring 30 minutes, the solvent was removed by vacuum to give a dark brown solid quantitatively. ^{1}H NMR (250 MHz, C_6D_6): δ 7.97 (br, s, 4H, py), 6.90 (br, s, 2H, py), 6.52 (br, s, 4H, py), 6.23 (t, $^3J_{HH}$= 7.3Hz, 6H, β-Pn*H*), 5.33 (d, $^3J_{HH}$= 7.3Hz, 12H, α-Pn*H*). A satisfactory elemental analysis could not be obtained.

$(Pn^{tBu})_2Yb(THF)$ (136)

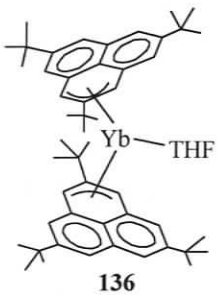

136

$Yb[N(SiMe_3)_2]_2(Et_2O)_2$ (89 mg, 0.14 mmol) and (Pn^{tBu})H (90 mg, 0.27 mmol) were dissolved in 10 mL hexane and heated for 8 days at 70 °C. The solvent was removed under vacuum in the glovebox and the resulting dark red solid was re-dissolved in 3 mL hexane and cooled in the fridge at -50 °C. After two weeks, 32 mg of **136** as dark red crystals was obtained from the solution. Yield: 26%. Mp 182°C (decompose). ^{1}H NMR (300 MHz, C_6D_6): δ5.63 (s, 12H, α-Pn*H*), 3.90 (s, 4H, α-THF CH_2), 1.25 (s, 6H, β-THF CH_2), 1.11 (s, 54H, *CMe*$_3$); ^{13}C NMR (75.5MHz C_6D_6): δ 152.94 (quaternary Pn*C*), 141.56 (β-Pn*C*), 104.52 (α-Pn*C*), 34.4 (*C*Me$_3$), 31.39 (C*Me*$_3$) (Resonances of THF were not observed). Anal. Calcd. for $C_{58}H_{82}O_2Yb$: C 70.77, H 8.39; found: C 71.31, H 9.22.

(Pn^{tBu})Yb[$N(SiMe_3)_2$]($THF)_2$ (137)

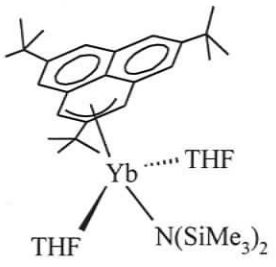

137

(Pn^{tBu})H (110 mg, 0.33 mmol) and Yb[$N(SiMe_3)_2]_2(THF)_2$ (220 mg, 0.33 mmol) were dissolved in 10 mL hexanes and heated overnight at 70 °C. The solvent was removed under vacuum in the glovebox to give 270 mg of **9** as a dark red oily solid. Yield: 90%. ^{1}H NMR (250MHz C_6D_6): δ5.73 (s, 6H, Pn ring *CH*), 3.44 (s, 4H, α-THF CH_2), 1.26 (s, 4H, β-THF CH_2), 1.22 (s, 27H, CMe_3), 0.28 (s, 18H, $SiMe_3$); ^{13}C NMR (63MHz, C_6D_6): δ153.54 (quaternary Pn*C*), 141.56 (β-Pn*C*), 103.59 (α-Pn*C*), 68.34 (α-THF CH_2) 34.37 (CMe_3), 31.04 (CMe_3), 25.55 (β-THF CH_2), 4.39 ($SiMe_3$).

(PCp^{Me})$_2$Y(CH_2SiMe_3)(THF) (147)

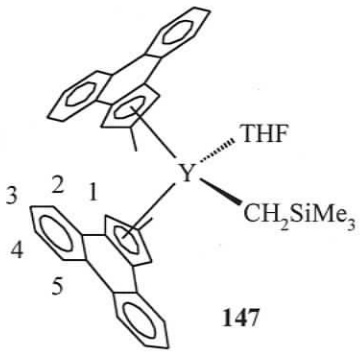

147

To a solution of (PCp^{Me})H (156 mg, 0.68 mmol) in 5 mL toluene was added a solution of Y(CH_2SiMe_3)$_3$($THF)_2$ (170 mg, 0.34 mmol) in 5 mL toluene. The reaction mixture was allowed to stir overnight at 0 °C, and after this time, the solvent was removed under vacuum. The Schlenk flask was transferred to the glovebox for workup. After addition of 20 mL hexane, the solution was filtered through Celite. The solvent was removed by vacuum to give 190 mg of **147** as a pale yellow powder. Crystallization of this pale yellow powder from hexane produced pale yellow crystals. Yield: 88%. Mp 136 °C (decompose). ^{1}H NMR (500

MHz, C_6D_6): δ 8.27 (d, $^3J_{HH}$ = 8.0Hz, 4H, *5,5'-arylH*), 8.00 (dd, $^3J_{HH}$ = 7.9Hz, $^4J_{HH}$ = 1.2Hz, 2H, *2' -arylH*), 7.56 (dd, $^3J_{HH}$ = 7.7Hz, $^4J_{HH}$ = 1.3Hz, 2H, *2-arylH*), 7.36-7.24 (m, 8H, *3,4,3',4' -arylH*), 6.72 (d, $^4J_{HH}$ = 2.0Hz, 2H, *1'-PCpCH*), 6.15 (d, $^4J_{HH}$ = 2.0Hz, 2H, *1-PCpCH*), 1.95 (t, $^3J_{HH}$ = 6.5Hz, 4H, α-THF CH_2), 1.94 (s, 6H, CH_3), 0.57 (s, 9H, SiMe_3), 0.50 (m, 4H, β-THF CH_2), -0.62 (d, $^2J_{YH}$ = 3.7Hz, 2H, CH_2SiMe_3); ^{13}C NMR (125.7 MHz, C_6D_6) δ130.53, 130.20, 127.69, 127.52, 127.21, 125.15, 125.01, 124.37, 124.26, 124.06, 124.03, 121.75, 120.91 (*arylC*), 104.97, 103.89 (PCp*C*H), 72.11, 24.90 (*THF*), 31.07 (d, J_{YC} = 45 Hz, CH_2), 15.56 (PCpCH_3), 5.75 (SiMe_3). Anal. Calcd. for $C_{44}H_{45}SiOY$: C 74.77, H 6.42; found: C 74.93; H 6.23.

$(PCp^{Ph})_2Y(CH_2SiMe_3)(THF)$ (148)

To a solution of $(PCp^{Ph})H$ (48 mg, 0.20 mmol) in 5 mL toluene was added a solution of $Y(CH_2SiMe_3)_3(THF)_2$ (49 mg, 0.10 mmol) in 5 mL toluene. The reaction mixture was allowed to stir overnight at 0 °C. After this time, the Schlenk flask was transferred to the glovebox for workup and the solvent was removed under vacuum. Hexane (10 mL) was added to the residue to extract the product. After filtration through Celite, the solvent was removed to give 69 mg of **148** as a pale yellow powder. Yield: 90%. Mp 102 °C (decompose). ^1H NMR (300MHz, C_6D_6): δ8.21 (m, 4H, *5,5'-arylH*), 7.82 (dd, $^3J_{HH}$ = 8.1Hz, $^4J_{HH}$ = 1.5Hz, 2H, *2'-arylH*), 7.63 (dd, $^3J_{HH}$ = 7.4Hz, $^4J_{HH}$ = 1.2Hz, 4H, *arylH*), 7.36-7.20 (m, 18H,

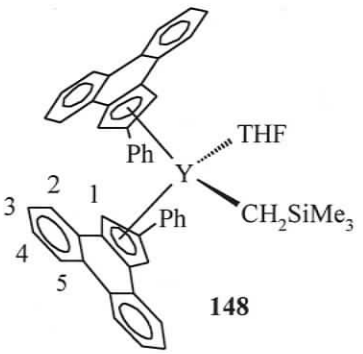

148

arylH), 6.84 (d, $^4J_{HH}$ = 2.4Hz, 2H, *1-PCpCH*), 1.99 (t, $^3J_{HH}$ = 6.6Hz, 4H, α-THF CH_2), 0.51 (t, $^3J_{HH}$ = 6.6Hz, 4H, β-THF CH_2), 0.14 (s, 9H, CH_2Si*Me*$_3$), -1.47 (d, $^2J_{YH}$ = 3.0Hz, 2H, CH_2SiMe$_3$); ^{13}C NMR (75.5MHz, C_6D_6): δ136.68, 130.42, 130.09, 129.68, 129.25, 127.65, 127.59, 126.93, 126.31, 125.55, 125.46, 124.59, 124.19 124.08, 123.87, 123.53, 122.44 (*arylC*), 101.54, 100.20 (CpCH), 71.84, 24.95 (*THF*), 32.40 (d, $^1J_{YC}$ = 46.0Hz, CH_2SiMe$_3$), 5.05 (Si*Me*$_3$). Anal. Calcd. for $C_{54}H_{49}SiOY$: C 78.05, H 5.94; found: C 73.86, H 5.46.

$(PCp)_2Y(CH_2SiMe_3)(THF)$ (149)

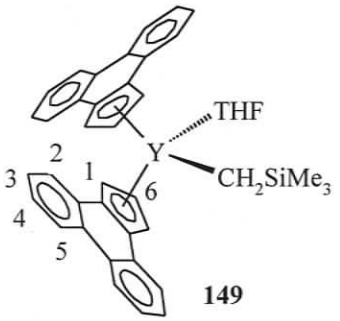

149

To a solution of (PCp)H (86 mg, 0.40 mmol) in 5 mL toluene was added a solution of $Y(CH_2SiMe_3)_3(THF)_2$ (99 mg, 0.20 mmol) in 5 mL toluene. The reaction mixture was allowed to stir overnight at 0°C. After this time, the Schlenk flask was transferred to the glovebox for workup and the solvent was removed under vacuum. After washing with 10 mL hexane, the residue was dried under vacuum to give 72 mg of **149** as a pale yellow powder. Yield: 88%. Mp 156 °C (decompose). ^{1}H NMR (250 MHz, C_6D_6): δ8.21 (d, $^3J_{HH}$ = 7.2Hz, 4H, *5,5'-arylH*), 7.95 (dd, $^3J_{HH}$ = 7.9Hz, $^4J_{HH}$ = 1.2Hz, 2H, *2'-arylH*), 7.56 (m, 2H, *2-arylH*), 7.28-7.20 (m, 8H, *3,4,3',4'-arylH*), 7.00 (t, $^3J_{HH}$ = 2.5Hz, 2H, *1'-CpCH*), 6.42 (t, $^3J_{HH}$ = 2.5Hz, 2H, *1-CpCH*), 6.35 (t, $^3J_{HH}$ = 2.5Hz, 2H, 6-CpC*H*), 1.75 (t, $^3J_{HH}$ =6.1Hz, 4H, α-THF CH_2), 0.59 (s, 9H, CH_2Si*Me*$_3$), 0.36 (m, 4H, β-THF CH_2), -0.62 (d, $^2J_{YH}$ =3.8Hz, 2H, CH_2SiMe$_3$); ^{13}C NMR (75.5 MHz C_6D_6) δ129.96,

128.70 , 128.38, 128.06, 127.82, 127.60, 125.51, 125.24, 124.07, 123.89, (*arylC*), 114.88, (Cp*C*H), 104.81, 102.42 (l,1'-Cp*C*H), 71.32, 24.636 (THF), 31.50 (d, $^{1}J_{YC}$ = 40.4Hz, CH_2SiMe_3), 5.42 ($SiMe_3$);

(PCp*)Y(CH_2SiMe_3)$_2$(THF) (150)

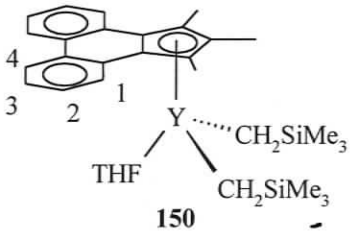

150

The ligand (PCp*)H (129 mg, 0.5 mmol) and $Y(CH_2SiMe_3)_3(THF)_2$ (250 mg, 0.5 mmol) were mixed in 5 mL toluene and stirred overnight. Removal of toluene gave a yellow residue which was re-dissolved in hexanes and filtered through Celite to give a clear yellow solution. Removal of hexanes afforded a yellow powder. Crystallization of this yellow powder afforded 80 mg **150** as pale yellow plates. Yield: 20%. Mp 110°C (decompose). ^{1}H NMR (500 MHz C_6D_6): δ 8.47 (dd, $^{3}J_{HH}$ = 8.2Hz, $^{4}J_{HH}$ = 0.8Hz, 2H, *1-arylH*), 8.25 (dd, $^{3}J_{HH}$ = 8.4Hz, $^{4}J_{HH}$ = 1.0Hz, 2H, *4-arylH*), 7.34 (m, 2H, *2-arylH*), 7.20 (m, 2H, *3-arylH*), 2.78 (s, 6H, Cp*Me*), 2.52 (t, 4H, α-THF CH_2), 2.32 (s, 3H, Cp*Me*), 0.60 (m, 4H, β-THF CH_2), 0.26 (s, 18H, $SiMe_3$), -0.60 (d, $^{2}J_{YH}$ = 3.2Hz, 4H, YCH_2); ^{13}C NMR (125.8 MHz, C_6D_6): δ131.73, 129.00, 128.58, 127.70, 124.72, 124.43, 123.94, 118.26, 113.70 (*arylC*), 70.21 24.69 (THF), 37.40 (d, $^{1}J_{YC}$ = 45 Hz, Y-CH_2), 16.30 (Cp*Me*), 11.75 (Cp*Me*), 4.76 ($SiMe_3$);; Anal. Calcd. for $C_{32}H_{47}OSi_2Y$: C 64.84, H 7.99; found: C 64.98, H 8.07.

(PCp*)Y(CH_2SiMe_3)$_2$(bipy) (151)

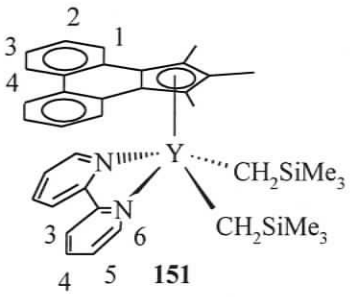

151

Addition of 11 mg 2.2'-bipyridine (0.07 mmol) in 1 mL toluene to 42 mg **150** (0.07mmol) in 5 mL toluene afforded a deep red solution. After gentle stirring for 5 minutes, the solvent was removed by vacuum to give a red solid in quantitative yield. ^{1}H NMR (300 MHz, C_6D_6): δ 8.26 (d, $^3J_{HH}$ = 5.2Hz, 2H, *6-bipy*), 7.94 (dd, $^3J_{HH}$ = 7Hz, $^4J_{HH}$ = 2.2Hz, 2H, *1-arylH*), 7.73 (dd, $^3J_{HH}$ = 7Hz, $^4J_{HH}$ = 2.6Hz, 2H, *4-arylH*), 7.03-6.91 (m, 4H, *2,3-arylH*), 6.64 (dt, 2H, $^3J_{HH}$ = 7Hz, *4-bipy*), 6.35 (d, 2H, $^3J_{HH}$ = 8Hz, *3-bipy*), 6.28 (dd, $^3J_{HH}$ = 6.6Hz, $^4J_{HH}$ = 2.2Hz, 2H, *5-bipy*), 2.76 (s, 6H, Cp*Me*), 2.58 (s, 3H, Cp*Me*), 0.29 (s, 18H, Si*Me*$_3$), -0.22 (dd, $^2J_{YH}$ = 3.0Hz, $^3J_{HH}$ = 11Hz, 2H, Y*CH*$_2$), -0.45 (dd, $^2J_{YH}$ =3.0Hz, $^3J_{HH}$ = 11Hz, 2H, Y*CH*$_2$), free THF resonances were observed at 3.57 and 1.45 ppm; ^{13}C NMR (75.5 MHz, C_6D_6) δ151.70, 138.64, 128.40, 128.08, 126.80, 124.35, 123.92, 123.35, 122.78, 120.47, 113.30 (*arylC*), 32.98 (d, J_{YC} = 38.6Hz, Y-*C*H$_2$), 16.44 (Cp*Me*), 12.47 (Cp*Me*), 5.27 (Si*Me*$_3$).

(sCp)Y(CH_2SiMe_3)$_2$(THF) (152)

To a solution of (sCp)H (156 mg, 0.68 mmol) in 5 mL toluene was added a solution of Y(CH_2SiMe_3)$_3$(THF)$_2$ (170 mg, 0.34 mmol) in 5 mL toluene. The reaction mixture was allowed to stir overnight at 0 °C and after this time, the solvent was

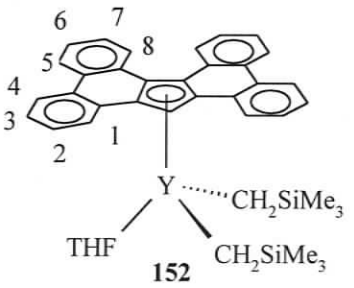

152

removed under vacuum. The Schlenk flask was transferred to the glovebox for workup. After addition of 40 mL hexanes, the solution was filtered through Celite and the solvent was removed by vacuum to give 190 mg of **152** as a pale yellow powder. Yield: 88%. Recrystallization of the pale yellow powder from hexane produced pale yellow crystals at -50 °C. Mp 134°C (decompose). ^{1}H NMR (500 MHz C_6D_6): δ 9.03 (dd, $^{3}J_{HH}$ = 8.0Hz, $^{4}J_{HH}$ = 1.2Hz, 2H, *8-arylH),* 8.40 (dd, $^{3}J_{HH}$ = 8.0Hz, $^{4}J_{HH}$ = 1.2Hz, 2H, *1-arylH*), 8.37 (m, 4H, *4,5-arylH*), 8.00 (s, 1H, Cp*H*), 7.48 (m, 2H, *2-arylH*), 7.38-7.34 (m, 4H, *3, 6-arylH*), 7.30 (m, 2H, *7-arylH*), 2.54 (br, 4H, α-THF CH_2), 0.59 (br, 4H, β-THF CH_2), 0.02 (s, 18H, SiMe_3), -0.98 (d, $^{2}J_{YH}$ = 3.1Hz, 4H, Y-CH_2); ^{13}C NMR (125MHz, C_6D_6): δ131.11, 130.69, 130.06, 129.16, 128.11, 127.26, 126.88, 126.52, 125.90, 125.64, 125.11, 125.07, 124.21, 115.53 (*arylC*), 92.41 (CpCH), 70.40, 24.66 (*THF*), 37.92 (d, $^{1}J_{YC}$ = 45Hz, Y-CH_2), 4.34 (SiMe_3). Anal. Calcd. for $C_{41}H_{47}Si_2OY$: C 70.26, H 6.76; found: C 70.31, H 6.67.

(sCp)Y(CH_2SiMe_3)$_2$(bipy) (154)

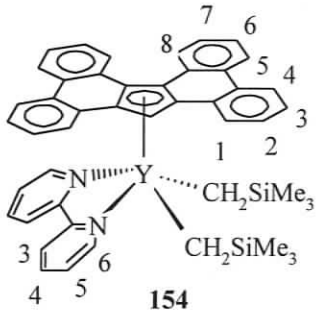

154

Addition of 3 mg 2.2'-bipyridine (0.02 mmol) to 14 mg **152** (0.02 mmol) in 0.5 mL C_6D_6 afforded a deep red solution. The ^{1}H NMR spectrum was obtained immediately. ^{1}H NMR (300 MHz, C_6D_6): δ 8.60 (d, $^{3}J_{HH}$ = 8.0Hz, 2H, *8-arylH),* 8.28 (d, $^{3}J_{HH}$ = 8.0Hz, 2H, *1-arylH*), 8.28 (s, 1H, sCpCp*H*), 8.18 (d, $^{3}J_{HH}$ = 8.4Hz , 4H, *4,5-arylH*), 7.63 (d, $^{3}J_{HH}$ = 5.2Hz, 2H, *6-bipy*), 7.55 (t, $^{3}J_{HH}$ = 7.4Hz, 2H, *7-arylH*), 7.37 (m, 2H, *2-arylH*), 7.09 (t, $^{3}J_{HH}$ = 7.8Hz, 2H,

6-arylH), 6.89 (t, $^3J_{HH}$ = 7.5Hz, 2H, *3-arylH*), 6.57 (dt, $^3J_{HH}$ = 7.8Hz, $^4J_{HH}$ = 1.5Hz, 2H, *4-bipy*), 6.36 (d, 2H, $^3J_{HH}$ = 7.8Hz, *3-bipy*), 6.11 (t, 2H, $^3J_{HH}$= 6.3Hz, *5-bipy*), 0.06 (s, 18H, Si*Me*$_3$), -0.82 (dd, $^2J_{YH}$ = 3.0Hz, $^2J_{HH}$= 11.5Hz, 2H, Y*CH*$_2$), -0.88 (dd, $^2J_{YH}$ = 3.0Hz, $^2J_{HH}$ = 11.0Hz, 2H, Y*CH*$_2$), free THF resonances were observed at 3.57 and 1.45 ppm. The carbon NMR spectrum was not obtained cleanly due to the low solubility of **154**.

(sCp)Y(CH$_2$SiMe$_3$)$_2$(DME) (155)

A large excess of DME (0.5 mL) was added to **152** (70 mg, 0.1 mmol) in 5 mL toluene. After stirring overnight, the color of the mixture changed from pale yellow to brown-yellow. After the solvent was removed by vacuum, the residue was washed by 10 mL hexanes and dried under vacuum to give 56 mg of **17** as a light brown product. Yield: 80%. Mp. (decompose slowly on heating). ^{1}H NMR (300 MHz C_6D_6): δ 8.99 (dd, $^3J_{HH}$ = 8.8Hz, $^4J_{HH}$ = 2.1Hz, 2H, *8-arylH*), 8.36-8.46 (m, 6H, *1,4,5-arylH*), 7.99 (s, 1H, sCpCpC*H*), 7.50 (t, 2H, *2-arylH*), 7.39-7.30 (m, 6H, *3,6,7-arylH*), 2.22 (s, 6H, C*H*$_3$O), 1.83 (s, 4H, OC*H*$_2$C*H*$_2$O), 0.11 (s, 18H, Si*Me*$_3$), -1.26 (d, $^2J_{YH}$ = 3.0 Hz, C*H*$_2$SiMe$_3$); ^{13}C NMR (75.5MHz, C_6D_6): δ131.40, 1, 130.52, 130.14, 128.08, 127.93, 127.39, 126.35, 126.23, 125.65, 125.34, 125.04, 124.92, 123.96, 115.37 (*arylC*), 93.08 (CpCH), 69.85, 62.43 (DME), 35.05 (d, $^1J_{YC}$ = 41.4Hz, *C*H$_2$SiMe$_3$), 4.96 (Si*Me*$_3$).

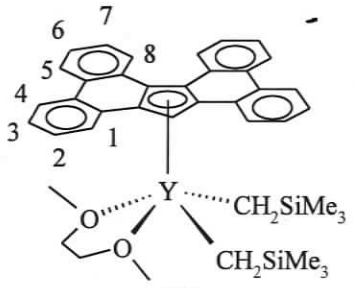

155

$(PCp^{Me})_2YCl(THF)$ (156)

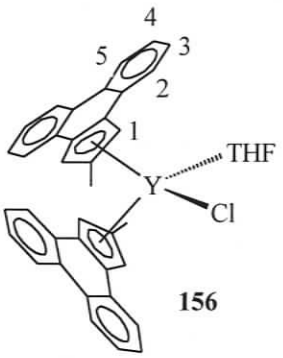

156

$PCp^{Me}Li^+$ (129 mg, 0.55 mmol) (precipitate from the reaction between neutral ligand and n-butyllithium in toluene) in 10 mL THF was transferred through a cannula to an YCl_3 (53 mg, 0.28 mmol) suspension in 10 mL THF while stirring. The mixture was allowed to stir overnight, and the color of solution changed from deep brown to deep red. After the removal of THF, the Schlenk flask was taken into the glovebox for workup. The residue was washed with 10 mL hexane and re-dissolved in 10 mL toluene. After filtration through Celite to give a clear yellow-brown solution, the solvent was evaporated under vacuum to give 110 mg of **156** as a yellow powder. ^{1}H NMR (250 MHz, C_6D_6) δ 8.18 (br, 4H, *5,5'-arylH*), 7.92 (br, 2H, *2'- arylH*), 7.30 (br, 2H, *2-arylH*), 7.15 (br, 8H, *3,3',4,4'-arylH*), 6.64 (br, 2H, *1'-CpCH)*, 6.48 (br, 2H, *1-CpCH*), 2.33 (br, 6H, $CpCH_3$), 1.93 (br, 4H, α-THF CH_2), 0.41 (br, 4H, β-THF CH_2). A clean ^{13}C NMR spectrum could not be obtained due to the presence of significant amount of impurities in this sample.

$(PCp^{Me})_2Y(\mu\text{-}Me)_2Li(THF)_2$ (157)

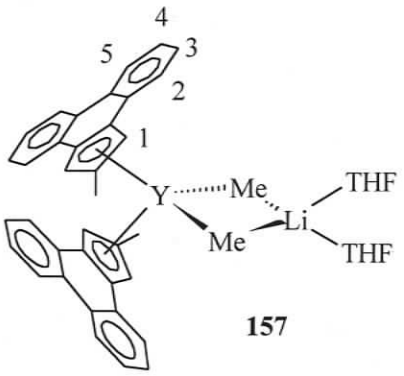

157

Methyllithium (0.21 mL of a 1.5 M solution in diethyl ether, 0.32 mmol) was added by syringe to **156** (60 mg, 0.094 mmol) in 10 mL THF while stirring. The mixture was allowed to stir overnight. The Schlenk flask was taken into the glovebox for workup after removal of solvent. Toluene (10 mL) was added to the solid residue and the resulting solution was filtered through Celite and evaporated under vacuum to give 25 mg of **157** as a brown-yellow product. Yield: 42%. ^{1}H NMR (500 MHz, C_6D_6): δ 8.37 (d, $^3J_{HH}$ = 7.0Hz, 4H, *5-arylH*), 7.81 (br, 4H, *2-arylH*), 7.32-7.22 (m, 8H, *3,4-arylH*), 6.41 (s, 4H, *1-CpCH*), 2.72 (br, 8H, α-THF CH_2), 2.22 (s, 6H, CpCH_3), 0.35 (br, 8H, β-THF CH_2), -2.25 (br, 6H, Y*Me*); ^{13}C NMR (125.7MHz, C_6D_6) δ131.10, 129.72, 128.67, 127.91, 127.50, 127.22, 123.17, 120.40 (*arylC*), 103.24 (CpCH), 68.41, 30.62 (THF), 32.68 (d, $^1J_{YC}$ = 50 Hz, CH_3).

$(PCp^{Me})_2Yb(THF)_2$ (158)

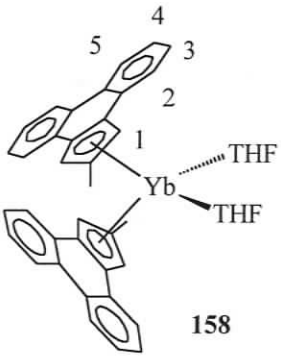

158

To a solution of $Yb[N(SiMe_3)_2]_2(THF)_2$ (85 mg, 0.13 mmol) in 5 mL toluene was added a solution of (PCp^{Me})H (60 mg, 0.26 mmol) in 5 mL toluene in the glovebox. On addition of ligand, the mixture changed color from bright red to dark red. The mixture was

allowed to stir overnight, and then was filtered through Celite. The solvent was removed by vacuum to give 75 mg of **158** as a red powder. Yield: 74%. ^{1}H NMR (300 MHz, C_6D_6): δ 8.26 (d, $^{3}J_{HH}$ = 7.9Hz, 4H, *5-arylH*), 7.82 (d, $^{3}J_{HH}$ = 7.9Hz, 4H, *2-arylH*), 7.26 (t, $^{3}J_{HH}$ =7.3Hz, 4H, *3 or 4-arylH*), 7.15 (t, $^{3}J_{HH}$ = 7.5Hz, 4H, *3 or 4-arylH*), 6.32 (s, 4H, *1-CpCH*), 2.36 (s, 6H, CpCH_3), 2.16 (br, 8H, α-THF CH_2), 0.71 (br, 8H, β-THF CH_2); ^{13}C NMR (75.5 MHz, C_6D_6) δ 130.31, 127.77, 126.89, 124.56, 124.09, 123.14, 122.98, 120.41 (*arylH*), 100.99 (CpCH), 69.81, 25.25 (THF), 16.20 (CH_3).

$(PCp^{Me})_2$Yb(S-p-tolyl)(THF) (159)

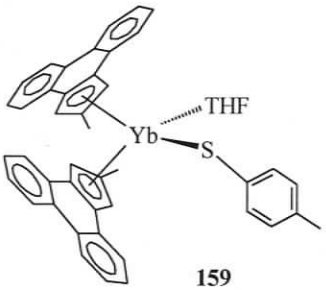

159

To a solution of **158** (39 mg, 0.05 mmol) in 5 mL toluene was added a solution of p-tolyldisulphide (6 mg, 0.025 mmol) in 1 mL toluene. The solution changed to deep purple immediately and was allowed to stir for another 10 minutes. After removing the solvent by vacuum, the residue was washed by hexane and then dried by vacuum to give 40 mg of **159** as a deep purple powder. Yield: (88%), ^{1}H NMR (300 MHz, C_6D_6, 300K) δ 90.05, 38.77, 29.19, 21.78, 17.78, 16.62, 15.22, -2.44, -28.12, -36.72, -97.66.

$(sCp)_2Yb(THF)$ (160)

To a solution of (sCp)H (68 mg, 0.2 mmol) in 10 mL toluene was added dropwise a solution of $Yb[N(SiMe_3)_2]_2(THF)_2$ (130 mg, 0.2 mmol) in 5 mL toluene. The reaction mixture was allowed to stir overnight, and after this time, the solvent was removed under vacuum to give a red-peach powder. Recrystallization of this powder from toluene produced 45 mg of **160** as red crystals at room temperature. Yield: 46%. Mp 134-136°C. ^{1}H NMR (500 MHz C_6D_6): δ 8.55 (d, $^3J_{HH}$ = 7.8Hz, 4H, *arylH*), 8.34 (d, $^3J_{HH}$ = 8.1Hz, 4H, *arylH*), 8.23 (d, 4H, *arlyH*), 8.19 (br, 4H, *arylH*), 7.77 (s, 2H, *CpH*), 7.57 (t, $^3J_{HH}$ = 7.3Hz, 4H, *arylH*), 7.45 (t, $^3J_{HH}$ = 7.5Hz, 4H, *arylH*), 7.13-7.00 (m, 8H, *arylH*), 1.47 (br, 4H, α-THF CH_2), 0.47 (br, 4H, β-THF CH_2); ^{13}C NMR (125.7 MHz, C_6D_6): δ131.89, 130.83, 129.58, 129.01, 127.87, 126.88, 125.26, 124.97, 124.93, 124.80, 124.74, 123.85, 123.36, 114.40 (*arylC*), 92.4 (Cp*CH*), 69.33, 24.94 (THF). Anal. Calcd. for $C_{62}H_{42}OYb$: C 76.30, H 4.34; found: C 70.25, H 4.41.

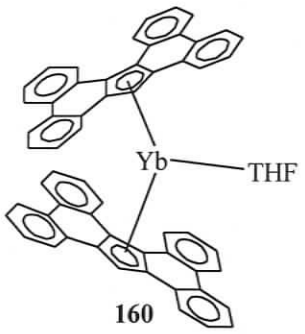

160

$[(PCp^{Ph})_2Y(\mu\text{-}H)]_2$ (161)

Phenylsilane (30 mg, 0.28 mmol) was added to **148** (135 mg, 0.16 mmol) in 5 mL hexanes solution. The mixture changed from pale yellow to light yellow-brown

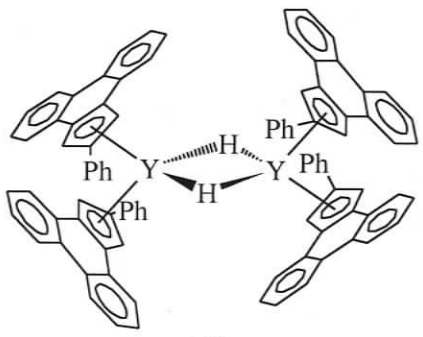

161

immediately. After one hour, a pale yellow precipitate formed in solution. The mixture was allowed to stir overnight. The color of precipitate changed to light orange yellow. Removal of the hexanes layer and drying of the precipitate gave 80 mg of **161** as a light orange-yellow product. ^{1}H NMR (300 MHz, C_6D_6): δ 8.90 (d, $^2J_{HH}$ = 7.5Hz, *arylH*), 8.67 (d, $^2J_{HH}$ = 8.1Hz, *arylH*), 8.33 (d, $^2J_{HH}$ = 8.1Hz, *arylH*), 7.68 (t, $^2J_{HH}$ = 7.5Hz, *arylH*), 7.59 (t, $^2J_{HH}$ = 7.2Hz, *arylH*), 8.90 (d, $^2J_{HH}$ = 7.5Hz, *arylH*), 7.42-7.00 (m, *arylH*), 6.72 (d, $^2J_{HH}$ = 6.6Hz, *arylH*), 6.62 (d, $^4J_{HH}$ = 2.4Hz, *arylH*), 6.23 (t, $^2J_{HH}$ = 7.5Hz, *arylH*), 5.30 (d, $^2J_{HH}$ = 8.1Hz, *arylH*), 3.50 (t, $^1J_{YH}$ = 34.5Hz). The resonances could not be assigned completely due to the presence of considerable impurities and failing to obtain resonanable integrations.

(PCp*)Y($O_2CCH_2SiMe_3$)$_2$ (162)

Into an evacuated Schlenk flask, CO_2, dried over sieves, was introduced into the flask along with **150** (50 mg, 0.082 mmol) in 5 mL hexanes. A white precipitate formed immediately. The mixture was allowed to stir overnight and then taken into the glovebox for workup. Decanting the hexanes layer from the white precipitate and drying the precipitate gave 30 mg of **162** as a white powder. Yield: 60%. ^{1}H NMR (C_6D_6, 500 MHz): δ 8.55 (d, $^3J_{HH}$ = 8.1Hz, 2H, *1-arylH*), 8.43 (d, $^3J_{HH}$ = 7.6Hz, 2H, *4-arylH*), 7.42 (m, 2H, *2-arylH*), 7.28 (m, 2H, *3-arylH*), 2.72 (s, 6H, Cp*Me*), 2.30 (s, 3H, Cp*Me*), 1.10 (s, 4H, CO_2CH_2), 0.00 (s, 18H, Si*Me*$_3$); ^{13}C NMR (125.7 MHz, C_6D_6):

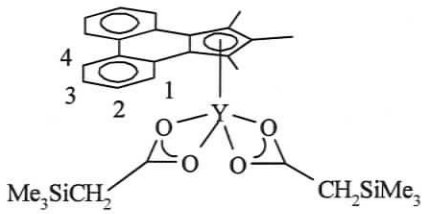

162

δ185.42 (*CO*$_2$), 132.57, 128.68, 128.39, 128.07, 127.05, 125.38, 124.22, 118.80, 114.46 (*arylC*), 29.63 (CO_2CH_2), 15.26 (Cp*Me*), 11.53 (Cp*Me*), -0.62 (Si*Me*$_3$). mp 234°C (decompose); Anal. Calcd. for $C_{30}H_{39}O_4Si_2Y$: C 59.20, H 6.46; found: C 60.18, H, 6.29.

(PCp*)Y[κ^2-(N,O)-Me$_3$SiN(CH$_2$SiMe$_3$)CO]$_2$ (163)

Me_3SiNCO (6 mg, 0.05 mmol) was added to 6 mg **150** (0.01 mmol) in 1 mL toluene solution and allowed to stir for 5 hours. Removal of solvent under vacuum afforded an off-white powder quantitatively.

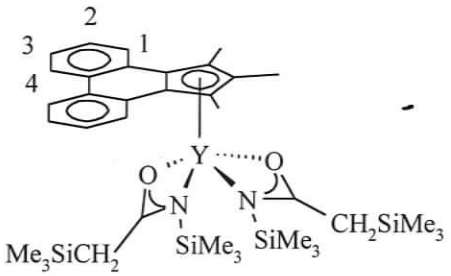

163

^{1}H NMR (C_6D_6, 300 MHz): δ 8.58 (d, $^3J_{HH}$= 8.0Hz, 2H, *1-aryl H*), 8.42 (d, $^3J_{HH}$ = 8.0Hz, 2H, *4-aryl H*), 7.45 (t, $^3J_{HH}$ = 7.3Hz, 2H, *2-aryl H*), 7.32 (t, $^3J_{HH}$ = 7.4Hz, 2H, *3-aryl H*), 2.79 (s, 6H, Cp*Me*), 2.31 (s, 3H, Cp*Me*), 1.65 (s, 4H, CH_2SiMe_3), 0.06 (s, 18H, CH_2Si*Me*$_3$), -0.05 (s, 18H, NSi*Me*$_3$); ^{13}C NMR (75.5 MHz, C_6D_6): δ 188.54 (*NCO*), 129.68, 128.72, 128.40, 127.25, 125.18, 124.33 (*arylC*), 31.40 (CH_2), 15.28 (Cp*Me*), 11.92 (Cp*Me*), 1.67 (CH_2Si*Me*$_3$), -0.28 (NSi*Me*$_3$).

(sCp)Y[κ^2-(N,O)- Me$_3$SiN(CH$_2$SiMe$_3$)CO]$_2$(THF) (164)

Me$_3$SiNCO (6 mg, 0.05 mmol) was added to 7 mg of **152** (0.01 mmol) in 1 mL toluene solution and allowed to stir overnight. Removal of solvent under vacuum afforded an oily solid quantitatively. ^{1}H(C$_6$D$_6$, 300MHz): δ 9.22 (d, $^3J_{HH}$ = 7.9Hz, 2H, *8-arylH*), 8.42-8.47 (m, 6H, *1,4,5,-arylH*), 7.90 (s, 1H, sCpCpC*H*), 7.52-7.35 (m, 8H, *2,3,4,5-arylH*), 2.99 (br, 4H, α-THF *CH$_2$*), 1.37 (s, 4H, C*H$_2$*SiMe$_3$), 1.01 (br, 4H, β-THF *CH$_2$*), 0.02 (s, 18H, CH$_2$*SiMe$_3$*), -0.22 (s, 18H, N*SiMe$_3$*); ^{13}C NMR (75MHz, C$_6$D$_6$): δ188.78 (N*C*O), 130.09, 128.70, 128.38, 127.57, 127.24, 126.11, 125.28, 125.07, 124.58, 124.25, 115.60 (*arylC*), 94.89 (Cp*C*H), 69.53, 25.51 (THF), 30.89 (C*H$_2$*SiMe$_3$), 1.53 (CH$_2$Si*Me$_3$*), -0.22 (NSi*Me$_3$*).

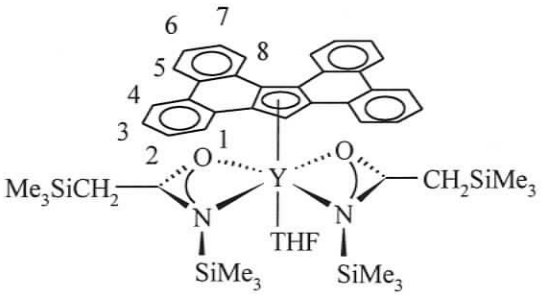

164

(PCp*)Y[κ^2-(N,N)-iPrN(CH$_2$SiMe$_3$)CN(i-Pr)]$_2$ (165)

Diisopropylcarbodiimide (6 mg, 0.05 mmol) Me$_2$CHNCNCHMe$_2$ was added to 6 mg **150** (0.01 mmol) in 1 mL toluene solution and allowed to stir overnight. Removal of solvent under vacuum afforded an off-white powder quantitatively. ^{1}H NMR (C$_6$D$_6$, 300MHz): δ 8.71 (d, $^3J_{HH}$ = 8.6 Hz, 2H, *1-aryl H*), 8.55 (d, $^3J_{HH}$ = 9.3Hz, 2H, *4-aryl H*), 7.53 (t, $^3J_{HH}$ = 7.8 Hz, 2H, *2-arylH*),

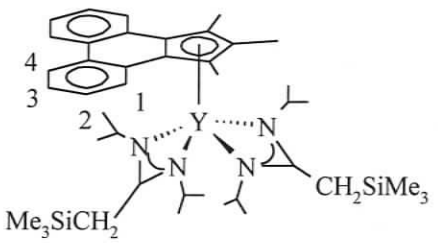

165

7.37 (m, $^3J_{HH}$ = 7.6 Hz, 2H, *3-aryl H*), 3.26 (m, 4H, C*H*Me$_2$), 2.87 (s, 6H, Cp*Me*), 2.41 (s, 3H, Cp*Me*), 1.83 (s, 4H, *CH*$_2$SiMe$_3$), 0.94 (d, 24H, $^3J_{HH}$ = 7.6 Hz, CH*Me*$_2$) 0.06 (s, 18H, Si*Me*$_3$); ^{13}C NMR (75.5 MHz, C_6D_6): δ 177.40 (*NCN*), 127.06, 125.88, 124.35, 124.31 (*arylC*), 48.15 (*CH*Me$_2$), 25.91 (CH*Me*$_2$), 18.96 (*C*H$_2$SiMe$_3$), 17.22 (Cp*Me*), 13.20 (Cp*Me*), 0.42 (Si*Me*$_3$).

(PCp*)Y(CCSiMe$_3$)$_2$(THF) (166), [PCp*Y(CCSiMe$_3$)(THF)]$_2$(μ^2-CCSiMe$_3$)$_2$] (167)

Trimethylsilylacetylene (20 mg, 0.2 mmol) was added to **150** (32 mg, 0.05 mmol) in a mixture of 0.5 mL THF and 3 mL toluene while stirring. The solution was allowed to stir overnight. Removal of solvent gave 30 mg of **166** (characterized by NMR) as a pale yellow residue. The residue was dissolved in hexanes and cooled at -40°C to give **167** (characterized by X-ray, **Fig 3.16**) as pale yellow crystals. Yield: 91%. Mp 102°C (decompose). ^{1}H NMR (C_6D_6, 500 MHz): δ 8.78 (d, $^3J_{HH}$ = 8.0Hz, 2H, *1-arylH*), 8.39 (d, $^3J_{HH}$ = 7.8Hz, 2H, *4-arylH*), 7.50 (m, 2H, *2-arylH*), 7.32 (m, 2H, *3-arylH*), 3.26 (t, 4H, α-THF *CH*$_2$), 2.98 (s, 6H, Cp*Me*), 2.36 (s, 3H, Cp*Me*), 0.60 (brs, 4H, β-THF *CH*$_2$), 0.28 (s, 18H, Si*Me*$_3$); ^{13}C NMR (125.7 MHz, C_6D_6): δ171.23 (d, $^1J_{YC}$ = 53.6Hz, α-YC), 132.37, 129.84, 129.47,

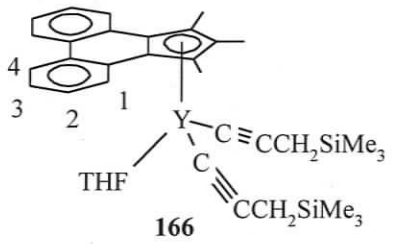

166

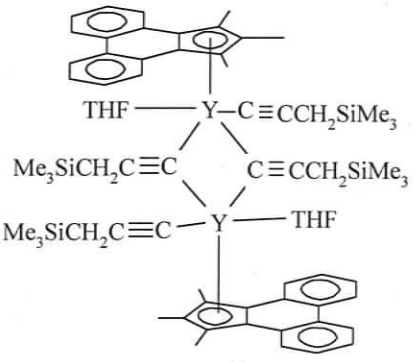

167

127.34, 126.35, 124.68, 123.85, 120.27, 117.23 (*arylC*), 71.95, 25.45 (*THF*), 16.53 (Cp*Me*), 13.80 (Cp*Me*), 1.09 (Si*Me*$_3$), β-carbon was not observed.

(sCp)Y(CCSiMe$_3$)$_2$(THF) (168) and (sCp)Y$_3$(CCSiMe$_3$)$_8$(THF)$_2$ (169)

(Trimethysilyl)acetylene (30 mg, 0.25 mmol) was added to **152** (43 mg, 0.06 mmol) in 5 mL hexanes solution and the mixture became cloudy immediately. Overnight reaction and removal of solvent under vacuum gave a pale yellow residue. The residue was washed with 1 mL hexanes and dried to give 30 mg of a toluene-insoluble pale yellow powder. The reaction attempted in toluene also afforded a toluene-insoluble pale yellow powder. In an NMR tube, several drops of D_8-THF were added to the mixture of pale yellow powder and C_6D_6. After one half hour, the mixture changed from cloudy suspension to a clear red-orange solution. Removal of the solvent gave **168** as a toluene-soluble light red-orange residue (characterized by NMR). Recrystallzation of **168** from toluene afforded very small amount of **169** as pale yellow crystals (characterized by X-ray, **Fig 3.19**). Yield: 70%. ^{1}H NMR (500 MHz, C_6D_6): δ 9.86 (d, $^3J_{HH}$ = 8.3Hz, 2H, *8-arylH*), 8.72 (dd, $^3J_{HH}$ = 7.9Hz, 2H, *1-arylH*), 8.59 (s, 1H, CpC*H*), 8.46 (d, 2H, $^3J_{HH}$ = 7.6Hz, *5-arylH*), 8.41 (d, $^3J_{HH}$ = 8.0Hz, 2H, *4-arylH*), 7.58 (m, 2H, *7-arylH*), 7.45(m, 2H, *2-arylH*), 7.40 (m, 2H, *6-arylH*), 7.33 (m, 2H, *3-arylH*), 3.55 (br, 4H, α-THF C*H*$_2$), 1.46 (br, 4H, β-THF C*H*$_2$), 0.21 (s, 18H, Si*Me*$_3$); ^{13}C NMR (125.8 MHz, C_6D_6):

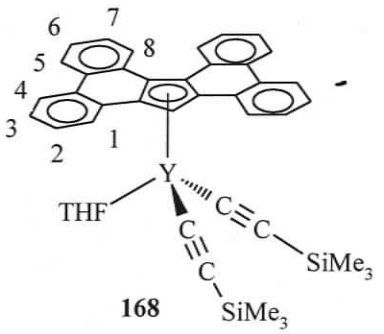

168

δ 172.46 (d, J_{YC} = 47.8Hz, Y-*C*CSiMe$_3$), 132.92, 131.16, 130.62, 129.88, 129.09, 127.03, 125.93, 125.86, 125.75, 125.54, 124.76, 123.71, 123.53, 116.87 (*arylC*), 111.95 (d, $^2J_{YC}$ = 8.8Hz, Y-C*C*SiMe$_3$), 98.99 (Cp*C*H), 1.69 (Si*Me*$_3$), THF resonances in this complex overlap with peaks of D_8-THF at 68 and 25 ppm.

(sCp)Y[κ^2-(N,C)-CH$_2$-(C$_5$H$_2$N-4,6-Me$_2$)]$_2$(collidine)$_3$ (170)

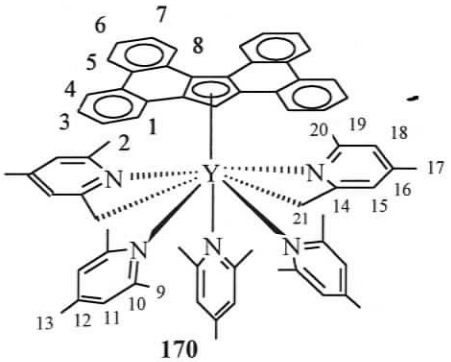

170

Collidine (dried over 4Å molecular sieves for two days) 20 mg (0.17 mmol) was added to 20 mg of **152** (0.03 mmol) in 2 mL toluene. The mixture was stirred overnight and the color changed from pale yellow to orange. After removal of solvent by vacuum, the red-orange residue was washed with hexanes to give 15 mg of **170** as an orange powder. Yield: 50%. ^{1}H NMR (500 MHz, C_6D_6): δ 9.16 (d, $^3J_{HH}$= 7.5Hz, 2H, *8-arylH*), 8.43 (d, $^3J_{HH}$= 7.2Hz, 2H, *4 or 5-arylH*), 8.38 (d, $^3J_{HH}$= 8.1Hz, 2H, *4 or 5-arylH*), 8.22 (d, $^3J_{HH}$= 6.8 Hz, 2H, *1-arylH*), 7.81 (s, 1H, Cp*C*H), 7.45-7.32 (m, 8H, *2,3,6,7-arylH*), 6.43(s, 6H, *11-colH*), 5.77(s, 2H, *15-colH*), 5.33 (s, 2H, *18-colH*), 2.45 (s, 18H, *9-colCH$_3$*) 1.87 (s, 9H, *13-colCH$_3$*) 1.62 (bs, 4H, *21-colCH$_2$*), 1.55 (s, 6H, *17-colCH$_3$*) 1.32 (s, 6H, *20-colCH$_3$*); ^{13}C NMR (125.7 MHz, C_6D_6): δ 164.97 (*14-colC*), 158.15 (*10-colC*), 154.93 (*19-colC*), 147.84 (*16-colC*), 146.97 (*12-colC*), 131.01, 130.69, 130.30, 129.62, 127.87, 127.57, 127.52, 126.61, 126.38, 126.31, 125.47, 124.88, 124.69, 124.23 (*arylC*), 121.30 (*11-colCH*), 117.40 (*15-colCH*),

115.93 (*arylC*), 111.94 (*18-colCH*), 92.78 (Cp*CH*), 50.13 (br, 21-*colCH*$_2$), 24.78 (*9-colCH*$_3$), 23.06 (*20-colCH*$_3$), 21.38 (*17-colCH*$_3$), 20.85 (*13-colCH*$_3$).

(sCp)$_2$YMe(THF) (171)

$AlMe_3$ 2 mL (2 M in hexanes, 4mmol) was added to **152** (80 mg, 0.11 mmol) in 2 mL toluene solution. After the mixture was stirred two days, a white-gray precipitate formed in solution. After separating this solid from the mother solution, it was washed with hexanes and dried under vacuum to give 15 mg of a toluene-insoluble product.

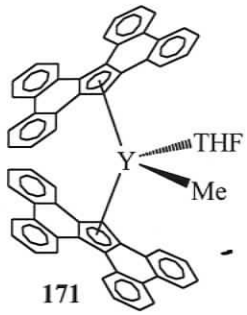

171

After several drops of THF were added to the suspension of this precipitate in toluene, a clear solution formed immediately. Evaporation of all the solvent under vacuum, followed by washing of the residue with hexanes and drying under vacuum gave 10 mg of **171** as a white toluene-soluble powder. Yield: 20%. ^{1}H NMR (500 MHz, C_6D_6/D_8-THF): δ 8.64 (d, 2H *arylH*), 8.55 (m, 6H, *arylH*), 8.49 (m, 2H, *arylH*), 8.19 (d, 2H, *arylH*), 7.67 (m, 4H, *arylH*), 7.60 (m, 2H, *arylH*), 7.55 (m, 4H, *arylH*), 7.38 (m, 2H, *arylH*), 7.30 (m, 4H, *arylH*), 7.24-7.07 (m, 6H, *arylH* and Cp*C*H), -0.95 (s, 9H, (D_8-THF)(Al*Me*$_3$), washed away), -2.80 (d, $^2J_{YH}$ = 2Hz , 3H, Y-C*H*$_3$); ^{13}C NMR (125.7 MHz, D_8-THF/C_6D_6): δ131.73, 131.27, 130.89, 130.74, 130.41, 130.16, 130.11, 129.76, 129.72, 128.95, 128.85, 128.08, 127.46, 126.63, 126.60, 126.35, 126.14, 126.09, 125.77, 125.58, 125.47, 125.32, 125.00, 124.96, 124.78, 124.69, 124.44, 124.30 (*arylC*), 94.54 (Cp*C*H), 24.01 (d, J_{YC} = 56.3Hz, Y-*C*H$_3$).

(PCp^{Me})(sCp)Y(CH$_2$SiMe$_3$)(THF) (174)

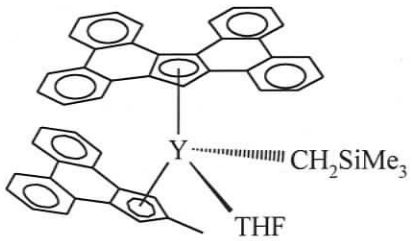

174

(PCp^{Me})H (12mg, 0.05 mmol) was added to **152** (35mg, 0.05 mmol) in 2 mL toluene and the mixture was stirred overnight. Removal of the solvent by vacuum afforded **174** as a pale yellow powder in quantitative yield. ^{1}H NMR (500MHz C_6D_6): δ 8.90 (d, 1H, *arylH*), 8.44-8.54 (m, 4H, *arylH*), 8.31 (dd, 1H, *arylH*), 8.13 (d, 2H, *arylH*), 8.03-7.99 (m, 2H, *arylH*), 7.94 (d, 1H, *arylH*), 7.89 (s, 1H, (sCp)Cp*H*), 7.54-6.96 (m, 14H, *arylH*, (PCp)Cp*H*), 5.24(d, $^4J_{HH}$ = 2 Hz, 1H, (PCp)Cp*H*), 1.54 (s, 3H, PCp*Me*), 1.35 (m, 2H, α-THF C*H*$_2$), 1.22 (m, 2H, α-THF C*H*$_2$), 0.48 (s, 9H, Si*Me*$_3$), 0.16 (m, 2H, β-THF C*H*$_2$), 0.09 (m, 2H, β-THF C*H*$_2$), -0.66 (dd, $^2J_{YH}$ = 3.7Hz, $^3J_{HH}$ = 10Hz, 1H, Y*CH*$_2$), -1.00 (dd, $^2J_{YH}$ = 3.8Hz, $^3J_{HH}$ = 10Hz, 1H, Y*CH*$_2$); ^{13}C NMR (125.8 MHz, C_6D_6): δ138.23, 131.87, 131.04, 130.52, 130.20, 130.09, 130.01, 129.99, 129.92, 129.86, 129.74, 129.66, 128.04, 127.85, 127.75, 127.72, 127.25, 126.67, 126.57, 126.54, 126.45, 126.24, 126.05, 126.03, 126.00, 125.91, 125.80, 125.52, 125.39, 125.21, 125.14, 125.10, 124.93, 124.82, 124.49, 124.29, 123.70, 123.51, 122.43, 121.06, 115.76, 114.94 (*arylC*), 105.91, 104.79 [(PCp)Cp*C*H)], 95.64 [(sCp)Cp*C*H)], 70.91 (α-THF C), 32.37 (d, $^1J_{YC}$= 46.1Hz, Y-*C*H$_2$), 24.63 (β-THF C), 14.66 (PCp*Me*), 5.68 (Si*Me*$_3$).

[(Me$_3$Si)$_2$Cp](sCp)YCH$_2$SiMe$_3$(THF) (175) and {[(Me$_3$Si)$_2$Cp]$_2$Y(μ-Cl)}$_2$ (176)

[(Me$_3$Si)$_2$Cp]H (12 mg, 0.05 mmol) was added to **152** (35 mg, 0.05 mmol) in 2 mL toluene and the mixture was stirred overnight. Removal of the solvent by vacuum followed by washing with hexane and drying under vacuum, afforded 30 mg of **175** (characterized by NMR) as a pale yellow powder. Yield: 68%. Recrystallization of **175** in toluene afforded very small amount of colorless X-ray quality crystals of **176** (characterized by X-ray, **Fig 3.20**). ^{1}H NMR (500 MHz, C_6D_6): δ 9.18 (dd, 1H, *arylH*), 9.13 (dd, 1H, *arylH*), 8.41(m, 2H, *arylH*), 8.34 (d, 2H, *arylH*), 8.32 (dd, 1H, *arylH*), 8.22 (dd, 1H, *arylH*), 7.77 (d, 1H, (sCp)Cp*H*), 7.51 (m, 1H, *arylH*), 7.43 (m, 2H, *arylH*), 7.30-7.40 (m, 5H, *arylH*), 6.19 (t, 1H, (Me$_3$Si)$_2$Cp*H*), 5.66 (t, 1H, (Me$_3$Si)$_2$Cp*H*), 4.61 (t, 1H, (Me$_3$Si)$_2$Cp*H*), 2.25 (m, 2H, α-THF C*H*$_2$), 2.16 (m, 2H, α-THF C*H*$_2$), 0.50 (m, 4H, β-THF C*H*$_2$), 0.41 (s, 6H, CpSi*Me*$_3$), 0.34 (s, 3H, CpSi*Me*$_3$), 0.31 (s, 3H, CpSi*Me*$_3$), 0.07 (s, 9H, CH$_2$Si*Me*$_3$), 0.00 (s, 3H, CpSi*Me*$_3$), -0.03 (s, 3H, CpSi*Me*$_3$), -1.82 (dd, $^2J_{YH}$= 3.7Hz, $^2J_{HH}$= 10Hz, 1H, Y*CH*$_2$), -2.16 (dd, $^2J_{YH}$= 3.8Hz, $^2J_{HH}$= 10Hz, 1H, Y*CH*$_2$); ^{13}C NMR (125.8 MHz, C_6D_6) δ 131. 87, 131.73, 130.50, 130.39, 130.08, 129.99, 129.90, 129.80, 129.66, 128.89, 127.86,

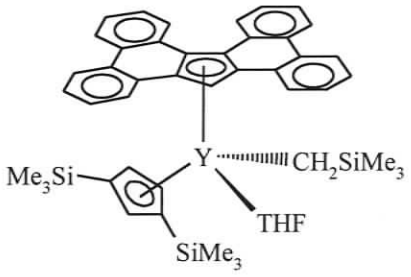

175

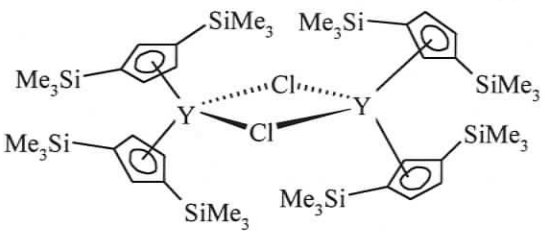

176

127.76, 127.70, 126.62, 126.55, 126.35, 126.28, 126.22, 125.57, 125.52, 125.28, 125.14, 124.94, 124.75, 124.56, 124.14, 121.89, 121.87, 121.70, 121.40, 121.06, 116.43, 114.57 (*arylC*, *CpC*), 91.65 [(sCp)Cp*C*H)], 70.97 (α-THF C), 25.82 (d, $^{1}J_{YC}$= 40.1Hz, Y-*C*H_2), 24.48 (β-THF C), 2.48, 1.58, 0.81, 0.36, -0.30 (CpSi*Me*$_3$), 1.29 (s, 9H, CH_2Si*Me*$_3$).

[(PCp*)YCH$_2$SiMe$_3$(THF)]$^+$[B(C$_6$F$_5$)$_4$]$^-$ (177) and its ethylene polymerization

$[Ph_3C]^+[B(C_6F_5)_4]^-$ (15 mg, 0.016mmol) in 1 mL toluene was added to complex **150** (10 mg, 0.016 mmol) in 3 mL toluene solution with rapid stirring. The color of solution changed from pale yellow to red immediately and faded away after two hours, indicating complete generation of **177**. The reaction mixture was exposed to vacuum for 20 seconds to remove the nitrogen gas in the reaction Schlenk. Ethylene gas, dried over sieves, was introduced into the flask at 1 bar pressure. After one half hour, the mixture changed to a yellow color with formation of a precipitate. Addition of methanol terminated the polymerization and the color of solution and precipitate changed to white immediately. Removal of solvent, followed by washing with HCl solution and methanol, afforded 170 mg polyethylene. The catalytic activity for polymerization of ethylene using cation **177** was calculated to be 21 kg mol^{-1} h^{-1} bar^{-1}.

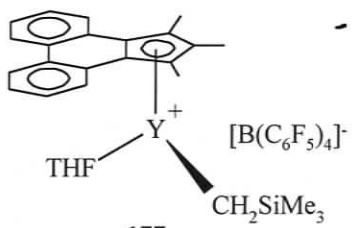

177

$[(sCp)YCH_2SiMe_3(THF)]^+[B(C_6F_5)_4]^-$ (178)

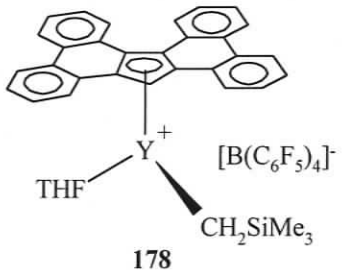

178

Similar reaction under the same conditions was carried out to generate cation **178**, except shorter reaction time as half hour. The catalytic activity for polymerization of ethylene for cation **178** was calculated to be 36 kg $mol^{-1}h^{-1}bar^{-1}$.

References

1 Kealy, T.J.; Pauson, P.L. *Nature* **1951**, *168*, 1039.

2 Pauson, P.L.; Kealy, T.J. *J. Chem. Soc.* **1952**, 632.

3 Birmingham, J.M.; Wilkinson, G. *J. Am. Chem. Soc.* **1956**, *78*, 42.

4 Mark, T.J.; Ernst, R.D. In *Comp. Organomet. Chem. I*; Abel, E.W.; Stone, F.G.; Wilkinson, G., Edit; Elsevier: Oxford, **1982**; *Vol. 3*.

5 Wayda, A.L.; Evans, W.J., *Inorg. Chem.* **1980**, *19*, 2190.

6 John, J.; Tsutsui, M., *J. Coord. Chem.* **1980**, *10*, 177.

7 Tsutsui, M.; Gysling, H.J., *J. Am. Chem. Soc.* **1969**, *91*, 3175.

8 Lappert, M.F.; Pearce, R., *J. Chem. Soc., Chem. Commun.* **1973**, 126.

9 Barker, F.K.; Lappert, M.F., *J. Organomet. Chem.* **1974**, *76*, C45.

10 Watson, P.L.; Whitney, J.F.; Harlow, R.L., *Inorg. Chem.* **1981**, *20*, 3271.

11 Tilley, T.D., Andersen, R.A.; Spencer, B.; Ruben, H.; Zalkin, A.; Templeton, D.H., *Inorg. Chem.* **1980**, *19*, 2999.

12 Williams, R.A.; Hanusa, T.P.; Huffman, J.C., *Organometallics* **1990**, *9*, 1128.

13 Evans, W.J., *Inorg. Chim. Acta* **1987**, *139*, 169.

14 Watson, P.L., *J. Chem. Soc., Chem. Commun.* **1980**, 652.

15 Schumann, H., *Angew. Chem.* **1984**, *96*, 475.

16 Schumann, H., *Angew. Chem. Int. Ed.* **1984**, *23*, 474.

17 Evans, W.J.; Grate, J.W.; Choi, H.W.; Bloom, I.; Hunter, W.E.; Atwood, J.L., *J. Am. Chem. Soc.* **1985**, *107*, 941.

18 Zinnen, H.A.; Pluth, J.J.; Evans, W.J., *J. Chem. Soc., Chem. Commun.* **1980**, 810.

19 Hollis, T.K.; Burdett, J.K.; Bosnich, B., *Organometallics* **1993**, *12*, 3385.

20 Kaupp, M.; Von Schleyer, P.R.; Dolg, M.; Stoll, H., *J. Am. Chem. Soc.* **1992**, *114*, 8202.

21 Evans, W.J.; Ulibarri, T.A.; Ziller, J.W., *J. Am. Chem. Soc.* **1988**, *110*, 6877.

22 Evans, W.J.; Ulibarri, T.A.; Ziller, J.W., *J. Am. Chem. Soc.* **1990**, *112*, 219.

23 Evans, W.J.; Giarikos, D.G.; Robledo, C.B.; Leong, V.S.; Ziller, J.W., *Organometallics*, **2001**, *20*, 5648.

24 Evans, W.J.; Gonzales, S.L.; Ziller, J.W., *J. Am. Chem. Soc.* **1994**, *114*, 2600.

25 Evans, W.J.; Ulibarri, T.A.; Ziller, J.W., *J. Am. Chem. Soc.* **1990**, *112*, 2314.

26 Evans, W.J.; Keyer, R.A.; Rabe, G.W.; Drummond, D.K.; Ziller, J.W., *Organometallics* **1993**, *12*, 4664.

27 Burns, C.J.; Andersen, R.A. *J. Am. Chem. Soc.* **1987**, *109*, 941.

28 Burns, C.J.; Andersen, R.A. *J. Am. Chem. Soc.* **1987**, *109*, 915.

29 Andersen, R.A.; Boncella, J.M.; Burns, C.J.; Green, J.C.; Hohl, D.; Rosch, N. *J. Chem. Soc., Chem. Commun.* **1986**, 405.

30 Evans, W.J.; Drummond, D.K. *J. Am. Chem. Soc.* **1989**, *111*, 3329.

31 Schultz, M.; Boncella, J.M.; Berg, D.J.; Tilley, T.D.; Andersen, R.A. *Organometallics* **2002**, *21*, 460.

32 Berg, D. J.; Boncella, J.M.; Andersen, R.A. *Organometallics* **2002**, *21*, 4622.

33 Evans, W.J.; Grate, J.W.; Bloom, I.; Hunter, W.E.; Atwood, J.L. *J. Am. Chem. Soc.* **1985**, *107*, 405.

34 Berg, D.J.; Burns, C.J.; Andersen, R.A.; Zalkin, A. *Organometallics* **1989**, *8*, 1865.

35 Berg, D.J.; Andersen, R.A.; Zalkin, A. *Organometallics* **1988**, *7*, 1858.

36 Recknagel, A.; Noltemeyer, M.; Stalke, D.; Pieper, U.; Schmidt, H.G.; Edelmann, F.T. *J. Organomet. Chem.* **1991**, *411*, 347.

37 Waston, P.L.; Tulip, T.H.; Williams, I. *Organometallics* **1990**, *9*, 1999.

38 Evans, W.J.; Chamberlain, L.R.; Ulibarri, T.A.; Ziller, J.W. *J. Am. Chem. Soc.* **1988**, *110*, 6423.

39 Evans, W.J.; Chamberlain, L.R.; Ziller, J.W. *J. Am. Chem. Soc.* **1987**, *109*, 7209.

40 Yamamoto, H.; Yasuda, H.; Yokota, K.; Nakamura, A.; Kai, Y.; Kasai, N; *Chem. Lett.* **1988** 1963.

41 den Hann, K. H.; de Boer, J. L.; Etuben, J. H.; Smeets, W. J. J.; Spek, A. L. *J. Organomet. Chem.* **1987**, *327*, 31.

42 Pfenning, B.z W.; Thompson, M. E.; Bocarsly, A. B. *Organometallics* **1993**, *12*, 649.

43 Watson, P. L.; *J. Chem. Soc., Chem. Commun.* **1983**, 276.

44 Watson, P. L. *J. Am. Chem. Soc.* **1983**, *105*, 6491.

45 Matsumaga, P. T. *Ph.D. Thesis* California Univ. Berkeley. Lawrence Berkeley Lab, **1991**.

46 Schumann, H.; Nichel, S.; Hahn, E.; Heeg, M. J. *Organometallics* **1985**, *4*, 800.

47 Piers, C. J.; Shapiro, P. J.; Bunel, E. E.; Bercaw, J. E. *Synth. Let.* **1990**, 74.

48 Thompson, M. E.; Baxter, S. M.; Bulls, A. R. ; Jurger, B. J.; Nolan, M. C. ; Santarsiero, B. D.; Schaefer, W. P.; Bercaw, J. E. *J. Am. Chem. Soc.* **1987**, *109*, 203.

49 den Haan, K. H.; de Boer, J. L.; Teuben, J. H. *Organometallics* **1986**, *5*, 1726.

50 Heeres, H. J.; Renkema, J.; Booij, M.; Meetsma, A.; Teuben, J. H. *Organometallics* **1988**, *7*, 2495.

51 Mauermann, H.; Swepston, P. N.; Marks, T. J. *Organometallics* **1985**, *4*, 200.

52 den Haan, K. H.; Luinstra, G. A.; Meetsma, A.; Teuben, J. H. *Organometallics* **1987**, *6*, 1509.

53 den Haan, K. H.; Wielstra, Y.; Teuben, J. H. *Organometallics* **1987**, *6*, 2053.

54 Heeres, H. J.; Maters, M.; Teuben, J. H. *Organometallics* **1992**, *11*, 350.

55 Booij, M.; Meetsma, A.; Teuben, J. H. *Organometallics* **1991**, *10*, 3246.

56 van der Heijden, H.; Schaverien, C. J. *Organometallics* **1989**, *8*, 225.

57 Schaverien, C. J. *Organometallics* **1994**, *13*, 62.

58 Camerson, T. M.; Gordon, J. C.; Scott, B. L. *Organometallics* **2004**, *23*, 2995.

59 Klooster, W. T.; Brammer, L.; Schaverien, C. J.; Budzelaar, P. H. M. *J. Am. Chem. Soc.* **1999**, *121*, 1381.

60 Fagan, P. J.; Manriquez, J. M.; Marks, T. J.; Day, V. W.; Vollmer, S. H.; Day, C. S. *J. Am. Chem. Soc.* **1980**, *102*, 5393.

61 Evans, W.J.; Chamberlain, L.R.; Ulibarri, T.A.; Ziller, J.W.; Alvarez, D. *Organometallics* **1990**, *9*, 2124.

62 Booij, M.; Deelman, B. J.; Duchateau, R.; Postma, D. S.; Meetsma, A.; Teuben, J. H. *Organometallics* **1993**, *12*, 3531.

63 den Haan, K. H.; Teuben, J. H. *J. Chem. Soc., Chem. Commun.* **1986**, 682.

64 Ringelberg, S.N.; Meetsma, A. Troyanov, S.I.; Hessen, B.; Teuben, J.H. *Organometallics* **2002**, *21*, 1759.

65 Schultz, M.; Burns, C. J.; Schwarts, D.J.; Andersen, R.A. *Organometallics* **2000**, *19*, 781.

66 Hultzsch, K.C.; Spaniol, T.P.; Okuda, J. *Angew. Chem. Int. Ed.* **1999**, *38*, 227.

67 Arndt, S.; Spaniol, T.S.; Okuda, J. *Organometallics* **2003**, *22*, 775.

68 van der Heijden, H.; Pasman, P.; de Boer, E. J. M.; Schaverien, C.J. *Organometallics* **1989**, *8*, 1459.

69 Tardif, O.; Nishiura, M.; Hou, Z. *Organometallics* **2003**, *22*, 1171.

70 Cui, D.; Tardif, O.; Hou, Z., *J. Am. Chem. Soc.* **2004**, *126*, 1312.

71 Tardif, O.; Hashizume, D.; Hou, Z. *J. Am. Chem. Soc.* **2004**, *126*, 8080

72 Evans, W. J.; Gummersheimer, T. S.; Boyle, T. J.; Ziller, J. W. *Organometallics* **1994**, *13*, 1281.

73 Nakamura, H.; Nakayama, Y.; Yasuda, H.; Maruo, T.; Kanehisa, N.; Kai, Y. *Organometallics* **2000**, *19*, 5392.

74 Atwood, J. L.; Burns, J. H.; Laubereau, P.G. *J. Am. Chem. Soc.* **1973**, *95*, 1830.

75 Guan, J.; Fischer, R. D. *J. Organomet. Chem.* **1998**, *564*, 167.

76 Guan, J.; Shen, Q.; Fischer, R. D. *J. Organomet. Chem.* **1997**, *549*, 203.

77 Shen, Q.; Qi, M.; Song, S.; Zhang, L.; Lin Y. *J. Organomet. Chem.* **1997**, *549*, 95.

78 Khvostov, A.V.; Bulychev, B. M.; Belsky, V. K.; Sizov, A. I. *J. Organomet. Chem.* **1999**, *584*, 164.

79 Kretschmer, W. P.; Troyanov, S. I.; Meetsma, A.; Hessen, B.; Teuben, J. H. *Organometallics* **1998**, *11*, 284.

80 Trifonov, A. A.; Kirillov, E. N.; Dechert, S.; Schumann, H.; Bochkarev, M. N. *Eur. J. Inorg. Chem.* **2001**, 2509.

81 Trifonov, A. A.; Fedorova, E. A.; Kukin, G. K.; Druzhkov, N. O.; Bochkarev, M. N. *Angew. Chem. Int. Ed.* **2004**, *43*, 5045.

82 Arndt, S.; Trifonov, A.; Spaniol, T.P.; Okuda, J. *Organometallics* **2000**, *19*, 4690.

83 Hultzsch, K.C.; Voth, P.; Beckerle, K.; Spaniol, T.P.; Okuda, J. *Organometallics* **2000**, *19*, 228.

84 Voth, P.; Arndt, S.; Spaniol, T. P.; Okuda, J. *Organometallics* **2003**, *22*, 65.

85 Arndt, S.; Trifonov, A.; Spaniol, T.P.; Okuda, J.; Kitamura, M.; Takahashi, T.; *J. Organomet. Chem.* **2002**, *647*, 158.

86 Arndt, S.; Trifonov, A.; Spaniol, T.P.; Okuda, J. *Eur. J. Inorg. Chem.* **2001**, 73.

87 Voth, P.; Spaniol, T. P.; Okuda, J. *Organometallics* **2003**, *22*, 3921.

88 Mu, Y.; Piers, W. E.; MacQuarrie, D. C.; Zaworotko, M. J.; Young, V. G. *Organometallics* **1996**, *15*, 2720.

89 Trifonov, A. A.; Spaniol, T. P.; Okuda, J. *Organometallics* **2001**, *20*, 4869.

90 Nishiura, M.; Hou, Z.; Wakatsuiki, Y.; Yamaki, T.; Miyamoto, T. *J. Am. Chem. Soc.*, **2003**, *125*, 1184.

91 Hou, Z. *Bull. Chem. Soc. Jap.* **2003**, *76*, 2253.

92 Kirillov, E.; Toupet, L.; Lehmann, C.W.; Razavi, A.; Carpentier, J. F. *Organometallics* **2003**, *22*, 4467.

93 Kirillov, E.; Toupet, L.; Lehmann, C. W.; Razavi, A.; Carpentier, J. F. *Eur. J. Inorg. Chem.* **2004**, 943.

94 Jeske, G; Schock, L. E.; Swepston, P. N.; Schumann, H.; Marks, T. J. *J. Am. Chem. Soc.* **1985**, *107,* 8103.

95 Stern, D.; Sabat, M.; Marks, T. J. *J. Am. Chem. Soc.***1990**, *112,* 9558-9575

96 Coughlin, E. B.; Bercaw, J. E. *J. Am. Chem. Soc.* **1992**,*114,* 7606.

97 Mitchell, J. P.; Hajela, S; Brookhart, S. K.; Hardcastle, K. I.Henling, L. M., Bercaw, J. E. *J. Am. Chem. Soc.* **1996**, *118,* 1045.

98 Gilchrist, J. H.; Bercaw, J. E. *J. Am. Chem. Soc.* **1996**, *118,* 12021.

99 Eppinger, J.; Spiegler, M.; Hieringer, W.; Herrmann, W. A.; Anwander, R. *J. Am. Chem. Soc.* **2000**, *122,* 3080.

100 Klimpel, M. J.; Sirsch, P.; Scherer, W.; Anwander, R. *Angew. Chem. Int. Ed.* **2003**, *5*, 42.

101 Lee, M. H.; Hwang, J.-W.; Kim, Y.; Kim, J.; Han, Y.; Do, Y. *Organometallics* **1999**, *18*, 5124.

102 Qian, C.; Nie, W.; Sun, J.; *Organometallics* **2000**, *19,* 4134.

103 Ihara, E.; Yoshioka, S.; Furo, M.; Katsura, K.; Yasuda, H.; Mohri, S.; Kanehisa, N.; Kai, Y. *Organometallics* **2001**, *20,* 1752.

104 Abrams, M. B.; Loever, C.; Day, M. W.; Bercaw, J. E. *Organometallics* **1999**, *18*, 1389.

105 Yoder, J. C.; Day, M. W.; Bercaw, J. E. *Organometallics* **1998**, *17*, 4946.

106 Ihara, E.; Nodono, M.; Adachi, Y.; Yasuda, H.; Yamagashira, M.; Hashimoto, H.; Hanehisa, N.; Kai, Y. *Organometallics* **1998**, *17*, 3945.

107 Piers, W. E.; Ferguson, G.; Gallagher, J. F. *Inorg. Chem.* **1994**, *33*, 3784.

108 Molander, G. A.; Dowdy, E. D.; Noll, B.C. *Organometallics* **1998**, *17*, 3754.

109 Maruo, T.; Kanehisa, N.; Kai, Y. *Organometallics* **2000**, *19*, 1812.

110 Conticello, V. P.; Brard, L.; Giardello, M. A.; Tsuji, Y.; Sabat, M.; Stern, C. L.; Marks, T. J. *J. Am. Chem. Soc.* **1992**, *114*, 2761.

111 Conticello, V. P.; Giardello, M. A.; Brard, L.; Sabat, M.; Rheingold, A. L.; Stern, C. L.; Marks, T. J. *J. Am. Chem. Soc.* **1994**, *116*, 10212.

112 Gagne, M. R.; Brard, L.; Conticello, V. P.; Giardello, M. A.; Sabat, M.; Rheingold, A. L.; Stern, C. L.; Marks, T. J. *Organometallics* **1992**, *11*, 2003.

113 Yasuda, H.; Furo, M.; Yamamoto, H. *Macromol.***1992**, *25*, 5115.

114 Yasuda, H.; Yamamoto, H.; Yamashita, M.; Yokota, K.; Nakamura, A.; Miyake, S.; Kai, Y.; Kanehisa, N. *Macromol.* **1993**, *26*, 7134.

115 Molander, G.A.; Romero, J.A.C. *Chem. Rev.* **2002**, *102*, 2161.

116 Luo, Y.; Baldamus, J.; Hou, Z. *J. Am. Chem. Soc.* **2004**, *126*, 13910.

117 Kaita, S.; Yamanaka, M.; Horiuchi, A. C.; Wakatsuki, Y. *Macromol.* 2006, 39, 1359.

118 Yamashita, M.; Takemoto, Y.; Ihara, E.; Yasuda, H. *Macromol.* **1996**, *29*, 1798.

119 Desurmont, G.; Tokimitsu, T.; Yasuda, H. *Macromol.* **2000**, *33*, 7679.

120 Zennen, H. A.; Pluth, J. J.; Evans, W. J. *Chem. Commun.* **1980**, 810.

121 Evans, W. J.; Meadows, J. H.; Wayda, A. L.; Hunter, W. E.; Atwood, J. L. *J. Am. Chem. Soc.* **1982**, *104*, 2008.

122 Schumann, H.; Genthe, W. *J. Organomet.c Chem.* **1981**, *213*, C7.

123 Jeske, G.; Lauke, H.; Mauermann, H.; Schumann, H.; Marks, T. J., *J. Am. Chem. Soc.* **1985**, *107*, 8111.

124 Molander, G. A.; Hoberg, J. O. *J. Org. Chem.* **1992**, *57*, 3266.

125 Molander, G. A.; Winterfeld, J. *J. Organomet. Chem.* **1996**, *524*, 275.

126 Tamao, K.; Ishida, N.; Tanaka, T.; Kumada, M. *Organometallics* **1983**, *2*, 1649.

127 Bergens, S. H.; Nogeda, P.; Whelan, J.; Bosnich, B. *J. Am. Chem. Soc.* **1992**, *114*, 2121.

128 Fu, P. F.; Brard, L.; Li, Y.; Marks, T. J. *J. Am. Chem. Soc.* **1995**, *117*, 7157.

129 Sakakura, T.; Lautenschlager, H. –J.; Tanaka, M. *Chem. Commun.* **1991**, 40.

130 Onozawa, S.; Sakakura, T.; Tanaka, M. *Tetra. Let.* **1994**, *35*, 8177.

131 Molander, G. A.; Dowdy, E. D.; Noll, B. C. *Organometallics* **1996**, *17*, 3754.

132 Molander, G. A.; Julius, M. *J. Org. Chem.* **1992**, *57*, 6347.

133 Molander, G. A.; Retsch, W. H. *Organometallics*, **1995**, *14*, 4570.

134 Giardello, M. A.; Conticello, V. P.; Brard, L.; Gagne, M. R.; Marks, T. J. *J. Am. Chem. Soc.* **1996**, *116*, 10241.

135 Gagne, M. R.; Stern, C. L.; Marks, T. J. *J. Am. Chem. Soc.* **1992**, *114*, 275.

136 Molander, G. A.; Dowdy, E. D. *J. Org. Chem.* **1998**, *63*, 8983.

137 Li, Y.; Marks, T. J. *J. Am. Chem. Soc.* **1996**, *118*, 9295.

138 Li, Y.; Marks, T. J. *J. Am. Chem. Soc.* **1996**, *118*, 707.

139 Arredondo, V. M.; McDonald, F. E.; Marks, T. J. *J. Am. Chem. Soc.* **1998**, *120*, 4871.

140 Li, Y.; Marks, T. J. *Organometallics* **1996**, *15*, 3770.

141 Molander, G. A.; Nichols, P. J. *J. Am. Chem. Soc.* **1995**, *117*, 4415.

142 Molander, G. A.; Hoberg, J. O. *J. Am. Chem. Soc.* **1992**, *114*, 3123.

143 Piers, W. E.; Shapiro, P. J.; Bunel, E. E.; Bercaw, J. E. *Synth. Let.* **1990**,74.

144 Visseaux, M.; Barbier-Baudry, D.; Blacque, O.; Hafid, A.; Richard, P.; Weber, F. *New. J. Chem.* **2000**, *24*, 939.

145 Evans, W. J.; Gummersheimer, T.S.; Boyle, T.J.; Ziller, J.W. *Organometallics* **1994**, *13*, 1281.

146 Keasey, A.; Bailey, P.M.; Maitlis, P.M. *J. Chem. Soc. Chem. Commun.* **1978**, 142.

147 Nakasuji, K.; Yamaguchi, M.; Murata, I. *J. Am. Chem. Soc.* **1986**, *108*, 325.

148 Reid, D.H., *Quart. Rev. Chem. Soc.* **1965**, *19*, 274.

149 Murata, I., *Topics Non-benzenoid Aromatic Chemistry*, **1973**, *1*, 159.

150 Bowden, K.; Cockerill, A. F. *J. Chem. Soc. (B)*, **1970**, *16*, 173.

151 Lin, S.; Boudjouk, P., *J. Organomet. Chem.* **1980**, *187*, C11.

152 Woell, J.B.; Boudjouk, P., *J. Organomet. Chem.* **1979**, *172*, C43

153 Keasey, A.; Bailey, P.M.; Maitlis, P.M. *J. Chem. Soc. Chem. Commun.* **1978**, 142.

154 Butcher, J.A.; Pagni, R.M. *J. Am. Chem. Soc.* **1979**, *101*, 3997.

155 Kazuhiro, N.; Masakazu, Y.; Ichiro, M.; Kazuyuki, T.; Akira, N. *Organometallics*, **1984**, *3*, 1257.

156 Cotton, F.A.; Wilkinson, G., *Adv. Inrog. Chem.*, *4th ed.* Interscience, New York, **1980**, Chapter 23.

157 Fieser, L.F; Novello, F.C. *J. Am. Chem. Soc.* **1940**, *62*, 1855.

158 Boudjouk, P.; Johnson, P.D. *J. Org. Chem.* **1978**, *43*, 3979.

159 Goto, K.; Kubo, T.; Yamamoto, K.; Nakasuji, K.; Sato, K.; Shiomi, D.; Takui, T.; Kubota, M.; Kobayashi, T.; Yakusi, K.; Ouyang, J. *J. Am. Chem. Soc.* **1999**, *121*, 1619.

160 Manchand, P.S. *Chem. Commun.* **1971**, 667.

161 Wolinska-Mocydlarz, J.; Canonne, P.; Leitch, L.C. *Synthesis* **1974**, 566.

162 Waston, P.L.; Whitney, J.F.; Harlow, R.L. *Inorg. Chem.* **1981**, *20*, 3271.

163 Hart, F.A.; Massey, A G.; Saran, M.S., *J. Organomet. Chem.* **1970**, *21*, 147.

164 Evans, W.J.; Boyle, T.J.; Ziller, J.W. *Inorg. Chem.* **1992**, *31*, 1120.

165 Schumann, H., *Angew. Chem.* **1984**, *96*, 475.

166 Schumann, H., *Angew. Chem. Int. Ed.* **1984**, *23*, 474.

167 Rogers, R.D.; Rogers, L.M. *J. Organomet. Chem.* **1992**, *442*, 225.

168 Day, C.S.; Day, V.W.; Ernst, R.D.; Vollmer, S.H. *Organometallics* **1982**, *1*, 998.

169 Tilley, T.D.; Boncellas, J.M.; Berg, D.J.; Burns, C.J.; Andersen, R.A. *Inorg Synth.* **1990**, *27*, 146.

170 Aspinall, H.C.; Bradley, D.C.; Hursthouse, M.B.; Sales, K.D.; Walker, N.P.C.; Hussain B. *J. Chem. Soc. Dalton Trans.* **1989**, 623.

171 Schumann, H.; Muller, J. *J. Organomet. Chem.* **1978**, *146*, C43.

172 Wilkinson, G.; Stone, F.G.A.; Abel, E.W. *Comp. Organomet. Chem. I*, **1982**, *3*, 175.

173 Fraser, R.R.; Mansour, T.S.; Savard, S. *J. Org. Chem.* **1985**, *50*, 3232.

174 Khvostov, A.V.; Sizov, A.I.; Bulychev, B.M.; Ya.Knjazhanski, S.; Belsky, V.K. *J. Organomet. Chem.* **1998**, *559*, 97.

175 Deacon, G.B.; Mackinnon, P.I.; Hambley, T.W.; Taylor, J.C. *J. Organomet. Chem.* **1983**, *259*, 91.

176 Schumann, M.; Glanz, H. *New. J. Chem.* **1995**, *19*, 491.

177 Drew, M.G.B.; Felix, V.; Concalves, I.S.; Romao, C.C.; Royo, B., *Organometallics*, **1998**, *17*, 5782.

178 Torschner, T.C.; Cutler, A.R.; Kullnig, R.K., *Organometallics* **1987**, *6*, 889.

179 Farrugia, L. J. ORTEP3 for Windows, *J. Appl. Cryst.* **1997**, *30*, 565.

180 Marsh, R.E., *Acta. Crysta: Sect. B: Struct. Sci.* **1997**, *53*, 317.

181 Qi, M.; Shen, Qi; Gong, X.; Shen, Z.; Weng, L. *Chin. J. Chem.* **2002**, *20*, 564.

182 Trifonov, A.T.; Spaniol, T.P.; Okuda, J. *Euro. J. Inorg. Chem.* **2003**, 926.

183 Yao, Y.; Zhang, Y.; Zhang, Z.; Shen, Q.; Yu, K. *Organometallics* **2003**, *22*, 2876.

184 Trifonov, A.A.; Kirillov, E.N.; Dechert, S.; Schumann, H.; Bochkarev, M.N. *Euro. J. Inorg. Chem.* **2001**, 3055.

185 Khvostov, A.V.; Bulychev, B.M.; Belsky, V.K.; Sizov, A.I. *J. Organomet. Chem.* **1999**, *584*, 164.

186 Nakamura, H.; Nakayama, Y.; Yasuda, H.; Maruo, T.; Kanehisa, N.; Kai, Y. *Organometallics* **2000**, *19*, 5392.

187 Drew, M.B.G.; Felix, V.; Conclaves, I.S.; Romao, C.C. *Organometallics* **1998**, *17*, 5782.

188 Camelas, C.A.; Herdtweck, E.; Lopes, J.P.; Romao, C.C. *Organometallics* 1999, 18, 506.

189 Forschner, T.C.; Cutler, A.R.; Kullnig, R.K. *Organometallics* **1987**, *6*, 889.

190 Alias, F. M.; Belderrain, T.R.; Carmona, E.; Graiff, C.; Paneque, M.; Tiripicchio, A. *J. Organomet. Chem.* **1999**, *577*, 316.

191 Bartsch, R.; Hitchcock, P.B.; Nixon, J.F. *Chem. Commun.* **1990**, 472.

192 Hazell, A.c.; Hazell, R.G.; Norskov-Lauritsen, L.; Briant, C.E.; Jones, D.W. *Acta Crysta: Sect. C. Cryst. Struc. Commun.* **1986**, *42*, 690

193 Jones, D.W.; McDonald, W.S. *Chem Commun.* **1990**, 417.

194 Cotton, F.A.; Lahuerta, P. *Inorg. Chem.* **1975**, *14*, 116.

195 Cope, A.C.; Field, L.; MacDowell, D. W. H.; Wright, E. *J. Am. Chem. Soc.* **1956**, 2547.

196 Collett, M. J.; Jones, D. W.; Renyard, S. *J. Chem. Soc., Perkin Trans. I*, **1986**, 1471.

197 Eliasson, B.; Nouri-Sorkhabi, M. H.; Trogen, L.; Sethson, I.; Edlund, U.; Sygula, A.; Rabinovitz, M. *J. Org. Chem.* **1989**, *54*, 171.

198 Adlington, R. M.; Barret, A. G.M. *Acc. Chem. Res.* **1983**, *16*, 55..

199 Jones, D. W. *J. Chem. Soc., Perkin Trans. I*, **1977**, 980.

200 Hay, A. M.; Hobbs-Dewitt, S.; MacDonald, A. A.; Ramage, R. *Synthesis* **1999**, *11*, 1979.

201 Evans, W. J.; Brady, J.C.; Ziller, J. W. *J. Am. Chem. Soc.* **2001**, *123*, 7711.

202 Emslie, D. J.; Piers, W. E.; Parvez, M.; Mcdanold, R. *Organometallics* **2002**, *41*, 4226.

203 Cai, C.X.; Toupet, L.; Lehmann, C.W.; Carpentier, J.-F. *J. Organomet. Chem.* **2003**, *683*, 131.

204 Brown, A.R.; Irving, S.L.; Ramage, R.; Raphy, G. *Tetrahedron* **1995**, *51*, 11815.

205 Zhang, J.; Ma, L.; Cai, R.; Weng, L.; Zhou, X.; *Organometallics* **2005**, *24*, 738.

206 Zalkin, A.; Henly, T. J.; Anderson, R. A. *Acta Crysta: Sect. C. Cryst. Struct. Commun.* **1987**, *43*, 233.

207 Atwood, J.L.; Hunter, W.E.; Wayda, A.L.; Evans, W.J. *Inorg. Chem.* **1981**, 20, 4115.

208 Shen, Q.; Zheng, D.; Lin, L.; Lin, Y. *J. Organomet. Chem.* **1990**, *391*, 307.

209 Tazelaar, C.G.J.; Bambirra, S.; van Leusen, D.; Meetsma, A.; Hessen, B., Teuben, J. H. *Organometallics* **2004**, *23*, 936.

210 Deelman, B.-J.; Stevels, W.J.; Teuben, J.H.; Lakin, L.T.; Spek, A.L. *Organometallics* **1994**, *13*, 3881.

211 Anwander, R.; Klimpel, M.G.; Dietrich, H.M.; Shorokhov, D.J.; Scherer, W. *Chem. Commun.* **2003**, 1008.

212 Song, X.; Thornton-Pett, M.; Bochmann, M. *Organometallics* **1998**, *17*, 1004.

213 Heeres, H.J.; Renkema, J.; Booij, M.; Meetmsa, A.; Teuben, J.H. *Organometallics* **1988**, *7*, 2495.

214 Jeske, J.; Lauke, H.; Mauermann, H.; Swepston, P.N.; Schumann, H.; Marks, T.J. *J. Am. Chem. Soc.* **1985**, *107*, 8091.

215 Gavenonis, J.; Don Tilley, T. *J. Organomet. Chem.* **2004**, *689*, 870.

216 Evans, W.J.; Grate, J.W.; Levan, K.R.; Bloom, I.; Peterson, T.T.; Doedens, R.J.; Zhang, H.; Atwood, J.L. *Inorg. Chem.* **1986**, *25*, 3614.

217 Lappert, M. F.; Singh, A.; Atwood, J. L.; Hunter, W. E. *Chem. Commun.* **1981**, 1190.

218 Xie, Z.; Chui, K.; Yang, Q.; Mak, T.C.W.; Sun J. *Organometallics* **1998**, *17*, 3937.

219 Beletskaya, I.P.; Voskoboynikov, A.Z.; Chuklanova, E.B.; Kirillova, N.I.; Shestakova, A.K.; Parshina, I.N.; Gusev, A.I.; Magomedov; G.K.-I. *J. Am. Chem. Soc.* **1993**, *115*, 3156.

220 Kirillov, E.; Lehmann, C.W.; Razavi, A.; Carpentier, J.F. *Organometallics* **2004**, *23*, 2768.

221 Lee, L.; Berg, D.J.; Bushnell, G.D. *Organometallics* **1995**, *14*, 8.

222 Lee, L.; Berg, D.J.; Bushnell, G.D. *Organometallics* **1997**, *16*, 2556.

223 Casey, C.P.; Klein, J.F.; Fagan, M.A. *J. Am. Chem. Soc.* **2000**, *122*, 4320.

224 Sandstrom, J. *Dynam. NMR Spect.* Pergamon: London, **1982**.

225 Zeimentz, P. M.; Arndt, S.; Elvidge, B. R.; Okuda, J. *Chem. Rev.* **2006**, 106, 2404/

Appendix: Crystallographic Data

Figure A.1. Complete Ortep3 diagram of 136

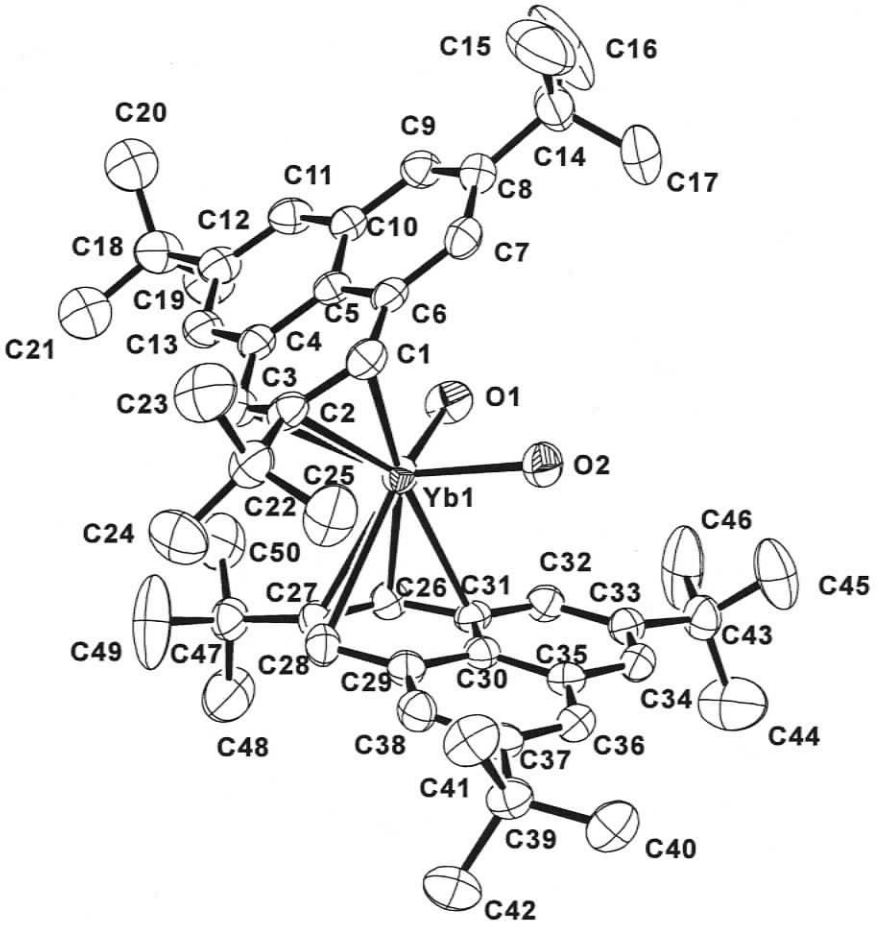

Table A.1. Crystal data and structure refinement for 136.

Empirical formula	C58 H82 O2 Yb	
Formula weight	984.28	
Temperature	235(2) K	
Wavelength	0.71073 Å	
Crystal system	Monoclinic	
Space group	C2/c	
Unit cell dimensions	a = 41.067(2) Å	α= 90°.
	b = 12.0077(7) Å	β= 104.579(1)°.
	c = 21.7474(12) Å	γ = 90°.
Volume	10378.7(10) $Å^3$	
Z	8	
Density (calculated)	1.260 Mg/m^3	
Absorption coefficient	1.841 mm^{-1}	
F(000)	4128	
Crystal size	0.47 x 0.39 x 0.28 mm^3	
Crystal color and habit	red plate	
Diffractometer	Bruker/Siemens SMART APEX	
Theta range for data collection	1.77 to 25.25°.	
Index ranges	-49<=h<=49, -14<=k<=14, -26<=l<=26	
Reflections collected	78029	
Independent reflections	9400 [R(int) = 0.0317]	
Completeness to theta = 25.25°	100.0 %	
Absorption correction	Semi-empirical from equivalents	
Max. and min. transmission	0.595 and 0.454	
Solution method	XS, Bruker SHELXTL v. 6.12	
Refinement method	Full-matrix least-squares on F^2	
Data / restraints / parameters	9400 / 18 / 571	
Goodness-of-fit on F^2	1.016	
Final R indices [I>2sigma(I)]	R1 = 0.0283, wR2 = 0.0692	
R indices (all data)	R1 = 0.0344, wR2 = 0.0726	
Largest diff. peak and hole	0.938 and -0.386 $e.Å^{-3}$	

Table A.2. Bond lengths [Å] and angles [deg] for 136

C(1)-C(2)	1.390(4)	C(28)-C(29)	1.437(4)
C(1)-C(6)	1.436(4)	C(28)-Yb(1)	2.864(3)
C(1)-Yb(1)	2.817(3)	C(29)-C(38)	1.393(4)
C(2)-C(3)	1.399(4)	C(29)-C(30)	1.434(4)
C(2)-C(22)	1.538(4)	C(29)-Yb(1)	3.022(3)
C(2)-Yb(1)	2.838(3)	C(30)-C(31)	1.426(4)
C(3)-C(4)	1.435(4)	C(30)-C(35)	1.426(4)
C(3)-Yb(1)	2.808(3)	C(30)-Yb(1)	3.013(3)
C(4)-C(13)	1.402(4)	C(31)-C(32)	1.406(4)
C(4)-C(5)	1.431(4)	C(31)-Yb(1)	2.886(3)
C(4)-Yb(1)	2.996(3)	C(32)-C(33)	1.402(4)
C(5)-C(6)	1.426(4)	C(33)-C(34)	1.381(4)
C(5)-C(10)	1.428(4)	C(33)-C(43)	1.532(4)
C(5)-Yb(1)	3.049(3)	C(34)-C(35)	1.414(4)
C(6)-C(7)	1.401(4)	C(35)-C(36)	1.411(4)
C(6)-Yb(1)	2.955(3)	C(36)-C(37)	1.375(4)
C(7)-C(8)	1.396(4)	C(37)-C(38)	1.409(4)
C(8)-C(9)	1.380(4)	C(37)-C(39)	1.531(4)
C(8)-C(14)	1.544(4)	C(39)-C(40)	1.531(5)
C(9)-C(10)	1.416(4)	C(39)-C(42)	1.538(5)
C(10)-C(11)	1.409(4)	C(39)-C(41)	1.539(4)
C(11)-C(12)	1.376(4)	C(43)-C(46)	1.505(5)
C(12)-C(13)	1.401(4)	C(43)-C(45)	1.522(5)
C(12)-C(18)	1.532(4)	C(43)-C(44)	1.525(6)
C(14)-C(16)	1.488(6)	C(47)-C(48)	1.510(5)
C(14)-C(17)	1.503(5)	C(47)-C(49)	1.510(6)
C(14)-C(15)	1.545(6)	C(47)-C(50)	1.520(6)
C(18)-C(20B)	1.502(8)	O(1A)-Yb(1)	2.435(2)
C(18)-C(21A)	1.491(5)	O(2)-Yb(1)	2.436(2)
C(18)-C(21B)	1.538(8)	C(2)-C(1)-C(6)	122.0(3)
C(18)-C(19A)	1.535(6)	C(1)-C(2)-C(3)	119.2(3)
C(18)-C(19B)	1.542(8)	C(1)-C(2)-C(22)	119.3(3)
C(18)-C(20A)	1.543(6)	C(3)-C(2)-C(22)	121.2(3)
C(22)-C(25)	1.527(5)	C(2)-C(3)-C(4)	121.1(3)
C(22)-C(23)	1.526(5)	C(13)-C(4)-C(5)	118.5(3)
C(22)-C(24)	1.530(6)	C(13)-C(4)-C(3)	123.1(3)
C(26)-C(27)	1.396(4)	C(5)-C(4)-C(3)	118.3(3)
C(26)-C(31)	1.437(4)	C(6)-C(5)-C(10)	119.8(3)
C(26)-Yb(1)	2.789(3)	C(6)-C(5)-C(4)	120.7(3)
C(27)-C(28)	1.393(4)	C(10)-C(5)-C(4)	119.4(3)
C(27)-C(47)	1.547(4)	C(7)-C(6)-C(5)	118.8(3)
C(27)-Yb(1)	2.869(3)	C(7)-C(6)-C(1)	123.2(3)

C(5)-C(6)-C(1)	117.9(3)	C(38)-C(29)-C(30)	118.8(3)
C(8)-C(7)-C(6)	122.1(3)	C(38)-C(29)-C(28)	123.3(3)
C(9)-C(8)-C(7)	118.7(3)	C(30)-C(29)-C(28)	117.8(3)
C(9)-C(8)-C(14)	121.2(3)	C(31)-C(30)-C(35)	120.0(3)
C(7)-C(8)-C(14)	120.1(3)	C(31)-C(30)-C(29)	120.9(3)
C(8)-C(9)-C(10)	122.4(3)	C(35)-C(30)-C(29)	119.1(3)
C(11)-C(10)-C(9)	123.0(3)	C(32)-C(31)-C(30)	118.8(3)
C(11)-C(10)-C(5)	118.8(3)	C(32)-C(31)-C(26)	123.0(3)
C(9)-C(10)-C(5)	118.1(3)	C(30)-C(31)-C(26)	118.1(3)
C(12)-C(11)-C(10)	122.3(3)	C(33)-C(32)-C(31)	121.8(3)
C(11)-C(12)-C(13)	118.7(3)	C(34)-C(33)-C(32)	118.5(3)
C(11)-C(12)-C(18)	121.2(3)	C(34)-C(33)-C(43)	119.7(3)
C(13)-C(12)-C(18)	120.1(3)	C(32)-C(33)-C(43)	121.8(3)
C(12)-C(13)-C(4)	122.2(3)	C(33)-C(34)-C(35)	122.9(3)
C(16)-C(14)-C(17)	110.6(4)	C(36)-C(35)-C(34)	123.0(3)
C(16)-C(14)-C(15)	107.5(4)	C(36)-C(35)-C(30)	119.1(3)
C(17)-C(14)-C(15)	105.7(4)	C(34)-C(35)-C(30)	117.9(3)
C(16)-C(14)-C(8)	113.7(3)	C(37)-C(36)-C(35)	122.3(3)
C(17)-C(14)-C(8)	110.3(3)	C(36)-C(37)-C(38)	118.3(3)
C(15)-C(14)-C(8)	108.7(3)	C(36)-C(37)-C(39)	122.4(3)
C(27)-C(26)-C(31)	121.4(3)	C(38)-C(37)-C(39)	119.3(3)
C(28)-C(27)-C(26)	119.5(3)	C(29)-C(38)-C(37)	122.5(3)
C(28)-C(27)-C(47)	121.0(3)	C(40)-C(39)-C(37)	112.5(3)
C(26)-C(27)-C(47)	119.3(3)	O(1A)-Yb(1)-O(2)	94.73(8)
C(27)-C(28)-C(29)	121.4(3)	O(1A)-Yb(1)-C(3)	112.39(8)

Figure A.2. Complete Ortep3 diagram of 147

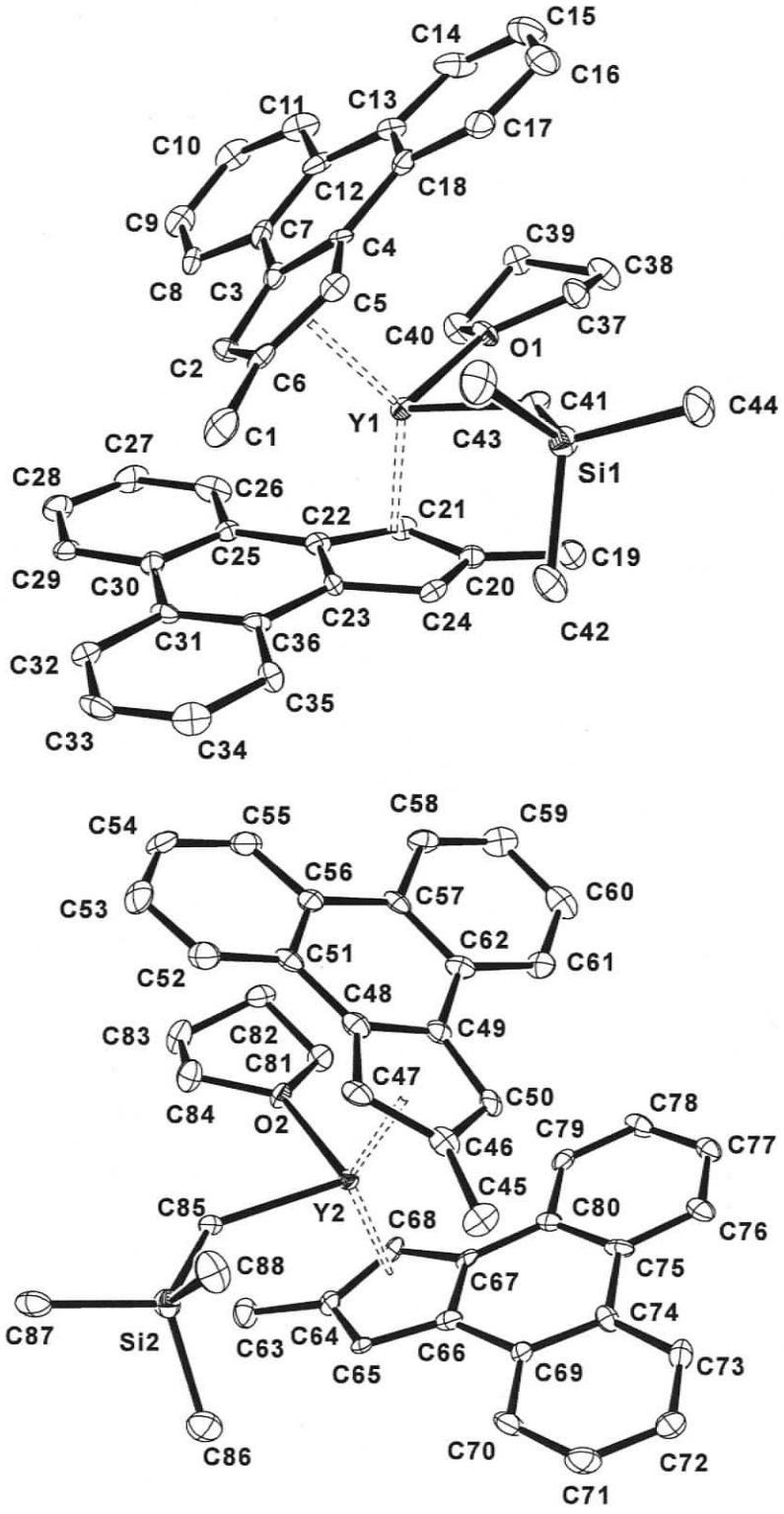

Table A.3. Crystal data and structure refinement for 147.

Empirical formula	C44 H45 O Si Y	
Formula weight	706.80	
Temperature	85(2) K	
Wavelength	0.71073 Å	
Crystal system	Orthorhombic	
Space group	Pca2(1)	
Unit cell dimensions	a = 23.301(5) Å	α= 90°.
	b = 12.701(3) Å	β= 90°.
	c = 23.859(5) Å	γ = 90°.
Volume	7061(3) Å^3	
Z	8	
Density (calculated)	1.330 Mg/m^3	
Absorption coefficient	1.720 mm^{-1}	
F(000)	2960	
Crystal size	0.24 x 0.14 x 0.08 mm^3	
Crystal color and habit	colorless fragment	
Diffractometer	Bruker/Siemens SMART APEX	
Theta range for data collection	0.85 to 25.25°.	
Index ranges	-27<=h<=27, -15<=k<=15, -28<=l<=28	
Reflections collected	94324	
Independent reflections	12768 [R(int) = 0.1240]	
Completeness to theta = 25.25°	99.9 %	
Absorption correction	Semi-empirical from equivalents	
Max. and min. transmission	0.8747 and 0.6830	
Solution method	XS, Bruker SHELXTL v. 6.12	
Refinement method	Full-matrix least-squares on F^2	
Data / restraints / parameters	12768 / 7 / 861	
Goodness-of-fit on F^2	1.014	
Final R indices [I>2sigma(I)]	R1 = 0.0510, wR2 = 0.1097	
R indices (all data)	R1 = 0.0793, wR2 = 0.1220	
Largest diff. peak and hole	2.208 and -0.396 e.Å^{-3}	

Table A.4. Bond lengths [Å] and angles [deg] for 147.

C(1)-C(6)	1.509(8)	C(27)-C(28)	1.390(9)
C(2)-C(6)	1.411(8)	C(28)-C(29)	1.361(8)
C(2)-C(3)	1.425(8)	C(29)-C(30)	1.408(8)
C(2)-Y(1)	2.661(6)	C(30)-C(31)	1.473(8)
C(3)-C(4)	1.435(8)	C(31)-C(32)	1.405(8)
C(3)-C(7)	1.455(8)	C(31)-C(36)	1.413(8)
C(3)-Y(1)	2.680(6)	C(32)-C(33)	1.390(9)
C(4)-C(5)	1.416(8)	C(33)-C(34)	1.379(9)
C(4)-C(18)	1.452(8)	C(34)-C(35)	1.373(8)
C(4)-Y(1)	2.676(5)	C(35)-C(36)	1.400(8)
C(5)-C(6)	1.400(8)	C(37)-O(1)	1.467(7)
C(5)-Y(1)	2.670(6)	C(37)-C(38)	1.530(8)
C(6)-Y(1)	2.666(6)	C(38)-C(39)	1.522(8)
C(7)-C(8)	1.402(8)	C(39)-C(40)	1.515(8)
C(7)-C(12)	1.417(9)	C(40)-O(1)	1.468(7)
C(8)-C(9)	1.367(8)	C(41)-Si(1)	1.843(6)
C(9)-C(10)	1.382(9)	C(41)-Y(1)	2.398(6)
C(10)-C(11)	1.372(10)	C(42)-Si(1)	1.881(6)
C(11)-C(12)	1.415(9)	C(43)-Si(1)	1.863(6)
C(12)-C(13)	1.454(9)	C(44)-Si(1)	1.871(6)
C(13)-C(14)	1.423(9)	C(45)-C(46)	1.492(8)
C(13)-C(18)	1.425(8)	C(46)-C(50)	1.417(8)
C(14)-C(15)	1.360(10)	C(46)-C(47)	1.439(8)
C(15)-C(16)	1.415(9)	C(46)-Y(2)	2.697(6)
C(16)-C(17)	1.358(9)	C(47)-C(48)	1.408(8)
C(17)-C(18)	1.414(8)	C(47)-Y(2)	2.664(6)
C(19)-C(20)	1.505(8)	C(48)-C(49)	1.433(8)
C(20)-C(24)	1.398(8)	C(48)-C(51)	1.435(8)
C(20)-C(21)	1.401(8)	C(48)-Y(2)	2.679(6)
C(20)-Y(1)	2.669(6)	C(49)-C(50)	1.420(8)
C(21)-C(22)	1.423(8)	C(49)-C(62)	1.444(8)
C(21)-Y(1)	2.706(6)	C(49)-Y(2)	2.684(6)
C(22)-C(23)	1.432(8)	C(50)-Y(2)	2.671(6)
C(22)-C(25)	1.449(7)	C(51)-C(52)	1.373(8)
C(22)-Y(1)	2.725(5)	C(51)-C(56)	1.427(8)
C(23)-C(24)	1.427(8)	C(52)-C(53)	1.374(9)
C(23)-C(36)	1.436(8)	C(53)-C(54)	1.404(9)
C(23)-Y(1)	2.708(5)	C(54)-C(55)	1.370(9)
C(24)-Y(1)	2.649(6)	C(55)-C(56)	1.407(8)
C(25)-C(30)	1.407(8)	C(56)-C(57)	1.464(9)
C(25)-C(26)	1.408(8)	C(57)-C(62)	1.424(9)
C(26)-C(27)	1.368(8)	C(57)-C(58)	1.433(8)

C(58)-C(59)	1.348(9)	C(8)-C(7)-C(12)	119.8(6)
C(59)-C(60)	1.425(9)	C(8)-C(7)-C(3)	121.2(6)
C(60)-C(61)	1.380(8)	C(12)-C(7)-C(3)	118.9(6)
C(61)-C(62)	1.389(9)	C(9)-C(8)-C(7)	121.1(6)
C(63)-C(64)	1.497(8)	C(8)-C(9)-C(10)	120.0(6)
C(64)-C(65)	1.411(8)	C(11)-C(10)-C(9)	120.2(6)
C(64)-C(68)	1.418(8)	C(10)-C(11)-C(12)	121.7(7)
C(64)-Y(2)	2.669(6)	C(11)-C(12)-C(7)	117.1(7)
C(65)-C(66)	1.402(8)	C(11)-C(12)-C(13)	122.5(7)
C(65)-Y(2)	2.644(5)	C(7)-C(12)-C(13)	120.4(6)
C(66)-C(67)	1.421(8)	C(14)-C(13)-C(18)	117.5(6)
C(66)-C(69)	1.462(8)	C(14)-C(13)-C(12)	121.6(6)
C(66)-Y(2)	2.711(6)	C(18)-C(13)-C(12)	120.8(6)
C(67)-C(68)	1.420(8)	C(15)-C(14)-C(13)	121.1(6)
C(67)-C(80)	1.434(8)	C(14)-C(15)-C(16)	121.3(7)
C(67)-Y(2)	2.712(5)	C(17)-C(16)-C(15)	118.8(6)
C(68)-Y(2)	2.681(6)	C(16)-C(17)-C(18)	121.8(6)
C(69)-C(74)	1.400(8)	C(17)-C(18)-C(13)	119.3(6)
C(69)-C(70)	1.417(8)	C(17)-C(18)-C(4)	121.8(6)
C(70)-C(71)	1.375(8)	C(13)-C(18)-C(4)	118.8(6)
C(71)-C(72)	1.387(9)	C(24)-C(20)-C(21)	108.7(5)
C(72)-C(73)	1.355(9)	C(24)-C(20)-C(19)	126.3(5)
C(73)-C(74)	1.413(8)	C(21)-C(20)-C(19)	125.0(5)
C(74)-C(75)	1.495(8)	C(20)-C(21)-C(22)	108.2(5)
C(75)-C(80)	1.409(8)	C(21)-C(22)-C(23)	107.8(5)
C(75)-C(76)	1.417(8)	C(21)-C(22)-C(25)	131.8(5)
C(76)-C(77)	1.379(8)	C(23)-C(22)-C(25)	120.3(5)
C(77)-C(78)	1.391(8)	C(24)-C(23)-C(22)	106.6(5)
C(78)-C(79)	1.369(8)	C(24)-C(23)-C(36)	131.7(5)
C(79)-C(80)	1.410(8)	C(22)-C(23)-C(36)	121.1(5)
C(85)-Y(2)	2.380(5)	C(20)-C(24)-C(23)	108.8(5)
O(1)-Y(1)	2.360(4)	C(30)-C(25)-C(26)	119.5(5)
O(2)-Y(2)	2.353(4)	C(30)-C(25)-C(22)	118.7(5)
C(6)-C(2)-C(3)	107.8(5)	C(26)-C(25)-C(22)	121.7(5)
C(2)-C(3)-C(4)	107.0(5)	C(27)-C(26)-C(25)	121.0(6)
C(2)-C(3)-C(7)	132.2(5)	C(26)-C(27)-C(28)	120.0(6)
C(4)-C(3)-C(7)	120.5(5)	C(29)-C(28)-C(27)	119.7(6)
C(5)-C(4)-C(3)	108.1(5)	C(28)-C(29)-C(30)	122.4(6)
C(5)-C(4)-C(18)	131.9(5)	C(25)-C(30)-C(29)	117.4(6)
C(3)-C(4)-C(18)	119.9(5)	C(25)-C(30)-C(31)	120.3(5)
C(6)-C(5)-C(4)	107.9(5)	C(29)-C(30)-C(31)	122.3(6)
C(5)-C(6)-C(2)	109.2(5)	C(32)-C(31)-C(36)	118.2(6)
C(5)-C(6)-C(1)	125.8(6)	C(32)-C(31)-C(30)	121.1(6)
C(2)-C(6)-C(1)	124.8(6)	C(36)-C(31)-C(30)	120.8(5)

C(33)-C(32)-C(31)	120.8(6)	C(61)-C(60)-C(59)	118.1(6)
C(34)-C(33)-C(32)	120.2(6)	C(60)-C(61)-C(62)	121.9(6)
C(35)-C(34)-C(33)	120.4(6)	C(61)-C(62)-C(57)	120.6(6)
C(34)-C(35)-C(36)	120.6(6)	C(61)-C(62)-C(49)	121.7(6)
C(35)-C(36)-C(31)	119.8(5)	C(57)-C(62)-C(49)	117.6(6)
C(35)-C(36)-C(23)	121.7(5)	C(65)-C(64)-C(68)	107.9(5)
C(31)-C(36)-C(23)	118.4(5)	C(65)-C(64)-C(63)	126.7(5)
O(1)-C(37)-C(38)	105.4(5)	C(68)-C(64)-C(63)	125.4(5)
C(39)-C(38)-C(37)	103.0(5)	C(66)-C(65)-C(64)	108.2(5)
C(40)-C(39)-C(38)	101.7(5)	C(65)-C(66)-C(67)	108.6(5)
O(1)-C(40)-C(39)	105.2(5)	C(65)-C(66)-C(69)	132.6(5)
C(50)-C(46)-C(47)	107.0(5)	C(67)-C(66)-C(69)	118.5(5)
C(50)-C(46)-C(45)	126.0(5)	C(68)-C(67)-C(66)	107.1(5)
C(47)-C(46)-C(45)	127.0(5)	C(68)-C(67)-C(80)	130.6(5)
C(48)-C(47)-C(46)	108.7(5)	C(66)-C(67)-C(80)	122.3(5)
C(47)-C(48)-C(49)	107.7(5)	C(64)-C(68)-C(67)	108.1(5)
C(47)-C(48)-C(51)	130.8(6)	C(74)-C(69)-C(70)	119.2(5)
C(49)-C(48)-C(51)	121.5(5)	C(74)-C(69)-C(66)	120.1(5)
C(50)-C(49)-C(48)	107.8(5)	C(70)-C(69)-C(66)	120.6(5)
C(50)-C(49)-C(62)	130.9(6)	C(71)-C(70)-C(69)	120.6(6)
C(48)-C(49)-C(62)	120.6(5)	C(70)-C(71)-C(72)	119.7(6)
C(46)-C(50)-C(49)	108.7(5)	C(73)-C(72)-C(71)	120.8(6)
C(52)-C(51)-C(56)	119.1(6)	C(72)-C(73)-C(74)	121.4(6)
C(52)-C(51)-C(48)	122.7(6)	C(69)-C(74)-C(73)	118.3(6)
C(56)-C(51)-C(48)	118.2(5)	C(69)-C(74)-C(75)	120.2(5)
C(51)-C(52)-C(53)	122.4(6)	C(73)-C(74)-C(75)	121.5(5)
C(52)-C(53)-C(54)	118.7(6)	C(80)-C(75)-C(76)	119.7(5)
C(55)-C(54)-C(53)	120.6(6)	C(80)-C(75)-C(74)	119.3(5)
C(54)-C(55)-C(56)	120.8(6)	C(76)-C(75)-C(74)	121.0(6)
C(55)-C(56)-C(51)	118.2(6)	C(77)-C(76)-C(75)	120.3(6)
C(55)-C(56)-C(57)	121.9(6)	C(76)-C(77)-C(78)	120.2(6)
C(51)-C(56)-C(57)	119.9(5)	C(79)-C(78)-C(77)	120.0(6)
C(62)-C(57)-C(58)	116.2(6)	C(78)-C(79)-C(80)	121.9(6)
C(62)-C(57)-C(56)	121.5(5)	Si(2)-C(85)-Y(2)	137.4(3)
C(58)-C(57)-C(56)	122.3(6)	O(1)-Y(1)-C(41)	92.99(17)
C(59)-C(58)-C(57)	122.4(6)	O(2)-Y(2)-C(85)	93.36(17)
C(58)-C(59)-C(60)	120.7(6)		

Figure A.3. Complete Ortep3 diagram of 150

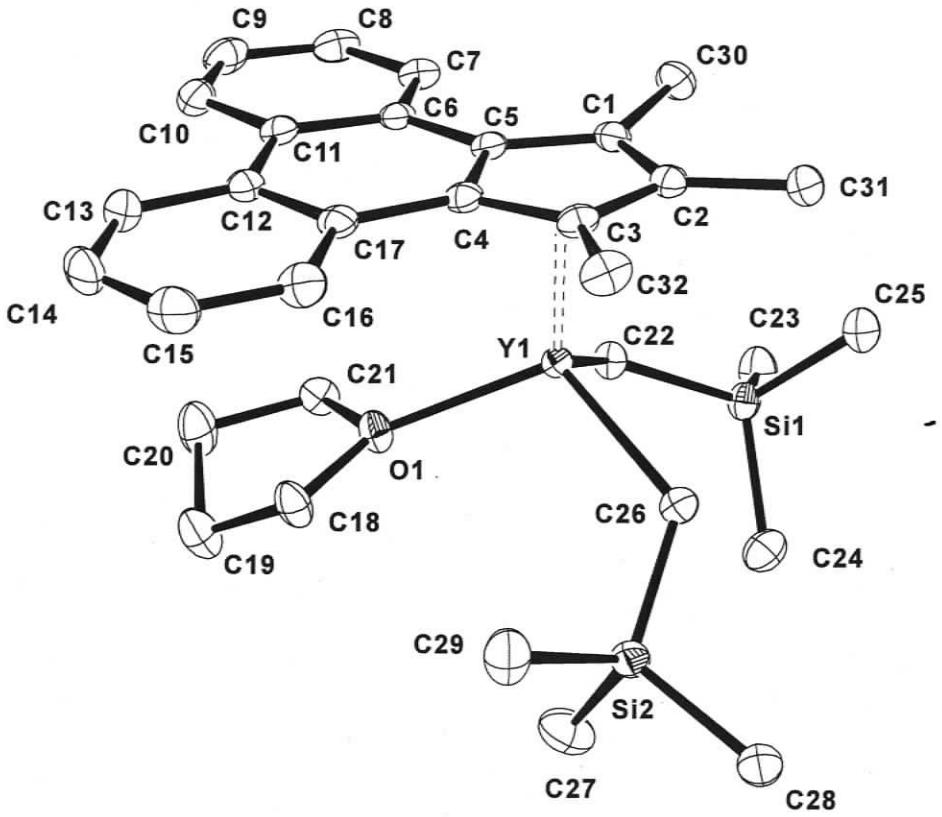

Table A.5. Crystal data and structure refinement for 150.

Empirical formula	C32 H47 O Si2 Y	
Formula weight	592.79	
Temperature	86(2) K	
Wavelength	0.71073 Å	
Crystal system	Triclinic	
Space group	P-1	
Unit cell dimensions	a = 11.1359(5) Å	α= 76.0030(10)°.
	b = 12.7246(6) Å	β= 74.1890(10)°.
	c = 12.9267(6) Å	γ = 64.5570(10)°.
Volume	1574.97(13) $Å^3$	
Z	2	
Density (calculated)	1.250 Mg/m^3	
Absorption coefficient	1.949 mm^{-1}	
F(000)	628	
Crystal size	0.32 x 0.28 x 0.21 mm^3	
Crystal color and habit	pale yellow parallelepiped	
Diffractometer	Bruker/Siemens SMART APEX	
Theta range for data collection	1.79 to 27.50°.	
Index ranges	-14<=h<=14, -16<=k<=16, -16<=l<=16	
Reflections collected	24128	
Independent reflections	7233 [R(int) = 0.0275]	
Completeness to theta = 27.50°	99.8 %	
Absorption correction	Semi-empirical from equivalents	
Max. and min. transmission	0.664 and 0.557	
Solution method	XS, Bruker SHELXTL v. 6.12	
Refinement method	Full-matrix least-squares on F^2	
Data / restraints / parameters	7233 / 0 / 334	
Goodness-of-fit on F^2	1.049	
Final R indices [I>2sigma(I)]	R1 = 0.0305, wR2 = 0.0750	
R indices (all data)	R1 = 0.0350, wR2 = 0.0770	
Largest diff. peak and hole	0.549 and -0.273 $e.Å^{-3}$	

Table A.6. Bond lengths [Å] and angles [deg] for 150.

C(1)-C(2)	1.418(2)	C(13)-C(14)	1.378(3)
C(1)-C(5)	1.427(2)	C(13)-H(13)	0.9500
C(1)-C(30)	1.509(2)	C(14)-C(15)	1.386(3)
C(1)-Y(1)	2.6747(17)	C(15)-C(16)	1.376(3)
C(2)-C(3)	1.420(2)	C(16)-C(17)	1.416(3)
C(2)-C(31)	1.509(2)	C(18)-O(1)	1.470(2)
C(2)-Y(1)	2.6952(17)	C(18)-C(19)	1.505(3)
C(3)-C(4)	1.426(2)	C(19)-C(20)	1.514(3)
C(3)-C(32)	1.505(2)	C(20)-C(21)	1.506(3)
C(3)-Y(1)	2.6786(17)	C(21)-O(1)	1.477(2)
C(4)-C(5)	1.434(2)	C(22)-Si(1)	1.8409(18)
C(4)-C(17)	1.452(2)	C(22)-Y(1)	2.3904(17)
C(4)-Y(1)	2.6313(16)	C(23)-Si(1)	1.886(2)
C(5)-C(6)	1.452(2)	C(24)-Si(1)	1.877(2)
C(5)-Y(1)	2.6297(16)	C(25)-Si(1)	1.872(2)
C(6)-C(7)	1.408(2)	C(26)-Si(2)	1.8327(18)
C(6)-C(11)	1.421(2)	C(26)-Y(1)	2.3832(17)
C(7)-C(8)	1.380(3)	C(27)-Si(2)	1.879(2)
C(8)-C(9)	1.392(3)	C(28)-Si(2)	1.882(2)
C(9)-C(10)	1.376(3)	C(29)-Si(2)	1.882(2)
C(10)-C(11)	1.409(3)	O(1)-Y(1)	2.3239(12)
C(11)-C(12)	1.473(3)	O(1)-Y(1)-C(26)	112.10(5)
C(12)-C(13)	1.411(2)	O(1)-Y(1)-C(22)	93.30(5)
C(12)-C(17)	1.417(3)	C(26)-Y(1)-C(22)	107.75(6)

Figure A.4. Complete Ortep3 diagram of 152

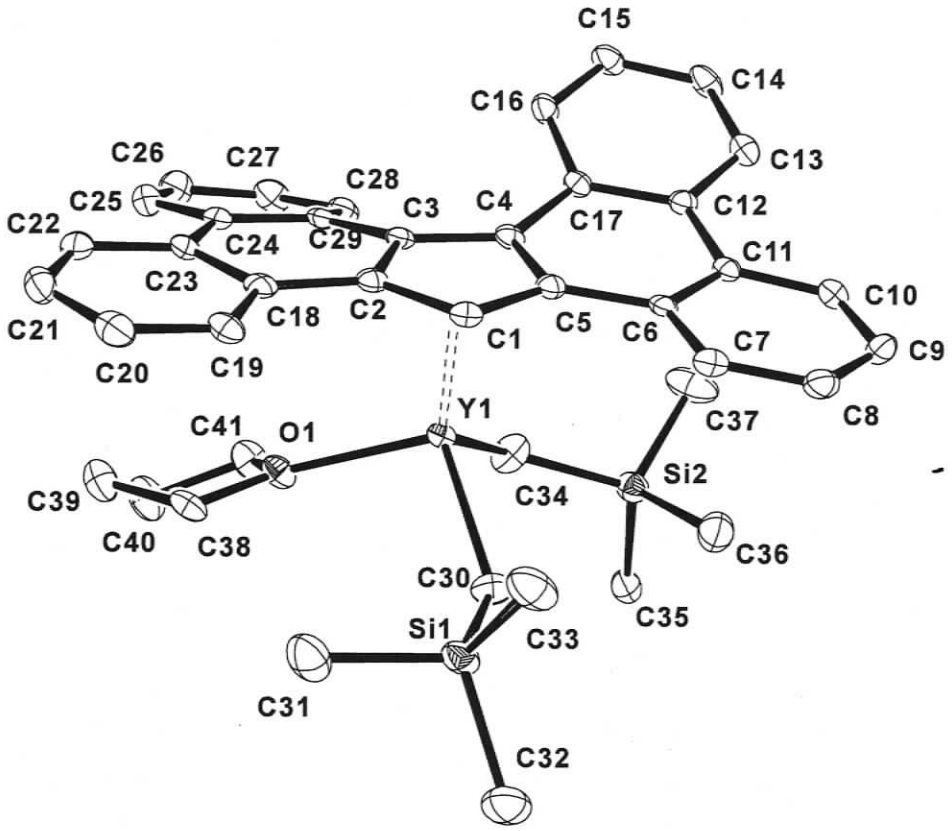

TableA.7. Crystal data and structure refinement for 152.

Empirical formula	C41 H47 O Si2 Y	
Formula weight	700.88	
Temperature	86(2) K	
Wavelength	0.71073 Å	
Crystal system	Monoclinic	
Space group	P2(1)/n	
Unit cell dimensions	a = 13.797(3) Å	α= 90°.
	b = 14.840(3) Å	β= 100.77(3)°.
	c = 18.047(4) Å	γ = 90°.
Volume	3630.0(13) $Å^3$	
Z	4	
Density (calculated)	1.282 Mg/m^3	
Absorption coefficient	1.703 mm^{-1}	
F(000)	1472	
Crystal size	0.42 x 0.17 x 0.07 mm^3	
Crystal color and habit	colorless plate	
Diffractometer	Bruker/Siemens SMART APEX	
Theta range for data collection	1.71 to 27.61°.	
Index ranges	-17<=h<=17, -19<=k<=19, -23<=l<=23	
Reflections collected	47751	
Independent reflections	8414 [R(int) = 0.1002]	
Completeness to theta = 27.61°	99.8 %	
Absorption correction	Semi-empirical from equivalents	
Max. and min. transmission	0.8901 and 0.5349	
Solution method	XS, Bruker SHELXTL v. 6.12	
Refinement method	Full-matrix least-squares on F^2	
Data / restraints / parameters	8414 / 0 / 412	
Goodness-of-fit on F^2	1.011	
Final R indices [I>2sigma(I)]	R1 = 0.0458, wR2 = 0.0924	
R indices (all data)	R1 = 0.0819, wR2 = 0.1045	
Largest diff. peak and hole	0.760 and -0.468 $e.Å^{-3}$	

Table A.8. Bond lengths [Å] and angles [deg] for 152.

C(1)-C(2)	1.411(4)	C(20)-C(21)	1.396(4)
C(1)-C(5)	1.413(4)	C(21)-C(22)	1.372(4)
C(1)-Y(1)	2.641(3)	C(22)-C(23)	1.404(4)
C(2)-C(3)	1.426(4)	C(23)-C(24)	1.470(4)
C(2)-C(18)	1.449(4)	C(24)-C(25)	1.409(4)
C(2)-Y(1)	2.645(3)	C(24)-C(29)	1.419(4)
C(3)-C(4)	1.432(4)	C(25)-C(26)	1.370(4)
C(3)-C(29)	1.457(4)	C(26)-C(27)	1.388(4)
C(3)-Y(1)	2.667(3)	C(27)-C(28)	1.377(4)
C(4)-C(5)	1.421(4)	C(28)-C(29)	1.401(4)
C(4)-C(17)	1.450(4)	C(30)-Si(1)	1.838(3)
C(4)-Y(1)	2.765(3)	C(30)-Y(1)	2.360(3)
C(5)-C(6)	1.450(4)	C(31)-Si(1)	1.865(3)
C(5)-Y(1)	2.699(3)	C(32)-Si(1)	1.880(3)
C(6)-C(7)	1.402(4)	C(33)-Si(1)	1.871(3)
C(6)-C(11)	1.412(4)	C(34)-Si(2)	1.838(3)
C(7)-C(8)	1.372(4)	C(34)-Y(1)	2.353(3)
C(8)-C(9)	1.386(4)	C(35)-Si(2)	1.868(3)
C(9)-C(10)	1.376(4)	C(36)-Si(2)	1.874(3)
C(10)-C(11)	1.404(4)	C(37)-Si(2)	1.870(3)
C(11)-C(12)	1.468(4)	C(38)-O(1)	1.466(3)
C(12)-C(13)	1.404(4)	C(38)-C(39)	1.510(4)
C(12)-C(17)	1.421(4)	C(39)-C(40)	1.519(4)
C(13)-C(14)	1.379(4)	C(40)-C(41)	1.501(4)
C(14)-C(15)	1.383(4)	C(41)-O(1)	1.472(3)
C(15)-C(16)	1.379(4)	O(1)-Y(1)	2.307(2)
C(16)-C(17)	1.401(4)	O(1)-Y(1)-C(34)	95.28(10)
C(18)-C(19)	1.407(4)	O(1)-Y(1)-C(30)	102.76(9)
C(18)-C(23)	1.408(4)	C(34)-Y(1)-C(30)	103.93(11)
C(19)-C(20)	1.372(4)		

Figure A.5. Complete Ortep3 diagram of 154

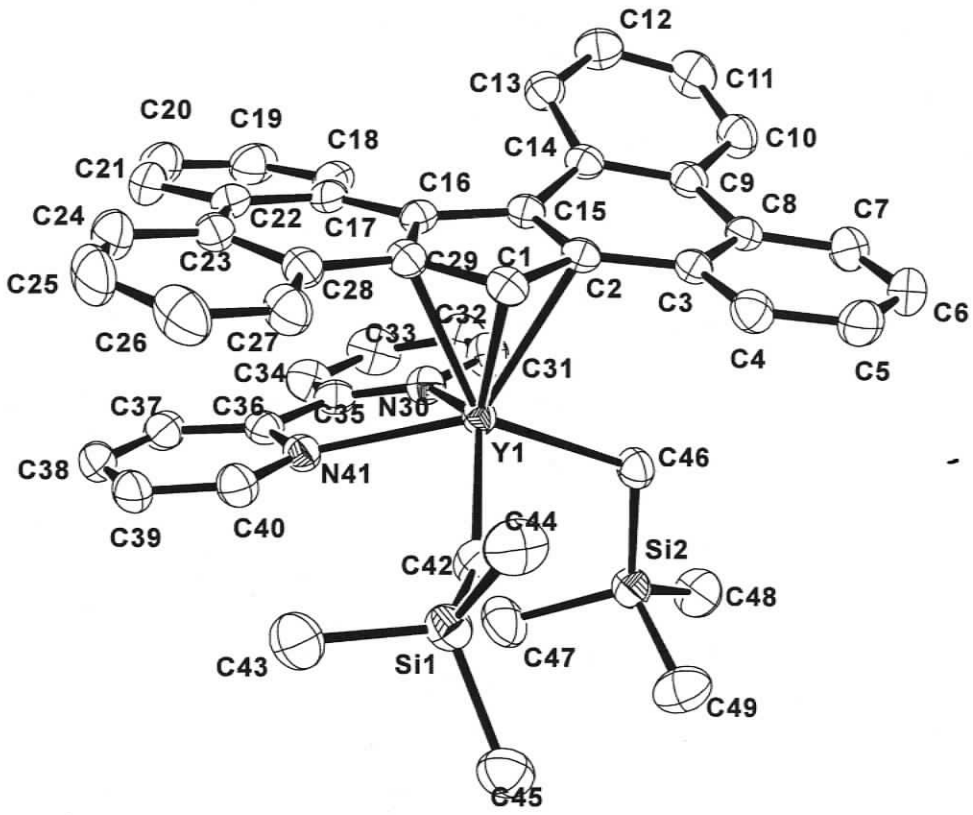

Table A.9. Crystal data and structure refinement for 154.

Empirical formula	C47 H47 N2 Si2 Y	
Formula weight	784.96	
Temperature	185(2) K	
Wavelength	0.71073 Å	
Crystal system	Monoclinic	
Space group	P2(1)/n	
Unit cell dimensions	a = 11.187(2) Å	α= 90°.
	b = 21.195(3) Å	β= 107.676(15)°.
	c = 17.318(3) Å	γ = 90°.
Volume	3912.6(11) $Å^3$	
Z	4	
Density (calculated)	1.333 Mg/m^3	
Absorption coefficient	1.588 mm^{-1}	
F(000)	1640	
Crystal size	0.34 x 0.26 x 0.17 mm^3	
Crystal color and habit	orange block	
Diffractometer	Bruker/Siemens SMART APEX	
Theta range for data collection	1.56 to 25.25°.	
Index ranges	-13<=h<=13, -25<=k<=25, -20<=l<=20	
Reflections collected	58200	
Independent reflections	7080 [R(int) = 0.0365]	
Completeness to theta = 25.25°	100.0 %	
Absorption correction	Semi-empirical from equivalents	
Max. and min. transmission	0.766 and 0.608	
Solution method	Bruker, 2003; XS, SHELXTL v. 6.14	
Refinement method	Full-matrix least-squares on F^2	
Data / restraints / parameters	7080 / 0 / 475	
Goodness-of-fit on F^2	1.032	
Final R indices [I>2sigma(I)]	R1 = 0.0317, wR2 = 0.0780	
R indices (all data)	R1 = 0.0402, wR2 = 0.0821	
Largest diff. peak and hole	0.477 and -0.215 $e.Å^{-3}$	

Table A.10. Bond lengths [Å] and angles [deg] for 154.

C(1)-C(29)	1.409(3)	C(27)-C(28)	1.401(3)
C(1)-C(2)	1.416(3)	C(28)-C(29)	1.455(3)
C(1)-Y(1)	2.640(2)	C(29)-Y(1)	2.721(2)
C(2)-C(15)	1.430(3)	C(31)-N(30)	1.346(3)
C(2)-C(3)	1.451(3)	C(31)-C(32)	1.378(3)
C(2)-Y(1)	2.689(2)	C(32)-C(33)	1.372(4)
C(3)-C(4)	1.397(3)	C(33)-C(34)	1.380(3)
C(3)-C(8)	1.414(3)	C(34)-C(35)	1.391(3)
C(4)-C(5)	1.374(3)	C(35)-N(30)	1.353(3)
C(5)-C(6)	1.388(4)	C(35)-C(36)	1.476(3)
C(6)-C(7)	1.370(3)	C(36)-N(41)	1.354(3)
C(7)-C(8)	1.404(3)	C(36)-C(37)	1.389(3)
C(8)-C(9)	1.467(3)	C(37)-C(38)	1.380(3)
C(9)-C(10)	1.406(3)	C(38)-C(39)	1.374(3)
C(9)-C(14)	1.424(3)	C(39)-C(40)	1.377(3)
C(10)-C(11)	1.369(3)	C(40)-N(41)	1.339(3)
C(11)-C(12)	1.381(3)	C(42)-Si(1)	1.829(2)
C(12)-C(13)	1.375(3)	C(42)-Y(1)	2.396(2)
C(13)-C(14)	1.410(3)	C(43)-Si(1)	1.877(3)
C(14)-C(15)	1.463(3)	C(44)-Si(1)	1.875(3)
C(15)-C(16)	1.445(3)	C(45)-Si(1)	1.894(2)
C(15)-Y(1)	2.804(2)	C(46)-Si(2)	1.836(2)
C(16)-C(29)	1.429(3)	C(46)-Y(1)	2.423(2)
C(16)-C(17)	1.469(3)	C(47)-Si(2)	1.875(2)
C(16)-Y(1)	2.780(2)	C(48)-Si(2)	1.880(2)
C(17)-C(18)	1.403(3)	C(49)-Si(2)	1.883(3)
C(17)-C(22)	1.425(3)	N(30)-Y(1)	2.5192(18)
C(18)-C(19)	1.377(3)	N(41)-Y(1)	2.4691(17)
C(19)-C(20)	1.382(4)	C(42)-Y(1)-C(46)	92.24(8)
C(20)-C(21)	1.376(4)	C(42)-Y(1)-N(41)	87.48(7)
C(21)-C(22)	1.410(3)	C(46)-Y(1)-N(41)	134.28(7)
C(22)-C(23)	1.462(3)	C(42)-Y(1)-N(30)	136.11(7)
C(23)-C(28)	1.410(3)	C(46)-Y(1)-N(30)	85.69(7)
C(23)-C(24)	1.410(3)	N(41)-Y(1)-N(30)	64.49(6)
C(24)-C(25)	1.370(4)	Si(2)-C(46)-Y(1)	115.24(10)
C(25)-C(26)	1.382(4)	Si(1)-C(42)-Y(1)	150.50(12)
C(26)-C(27)	1.370(3)		

Figure A.6. Complete Ortep3 diagram of 161.

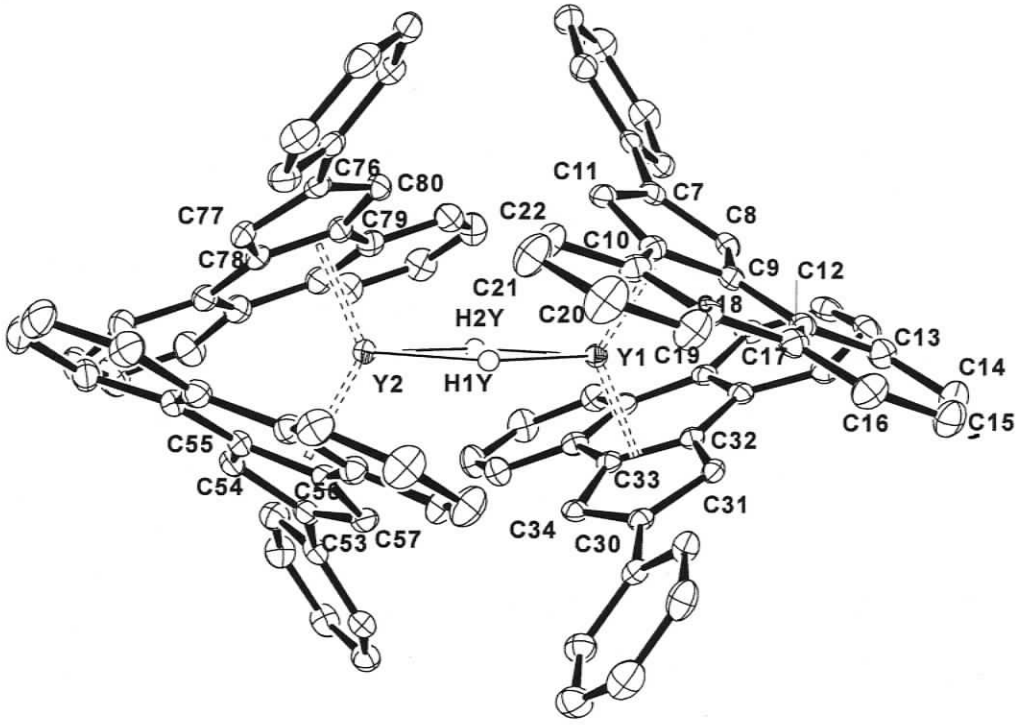

Table A.11. Crystal data and structure refinement for 161.

Identification code	bt685	
Empirical formula	C109.50 H82 Y2	
Formula weight	1575.57	
Temperature	86(2) K	
Wavelength	0.71073 Å	
Crystal system	Monoclinic	
Space group	P2(1)/c	
Unit cell dimensions	a = 23.4906(14) Å	α= 90°.
	b = 19.2945(11) Å	β= 112.7740(10)°.
	c = 18.5459(11) Å	γ = 90°.
Volume	7750.4(8) $Å^3$	
Z	4	
Density (calculated)	1.350 Mg/m^3	
Absorption coefficient	1.544 mm^{-1}	
F(000)	3268	
Crystal size	0.39 x 0.37 x 0.27 mm^3	
Crystal color and habit	colorless needle	
Diffractometer	Bruker/Siemens SMART APEX	
Theta range for data collection	1.41 to 27.50°.	
Index ranges	-30<=h<=30, -25<=k<=25, -24<=l<=24	
Reflections collected	117274	
Independent reflections	17801 [R(int) = 0.0524]	
Completeness to theta = 27.50°	100.0 %	
Absorption correction	Semi-empirical from equivalents	
Max. and min. transmission	0.660 and 0.566	
Solution method	XS, Bruker SHELXTL v. 6.12	
Refinement method	Full-matrix least-squares on F^2	
Data / restraints / parameters	17801 / 0 / 905	
Goodness-of-fit on F^2	1.029	
Final R indices [I>2sigma(I)]	R1 = 0.0442, wR2 = 0.1058	
R indices (all data)	R1 = 0.0616, wR2 = 0.1146	
Largest diff. peak and hole	1.485 and -0.885 $e.Å^{-3}$	

Table A.12. Bond lengths [Å] and angles [deg] for 161.

C(1)-C(2)	1.390(4)	C(30)-Y(1)	2.620(2)
C(1)-C(6)	1.397(4)	C(31)-C(32)	1.422(3)
C(2)-C(3)	1.382(4)	C(31)-Y(1)	2.599(2)
C(3)-C(4)	1.387(4)	C(32)-C(33)	1.421(3)
C(4)-C(5)	1.387(4)	C(32)-C(35)	1.453(3)
C(5)-C(6)	1.395(4)	C(32)-Y(1)	2.686(2)
C(6)-C(7)	1.474(3)	C(33)-C(34)	1.420(3)
C(7)-C(11)	1.417(3)	C(33)-C(46)	1.449(3)
C(7)-C(8)	1.420(3)	C(33)-Y(1)	2.711(2)
C(7)-Y(1)	2.650(2)	C(34)-Y(1)	2.660(2)
C(8)-C(9)	1.421(3)	C(35)-C(36)	1.404(3)
C(8)-Y(1)	2.633(2)	C(35)-C(40)	1.418(3)
C(9)-C(10)	1.414(3)	C(36)-C(37)	1.377(4)
C(9)-C(12)	1.454(3)	C(37)-C(38)	1.394(4)
C(9)-Y(1)	2.715(2)	C(38)-C(39)	1.375(4)
C(10)-C(11)	1.422(3)	C(39)-C(40)	1.412(3)
C(10)-C(23)	1.447(3)	C(40)-C(41)	1.474(3)
C(10)-Y(1)	2.712(2)	C(41)-C(46)	1.410(3)
C(11)-Y(1)	2.664(2)	C(41)-C(42)	1.411(4)
C(12)-C(13)	1.399(3)	C(42)-C(43)	1.377(4)
C(12)-C(17)	1.419(3)	C(43)-C(44)	1.398(4)
C(13)-C(14)	1.380(4)	C(44)-C(45)	1.377(4)
C(14)-C(15)	1.393(4)	C(45)-C(46)	1.405(3)
C(15)-C(16)	1.375(4)	C(47)-C(48)	1.389(4)
C(16)-C(17)	1.405(3)	C(47)-C(52)	1.399(4)
C(17)-C(18)	1.473(3)	C(48)-C(49)	1.389(4)
C(18)-C(19)	1.411(4)	C(49)-C(50)	1.383(4)
C(18)-C(23)	1.414(3)	C(50)-C(51)	1.387(4)
C(19)-C(20)	1.370(4)	C(51)-C(52)	1.397(4)
C(20)-C(21)	1.401(4)	C(52)-C(53)	1.476(3)
C(21)-C(22)	1.371(4)	C(53)-C(54)	1.419(3)
C(22)-C(23)	1.410(4)	C(53)-C(57)	1.420(3)
C(24)-C(25)	1.387(4)	C(53)-Y(2)	2.657(2)
C(24)-C(29)	1.400(4)	C(54)-C(55)	1.420(3)
C(25)-C(26)	1.388(4)	C(54)-Y(2)	2.641(2)
C(25)-H(25)	0.9500	C(55)-C(56)	1.420(3)
C(26)-C(27)	1.378(4)	C(55)-C(69)	1.450(3)
C(27)-C(28)	1.388(4)	C(55)-Y(2)	2.704(2)
C(28)-C(29)	1.398(3)	C(56)-C(57)	1.422(3)
C(29)-C(30)	1.473(3)	C(56)-C(58)	1.449(3)
C(30)-C(34)	1.414(3)	C(56)-Y(2)	2.691(2)
C(30)-C(31)	1.419(3)	C(57)-Y(2)	2.658(2)

C(58)-C(59)	1.403(3)	C(79)-C(80)	1.423(3)
C(58)-C(63)	1.417(3)	C(79)-C(81)	1.448(4)
C(59)-C(60)	1.373(4)	C(79)-Y(2)	2.697(2)
C(60)-C(61)	1.390(4)	C(80)-Y(2)	2.665(2)
C(61)-C(62)	1.369(4)	C(81)-C(82)	1.410(4)
C(62)-C(63)	1.405(4)	C(81)-C(86)	1.414(4)
C(63)-C(64)	1.474(4)	C(82)-C(83)	1.378(4)
C(64)-C(65)	1.407(4)	C(83)-C(84)	1.392(4)
C(64)-C(69)	1.413(4)	C(84)-C(85)	1.374(4)
C(65)-C(66)	1.375(4)	C(85)-C(86)	1.410(4)
C(66)-C(67)	1.397(4)	C(86)-C(87)	1.471(4)
C(67)-C(68)	1.371(4)	C(87)-C(88)	1.407(4)
C(68)-C(69)	1.409(3)	C(87)-C(92)	1.416(4)
C(70)-C(71)	1.387(4)	C(88)-C(89)	1.372(4)
C(70)-C(75)	1.400(4)	C(89)-C(90)	1.393(4)
C(71)-C(72)	1.380(4)	C(90)-C(91)	1.377(4)
C(72)-C(73)	1.384(4)	C(91)-C(92)	1.408(4)
C(73)-C(74)	1.391(4)	Y(1)-H(1Y)	2.10(2)
C(74)-C(75)	1.397(4)	Y(1)-H(2Y)	2.14(3)
C(75)-C(76)	1.475(4)	Y(1)-H(1Y)	2.10(2)
C(76)-C(77)	1.415(3)	Y(1)-H(2Y)	2.14(3)
C(76)-C(80)	1.418(4)	Y(2)-H(2Y)	2.10(3)
C(76)-Y(2)	2.636(2)	Y(2)-H(1Y)	2.16(2)
C(77)-C(78)	1.425(4)	Y(2)-H(1Y)	2.16(2)
C(77)-Y(2)	2.589(2)	Y(2)-H(2Y)	2.10(3)
C(78)-C(79)	1.419(3)	H(1Y)-Y(1)-H(2Y)	67.5(9)
C(78)-C(92)	1.452(3)	H(2Y)-Y(2)-H(1Y)	67.1(10)
C(78)-Y(2)	2.667(2)		

Figure A.7. Complete Ortep3 diagram of 167

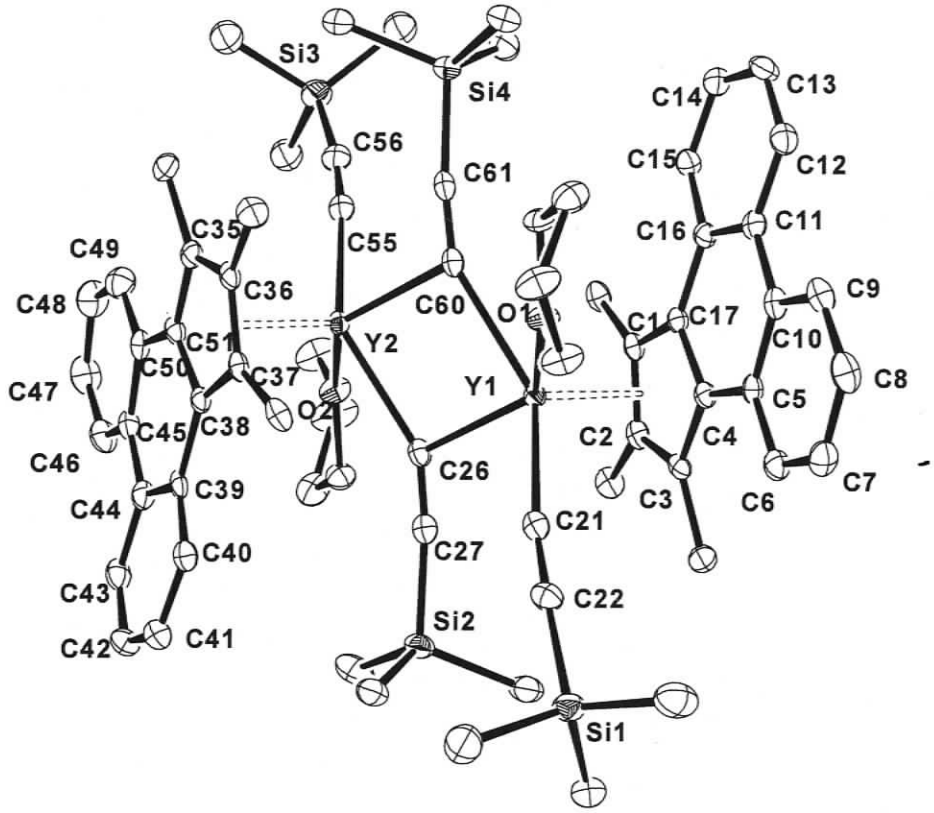

Table A.13. Crystal data and structure refinement for 167.

Empirical formula	C75 H94 O2 Si4 Y2	
Formula weight	1317.68	
Temperature	89(2) K	
Wavelength	0.71073 Å	
Crystal system	Monoclinic	
Space group	P2(1)/c	
Unit cell dimensions	a = 10.5591(12) Å	α= 90°.
	b = 24.499(3) Å	β= 100.724(10)°.
	c = 27.461(3) Å	γ = 90°.
Volume	6979.7(13) $Å^3$	
Z	4	
Density (calculated)	1.254 Mg/m^3	
Absorption coefficient	1.767 mm^{-1}	
F(000)	2776	
Crystal size	0.21 x 0.13 x 0.07 mm^3	
Crystal color and habit	colorless plate	
Diffractometer	Bruker/Siemens SMART APEX	
Theta range for data collection	1.51 to 25.25°.	
Index ranges	-12<=h<=12, -29<=k<=29, -32<=l<=32	
Reflections collected	104015	
Independent reflections	12642 [R(int) = 0.0808]	
Completeness to theta = 25.25°	100.0 %	
Absorption correction	Semi-empirical from equivalents	
Max. and min. transmission	0.8863 and 0.7080	
Solution method	XS, Bruker SHELXTL v. 6.10	
Refinement method	Full-matrix least-squares on F^2	
Data / restraints / parameters	12642 / 15 / 764	
Goodness-of-fit on F^2	1.030	
Final R indices [I>2sigma(I)]	R1 = 0.0425, wR2 = 0.0849	
R indices (all data)	R1 = 0.0662, wR2 = 0.0926	
Largest diff. peak and hole	0.573 and -0.438 $e.Å^{-3}$	

Table A.14. Bond lengths [Å] and angles [deg] for 167.

C(1)-C(2)	1.424(4)	C(31)-O(1)	1.472(3)
C(1)-C(17)	1.426(4)	C(31)-C(32)	1.511(4)
C(1)-C(18)	1.509(4)	C(32)-C(33)	1.508(4)
C(1)-Y(1)	2.670(3)	C(33)-C(34)	1.510(4)
C(2)-C(3)	1.418(4)	C(34)-O(1)	1.473(3)
C(2)-C(19)	1.505(4)	C(35)-C(36)	1.414(4)
C(2)-Y(1)	2.713(3)	C(35)-C(51)	1.427(4)
C(3)-C(4)	1.424(4)	C(35)-C(52)	1.505(4)
C(3)-C(20)	1.500(4)	C(35)-Y(2)	2.698(3)
C(3)-Y(1)	2.693(3)	C(36)-C(37)	1.414(4)
C(4)-C(17)	1.428(4)	C(36)-C(53)	1.507(4)
C(4)-C(5)	1.465(4)	C(36)-Y(2)	2.718(3)
C(4)-Y(1)	2.637(3)	C(37)-C(38)	1.427(4)
C(5)-C(6)	1.404(4)	C(37)-C(54)	1.512(4)
C(5)-C(10)	1.419(4)	C(37)-Y(2)	2.672(3)
C(6)-C(7)	1.377(4)	C(38)-C(51)	1.438(4)
C(7)-C(8)	1.381(4)	C(38)-C(39)	1.456(4)
C(8)-C(9)	1.373(4)	C(38)-Y(2)	2.663(3)
C(9)-C(10)	1.414(4)	C(39)-C(40)	1.404(4)
C(10)-C(11)	1.466(4)	C(39)-C(44)	1.415(4)
C(11)-C(12)	1.408(4)	C(40)-C(41)	1.378(4)
C(11)-C(16)	1.421(4)	C(41)-C(42)	1.380(4)
C(12)-C(13)	1.370(4)	C(42)-C(43)	1.367(5)
C(13)-C(14)	1.392(4)	C(43)-C(44)	1.410(4)
C(14)-C(15)	1.377(4)	C(44)-C(45)	1.473(4)
C(14)-H(14)	0.9500	C(45)-C(46)	1.408(4)
C(15)-C(16)	1.403(4)	C(45)-C(50)	1.415(4)
C(16)-C(17)	1.460(4)	C(46)-C(47)	1.371(5)
C(17)-Y(1)	2.657(3)	C(47)-C(48)	1.388(5)
C(21)-C(22)	1.219(4)	C(48)-C(49)	1.378(4)
C(21)-Y(1)	2.412(3)	C(49)-C(50)	1.404(4)
C(22)-Si(1)	1.831(3)	C(50)-C(51)	1.463(4)
C(23)-Si(1)	1.864(3)	C(51)-Y(2)	2.634(3)
C(24)-Si(1)	1.871(3)	C(55)-C(56)	1.217(4)
C(25)-Si(1)	1.863(4)	C(55)-Y(2)	2.397(3)
C(26)-C(27)	1.221(4)	C(56)-Si(3)	1.826(3)
C(26)-Y(1)	2.507(3)	C(57)-Si(3)	1.866(4)
C(26)-Y(2)	2.517(3)	C(58)-Si(3)	1.861(4)
C(27)-Si(2)	1.862(3)	C(59)-Si(3)	1.865(4)
C(28)-Si(2)	1.855(3)	C(57B)-Si(3)	1.866(4)
C(29)-Si(2)	1.860(3)	C(58B)-Si(3)	1.869(4)
C(30)-Si(2)	1.858(3)	C(59B)-Si(3)	1.870(4)

C(60)-C(61)	1.226(4)	C(73)-C(74)	1.383(5)
C(60)-Y(2)	2.499(3)	C(74)-C(75)	1.360(5)
C(60)-Y(1)	2.521(3)	C(27)-C(26)-Y(1)	105.8(2)
C(61)-Si(4)	1.865(3)	C(27)-C(26)-Y(2)	151.2(2)
C(62)-Si(4)	1.860(3)	Y(1)-C(26)-Y(2)	100.85(10)
C(63)-Si(4)	1.855(3)	C(61)-C(60)-Y(2)	102.2(2)
C(64)-Si(4)	1.862(3)	C(61)-C(60)-Y(1)	154.9(2)
C(65)-O(2)	1.472(4)	Y(2)-C(60)-Y(1)	100.98(11)
C(65)-C(66)	1.493(5)	O(1)-Y(1)-C(21)	83.78(8)
C(66)-C(67)	1.513(5)	O(1)-Y(1)-C(26)	136.37(8)
C(67)-C(68)	1.514(4)	C(21)-Y(1)-C(26)	93.12(10)
C(68)-O(2)	1.468(4)	O(1)-Y(1)-C(60)	78.57(8)
O(1)-Y(1)	2.3609(19)	C(21)-Y(1)-C(60)	143.83(10)
O(2)-Y(2)	2.380(2)	C(26)-Y(1)-C(60)	78.94(10)
C(69)-C(70)	1.493(5)	O(2)-Y(2)-C(55)	80.97(9)
C(70)-C(75)	1.366(5)	O(2)-Y(2)-C(60)	136.06(9)
C(70)-C(71)	1.406(5)	O(2)-Y(2)-C(26)	79.83(8)
C(71)-C(72)	1.380(5)	C(55)-Y(2)-C(26)	142.03(10)
C(72)-C(73)	1.372(5)	C(60)-Y(2)-C(26)	79.17(10)

Figure A.8. Complete Ortep3 diagram of 169.

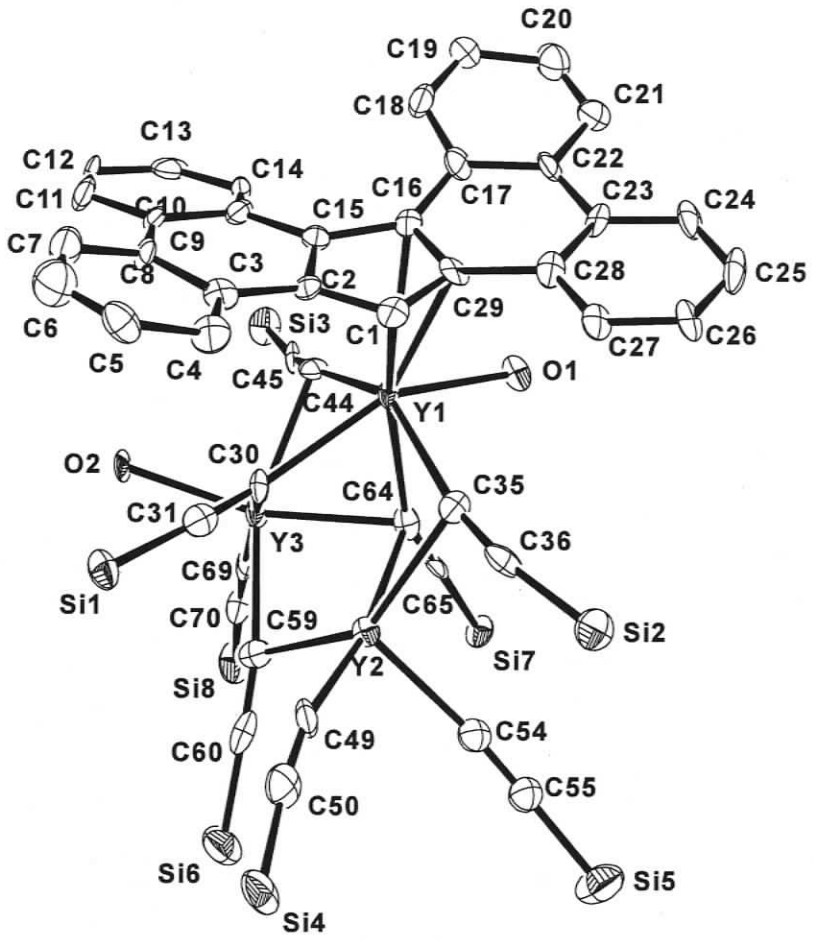

Table A.15. Crystal data and structure refinement for 169.

Empirical formula	C79.50 H110 O2 Si8.50 Y3	
Formula weight	1603.17	
Temperature	87(2) K	
Wavelength	0.71073 Å	
Crystal system	Monoclinic	
Space group	P(2)1/c	
Unit cell dimensions	a = 16.685(2) Å	α= 90°.
	b = 14.4172(17) Å	β= 98.696(2)°.
	c = 38.023(5) Å	γ = 90°.
Volume	9041.3(19) $Å^3$	
Z	4	
Density (calculated)	1.178 Mg/m^3	
Absorption coefficient	2.061 mm^{-1}	
F(000)	3356	
Crystal size	0.29 x 0.08 x 0.04 mm^3	
Crystal color and habit	colorless needle	
Diffractometer	Bruker/Siemens SMART APEX	
Theta range for data collection	1.51 to 22.50°.	
Index ranges	-17<=h<=17, -15<=k<=15, -40<=l<=40	
Reflections collected	75831	
Independent reflections	11808 [R(int) = 0.2455]	
Completeness to theta = 22.50°	99.9 %	
Absorption correction	Semi-empirical from equivalents	
Max. and min. transmission	0.9221 and 0.5863	
Solution method	SHELXS-97 (Sheldrick, 1990)	
Refinement method	Full-matrix least-squares on F^2	
Data / restraints / parameters	11808 / 72 / 861	
Goodness-of-fit on F^2	1.085	
Final R indices [I>2sigma(I)]	R1 = 0.0933, wR2 = 0.2100	
R indices (all data)	R1 = 0.1624, wR2 = 0.2418	
Extinction coefficient	0.0052(3)	
Largest diff. peak and hole	1.677 and -0.975 $e.Å^{-3}$	

Table A.15. Bond lengths [Å] and angles [deg] for 169.

C(1)-C(29)	1.402(17)	C(30)-Y(2)	2.789(12)
C(1)-C(2)	1.422(16)	C(35)-C(36)	1.242(17)
C(1)-Y(1)	2.657(11)	C(35)-Y(1)	2.463(13)
C(2)-C(15)	1.408(17)	C(35)-Y(2)	2.552(12)
C(2)-C(3)	1.448(17)	C(36)-Y(2)	2.849(12)
C(2)-Y(1)	2.791(11)	C(44)-C(45)	1.241(17)
C(3)-C(4)	1.393(18)	C(44)-Y(3)	2.515(12)
C(3)-C(8)	1.430(18)	C(44)-Y(1)	2.530(14)
C(4)-C(5)	1.501(18)	C(45)-Y(3)	2.873(12)
C(5)-C(6)	1.272(19)	C(49)-C(50)	1.254(18)
C(6)-C(7)	1.38(2)	C(49)-Y(2)	2.340(14)
C(7)-C(8)	1.410(18)	C(59)-C(60)	1.255(17)
C(8)-C(9)	1.429(18)	C(59)-Y(3)	2.400(13)
C(9)-C(10)	1.388(17)	C(59)-Y(2)	2.517(13)
C(9)-C(14)	1.447(17)	C(64)-C(65)	1.235(17)
C(10)-C(11)	1.334(18)	C(64)-Y(3)	2.504(12)
C(11)-C(12)	1.399(18)	C(64)-Y(1)	2.563(13)
C(12)-C(13)	1.372(17)	C(64)-Y(2)	2.656(12)
C(13)-C(14)	1.391(17)	C(69)-C(70)	1.242(17)
C(14)-C(15)	1.465(16)	C(69)-Y(3)	2.364(14)
C(15)-C(16)	1.460(16)	C(74)-O(2)	1.409(14)
C(15)-Y(1)	2.773(11)	O(1)-Y(1)	2.350(8)
C(16)-C(29)	1.422(17)	O(2)-Y(3)	2.285(7)
C(16)-C(17)	1.483(17)	Y(1)-Y(3)	3.5698(16)
C(16)-Y(1)	2.721(11)	Y(1)-Y(2)	3.7301(17)
C(17)-C(18)	1.388(18)	Y(2)-C(54)	2.394(13)
C(17)-C(22)	1.425(17)	Y(2)-Y(3)	3.6367(17)
C(18)-C(19)	1.342(18)	C(54)-C(55)	1.229(16)
C(20)-C(21)	1.356(19)	C(80)-C(81)	1.226(18)
C(21)-C(22)	1.424(18)	Y(1)-C(30)-Y(3)	87.3(4)
C(22)-C(23)	1.468(18)	Y(1)-C(30)-Y(2)	89.5(4)
C(23)-C(24)	1.404(17)	Y(3)-C(30)-Y(2)	83.6(3)
C(23)-C(28)	1.408(18)	Y(1)-C(35)-Y(2)	96.1(4)
C(24)-C(25)	1.385(19)	Y(3)-C(44)-Y(1)	90.1(4)
C(25)-C(26)	1.395(19)	Y(3)-C(59)-Y(2)	95.4(4)
C(26)-C(27)	1.355(17)	Y(3)-C(64)-Y(1)	89.6(4)
C(27)-C(28)	1.400(17)	Y(3)-C(64)-Y(2)	89.6(4)
C(28)-C(29)	1.463(17)	Y(1)-C(64)-Y(2)	91.2(4)
C(29)-Y(1)	2.610(11)	Y(1)-Y(3)-Y(2)	62.33(3)
C(30)-C(31)	1.202(17)	Y(3)-Y(1)-Y(2)	59.71(3)
C(30)-Y(1)	2.500(13)	Y(3)-Y(2)-Y(1)	57.95(3)
C(30)-Y(3)	2.668(12)		

Figure A.9. Complete Ortep3 diagram of 176.

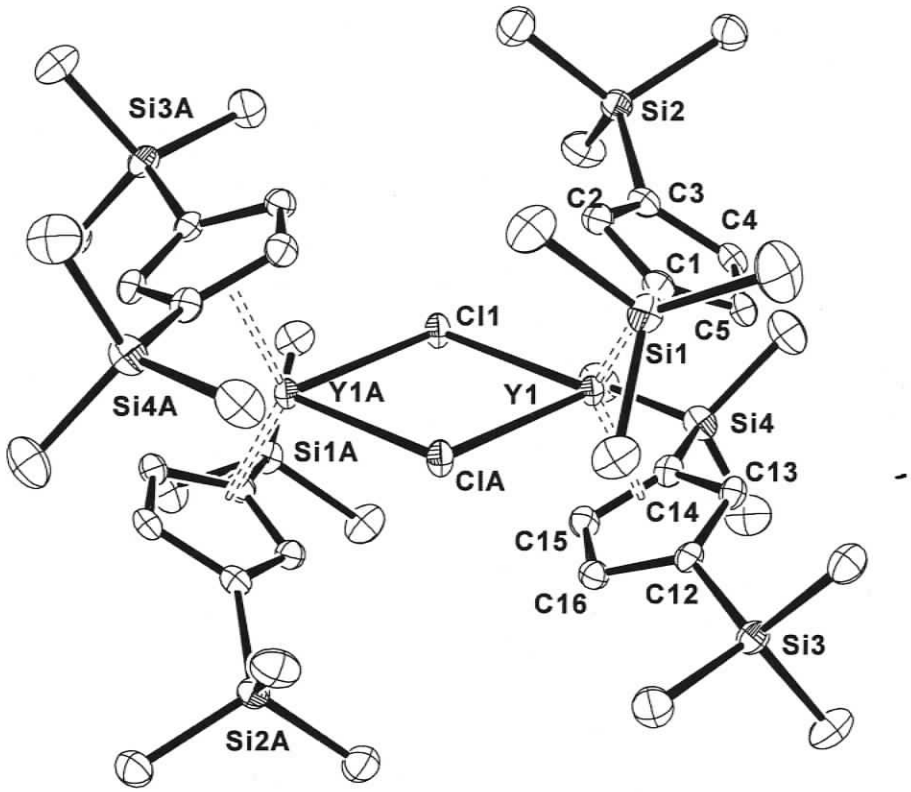

Table A.17. Crystal data and structure refinement for 176.

Empirical formula	C44 H84 Cl2 Si8 Y2	
Formula weight	1086.55	
Temperature	89(2) K	
Wavelength	0.71073 Å	
Crystal system	Triclinic	
Space group	P-1	
Unit cell dimensions	a = 10.5621(17) Å	α= 72.286(3)°.
	b = 11.6017(19) Å	β= 84.922(3)°.
	c = 13.022(2) Å	γ = 74.842(3)°.
Volume	1467.1(4) $Å^3$	
Z	1	
Density (calculated)	1.230 Mg/m^3	
Absorption coefficient	2.249 mm^{-1}	
F(000)	572	
Crystal size	0.36 x 0.25 x 0.07 mm^3	
Crystal color and habit	colorless plate	
Diffractometer	Bruker/Siemens SMART APEX	
Theta range for data collection	1.90 to 25.25°.	
Index ranges	-12<=h<=12, -13<=k<=13, -15<=l<=15	
Reflections collected	21697	
Independent reflections	5306 [R(int) = 0.0288]	
Completeness to theta = 25.25°	100.0 %	
Absorption correction	Semi-empirical from equivalents	
Max. and min. transmission	0.8585 and 0.4982	
Solution method	XS, Bruker SHELXTL v. 6.12	
Refinement method	Full-matrix least-squares on F^2	
Data / restraints / parameters	5306 / 0 / 265	
Goodness-of-fit on F^2	1.056	
Final R indices [I>2sigma(I)]	R1 = 0.0276, wR2 = 0.0667	
R indices (all data)	R1 = 0.0317, wR2 = 0.0685	
Largest diff. peak and hole	0.424 and -0.258 $e.Å^{-3}$	

Table A.18. Bond lengths [Å] and angles [deg] for 176.

C(1)-C(5)	1.422(3)
C(1)-C(2)	1.425(3)
C(1)-Si(1)	1.879(2)
C(1)-Y(1)	2.657(2)
C(2)-C(3)	1.429(3)
C(2)-Y(1)	2.656(2)
C(3)-C(4)	1.425(3)
C(3)-Si(2)	1.872(2)
C(3)-Y(1)	2.666(2)
C(4)-C(5)	1.406(3)
C(4)-Y(1)	2.616(2)
C(5)-Y(1)	2.613(2)
C(12)-C(13)	1.421(3)
C(12)-C(16)	1.432(3)
C(12)-Si(3)	1.865(2)
C(12)-Y(1)	2.651(2)
C(13)-C(14)	1.419(3)
C(13)-Y(1)	2.644(2)
C(14)-C(15)	1.430(3)
C(14)-Si(4)	1.863(2)
C(14)-Y(1)	2.657(2)
C(15)-C(16)	1.400(3)
C(15)-Y(1)	2.636(2)
C(16)-Y(1)	2.637(2)
Cl(1)-Y(1)A	2.6909(6)
Cl(1)-Y(1)	2.6987(6)
Y(1)-Cl(1)A	2.6909(6)
Cl(1)A-Y(1)-Cl(1)	79.60(2)